An evaluation of remote sensing techniques for the detection of archaeological features

James Scott Lyall

An evaluation of remote sensing techniques for the detection of archaeological features

James Scott Lyall, M.A. (Hons)

Thesis submitted for the Degree of Master of Science

Department of Geography, University of Durham

January 2007

Abstract

An evaluation of remote sensing techniques for the detection of archaeological features.

Submitted in January 2007 for the Degree of Master of Science.

J. S. Lyall.

The thesis evaluates the potential for using multiple remote sensing techniques to identify archaeological features buried beneath vegetation. The research is carried out on data acquired by the Natural Environmental Research Council (henceforth NERC), who have provided multispectral, LIght Detection and Ranging (henceforth LiDAR) and high resolution colour aerial photographic data. The returns from these techniques are compared with ground-based geophysical survey data carried out by the Landscape Research Centre (henceforth LRC) on four major projects funded by English Heritage (henceforth EH), as well as aerial photographs collected by the LRC.

The methodology adopted for this research uses primarily qualitative techniques, where images from different forms of remote sensing are processed, georeferenced and then compared for their ability to identify archaeological features. A process has been developed where the returns from each form of remote sensing are interpreted and then digitised as vector polygons with individual database entries for each polygon, which allows a direct comparison between the different datasets to be conducted.

The timing of the data acquisition is shown to be critical if the data is to be used for small scale anomaly detection, as is the case with archaeological features. This is particularly true for airborne sensors, although the returns from ground-based geophysical surveys can also be affected if carried out under unfavourable circumstances. It was established that the different underlying drift geologies of the

Vale of Pickering also affected the returns from remote sensing sources, with the calcareous and sandy zones of the southern part of the research area generally (though not exclusively) providing better results than the more alluvial zones to the north.

The use of different forms of airborne remote sensing and geophysical survey are demonstrated to be complementary, with each form of remote sensing identifying different, though not always exclusively different, archaeological anomalies.

Contents

Figures

Tables

Declaration

The material submitted in this thesis has not previously been submitted by the candidate for a degree in this or any other university.

Statement of copyright

Acknowledgements

Many organisations and individuals have helped and facilitated the preparation of this research, and thanks must go primarily to LRC, which has funded me from the inception of the research design to the completion of the thesis.

Thanks must also go to NERC, who have provided multispectral, LiDAR and aerial photographic data, without which this research could not have been undertaken. English Heritage, both through commissions and the Aggregates Levy Sustainability Fund (henceforth ALSF) have funded four separate projects which together have resulted in the acquisition of the largest contiguous gradiometer survey ever undertaken, the partial results of which are presented here. Keith Challis (Birmingham University) kindly sent pre-publication articles on LiDAR and other remote sensing techniques, for which I am very grateful.

All Ordnance Survey digital maps used in this thesis are licensed through the Geography Department academic agreement. All GetMapping images are used through the LRC academic license.

Unless otherwise stated, all geophysical imagery is owned by the LRC, and must not be copied or used without consent being sought. All web addresses referenced in the text were checked at the time of submission (January 2007), and were found to be active.

My final thanks must go to my supervisors, Dr Danny Donoghue (Geography Dept, University of Durham) and Professor Dominic Powlesland (Director, LRC), who have kept me from straying too far from the straight and narrow path of academic rigour, while allowing me both the time and resources to explore these rich and diverse datasets. However, the responsibility for any errors, whether in fact, omission or interpretation must remain firmly my own.

Chapter 1 Introduction

This chapter explains the concept behind this thesis, clearly stating the aims, objectives and the rationale for carrying out the research, continues with the existing framework to which the research will contribute and concludes with a brief overview of the structure of the thesis.

1.1 Context

Archaeological excavation is an expensive, labour intensive and time-consuming process. Any method that will enable archaeologists to inform their understanding of past human activity is therefore of a huge benefit. However, a bewildering array of remote sensing and geophysical techniques, both well established and novel, now face the non-specialised archaeologist. These include geophysical survey methods (magnetometry, resistivity and ground penetrating radar are currently the most often used) as well as aerial photography and newer airborne techniques (such as LiDAR and multi or hyperspectral scanning). Because of a lack of in-depth knowledge about how, when and why these techniques work, in many cases the criteria used to choose which form of remote sensing or geophysical survey to be adopted tends to be the availability of equipment (or data) rather than the method which would provide the best results in a given environment.

The project area for this research is located in the Vale of Pickering, North Yorkshire, England (see Figure 1), and was chosen for a variety of reasons. Firstly, the area has been the setting for one of the longest running archaeological research programs ever undertaken in this country. In addition, a number of smaller trial excavations have been conducted across the project zone. Combined, these excavations provide a transect of over 20 hectares of securely dated evidence which can be used to help confirm the interpretation of the remotely sensed data. Secondly, the area comprises a number of

different local geological environments, allowing different remote sensing techniques to be assessed over different underlying soil and drift geological conditions (see Figure 5). Finally, and perhaps most importantly for this research, the project area has seen the application of a battery of remote sensing techniques over the last 30 years, providing a range of comparative datasets against which any experimental work could be compared. These include a largest area magnetometer survey yet undertaken, a long-running and ongoing aerial photographic campaign, and an initial multispectral flight in 1992.

1.2 Aim

The research aims to evaluate a number of remote sensing and geophysical surveying techniques, in order to compare, contrast and quantify their ability to detect archaeological features on both a landscape and a local scale, across a range of geological zones.

In order to achieve this, the research will draw on the previously acquired multispectral data, geophysical surveys and aerial photographs, as well as two new remote sensing flights which include both LiDAR and newly acquired multispectral data. Targeted geophysical surveys have been carried out to confirm results, where these techniques are applicable.

1.3 Objectives

1) To quantify, contrast and compare the returns from a number of remote sensing techniques, primarily using four areas as case studies, although also illustrated with data from the extended project zone. To achieve this objective, a methodology using a combination of vector polygons linked to a relational database already designed for excavation datasets has been enhanced for remote sensing applications.

2) To integrate the results from the research within a GIS and data management framework, to allow analysis to be easily visualised.

1.4 Research Framework

The research has been funded in full by the Landscape Research Centre, as part of an ALSF funded project investigating the returns from different remote sensing sources. The LRC has also benefited from data grants from NERC, which include two multispectral sorties, flown on the 27/06/1992 and the 23/06/2005.

The project area is a located within a landscape which has long been known to be rich in cropmarks, and has been intensively studied from the air and on the ground for the past 25 years. The preliminary results from the initial NERC Airborne Research Survey Facility (henceforth ARSF) flight in 1992 have significantly enhanced the archaeological record in the area (Powlesland, Lyall and Donoghue, 1997) and have posed new questions that challenge the existing interpretation of human occupation and use of the Vale from Neolithic to the late Saxon period (Powlesland, 2001, p.233-235: 2003, p.275-292). It is of great significance that the study area contains three distinctly different aggregate geological environments: the chalk of the northern edge of the Wolds; the sand and calcareous chalk and chert gravel and windblown sand extending north from the foot of the Wolds; and the area in the centre of the Vale, primarily an alluvial sand and silicaceous gravel environment which also includes desiccating peat and lacustrine deposits.

The archaeological sites occur in an area of intensive agriculture that is being actively damaged by a combination of ploughing, subsoiling and intense drainage. Data from ground based magnetic survey and airborne imagery, including the NERC ARSF 1992 imagery, has revealed a landscape rich in archaeological remains, demonstrating a much

more intensive occupation than had been previously understood. David Miles, the chief archaeologist of English Heritage has said "*This site is as important as Stonehenge or Avebury. The graves, burial mounds, and houses have been left untouched by mechanized farming which has wrecked so much of the rest of our archaeology*". Original source: The Telegraph 26/11/02. Alternative web source http://news.bbc.co.uk/1/hi/england/north_yorkshire/3275377.stm

One of the key aspects of this research is the re-examination of the same targets after a gap of 13 years, using improved instrumentation to analyse areas where archaeological remains are known from the 1992 multispectral data but are not detected by the magnetometer surveys (Donoghue et al 2003). The acquisition of LiDAR data has facilitated the creation of a high resolution digital elevation model, and all of the other remotely sensed data has been draped over the model, a process which is of great significance for the analysis of the steeper slopes on the Wold scarp, and the flatter wetland areas of the valley floor.

This project area is situated in one of the most intensively studied landscapes in Britain and includes over 20 hectares of excavation and 25 years of study using aerial photography, ground examinations and remote sensing. This has had the effect of creating a major comparative archaeological landscape dataset. This systematic survey of the Vale of Pickering by the LRC provides an unparalleled opportunity to test the returns of the 2005 airborne multispectral imagery against the largest contiguous geophysical survey yet undertaken in Britain (see Figure 18).

Although conventional air photography and magnetometry can often yield spectacular results, it is currently impractical to undertake detailed magnetometer survey on a routine basis over large areas. The proposed research will help to assess cost effective

airborne survey techniques that can identify the archaeological returns from large areas quickly and cheaply, as well as identifying target areas for ground based geophysical investigation. The archaeological community at large will benefit from this research, as it looks at novel ways of interpreting remotely sensed data. It will also help to identify times when certain techniques are inapplicable, or at least assess the appropriateness of the times when the best returns can be expected.

1.5 Displaying the data

In order to correlate and visualise the different datasets, it is essential to use a Geographic Information System (GIS). This allows multiple layers of both vector and raster data to be displayed at the same time, which in turn allows a direct visual comparison between the different data sources to be made. Without this functionality, it would be virtually impossible to carry out research of this type.

1.6 Chapter overview

The thesis begins with a chapter outlining the context, aims and objectives of the research. Chapter 2 defines the archaeological and geological background of the project area. This is followed by Chapter 3, an introduction to the instruments used for data collection, which includes a short history of their use and development (mainly within British archaeology). The methodology adopted for each of the instruments is also discussed here. Chapter 4 discusses the data processing which each type of remote sensing underwent, as well as introducing the concepts of quantification of remotely sensed data. Chapter 5 looks at interpretation and data integration, using a case study to show how large and different datasets can be combined. The chapter also outlines the interpretative process involved, and how problems encountered were dealt with. Chapter 6 analyses the results of the data. Chapter 7 discusses the results and their impact on our understanding of the archaeological landscape. Chapter 8 draws the conclusions from the research, and lists a number of recommendations for further study.

Chapter 2 The geological and archaeological background of the project area

2.1 Location

The research project zone is located in Ryedale county, North Yorkshire, England, in an area where the low-lying Vale of Pickering meets the north-facing slopes of the Cretaceous Yorkshire Wolds. The full project area is a rectangle of 10 kilometres long by 7 kilometres wide, thus covering an area of 70 square kilometres. The south-west corner of the project area is at Ordnance Survey (OS) grid reference SE 88/73 and the north-west corner is at SE 98/80 (see Figure 2).

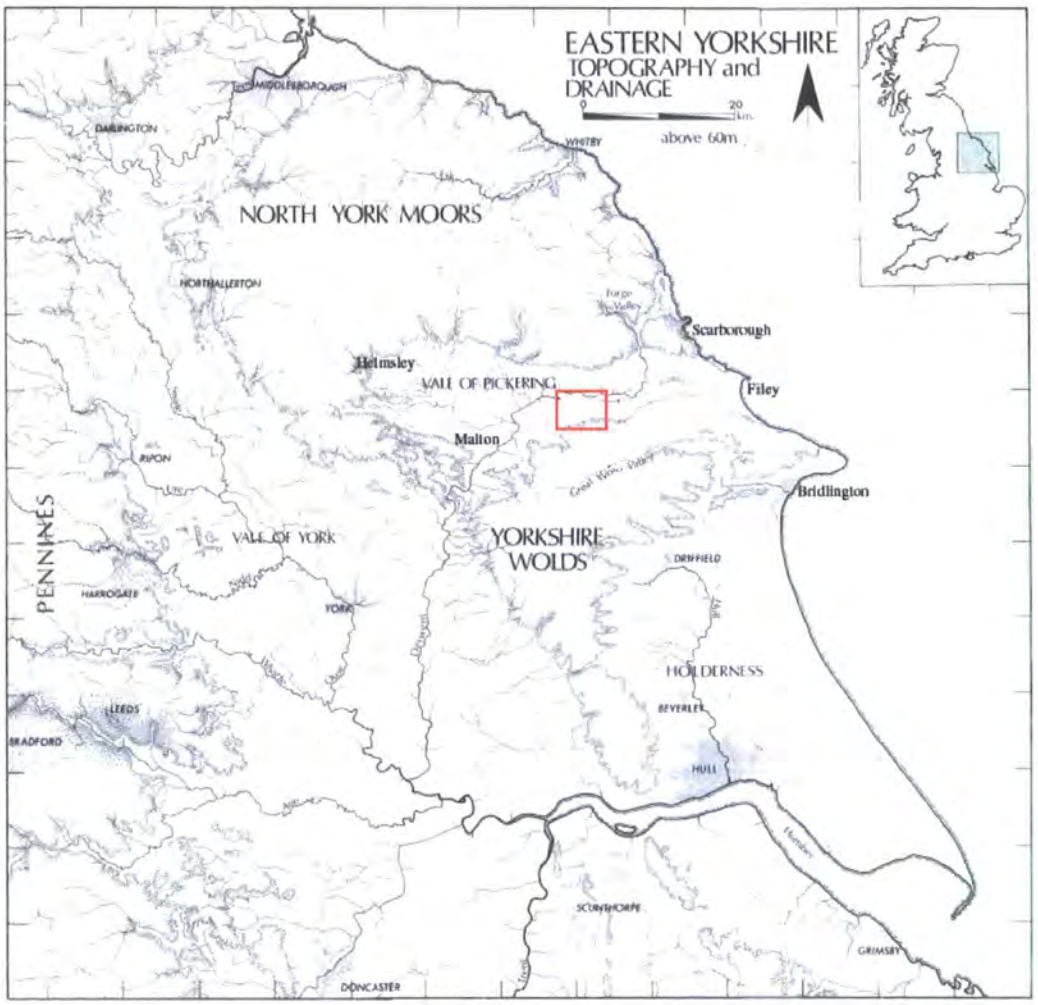

Figure 1 Location of the project area. After Powlesland et al, 1986

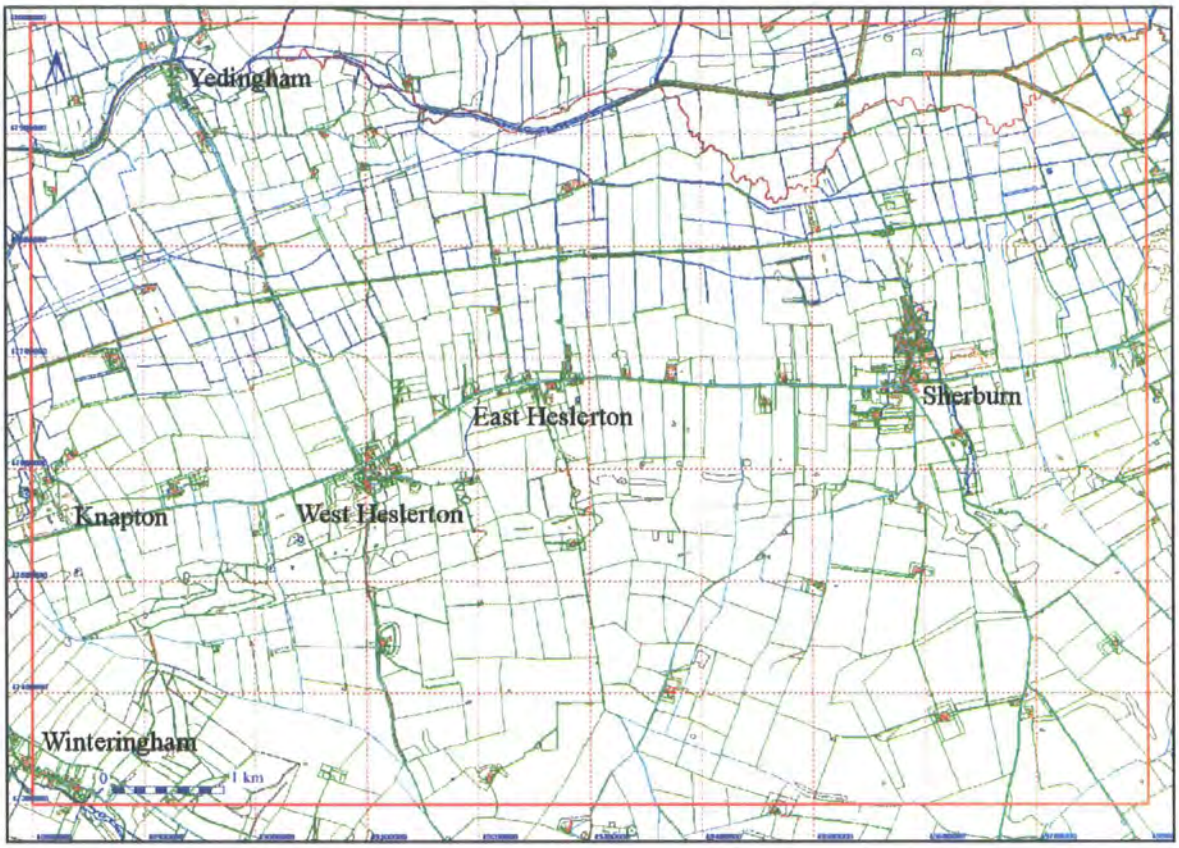

Figure 2 The location of the project zone in relation to modern villages

2.2 The geology of the area

The Vale of Pickering is a fairly flat, broad plain, extending from Helmsley in the west to Filey on the east coast, a distance of some 37 kilometres. The central zone is covered by a variable thickness of drift deposits, mostly fluvial and lacustrine clays, with sand and gravel deposits, all of which overlie Upper Jurassic mudstones (Kent, 1980, p. 7).

As the southern margins of the Vale meet the northern edge of the chalk Wolds, a zone of drifting windblown sand is encountered (see Figure 3, where active aeolian deposition is occurring in the background). This zone is particularly significant for archaeological reasons, as the aeolian sand serves to protect relict landscapes from modern agricultural techniques, such as deep ploughing and sub-soiling, one of the major threats to archaeological survival (see the English Heritage document, Ripping up

History, also available for downloading from the website http://www.english-heritage.org.uk/server/show/conWebDoc.3932.

During the latter stages of the Devensian Ice Age, the area which drained the waters from the eastern end of the higher ground (now part of the North York Moors) was cut off from the North Sea by a lateral moraine, causing the floodwaters to drain southward through what is now Forge Valley. Thus the river Derwent, running centrally through the Vale, is the only river in England to flow away from the sea for much of its 120 km length, eventually joining with the river Ouse before draining into the Humber estuary.

Figure 3 Active aeolian deposition 13 April 2006 (Looking SSW across the southern Vale towards the Wolds).

The Vale is bounded in the north and north-west by the Jurassic (Corallian division) limestones and sandstones of the Tabular Hills and the North York Moors, and in the west by the Jurassic limestone and sandstone of the Howardian Hills. To the south, the upper Cretaceous chalk of the Yorkshire Wolds forms a picturesque limit (see Figure 3).

Dominic Powlesland (Powlesland et al, 1986, pp.56-58) defined six distinct geomorphological zones across a parish transect (see Figure 4 for transect and Figure 5 for plan view).

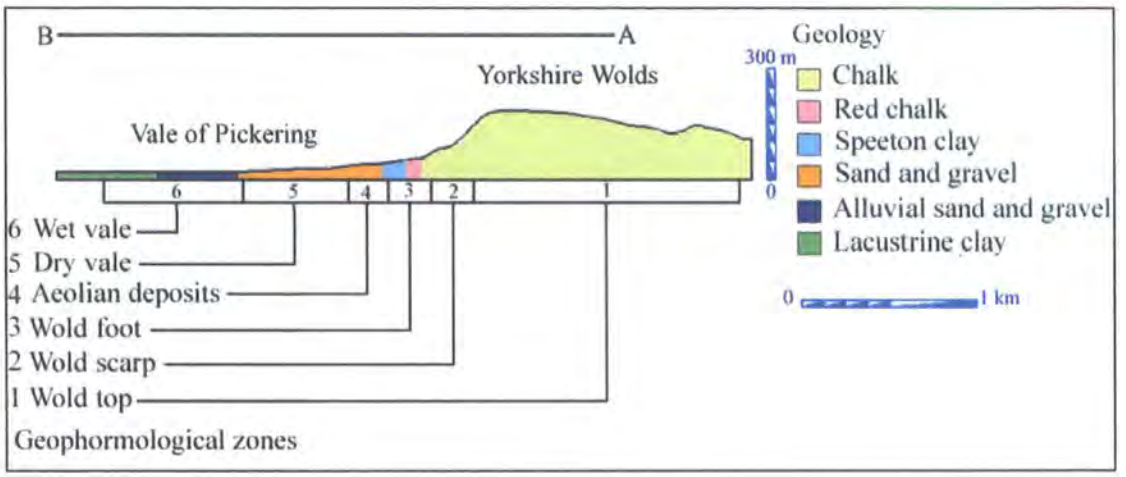

Figure 4 Transect through the project area. After Powlesland et al, 1986

The reason for this "zoning" was twofold. Firstly, it reflected genuine differences in the geomorphology of the area, relative to the underlying geology, and secondly, the archaeology seemed to reflect these broad geomorphological zones, with different activities occurring across the areas.

2.2.1 Zone 1 the Wold top

The largest zone comprises an area of open chalk downland, previously used mainly for pasture, although it is now under an intensive arable farming regime. The chalk is divided by a number of dry valleys (including the Great Wold valley), which are often sealed by deposits of alluvial sands and gravels, themselves commonly capped by colluvium (hillwash). The archaeology of this zone is dominated by upstanding monuments: the ditch and bank systems of the Wold entrenchments and funerary monuments, including both long barrows and round barrows. Because of the extent of modern ploughing, it is only beneath the upstanding earthworks or beneath colluvial deposits in the dry valleys that significant archaeological remains may be preserved,

though important environmental deposits could still be preserved beneath the banks of the entrenchments (Powlesland, 1986, pp.56; Powlesland, 2003, p.277-280).

2.2.2 Zone 2 the Wold scarp

This zone is one of the most picturesque, and comprises the steep, north-facing scarp of the Wolds, where the incline has restricted the build up of fertile soils. Any soil in this zone has tended to wash down into the dry valleys as colluvium, in some cases sealing archaeological deposits. The archaeological importance of this zone is demonstrated by the situation of two late Bronze/early Iron age palisaded enclosures on steep-sided knolls, at Staple Howe (Brewster 1963) and Devil's Hill (Brewster 1981). It is postulated that similar defended sites will be found at regular intervals both to the east and west (Powlesland, 1986, pp.56; Powlesland, 2003, p.280), although to date these have proved elusive to find.

2.2.3 Zone 3 the Wold foot

This zone incorporates the basal red chalk and the Speeton and Kimmeridge clay deposits. The location of a spring line where the chalk meets the clay is highly significant, as these water sources attracted human activity from the earliest times. Both the present day villages of East and West Heslerton are to be found in this zone (Powlesland, 1986, pp.56-58; Powlesland, 2003, p.280). The Anglian settlement of West Heslerton, located some 500m to the east of the present village, was located around one of these springs, which continues to produce water to this day. A number of current, buried or relict stream channels are known, extending out from their parent springs, although many of the still active springs have long since been diverted from their original courses (for instance, the stream which ran through the Anglian settlement is now diverted to the west, where it feeds the village bowling green across the A64).

2.2.4 Zone 4 the aeolian deposits

Zone four was originally identified by the excavations of 1977-1985 (see The Heslerton Parish Project), and comprises areas of windblown sand, which protect a number of archaeological deposits, including old ground surfaces and structural remains. The blown sands are derived from a deposit of post glacial sands and gravels beneath them, and have been accumulating since the late Mesolithic period at least, although how the deposits accumulate over time is still not well understood. (Powlesland, 1986, pp.58; Powlesland, 2003, p.280-282).

2.2.5 Zone 5 the dry Vale

Zone five consists of an area of post glacial sand and gravel, and is bounded to the south by the aeolian sand deposits and to the north by the lacustrine clays of zone six. The dry vale contains a continuous series of ladder settlements and field systems (of late Iron Age/Romano British date), which can be traced for circa 8km along the 27 to 30m contour lines in the southern part of the Vale. There is another ladder settlement in the northern part of the Vale (not part of the project area), although for this feature there is much less in the way of aerial photographic evidence. Gaps in the aerial photographic record and geophysical survey data could indicate either that these areas are well sealed beneath aeolian deposits, or could indicate genuine breaks in the ladder. It is probable that the areas which are very well-defined are those which have been the most seriously damaged by modern agricultural methods. (Powlesland, 1986, pp.58; Powlesland, 2003, p.282).

2.2.6 Zone 6 the wet Vale

Zone six is mainly comprised of a complex sequence of alluvial sands and silicaceous gravels and lacustrine clay deposits in the central area of the Vale. It is cut by relict stream channels, and includes a number of slightly elevated sand and gravel areas. This would have been a fenland or marshy environment in the past, although successive

drainage schemes, particularly during and after the Second World War last century have dried out much of the area. Trial trenching has indicated that blanket areas of peat are now rapidly drying out in this central zone (Powlesland, 1986, pp.58; Powlesland, 2003, p.282).

The geomorphological zones do not precisely follow the boundaries of the underlying geological layers, with the blown sand occurring across the Speeton clay and sand and gravel deposits, the wet vale across alluvial sands and gravels and clay deposits, and the Wold foot area across chalk, red chalk and the Speeton clay. Figure 5 shows the plan view of the transect illustrated in Figure 4 (A-B), and a comparison of the geomorphological zones overlain onto a geological map.

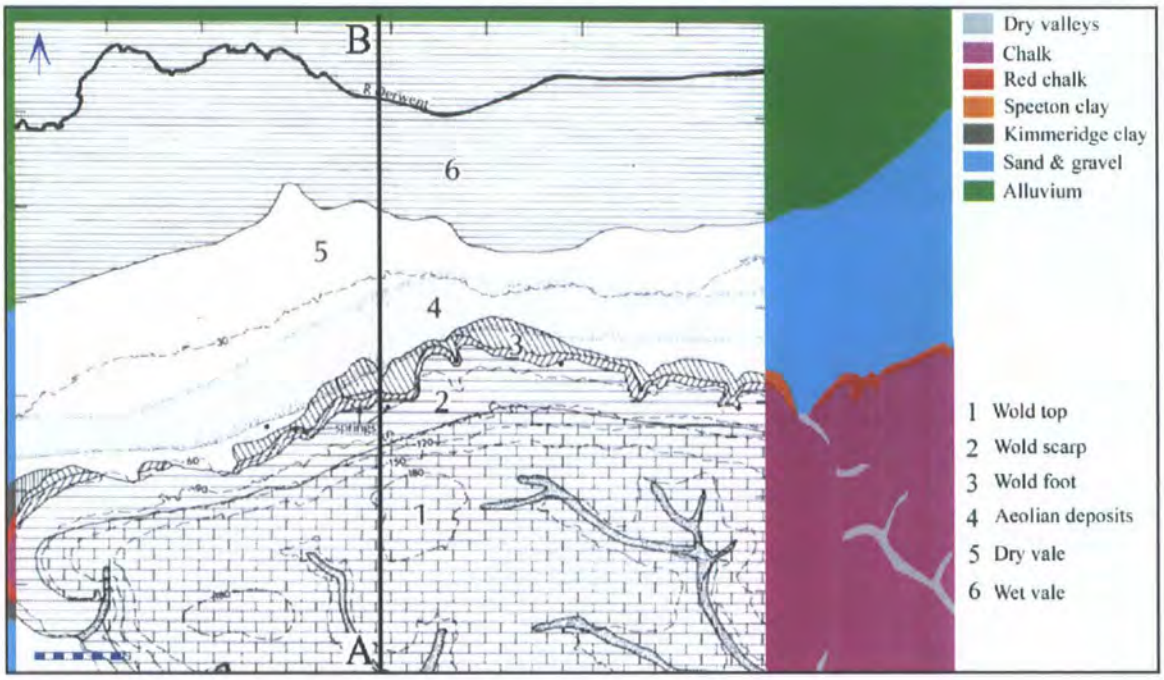

Figure 5 Geomorphology of the project area, overlaid onto a geological background. (After Powlesland et al, 1986 and Pryor, 1992)

Although most geological maps indicate fairly distinct zones in the region (see Figure 5), excavation and auguring over a large sample area have demonstrated that the real situation is of a much more complex nature (see Figure 73). Archaeologically, drift geology is the most important consideration, with colluvium (hillwash) filling in dry

valleys and spreading down into the windblown sand zone in the south, where areas of parent sand, windblown sand and alluvial sands and gravels all coincide within a landscape which was and remains intensively occupied. This zone is also cut by a number of existing and relict stream channels, which drain into the more alluvial, lacustrine area to the north.

The project area (see Figure 1 and Figure 2) is located in the southern central part of the Vale, extending south from the River Derwent across mainly alluvial clays, sands and gravels, before meeting the windblown sand zone, and ending on the steep north-facing scarps of the chalk Wolds.

Figure 6 Looking north across the Vale from the Wold scarp, with the Wold foot in the foreground

2.3 Soil type

The soils map for the area (Figure 7) reveals a more complex patterning, although the broad underlying geomorphological zones can still be identified.

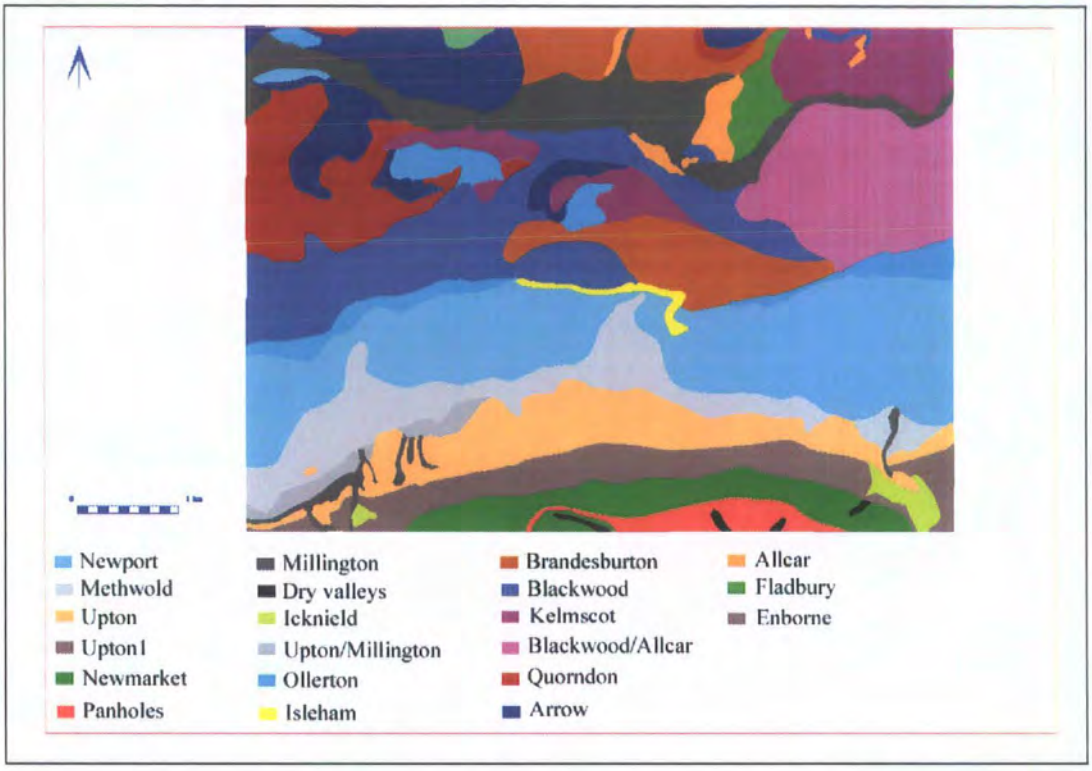

Figure 7 Soils encountered in a subset of the project area (shown in a red outline). Source: King, 1986. Polygons derived from Caldwell, 1996.

Table 1 gives a list of the soils found within the project area, a brief description of their characteristics, and the geomorphological zone in which they occur.

Name	Soil type	Description	Zone	Zone 2
Allcar	Earthy peat soils	Earthy eu-fibrous peat soils/grass sedge peat	6	
Arrow	Brown earths	Gleyic brown earths over coarse loamy drift with silicaceous stones	5	6
Blackwood	Sandy gley soil	Sandy drift with silicaceous stones	6	
Brandesburton	Cambic gley soil	Coarse loamy material over calcareous gravel	6	
Enborne	Alluvial gley soils	Fine loamy river alluvium	6	
Fladbury	Alluvial gley soils	Clayey river alluvium	6	
Icknield	Rendzina	Loamy lithoskeletal chalk	2	
Isleham	Humic sandy gley soil	Sandy drift with silicaceous stones	4	
Kelmscot	Cambic gley soil	Fine loamy material over calcareous gravel	6	
Methwold	Brown calcareous sands	Sandy chalky drift	4	3
Millington	Brown calcareous earth	Fine silty calcareous colluvium (dry valleys)	3	2
Newmarket	Rendzina	Coarse loamy lithoskeletal chalk	1	
Newport	Brown sands	Sandy drift with silicaceous stones	4	
Ollerton	Brown sands	Gleyic brown sands on sandy drift with silicaceous stones	4	5
Panholes	Brown calcareous earth	Fine silty material over lithoskeletal chalk	1	
Quorndon	Cambic gley soil	Coarse loamy drift with silicaceous stones	6	5
Upton	Rendzina	Loamy lithoskeletal chalk	2	

Table 1 The soils encountered in the main project area (after Caldwell, 1996)

A number of these soils are to be found in more than one zone, and this is indicated by a value in the zone 2 column. Although the soils map appears to give an in depth coverage of the area, the micro-variations which are to be found within fields are not reflected on this map. Figure 73 shows how much local variation can occur within a small area.

2.4 Case study areas

To achieve the objectives outlined above (see Objectives), it was necessary to focus on four specific case study areas (see Figure 8), although data from the wider project zone is also used where this helps to elucidate specific points. The four areas represent different underlying geologies; two in an area of alluvial sands and silicaceous gravel, where peat has also developed on at least two separate occasions in the post-glacial period, the third in a post-glacial sand and calcareous gravel area with a sealing aeolian sand component and the fourth covering the aeolian sand zone as well the predominantly chalk area to the south.

Case study areas one and three were located where the sand and calcareous chalk gravel and windblown sand zone has given way to the alluvial sands and silicaceous gravels to the north (zones 5 and 6), and it is in this zone where magnetic surveying techniques tend to be less successful. The test areas were chosen because they contain the remains of an extensive Middle Iron Age square barrow cemetery, which reacts to different forms of remote sensing with varying degrees of responsivity, depending on a number of contributing factors, as well as an (as yet undated) prehistoric enclosure system.

Case study area two is located in the windblown sand area (zones 4 and 5), with underlying sand and calcareous chalk gravels. It was chosen because it is known to respond well to a number of different remote sensing techniques. In addition, three sample excavations were carried out in 2001, so the relative depths of ploughsoil and windblown sand can to a certain extent be extrapolated.

Area four extends from the windblown sand zone southwards to the Wold scarp (zones 4, 3 and 2), and was chosen because the prehistoric trackway and pit alignments located here extend across all three zones, and often give exceptional cropmarks.

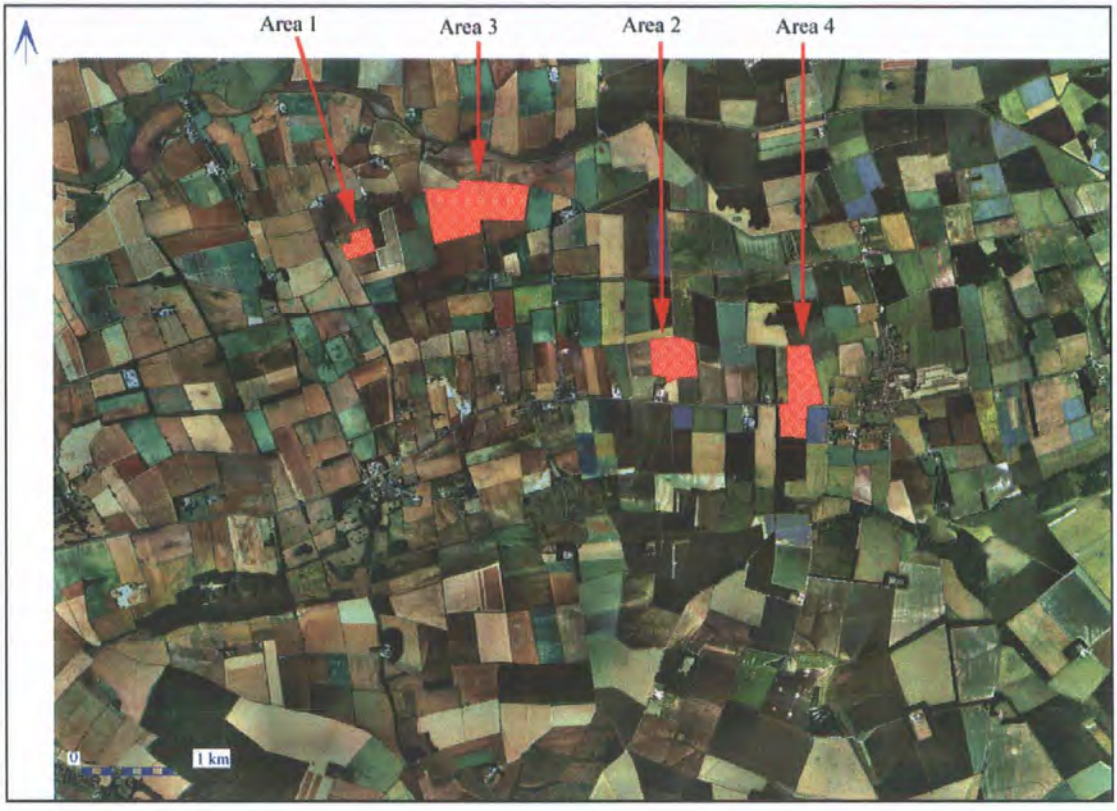

Figure 8 Location of case study areas within the project zone, on a Getmapping background

2.5 Archaeological background

2.5.1 Earlier archaeological work

Heslerton and the surrounding parishes were initially the focus of antiquarian investigations, culminating with Canon Greenwell's excavation of three round barrows in the parish during the mid 19th century (Greenwell and Rolleston, 1877, p.141-145). Greenwell also mentions a ploughed-out long barrow "at no great distance" from the third round barrow, which was partially removed prior to, and then "completely removed" in 1868. As Greenwell left no plan of his excavations, it is not clear whether he was referring to the East Heslerton long barrow, as this is still visible as a low upstanding monument today.

It was with Tony Brewster that the first modern excavations in the Vale were undertaken, beginning in the early 1950's (Brewster, 1952; Brewster, 1957). As well as being an accomplished archaeologist, Brewster was also the local schoolteacher for a number of years, and lost no opportunity in using archaeology to illustrate many of his lessons. His legacy lives on today in West Heslerton, where the villagers have maintained a keen interest in their surrounding archaeological remains. Brewster excavated a number of important sites in the region, including the major excavations at Garton Slack on the Wolds (Brewster, 1980), as well as the defended, palisaded enclosures of Staple Howe (Brewster 1963) and Devil's Hill (Brewster 1981), both located within the project zone. Devil's Hill was subsequently issued with LRC site number 31.

During the 1960's an investigation of the eastern end of the East Heslerton long barrow (site 32) was conducted by Faith Vatcher (Vatcher, F de M. and H. L, 1965). This revealed that the monument was one of the Yorkshire cremation series of long barrows, although unfortunately much of the northern half of the facade had been destroyed by a lime kiln. The long barrow is located just over the edge of the Wold scarp, and is not visible from the Vale below.

2.5.2 The Heslerton Parish Project

Since 1978, the archaeological team working at West Heslerton under the direction of Dominic Powlesland has developed a site code system, where each field is assigned a number, with all further work carried out in that field being related to this specific site number. All fieldwork carried out in the project area will refer to these site numbers, a location map of which is illustrated in Figure 9.

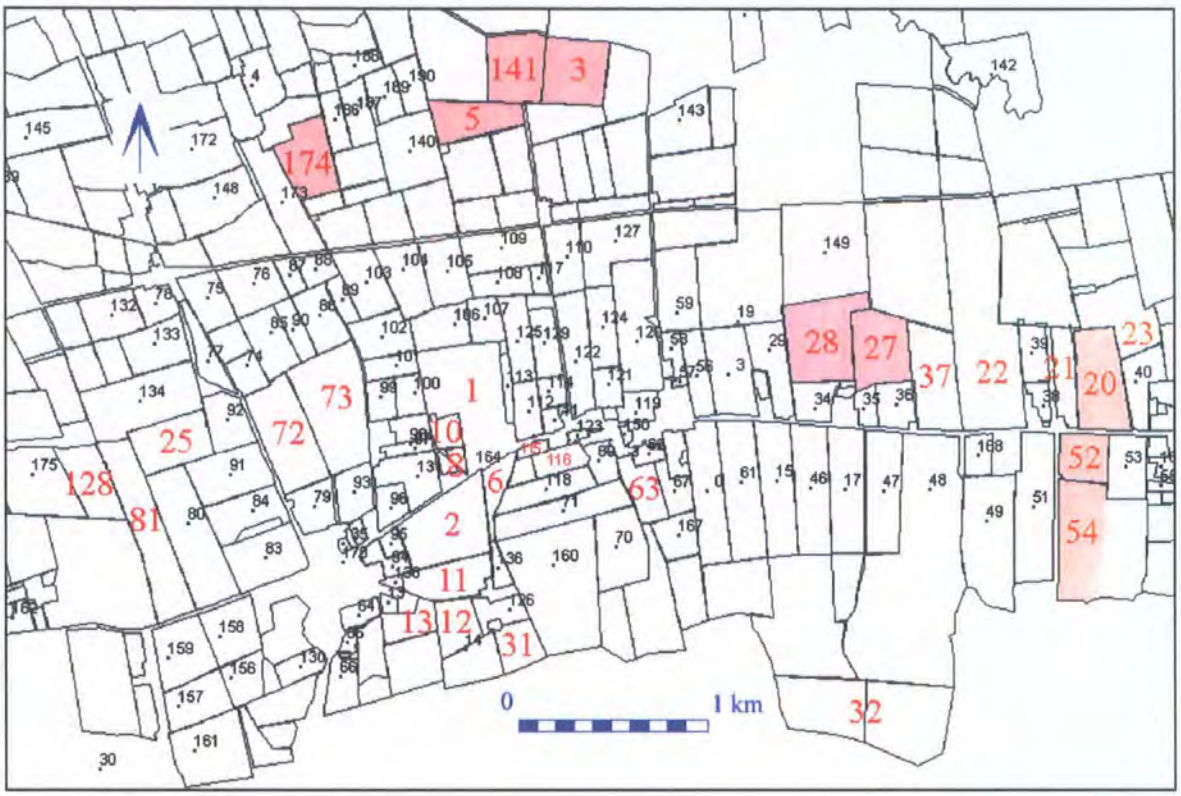

Figure 9 Site numbers, with those mentioned in the text in red. Case study areas are highlighted.

In 1977, a chance find at Cooks Quarry by one of Brewster's former pupils, Jim Carter, was to lead to one of the longest running excavations ever conducted in England, which is only now nearing completion. This initial find led to the discovery of an Anglian cemetery, which was excavated in 1977 (site 1 see Figure 10 for location) by John Dent and between 1978 and 1986 (sites 1, 2, 6 and 8) by Dominic Powlesland (Haughton and Powlesland, 1999). These early investigations prompted the formation of the Heslerton Parish Project in 1980, which initiated a research framework with the primary aim being to place the results of the excavations into a wider landscape context. Besides the Anglian cemetery, a late Bronze Age settlement site was also encountered, as well as an extensive Neolithic and early Bronze Age ritual complex, incorporating a timber post circle, a henge monument and part of two round barrow cemeteries (Powlesland et al, 1986; Haughton and Powlesland, 1999). These initial investigations led to the excavation (1987-1995) of the Anglo-Saxon settlement (sites 2, 11, 12 and part of 13) directly associated with the cemetery; the first time that such a relationship had been

excavated in the north of Britain, and the first using modern excavation techniques. More recently, the excavation of the prehistoric landscape has continued, in advance of sand extraction at Cooks Quarry (Site 10 1999-2006). To date a total of 20.3638 hectares has been excavated.

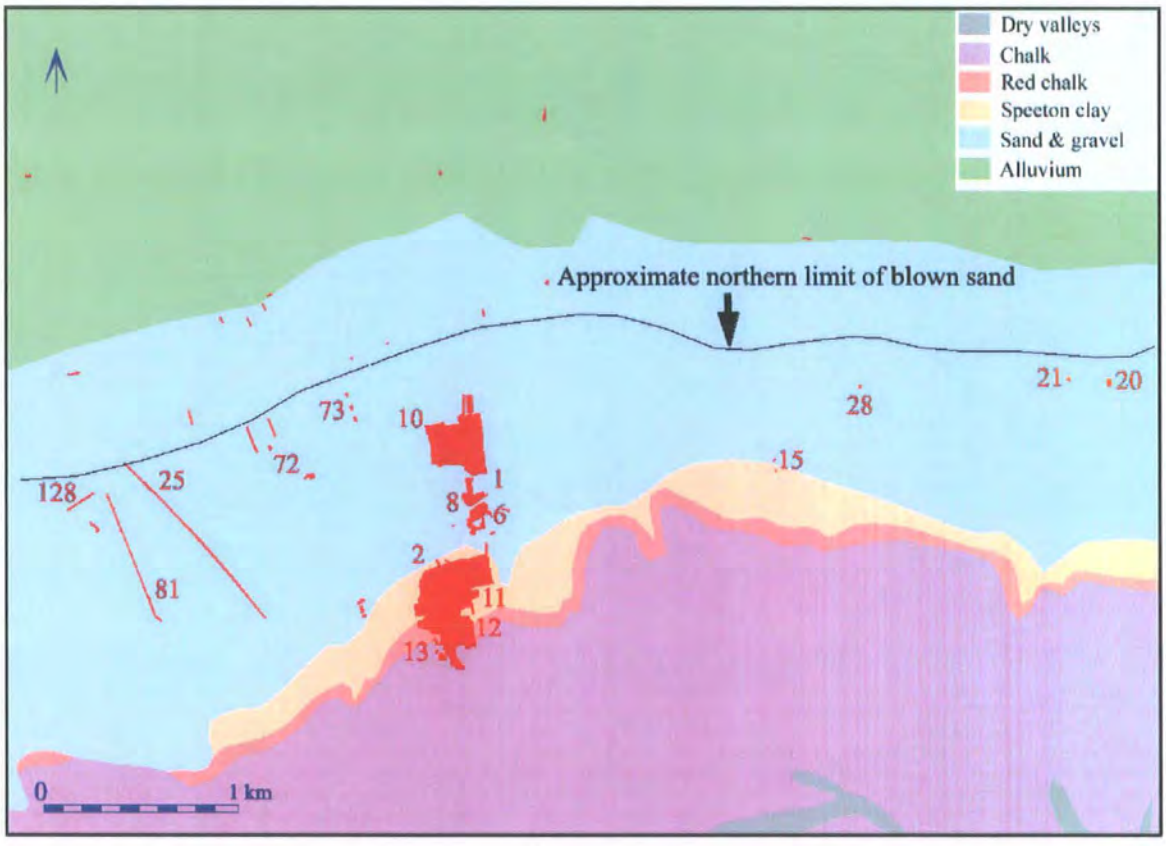

Figure 10 Map of the location of the excavated areas mentioned in the text, on a geological background

In addition to the main excavation area, a number of relatively small scale observation trenches have been excavated over the years (Figure 10). These include trenches over an Iron Age/Romano-British ladder settlement (sites 20 and 21 in 1984, site 25 in 1995, site 28 in 2001 and sites 72, 81 and 128 in 2003), with further trenches investigating the presence of Anglian Grubenhäuser (site 28 in 2001 and site 73 in 2003). Additionally, a number of small trenches have been cut in the wet Vale to collect the environmental evidence required to establish the environmental context of the larger excavations.

The value of these excavations for remote sensing purposes cannot be overestimated, as they allow an insight into the nature and character of the subsoil as well as the archaeological features in the project area. This allows the interpretation of both geophysical and remotely sensed anomalies to be made with a high level of confidence in these areas, in effect extrapolating the known archaeological features outwards from the excavations.

2.6 Previous remote sensing work

2.6.1 Aerial Photography

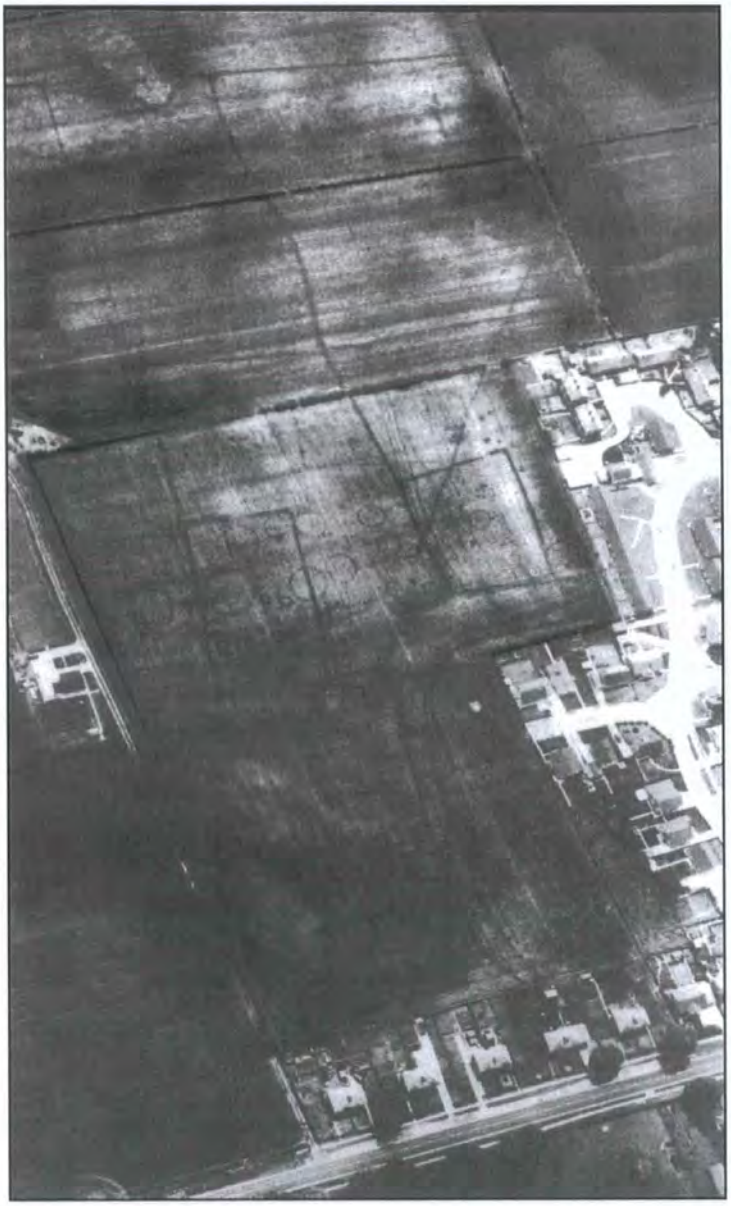

Figure 11 Rillington barrow complex (source A. L. Pacitto)

A number of the famous figures in aerial photography have flown campaigns over Yorkshire, including J.K. St Joseph and D.R. Wilson, both of whose collections are now held in the Cambridge University collection, as well as Derek Riley and Tony Pacitto (Riley, (ed) 1988). Figure 11 shows an example of one of Tony Pacitto's photographs of the Rillington barrow complex (located 3 kilometres to the west of the project area). The photograph was scanned from Yorkshire's Past from the Air (Riley

(ed), 1988, p.47), and has been slightly contrast enhanced to bring out some of the square barrows in the bottom (northern) part of the photograph. The photograph is oblique and is not geocorrected. The Vale has also been flown by the Aerial Photographic Unit of the RCHAM (now the Aerial Survey team, part of English Heritage), and fortunately the project zone was sufficiently close to the edge of the Yorkshire Wolds to be partially included in the plotted maps from the Ancient Landscapes of the Yorkshire Wolds volume (Stoertz, 1997).

At the same time as the multispectral flight was undertaken in 1992 (see Multispectral imagery), a series of 92 high resolution colour near vertical large format prints was also acquired. As the near drought conditions in the summer of 1992 were ideal for good cropmark formation, the photographs provided enhanced detail on a number of known sites, as well as finding new cropmarks (see Figure 21).

However, by far the most important aerial photographic resource is that collected and collated by Dominic Powlesland. In a ongoing campaign which has to date spanned 28 years, he has taken thousands of photographs, both black and white prints and colour slides, which have provided a wealth of detail about the extent of archaeological activity in the area. Compare Figure 11 with Figure 12, another oblique view of the Rillington complex, taken from the west looking east. Both photographs provide good coverage of the main area, but the different view angles allow the cropmarks in the surrounding fields to be identified.

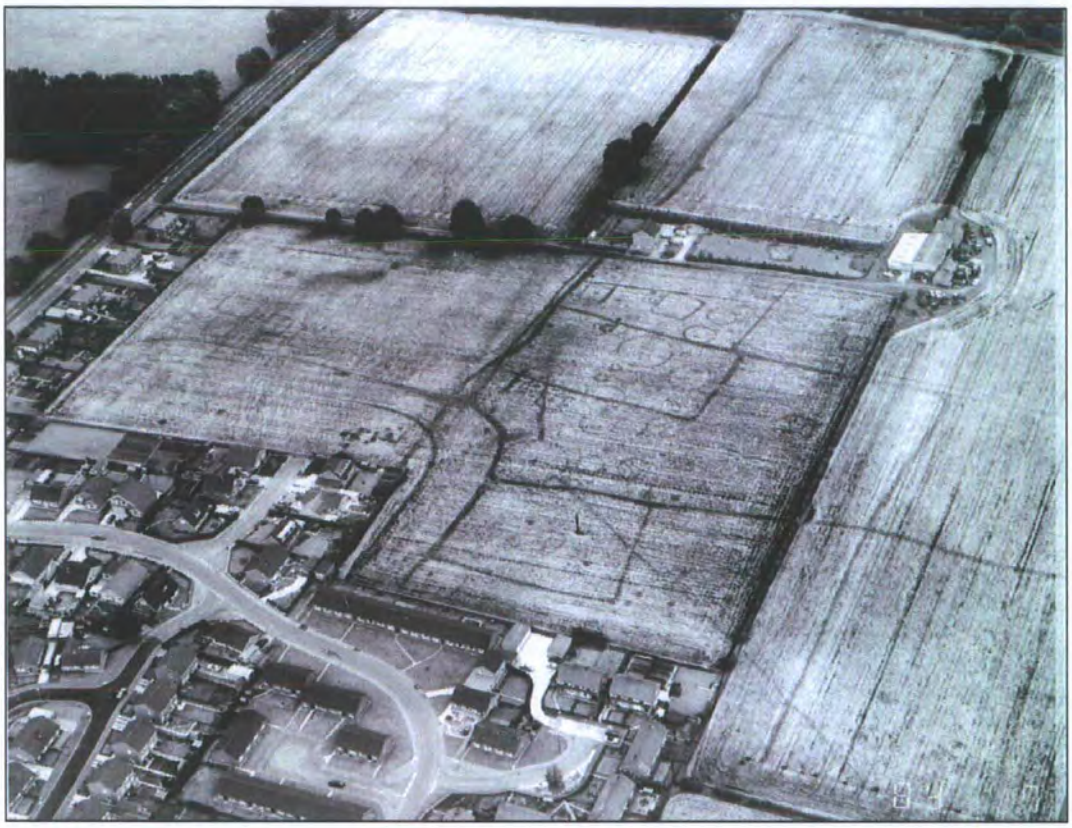

Figure 12 Rillington barrow complex (source D. J. Powlesland)

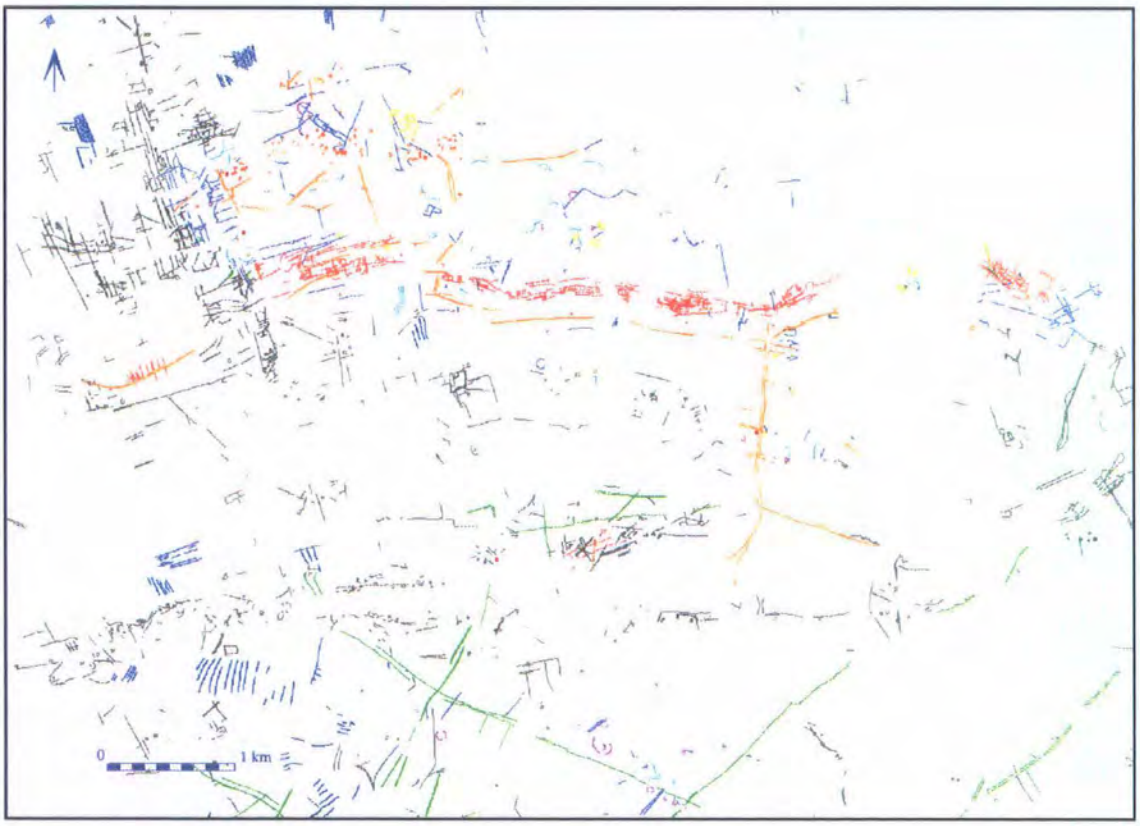

Figure 13 Cropmark plot of the main project area

Figure 13 shows a plot of the combined results from all aerial photographs taken up to the end of 1994. The detail and extent of the coverage provides a yardstick against which all of the other forms of remote sensing can be compared.

2.6.2 Geophysical Surveys

A proton magnetometer survey was carried out over the Iron Age square barrow site at Arras on the Yorkshire Wolds in 1959 (Stead, 1979, p.10). This was one of the earliest surveys of its type in Yorkshire, and a very creditable area of almost 3 hectares was covered. Unfortunately, in an area where 19 square barrows were subsequently shown by excavation to exist, only 2 were detected magnetically, and even these not completely (only 3 sides of each barrow ditch appeared as magnetic anomalies).

Initial trials by Arnold Aspinall over a known round barrow at the Cook's Quarry excavations (Site 1) using both magnetometry and resistivity in 1980 were also inconclusive (Dominic Powlesland pers comm.). However, further work by Arnold Aspinall and Tony Pacitto demonstrated that sites on the chalk Wolds, for example the East Heslerton long barrow and areas around Rudston, responded well to magnetic survey (Arnold Aspinall pers comm).

In April 1986, the English Heritage (Ancient Monuments Laboratory) team carried out a magnetometer and magnetic susceptibility survey at site 2, over an area suspected to be part of an Anglian settlement, as a precursor to excavation.

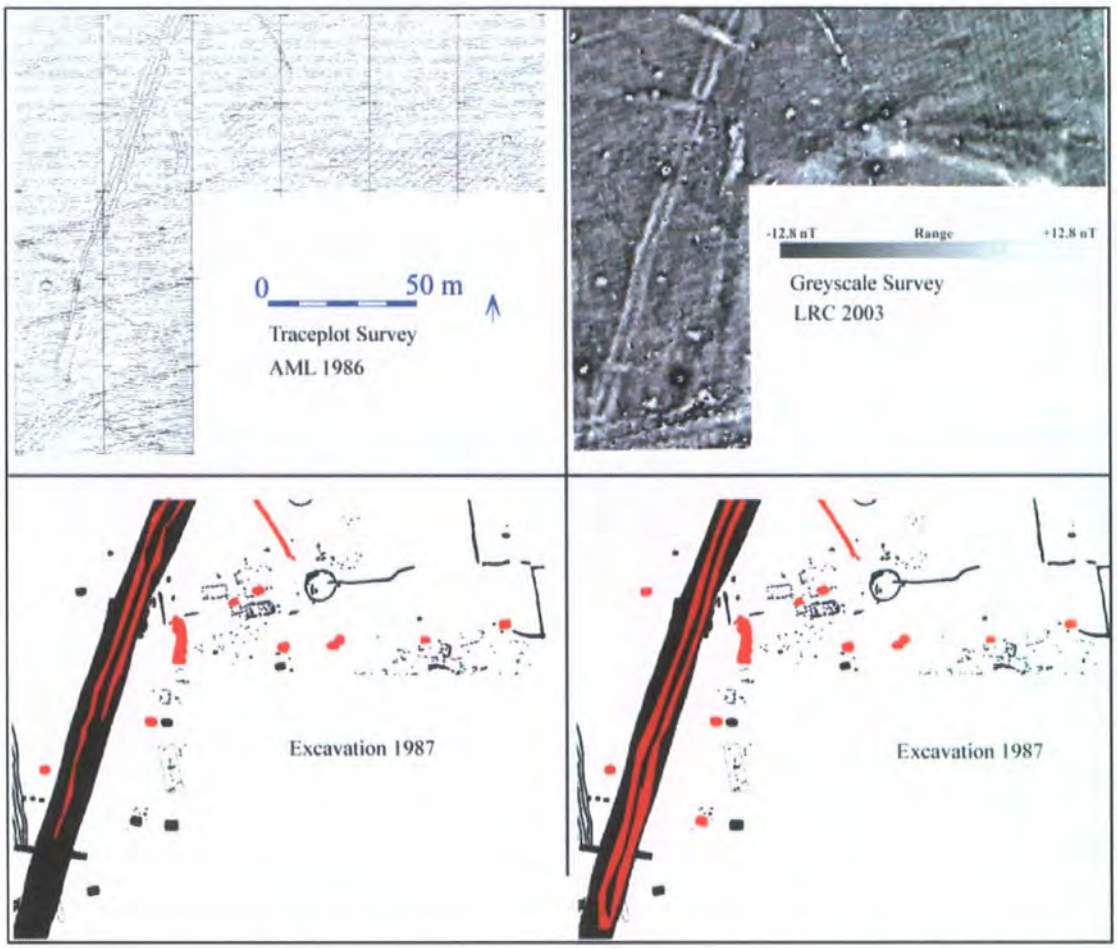

Figure 14 Comparative magnetometer plots related to excavated features (in red)

The magnetometer survey was carried out with an instrument which produced trace plots only (see Figure 14), and is documented in the AML report Series/No Geophysics G 3/86. The results clearly indicated the presence of a number of localised anomalies, some linear anomalies, as well as a number of less clearly defined linears. The area was resurveyed by the LRC team in 2003, and the greyscale plot is included as a comparison in Figure 14. The 1986 survey demonstrated that magnetic techniques would work well on the areas away from the sands of the quarry zone, but failed to reveal the full complexity of the underlying archaeology. Further work by the AML team, using a fluxgate gradiometer (model FM36) confirmed the effectiveness of the technique in this zone, with another 10 hectares of the Anglian settlement surveyed during 1990 and 1991, providing some stunning results (see Figure 15 below).

These results were enhanced by carrying out high resolution surveys (LRC surveys, 1991 and 1995) over the same areas (parts of sites 11 and 12), after removing the ploughsoil. This allowed the archaeological features to be mapped long before they became visible to the naked eye, as well as providing a number of other benefits. (Lyall and Powlesland, 1996).

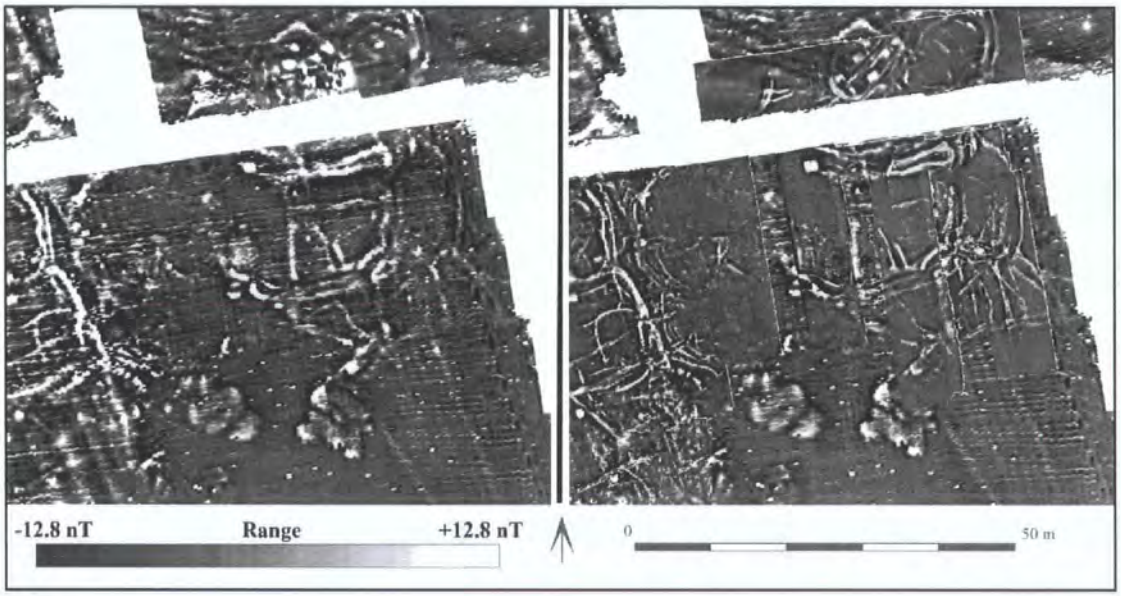

Figure 15 Comparison of normal and superimposed high resolution magnetic survey over Sites 11 and 12

In Figure 15, the same area surveyed at a normal resolution (25cm by 100cm) prior to the removal of the topsoil (left, survey by the AML team) can be compared with the high resolution survey (25cm by 25cm) carried out after topsoil stripping. A detail view of the eastern part of this image can be seen in Figure 155.

The technique of using high resolution surveying has been used twice more over different areas of the project zone, once after the removal of topsoil, and once on the current ground surface. In both cases, enhanced detail over the usual survey resolution was apparent.

The second test was in a different geological zone, where deep bands of sand and chalk gravel are overlain in parts by windblown sand. It was located just to the west of the area where Arnold Aspinall had carried out the initial geophysical tests. The effect of more magnetically susceptible ploughsoil masking underlying features is graphically demonstrated in Figure 16, which shows the results of two gradiometer surveys conducted at Site 10, one carried out before the removal of the topsoil, and one shortly afterwards.

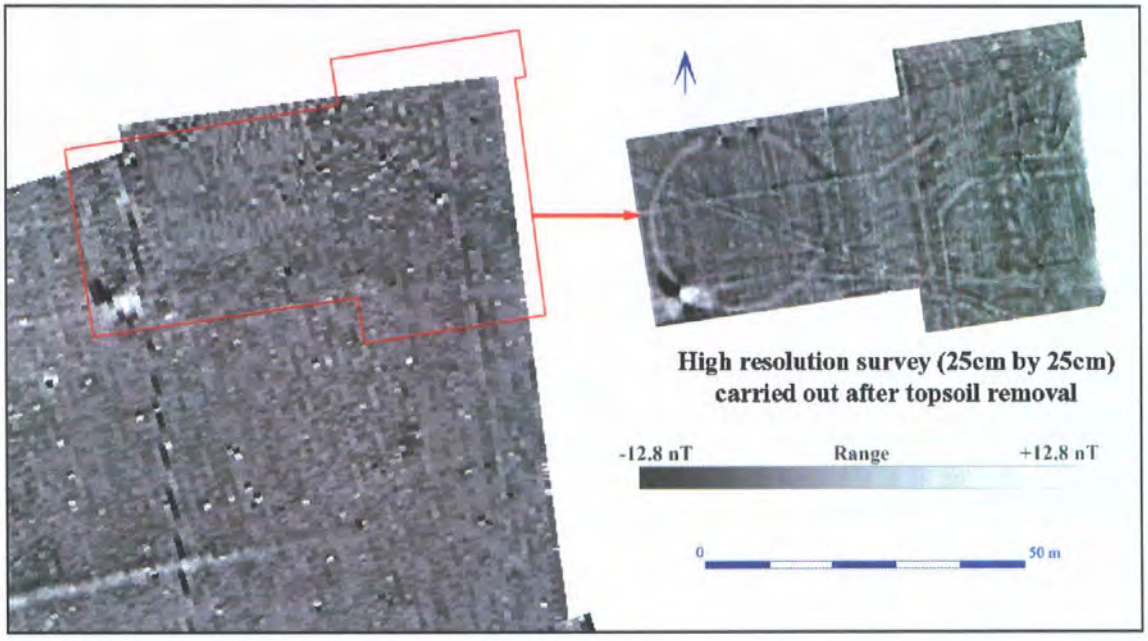

Figure 16 High resolution results after the removal of the topsoil on Site 10

The two surveys are not directly comparable, as the initial survey had a spatial resolution of 25cm north-south and 100 cm east-west, while the second survey had a higher spatial resolution of 25cm in both directions. Nevertheless, the difference in anomaly detection is quite remarkable, especially when considering that the overburden of ploughsoil removed from the western half of the second surveyed area was no more than 30-35cm in depth. During this second high resolution survey, it was noticed that the difference in magnetic contrast between the filled archaeological features and the parent sand and chalk gravel subsoil was slight; no more than 1 or 2 nT.

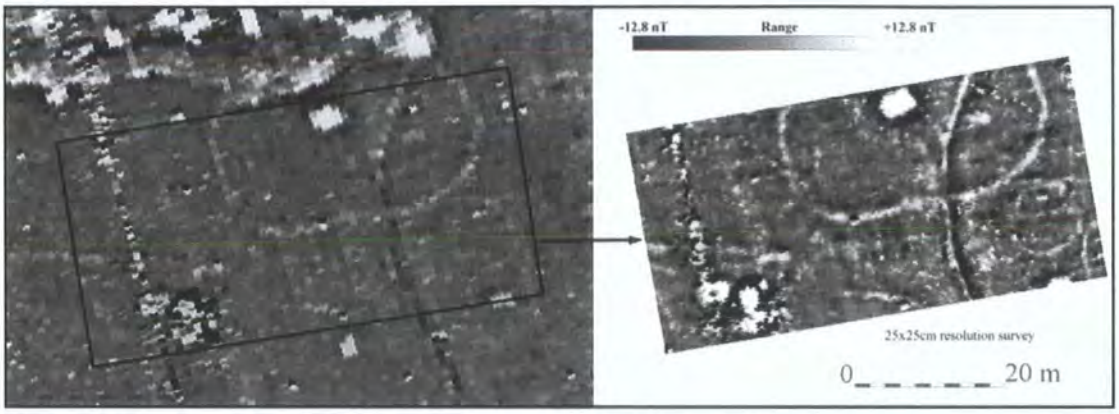

Figure 17 Comparison of normal and high resolution magnetic survey over Site 63

The third trial of high resolution surveying was carried out just to the south-east of the earthworks associated with the deserted medieval village, located to the south of the present village of East Heslerton (Site 63, see Figure 17). The original survey results were good, showing a curvilinear enclosure, a potential *Grubenhaus* and a circular anomaly just to the south-east of the enclosure, but it was felt that further enhancement of detail could be achieved if a closer traverse interval was used. A small test area (30m by 60m) was then surveyed.

The results of the high resolution survey (25cm by 25cm) were generally excellent, defining the enclosure, as well as confirming the ring ditch feature to the south-east. The potential *Grubenhaus* looks even more convincing in this dataset. Further anomalies not easily defined in the first dataset were obvious in the second. Although the ploughsoil had not been stripped away prior to the high resolution survey, the location of the surveyed area was on the brow of a small chalky knoll, and it is likely that the ploughsoil depth here is extremely shallow. The implication is that in areas where magnetic techniques are known to give good results and thin layers of topsoil are present, the use of close traverse surveys should give an improved definition of anomalies.

Large scale geophysical survey

Perhaps the most significant advance in recent years has been the application of magnetometry over a large (>1000 hectare) contiguous area, covering much of the central project zone. This was a major undertaking, but has provided a detailed interpretative map which both complements and enhances the aerial photographic plots. The surveys have been part of a number of different projects, funded by English Heritage, the ALSF (through English Heritage) as well as the LRC. The first surveys in this campaign were carried out in 1993 as part of an English Heritage funded project which also provided a preliminary assessment of the returns from the first multispectral flight in 1992 (Powlesland, Lyall and Donoghue, 1997). These initial geophysical surveys were targeted to achieve two aims, the first being to confirm the returns from both the cropmark and multispectral sources, and the second to test the magnetic response over three different geological zones. These were the chalk bedrock of the Wold tops (1.26 Ha), the Wold foot where a mixture of windblown sand, chalk and colluvial deposits are found (1.45 Ha), and finally the dry Vale (6.65 Ha), where drifts of windblown sand overlie areas of parent sand and gravel (see Powlesland et al, 1997 for images). To some extent, the first two zones were already known to be magnetically responsive, but the windblown sand zone had not yet been tested geophysically. This zone proved to be very receptive to magnetic surveying techniques, and further research surveys by the LRC (totalling 27.765 Ha) over the next few years confirmed these promising initial results.

With the knowledge that almost the entire area of the central sand and calcareous chalk gravel zone was responsive to magnetic surveying, a number of projects targeting different aspects of archaeological activity across the geological zones were proposed and accepted by English Heritage. These were the Landscape Evaluation Project

(funded by English Heritage, Project number 2804, carried out from 2000-2006, to date totalling 441.705 Ha) and the Landscape Characterisation Project (EH Project number 3409 supported by the ALSF, carried out from 2003-2004, 393.808 Ha). Latterly, a further project, Mapping the Archaeological Resource (EH Project number 3841, supported by the ALSF) has conducted 72.75 hectares in the less responsive zone to the north, as well as a further 137.458 hectares of survey to the east of Sherburn, during 2005-2006.

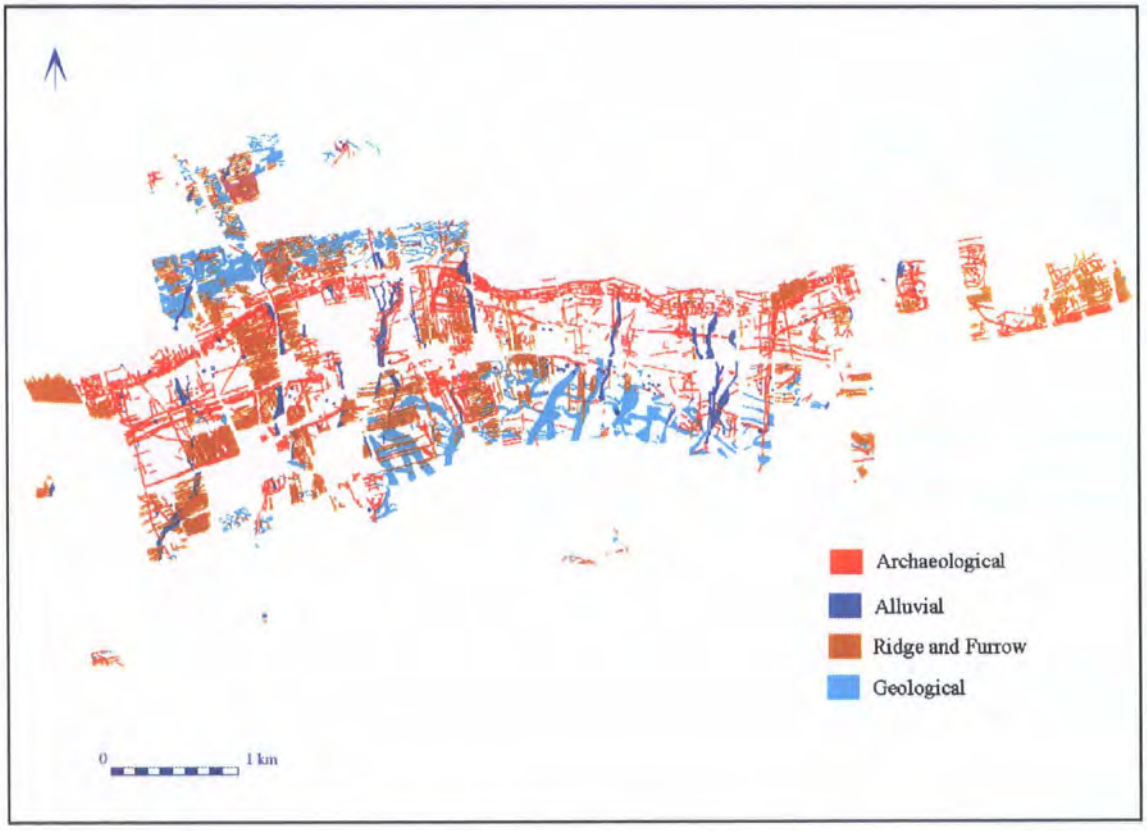

Figure 18 Magnetometer anomaly plot coloured by interpretative overlay

The combined interpretative results from all of the projects is shown in Figure 18, covering the same area as the cropmark plot in Figure 13, allowing a direct comparison to be made between the returns from these two methods.

2.6.3 Multispectral imagery

In June 1992, a multispectral flight covering an area of 33.63 square kilometres was flown by the NERC. Initial work on the data demonstrated its ability to enhance

archaeological understanding of the area, even in areas where other forms of remote sensing were not successful (Powlesland, Lyall and Donoghue, 1997). This was particularly true of the infra-red and thermal bands, which defined cropmarks not visible in the colour aerial photographs taken at the same time (see Figure 95 and Figure 100).

Due to time constraints, only some small sample areas of the multispectral data were georeferenced following the 1992 flight, although most of the area covered has now been geocorrected as part of this research. See Chapter 4 Correcting geometric distortions (georeferencing the image files) for further details.

Two postgraduate student theses (Pryor, C.M. 1992 and Caldwell, A.E. 1996) have also looked at specific aspects of the data from the 1992 multispectral flight (see Appendix three for a short discussion on the work they undertook.

Chapter 3 Instruments and methodology

This chapter describes the instruments and techniques used to conduct the data collection, and the methodologies employed in their use. A short summary of the concepts and principles underlying each technique is also presented and, where appropriate, a history of their use in an archaeological context (primarily in the UK) is discussed. Remote sensing is divided into two main types, either active or passive. Active remote sensing supplies its own source of energy or illumination (Lillesand and Kiefer, 1999, p.617) onto a surface in order to measure the return (e.g. resistivity, LiDAR). Passive remote sensing records an extant form of energy or radiation (e.g. magnetometry, multispectral imagery and aerial photography).

3.1 Aerial photography

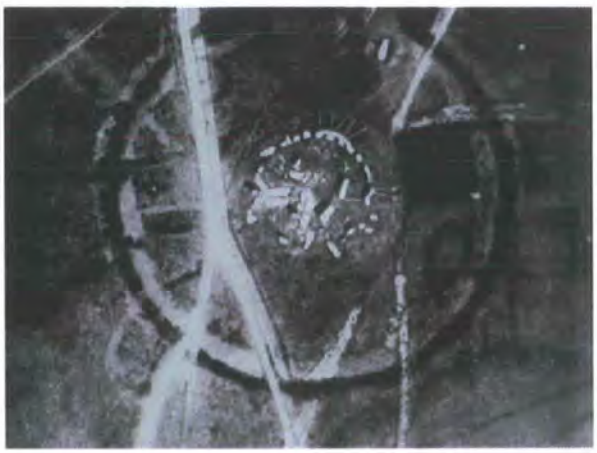

Figure 19 Stonehenge from a balloon, 1906 (Source http://www.english-heritage.org.uk/server/show/ConMediaFile.16001

Without doubt, aerial photography is the most widespread form of remote sensing used in the United Kingdom today. Aerial photography as a means of detecting archaeology has been used in Britain since 1906, where photographs of Stonehenge were taken from an army balloon by a lieutenant P. Sharpe (Wilson, 2000, p17: Bewley, 2003, pp.274).

However, the real advances came during the next two decades, after fixed-wing aircraft development continued apace during the First World War. O. G. S. Crawford, the first archaeological officer of the Ordnance Survey, quickly realised the potential of aerial photographs to discover new archaeological sites, as well as enhancing the detail of previously known areas. The publication of Wessex from the Air (Crawford and Keiler, 1928) demonstrated this potential both to archaeologists and the wider public alike. The Second World War and the years following conversely proved to be a boom time for aerial photography for two reasons: many more planes were flying and taking photographs for military purposes and land previously used for pasture was brought under cereal cultivation for this first time since antiquity. Many of the photographs taken during the war (by both British and German pilots) and immediately thereafter form the basis of most of the large aerial photographic collections in the country (for instance, the Cambridge University collection of Air Photos, or CUCAP, web address http://venus.uflm.cam.ac.uk/, currently curates the entire collection of photographs taken by J. K. St Joseph and David R. Wilson).

Until the late 1950's however, the emphasis was on collecting aerial photographs on a somewhat ad-hoc basis. However, the publication by the Royal Commission on the Historical Monuments of England (RCHME) of A Matter of Time in 1960 served to open people's eyes both to the potential of aerial photographic mapping and to the ongoing destruction of the archaeological resource by gravel extraction.

Debate among the aerial photography fraternity in the 1960's and 1970's developed from a need to document the vanishing archaeological resource to a desire to move in a more quantitative direction, initially by the mapping of landscape areas and then in the subsequent interpretation of the cropmarks (Palmer, 1989). John Hampton, head of the

Aerial Photographic Unit of the RCHAM from 1965 to 1985, documents this changing direction towards "aerial archaeology" and landscape studies (Hampton, 1989).

The National Mapping Programme (NMP) was established in 1992 (Bewley, 2003, pp.278-282), developing out of both (then) current and earlier projects, including the Yorkshire Wolds Survey (Stoertz, 1997), the Danebury Project (Palmer, 1984) and a number of pilot study areas for the Monuments Protection Programme (MPP). The MPP. was set up in 1986 to catalogue the monuments of England. Its main aim was to identify sites or monuments which would benefit from a form of statutory protection (generally scheduling). See website http://pcwww.liv.ac.uk/~Sinclair/ALGY399_Site/scheduling.html #mpp for more information on the MPP.

The NMP is an ambitious undertaking, but its success is essential if the full benefit of the returns from many decades of aerial photography are to be fully utilised. See website http://amaxus.english-heritage.org.uk/server/show/conWebDoc.4223 for more background on the NMP.

The cameras used for aerial photography varied from standard 35mm single lens reflex cameras to high resolution medium format types, such as the Wild RC10, which uses 230mm negatives. Today, digital cameras are being used more and more frequently and, as CCD technology advances, will eventually replace film cameras for this purpose. The two main forms of aerial photography are oblique and vertical, both of which can use black and white, colour or infrared film.

3.1.1 Oblique aerial photography

Many archaeological cropmarks are only visible from certain orientations, and oblique aerial photography is required to record these features. One drawback of oblique cropmark detection is that if the flight line is not at the correct angle or height, than the cropmarks could easily be virtually invisible, or at least very difficult to photograph. It is thus necessary to fly around the target in order to ascertain whether cropmarks are present, or to find the best angle from which to view them.

3.1.2 Vertical aerial photography

Vertical or near vertical photographs taken with a reasonable degree of overlap, (Wilson suggests 60%, Wilson, 2000, p.32) have the advantage of being able to be viewed with a stereoscope, which gives the impression of a 3-dimensional relief. This allows features such as earthworks to be more easily identified. By their nature, vertical photographs also make it easier to ensure that all of a given area is covered. This helps to make landscape interpretation possible, whereas a collection of oblique photographs, even if taken in the same general area over a number of years, tend to focus on known or newly visible sites, and as such can be seen as a selective (non-arbitrary) method of data collection. This is not to minimise the importance of oblique aerial photographs, because as stated above, some cropmarks are only visible from specific angles, and might not be detected using vertical photography alone.

A number of different types of marks relating to archaeological features can be identified from the air. These were originally classified by Crawford, and are discussed below.

3.1.3 Cropmark formation

It has often been stated that in order to obtain a reasonable return from aerial photography a flying campaign over many years is required. Bewley suggests that 50

years may be necessary in order to begin to understand an area (Bewley, 2003, pp.276). This is because the formation of cropmarks is dependent upon a number of different, often transient, factors, all of which vary considerably from year to year.

These factors include geology and soil type, the species of crop, the stage of growth of the crop and the amount of moisture (or rather lack of moisture) available to the root system of plants throughout their growth cycle, but particularly towards the end of this cycle. The soil type and composition play a significant part in the amount of moisture which can be retained, thus affecting the potential formation of cropmarks. Cropmarks may take weeks to develop on heavy clay soils, whereas they can form over a period of as little as three days on sandy, well drained soils (Wilson, 2000, p.69). Also, certain types of soil (i.e. soils with a greater clay component) are generally not responsive to magnetic surveying techniques.

The crop type will also play a part in the formation of cropmarks, with wheat, barley and oats being good in June and July, sugar beet good in August, and potatoes generally poor (Riley, 1944). Modern fertilizers and weed killers also have an effect on cropmark formation, as they can now be applied (using the results of prior soil sampling combined with a GPS) only to the specific parts of the field which require treatment.

One of the most significant factors in the development of cropmarks is the potential soil moisture deficit (PSMD). When transpiration exceeds rainfall, there is said to be a PSMD, although the actual soil moisture deficit is influenced by the stage of growth of a crop (where greater or lesser transpiration can occur) and the amount of bare soil between the young shoots. Because of this, measuring the actual soil moisture deficit is rarely carried out (Jones and Evans, 1975, p.3), rather the PSMD is calculated using a

formula based on the monthly rainfall data and the mean potential transpiration figures tabulated in Smith, 1967 (see Figure 22 for potential transpiration curve).

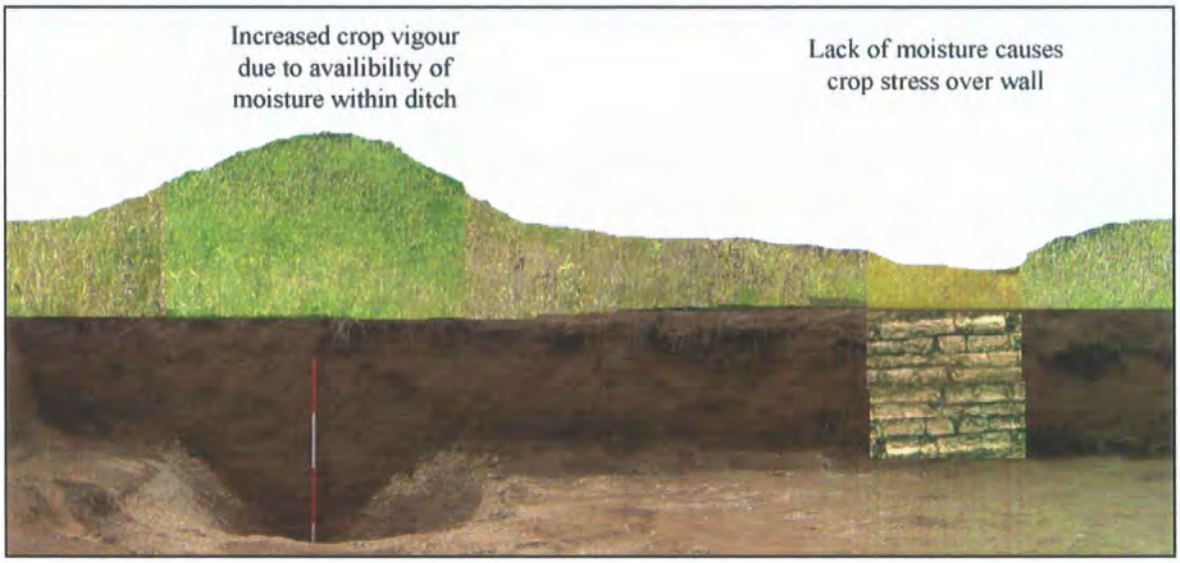

Figure 20 Stylised representation of cropmark formation

Figure 20 indicates in a stylised fashion how both positive and negative cropmarks are formed. The positive cropmark is visible because the root system has access to a more plentiful supply of moisture, which is provided by the fill of the ditch. This has the effect of making these plants slightly greener, as well as allowing a more vigorous growth. Negative cropmarks occur when the root system has less moisture available than the surrounding crop, causing a stress in the crop at this point (i.e. over a buried wall), as well as stunted growth.

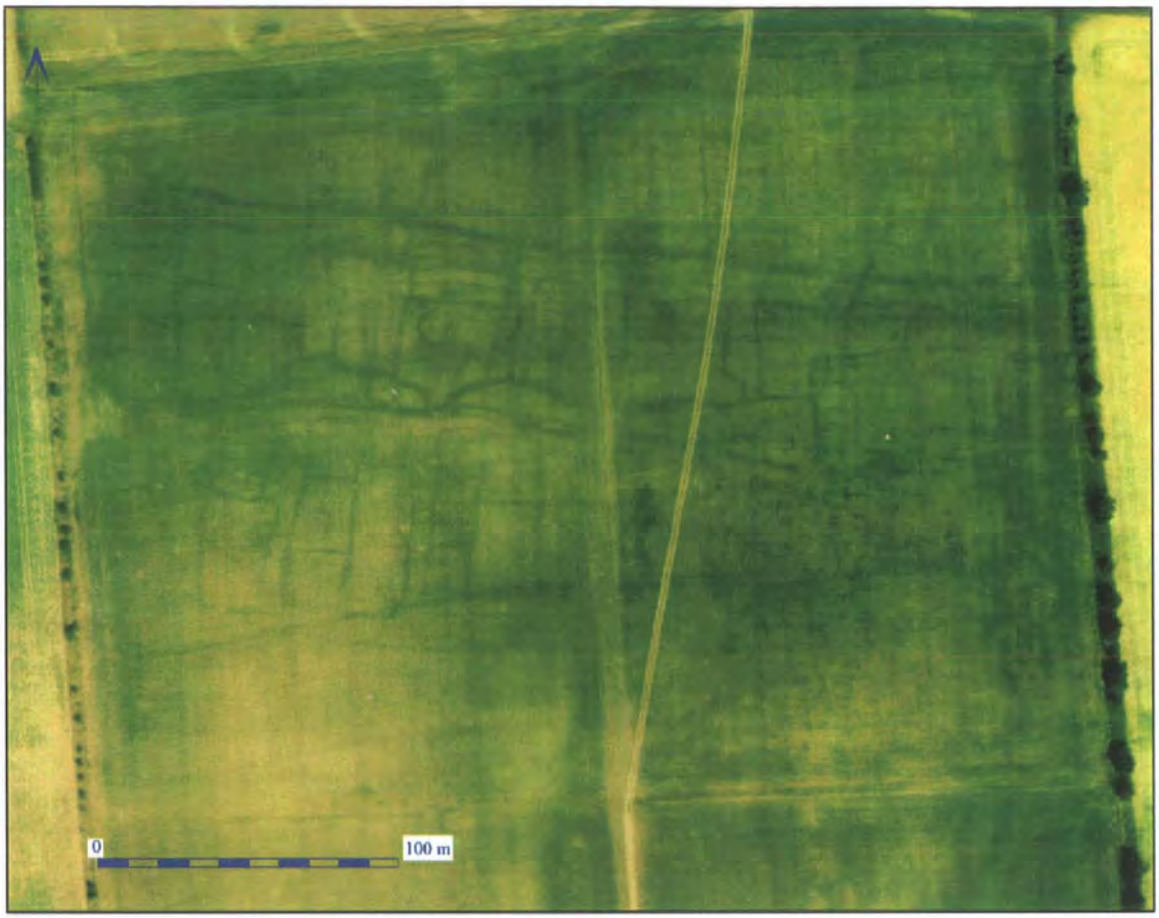

Figure 21 The northern part of Site 022, with the ladder settlement clearly visible. (source NERC 27 June 1992, vertical photograph over a turf crop).

Figure 21 demonstrates the formation of cropmarks on a turf field, something which is very unusual, and has occurred here because of the very dry conditions in the summer months of 1992. Figure 22 shows the PMSD for 1992, with rainfall as recorded at High Mowthorpe (located some 8.5 kilometres to the SSW of West Heslerton), and the PMSD for 2005, for the north-east region.

The formation of good cropmarks cannot be assumed just because one of the contributing factors is in place. For instance, even though the PSMD in May and June may indicate that cropmarks should be forming, the months during the germination and young growth of the plants also play a part. Also, the PSMD for grass (and other shallow rooted crops) is different to that which will allow cropmarks to form in cereals. However, it is certainly true that in summer drought years spectacular cropmark

formation is most widely encountered. In 1976, a great increase in the cropmark record across Northern Europe was encountered (Scollar et al, 1990, p.33), and the same was found at West Heslerton in 1992 (NERC Wild RC10 colour vertical photographs, see Figure 21), which was also a long, dry summer. Irrigation can have the effect of restricting cropmark development, particularly if only certain parts of the field are being irrigated.

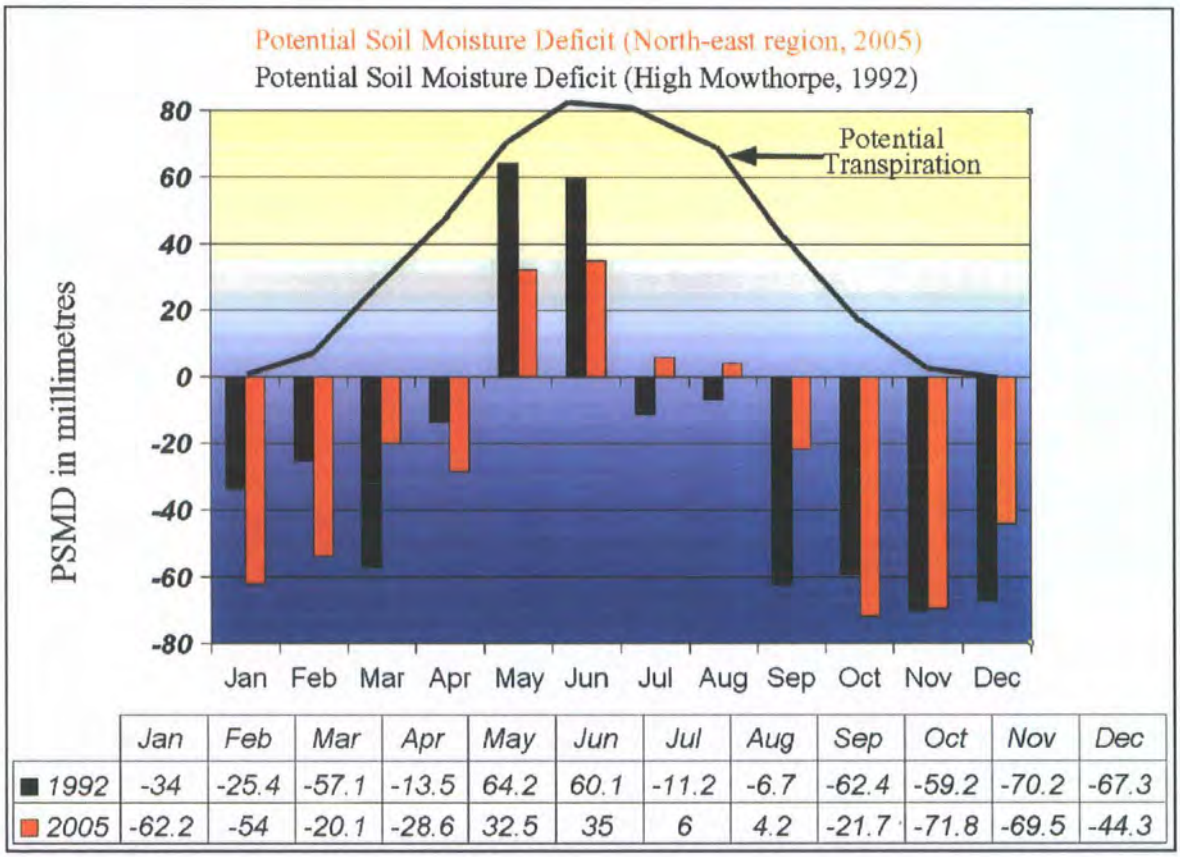

	Jan	Feb	Mar	Apr	May	Jun	Jul	Aug	Sep	Oct	Nov	Dec
1992	-34	-25.4	-57.1	-13.5	64.2	60.1	-11.2	-6.7	-62.4	-59.2	-70.2	-67.3
2005	-62.2	-54	-20.1	-28.6	32.5	35	6	4.2	-21.7	-71.8	-69.5	-44.3

Figure 22 The PSMD for 1992 (after Caldwell, 1996) and 2005 (data from the Met Office)

Jones and Evans have observed that cropmarks form when the PSMD is between 30-90mm, and that a successful flying campaign generally requires a PSMD of over 50mm (Jones and Evans, 1975, p.1). Figure 22 shows that this threshold was reached in 1992, but that in 2005, the PSMD was only just over the 30mm mark, and this is reflected in the generally lower returns from the 2005 flying campaign (although see Figure 107 for an exception).

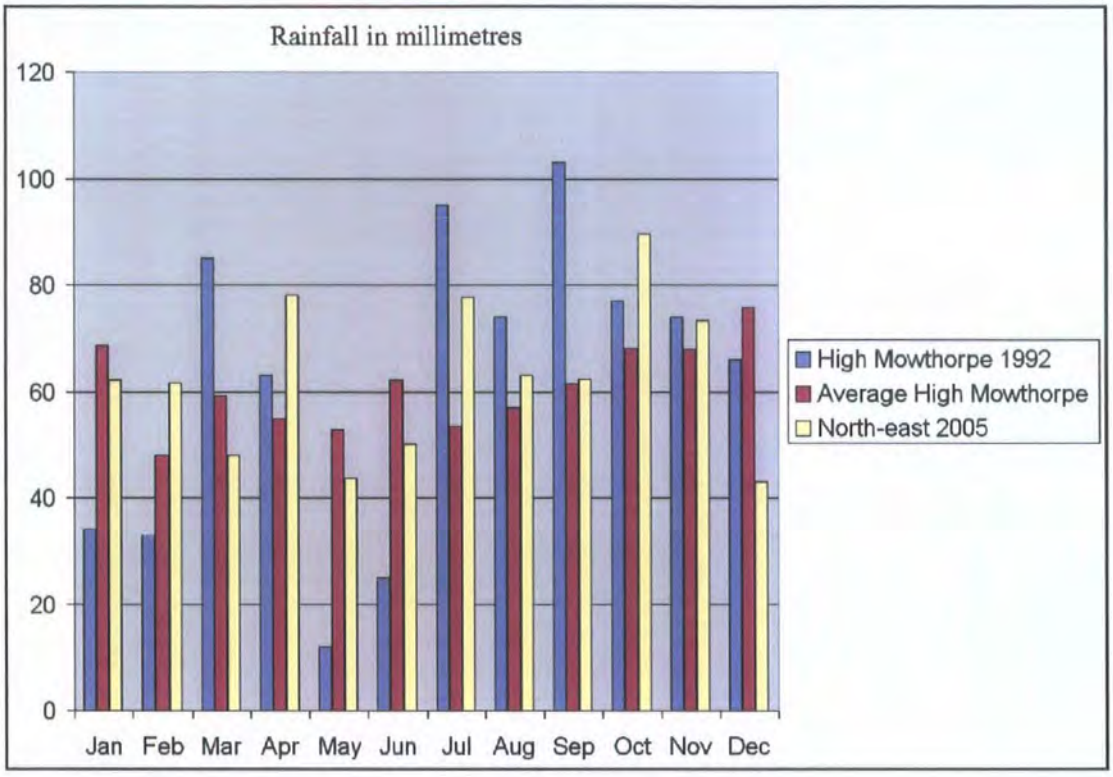

Figure 23 Rainfall per month in mm for 1992 and 2005 compared with the average rainfall from 1971 to 2001

Figure 23 shows that the rainfall pattern in 1992 was unusual, with two wetter than average months in March and April, followed by two very dry months in May and June. This combination of rainfall was ideal for the formation of cropmarks. Compare this to the rainfall in 2005, which is generally near the average, although still slightly down in May and June.

Average rainfall by month for the north-east region was taken from the Meteorological Office website at http://www.metoffice.gov.uk/climate/uk/2005/index.html

The average rainfall for the station at High Mowthorpe over the period 1971 to 2000 was taken from the website http://www.metoffice.gov.uk/climate/uk/averages/19712000/sites/high_mowthorpe_.html

Soilmarks

Soilmarks reflect plough damaged features and are visible after ploughing and harrowing, and generally remain visible until the crop begins to grow. They can be formed in two ways. If a site containing earthworks is to be ploughed for the first time, the site is generally levelled prior to ploughing. This has the effect of removing the tops of the earthworks, and depositing this material in any remaining hollows or ditches. These features will then show as soil marks when ploughed, particularly on light coloured soils (Wilson, 2000, p.53).

They can be also seen when the plough is cutting down to contrasting subsoil, and where the archaeological or geological features cut into the bedrock are filled with remaining ploughsoil, they stand out as darker anomalies.

Figure 24 Soilmarks in the middle distance visible from ground level

This is demonstrated in Figure 24, where the darker linear features can be seen in the background extending down from the Wolds towards a dry valley. These features could be the remains of early linear boundaries, but it is more likely that they are natural in origin. The photograph was taken at ground level, looking south-west.

Shadow marks

Figure 25 Shadow marks above (source English Heritage Aerial Survey team) with gradiometer survey by the LRC below

Shadow marks are formed when low angle sunlight shines across standing earthworks, forming shadows. Very subtle features can be detected this way, with the best time of year being winter, because of the low angle of the sun during this season. This serves to enhance the view of the earthworks, often allowing previously unknown features to be detected. Some difficulties can arise when a number of

trees are present, as they cast long shadows across the area of interest. An example of earthworks causing shadow marks can be seen in Figure 25, source English Heritage Aerial Survey team), where the deserted part of the Medieval village of East Heslerton can be seen, located to the south of the modern village. As a comparison, the returns from a fluxgate gradiometer survey over the same area are also shown.

Snow marks

A variation on this theme is also found during winter, when light snowfall begins to thaw, leaving snow in the shadows (lee) of the earthworks (see Figure 26). Other snow marks can be found when snow fills depressions, which are wetter, causing freeze and thaw effects. The remains of Medieval villages and rig and furrow ploughing are often best seen from the air when snow marks have formed.

Figure 26 Snow marks from ground level showing West Heslerton DMV looking north-east.

3.2 Geophysical surveys

Two main forms of geophysical survey have been used in the sample areas, with over 960 hectares of fluxgate gradiometery (a form of magnetometry) forming the major component.

One definition of something which differs from the norm is an anomaly. Conventionally, this is the term used both in remote sensing and geophysical surveying to describe an entity perceived as being significantly different to the background average. The anomalies may relate to archaeological features, or to a features of a natural or geological origin. Anomalies are also caused by modern human activity.

3.2.1 Magnetometry

Magnetometry is a passive form of geophysical survey, and was tested in the United Kingdom for the first time in an archaeological context in 1958, when a proton magnetometer designed and constructed by Martin Aitken and Edward Hall at the research Laboratory for Archaeology and the History of Art at Oxford University successfully detected, among other features, a kiln at a site at Water Newton (Aitken, 1958). For a detailed discussion on how magnetic surveying operates and the development of fluxgate gradiometers see Appendix one.

Fluxgate gradiometer types

Two different commercially available fluxgate gradiometers were used for the collection of the magnetic data in the project areas. These are the *Geoscan Research* fluxgate gradiometer (model number FM36), and the Bartington dual sensor Grad 601-2 fluxgate gradiometer.

Geoscan Research FM36 fluxgate gradiometer

The instrument is a light, rigid aluminium tube 50 centimetres long, with a fluxgate sensor mounted at either end. A data logger, the power supply and the controls are also mounted on the carrying handle to make the instrument fully portable. In use, the two sensors are aligned, balanced, and zeroed manually (see Data collection for further details), and the instrument is then carried vertically alongside the operator's body. The measurements taken are stored in the data logger, periodically transferred to a portable computer in the field. With the FM36, this needed to be done every four 30m grids, and took 20 minutes to download.

Figure 27 James Lyall and Kay McManus with two FM36 gradiometers, carrying out a survey near Bosworth battlefield.

Bartington Grad 601-2 fluxgate gradiometer

The Bartington Grad 601-2 is a lightweight construction, with a crossbar containing the memory, controls and power supply, supporting 2 one metre long tubes, with each tube containing a fluxgate at either end. This dual sensor mode has the advantage of cutting surveying time almost in half, compared to the use of a single sensor. In use, the Grad 601-2 is carried to a zero reference point and then zeroed, this being an automatic rather

than a manual process as with the FM36. See choice of instrument in Appendix one which looks at the current reasons for using a fluxgate gradiometer rather than choosing a caesium instrument.

Figure 28 James Lyall with the Bartington Grad 601-2 fluxgate gradiometer. The northern slopes of the Upper Cretaceous Yorkshire Wolds can be seen the background.

Data collection

Each field was treated as a separate entity (or site), and divided into a number of whole or partial 30 metre square grids. A base line along one of the field boundaries was established, and then the grids were generally set out using ranging rods and an optical square, although when required either a total station or kinematic Global Positioning System (GPS) was used. See Appendix one for details on how to carry out a successful magnetometer survey.

Figure 29 The GPS collected points at the corner of each 30 metre geophysics grid

Where possible, all surveys carried out from September 2004 have also had the corner of each 30m square logged by a kinematic GPS, to allow variations in slope across the surveyed area to be accounted for (see Figure 29). The missing points in the fields are because the pegs or pin flags used to mark the corners of the grids had been moved by animals (or humans) prior to logging the GPS points. Logging the exact location of each corner is more vital when the work is conducted on a slope, as normal geophysical survey assumes a flat plane. These accurate 3-dimensional coordinates allow the results of the survey to be warped onto a digital elevation model.

Traverse method

Two methods of collecting the data are possible. The parallel (also unidirectional or normal) traverse method requires that the instrument is maintained in the same orientation, and that each line is walked in the same direction (i.e. south to north). This requires the operator to walk the first 30 metre line, then return to the beginning of the next line, before beginning the second traverse. The zigzag (also bi-directional) traverse method has the operator returning down the second traverse north to south. If using the FM36 the machine is turned so it is facing in the same direction as in the first traverse. The Bartington Grad 602-1 does not require to be turned round in this way. The choice of traverse method depends to a large extent upon the experience of the surveyor. With experienced surveyors, no appreciable difference will be noted between the two traverse methods.

Spatial resolution and machine sensitivity

The surveys were conducted by taking readings every 25cm along the north-south axis and every metre along the east-west axis (thus 3600 readings for each 30m by 30m grid). The sensitivity of both the FM36 and the Grad 601-2 were set to detect magnetic variation in the order of 0.1 nT.

3.3 Surface or near-surface thermal data collection

3.3.1 Thermal properties

The thermal properties of materials are the factors which influence how heat derived from the sun is distributed both through time and through depth, and these vary due to differences in mineral composition, moisture content, grain or particle size and the physical properties of the material (Price, 1977).

As shown in Figure 31, the AZ-16 ATM collects thermal data between the 8.5μm and 13μm part of the electro magnetic spectrum (henceforth EMS). The thermal properties of a material can be defined in a number of different ways. Thermal conductivity measures the rate at which heat passes through a material. Thermal capacity determines how well a material stores heat. Thermal diffusivity is a chronological measure of temperature change in a material. Thermal inertia can be defined as the measure of the response of a material to temperature change (Lillesand and Kiefer, 2000, p.336) or the resistance of a material to a change in temperature (Price 1989). It is thermal inertia which is of most significance for the purposes of detecting differences in the returns from day and night flights over the same area. Physical thermal inertia cannot be measured from remote sensing techniques alone, as this would require actual ground-based data collection. However, apparent thermal inertia can be measured by subtracting the thermal returns from a midday flight from those acquired during an early morning (pre-dawn) flight.

Thermal inertia can be informative in identifying archaeological features, as demonstrated by McManus (2003, p.204-206), where she uses an arithmetic subtraction routine to enhance the differences between the two datasets.

3.3.2 Temperature data loggers

The TEMPCON® HOBO-H8 thermal data loggers are small self-contained waterproof instruments which can record temperature at four different depths, both above and under the ground surface. The instrument is buried at a depth of around 30-60cm, and the temperature sensors are placed at depths from 60cm to above ground level. In this way, differences in ground and subsurface temperature can be logged over a period of time, which depends on the rate at which the readings are logged. Three data loggers were buried on the 13/06/2005.

No	Rate	Date	Time	S1	S2	S3	S4
H3	5 min	13/06/2005	12:00:00	Under surface (under water)	On the surface (under water)	On the surface (under water)	In the air above water
H4	5 min	13/06/2005	12:30:00	60cm	30cm	10cm	In the air
H5	10 Min	13/06/2005	12:35:00	30cm	60cm	10cm (in trackway deposit	In the air

Table 2 The location of the thermal data sensors

Table 2 indicates the location of each of the three sensors relative to the others, so that direct comparisons between the different loggers can be made. Note that Hobo 5 was set to take readings every 10 minutes, while the other two were set to take a reading every 5 minutes. This was done in order to see whether the closer chronological spacing would provide any significant benefit over the 10 minute spacing. A set of data was acquired from the 08/06/2004 to the 15/09/2004, all at 10 minute collection times, and this provides a comparable dataset to test the 5 minute data. Unfortunately, when recovering the loggers, the Hobo which had been placed in a pool of water had been removed by persons unknown, thus the data from this source is not available.

The loggers are initiated in the field by using a portable computer, and are downloaded in the same way. It is important to launch all of the loggers at the same session, so that

they are all stamped with the date and time from the portable computer. This allows the data from all of the loggers to be compared with each other. The data can be downloaded in either Fahrenheit or Centigrade.

3.4 Multispectral data

Multispectral data is collected from a number of different wavelengths along the electromagnetic spectrum (EMS), ranging from the visible to the thermal infrared bandwidths. As can be seen in Figure 30, visible light, or what the human eye can see, is only a very small part of the EMS. Multispectral data increases this range into the near and short wave infrared (SWIR) and the thermal parts of the EMS.

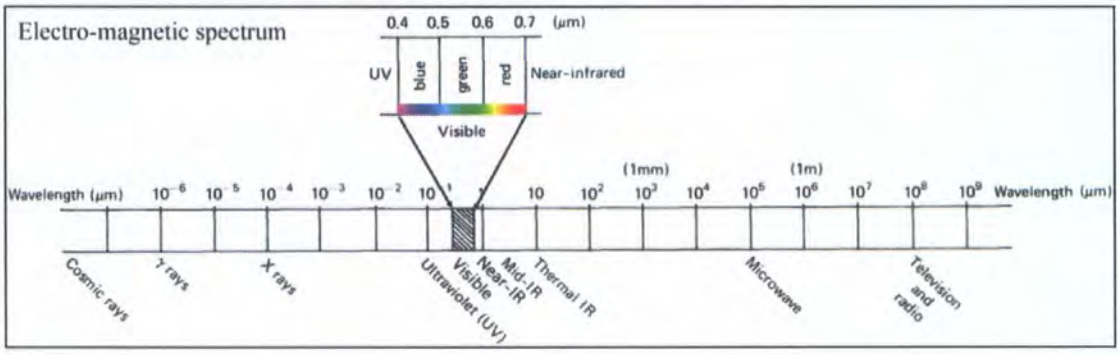

Figure 30 The electromagnetic spectrum (after Lillesand and Kiefer, 1999 p.5)

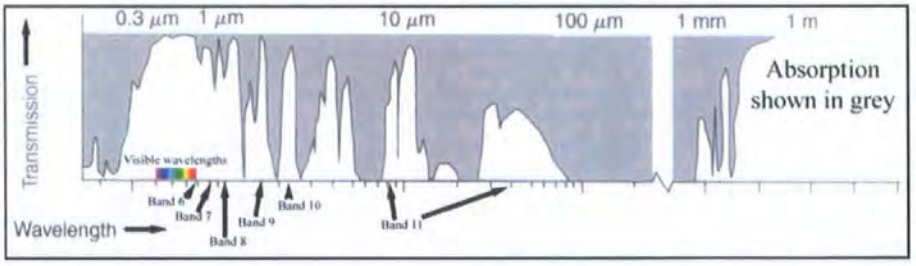

Figure 31 Showing atmospheric transmittance in white and absorption in grey (taken from Lillesand and Kiefer, 1999, p11)

As Figure 31 clearly demonstrates, at certain wavelengths atmospheric absorption is almost total, and data from these wavelengths are not collected. There are thus a specific set of wavelengths where it is possible to record good data, and it is in these wavelengths that multispectral scanners are active.

3.4.1 Daedalus 1268 Airborne Thematic Mapper 1992 multispectral flight

The Daedalus 1268 Airborne Thematic Mapper (ATM) collects radiation from the Earth's surface in 11 different bandwidths, in the visible, near infrared and thermal

bands of the EMS (see Table 3). The scanner is a passive remote sensing device, and is designed for use on an airborne platform. It operates by using a rotating scan mirror to capture the radiated light, with both visible and near infrared being split and then imaged onto a number of silicon detectors. The middle infrared and thermal radiation is dealt with slightly differently, as they are split and then recorded onto three single detector elements, which are enclosed within liquid nitrogen cooled containers.

Bands one to five collect data in the visible part of the spectrum, with bands six to eight in the near infrared, bands nine and ten in the short-wave infrared, and bands eleven and twelve in the same mid infra-red or thermal wavelength, but with channel 12 collected using half the gain setting, thus utilising a different radiometric sensitivity to help alleviate any potential over-exposure problems.

The scan mirror can be set to three different synchronised speeds (12.5, 25 and 50 Hz), so that data collection at different altitudes can be linked to ground coverage. In order to avoid any gaps in the area coverage along the flight lines, around a 10% overlap between alternate scanlines is employed. The ground resolution of multispectral data is both altitude and airspeed dependent.

Band	Lower wavelength in µm	Upper wavelength in µm	Spectral component
One	0.42	0.45	Blue
Two	0.45	0.52	Blue-green
Three	0.52	0.605	Green
Four	0.605	0.625	Red
Five	0.63	0.69	Red
Six	0.695	0.75	Near Infra-red
Seven	0.76	0.9	Near Infra-red
Eight	0.91	1.05	Near Infra-red
Nine	1.55	1.75	Short wave Infra-red
Ten	2.08	2.35	Short wave Infra-red
Eleven	8.5	13	Mid Infra-red or thermal
Twelve	8.5	13	Half the gain setting of 11

Table 3 indicating the upper and lower wavelengths of the EMS collected by the Daedalus 1268, in µm

The data were originally supplied on a reel of magnetic tape, and were initially read off the tape using specialist equipment in the Durham Geography department. It was then "byte-swapped" into a standard Band Interleaved (BIL) format which could be imported into any of the main image processing packages.

3.4.2 Enhanced AZ-16 ATM 2005 multispectral flight

Since the 1992 flight, a number of enhancements have been made to the NERC multispectral equipment. The Daedalus (now ArgonST) 1268 ATM has now been upgraded to an AZ-16 ATM, which offers a number of refinements when compared with the older machine.

Specification	Daedalus 1268 (ATM)	AZ-16 (ATM)
A/D resolution	8 bits	16 bits
Range of DN levels	0 - 255	0 - 65535
Gain-settings	0.5, 1, 2, 4, 8	None required
Total digitised FOV	85.92	90
Actual FOV	72.86 with S-bend correction	90.0 (S-bend correction in post-processing)
Roll correction (in-flight)	15 from single axis mechanical gyro	None (3-axes correction in post-processing)
Number of pixels/scan-line	716	938
Mirror scan	12.5 / 25 / 50	12.5 / 25 / 50
Black Bodies	1 digitised pixel/black body	16 digitised pixels/blackbody
Data recording	1" HDDT tape drive	9 Gbyte removable HD
Data visualisation	Oscilloscope of digitised signal	Waterfall image of selected band(s) on colour monitor

Table 4 Listing the enhancements of the AZ-16 over the Daedalus 1268 (Data downloaded from NERC website_http://arsf.nerc.ac.uk/instruments/atm.asp)

One of the most significant enhancements for archaeological feature detection is the move from 8 to 16 bit data, where the subsequent increase in sensitivity has the advantage of allowing a much greater range of detail to be extracted from the data. The thermal data collection is much improved by the use of two onboard blackbodies, which are imaged during each scan. The temperatures and responses of the blackbodies are

recorded, in order to facilitate the radiometric corrections required in the post-processing phase.

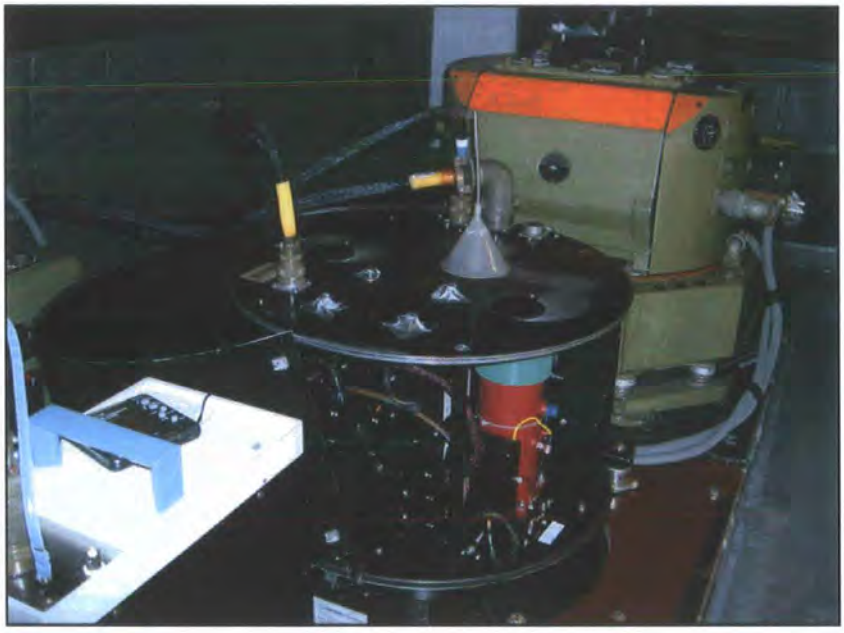

Figure 32 The internal workings of the AZ-16, with the CASI instrument in the foreground and the Wild RC10 in the background.

Another improvement is the use of the Integrated Data System (IDS), which collects navigation and attitude information (obtained by onboard instruments and global positioning system technology on the wings and at the front and rear of the plane during the flight). This technology, combined with a GPS system collecting data on the ground, mean that many of the problems with geometric correction of the data using the former instrument are now dealt with "on the fly", or at least in the immediate post-flight processing phase.

3.4.3 Compact Airborne Spectrographic Imager (CASI) data

The system used is a CASI-2, made by Itres Research of Canada, and uses a two dimensional CCD array imaging spectrograph. It utilises a pushbroom scanning mode, with the full swath width (54.4 degrees field of view) imaged simultaneously over a large number of spectral bands (up to as many as 288 in hyperspectral mode), between the visible and near infra-red areas of the EMS (between 405 and 950nm). The resolution of the data varies depending on both altitude and the number of bands being

collected. For the 2005 data flight, 48 bands were collected at a height of 800 metres, giving a nominal resolution of around 1.5 metres per pixel. This is the same nominal ground resolution as that collected by both the 1992 Daedalus 1268 flight and the 2005 AZ-16 flight, so all three of the multi spectral datasets could be directly compared.

Parameter	Description
IFOV (Instantaneous Field Of View) Across Track	54.4 degrees (custom lens)
IFOV (Instantaneous Field Of View) Along Track	0.1151 degrees
Aperture	f/2.8 - f/11 (Automated iris control)
Spectral range	405 - 950 nm
Spatial samples	512 spatial pixel
Spectral samples	288 at 1.8nm intervals (2.2nm FWHM @ 650nm)
Dynamic range	12-bits (4096 levels)
Recording	1 removable 9 GByte Hard Disk

Table 5 CASI-2 characteristics. From PDF file available for download on website http://arsf.nerc.ac.uk/instruments/casi.asp

Operating Mode	Description
Spatial Mode	512 pixels across swath, up to 18 spectral bands (fully programmable)
Spectral Mode	Full spectrum (288 channels) for up to 39 look directions spread across swath (4, 8, 12, or 16 pixel spacing between look directions). Includes a monochromatic image at full spatial resolution (Scene Recovery Channel).
Enhanced Spectral Mode	Full spectrum (288 channels) in a block of 101 adjacent spatial pixels.
Full Frame	512 pixels across swath x 288 spectral pixels (~1-2 sec. Integration time limits use to laboratory calibration or ground-based field use)

Table 6 CASI-2 operating modes. From PDF file available for download on website http://arsf.nerc.ac.uk/instruments/casi.asp

The data on CASI is derived from the NERC website http://arsf.nerc.ac.uk/instruments/casi.asp

Band	Centre	Lower wavelength in µm	Upper wavelength in µm	Band	Centre	Lower wavelength in µm	Upper wavelength in µm
1	0.407743	0.404873975	0.410612025	25	0.679191	0.676253745	0.682128255
2	0.418883	0.41601037	0.42175563	26	0.690655	0.687715735	0.693594265
3	0.43004	0.42716383	0.43291617	27	0.702128	0.699186795	0.705069205
4	0.441214	0.438334355	0.444093645	28	0.71361	0.710666905	0.716553095
5	0.452405	0.449521955	0.455288045	29	0.725101	0.722156085	0.728045915
6	0.463611	0.46072461	0.46649739	30	0.736601	0.73365435	0.73954765
7	0.474834	0.47194433	0.47772367	31	0.748109	0.745160655	0.751057345
8	0.486072	0.483179125	0.488964875	32	0.759625	0.75667505	0.76257495
9	0.497325	0.494428985	0.500221015	33	0.771149	0.768197495	0.774100505
10	0.508593	0.5056939	0.5114921	34	0.782679	0.779726	0.785632
11	0.519876	0.516973905	0.522778095	35	0.794217	0.791262595	0.797171405
12	0.531173	0.52826796	0.53407804	36	0.805762	0.802806255	0.808717745
13	0.542484	0.53957609	0.54539191	37	0.817312	0.81435497	0.82026903
14	0.553809	0.55089828	0.55671972	38	0.828869	0.825910735	0.831827265
15	0.565147	0.562233535	0.568060465	39	0.840431	0.83747159	0.84339041
16	0.576498	0.57358185	0.57941415	40	0.851999	0.84903851	0.85495949
17	0.587862	0.58494324	0.59078076	41	0.863572	0.8606105	0.8665335
18	0.599238	0.59631671	0.60215929	42	0.87515	0.87218754	0.87811246
19	0.610627	0.60770322	0.61355078	43	0.886732	0.883768655	0.889695345
20	0.622026	0.61909981	0.62495219	44	0.898318	0.89535383	0.90128217
21	0.633438	0.63050946	0.63636654	45	0.909907	0.90694207	0.91287193
22	0.64486	0.641929185	0.647790815	46	0.921501	0.91853538	0.92446662
23	0.656293	0.653359975	0.659226025	47	0.933097	0.93013077	0.93606323
24	0.667737	0.66480182	0.67067218	48	0.944696	0.941729205	0.947662795

Table 7 indicating the upper and lower wavelengths of the 48 bands collected by the CASI, in µm
For a comparison of the comparative wavelengths of the CASI and ATM machines, see Appendix seven)

Even though the use of multispectral data for defining archaeological features was pioneered in Britain as far back as 1985 (see Donoghue and Shennan 1988a and 1988b), the uptake of this method as a means of archaeological prospection has been limited. A paper on the 1992 multispectral dataset for the Heslerton project area looked at how the data could fill in "gaps" left by other forms of remote sensing (Powlesland, Lyall and Donoghue, 1997). Kay McManus (McManus, 2003, p.126-132) had some success at using multispectral data as a prospection tool, defining archaeological features at one (Bosworth Battlefield) of her target areas. McManus also used thermal inertia to define quite subtle differences in the returns at Bosworth. More recently, a team in Scotland

(Winterbottom and Dawson, 2005), have used ATM data acquired by NERC in 2002 to identify a number of different archaeological remains on the islands of Coll and Tiree off the west coast of Scotland. Apart from these few examples, Donoghue's hope that "this research will alert archaeologists to the potential of using multispectral imagery" (Donoghue and Shennan 1988b) has remained largely unfulfilled.

3.4.4 High resolution near vertical photography

At the same time as the multispectral data is acquired, NERC also collect high resolution colour photographs. Prior to 2004, these were taken by the Wild (now Leica) RC10. The RC10 provides very high resolution photographs, with a negative format of 230 by 230mm. If full georeferencing of these images is required, it is preferable to scan in the original negatives at a high resolution, which is best carried out by a specialist company (i.e. BKS. website http://www.bks.co.uk/ or Bluesky, website http://www.bluesky-world.com/aerialphotography.html). However, all prior images acquired by NERC are currently in the process of being scanned in by NERC Earth Observation Data Centre (NEODC). The website address is http://www.neodc.rl.ac.uk/, and you can register here to use the scanned images, which, after you have been given permission, allows you to download the images from the website data browser.

After 2004, the choice of using the Rollei medium format digital camera was offered, which had the advantage of providing images which could be directly georeferenced. The CCD resolution (see Table 8) of the camera is around 16.64 megapixels. In practice, the actual spatial resolution of the images depends on the altitude of the aircraft during the acquisition phase, in our case up to 800 metres, which gives a nominal resolution of around 14cm per pixel.

Capture rate	2s
CCD size	36.9mm x 36.9mm
CCD resolution	4080 x 4080
Bits per colour	16 bit
Output image size	96MB
Image capacity	1000 images
Field of view	40.5 degrees

Table 8 The characteristics of the Rollei digital camera (from NERC website http://arsf.nerc.ac.uk/instruments/rollei.asp)

Data on the RC10 can be obtained from the NERC website at http://arsf.nerc.ac.uk/instruments/rc-10.asp and on the Rollei at http://arsf.nerc.ac.uk/instruments/rollei.asp.

3.5 LiDAR data

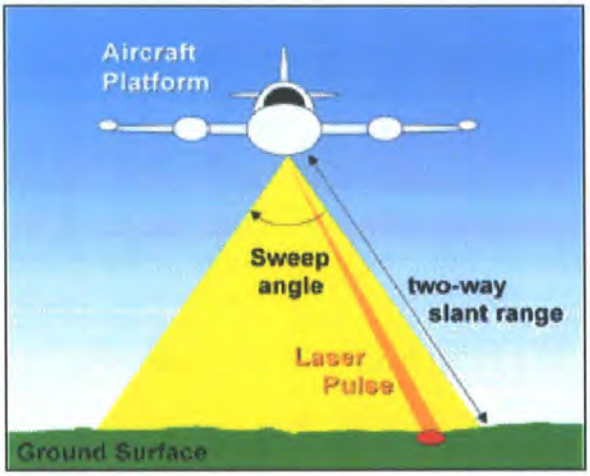

Light Detection and Ranging, or LiDAR, is an active method of obtaining an accurate, large scale elevation coverage over a specific area of interest. It works by using a coherent laser beam which is directed in pulses towards the ground.

Figure 33 LiDAR operation (taken from the Environment Agency) website address http://www.environment-agency.gov.uk/science/monitoring/131047/?version=1&lang=_e)

The return time for each pulse is recorded and used to calculate the distance between the sensor and the surface (Lillesand and Kiefer, 1999, p.700).

LiDAR data allows the creation of high resolution digital surface models or digital elevation models. These are created by using the first pulse data to detect the tree canopy and other terrain features, and the last pulse data to detect the ground surface elevation. There are three factors which could influence the accuracy of the returns;

very bright sunlight on a highly reflective surface could provide an invalid reading, and dust or vapour particles in the atmosphere can scatter the signal returning from the target (data from http://www.optech.ca/aboutlaser.htm). It is also possible to get errors in readings where multiple reflected bounces occur. The ground resolution of the data depends on the height of the aircraft acquiring the data, and the frequency of the pulse and the number of passes made over the area.

The LiDAR data for the project area were collected on the 11th and 19th of April, 2005, by the Unit for Landscape Modelling (ULM), part of the Environment Agency based in Cambridge. The data was collected using an Optech ALTM3033 (Airborne Laser Thematic Mapper). The device collects 33,000 laser observations per second. From an altitude of 1000 metres the height data is accurate to +-15 cms. (data from http://arsf.nerc.ac.uk/instruments/altm.asp). Nominally the machine can collect data both across track and along track at a resolution of about 1 metre. The actual resolution of the data depends to an extent on the slope of the surface being measured and the position of the laser at the time of collection. The resolution of our data ranges from around 1 metre to 2.5 metres.

It is also possible to collect the intensity (or amplitude) readings from each light pulse. This intensity value can be affected by a number of different variables, and damp or moist soil conditions are known to cause reduced reflectivity (Challis 2005, p.47)

LiDAR is a relatively new technique applied to archaeological feature detection, although a number of trial projects have demonstrated its potential. These include the Stonehenge Environs Project (Barnes 2003; Bewley, 2003) and detecting archaeological features in three riverine environments (Challis 2006). Recent work by the English

Heritage aerial photographic team have looked at the Witham valley in Lincolnshire (Crutchley, 2006) and again the area around Stonehenge (Bewley et al, 2005).

Chapter 4 Data Processing

4.1 Image manipulation

As the raw data used in this research is virtually all imagery of one type or another, the data processing discussed here refers almost exclusively to image manipulation, which can be defined as a number of processes, each of which is dependent on the successful completion of the earlier stages (see Figure 34).

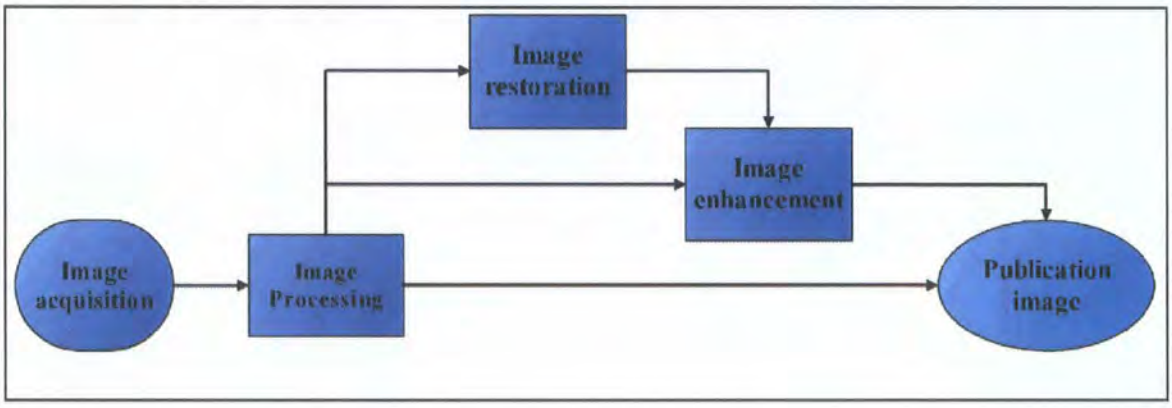

Figure 34 Flowchart of image manipulation stages

4.1.1 Image acquisition

In all forms of geophysical and remote sensing data collection, including those where data is directly acquired onto a subsequently visible source (such as the imprinting of the image onto a photographic or infra-red film or plate), the method of acquisition of the raw data is of the utmost importance. Faulty data collection can be very difficult, if not impossible to correct at a later date. To this end, it is vital that in the data collection phase of the project, every effort is made to ensure that the initial data is of the highest quality.

4.1.2 Image processing

No matter how the data are collected, the raw data from every form of remote sensing will still need some form of processing in order to be visualised in a way that the human eye can understand, (at the base level, the numbers collected by the various devices

must be converted into some form of either colour or greyscale image). This is demonstrated by Figure 35, which shows a sequence of numbers converted into a greyscale image; here the original data are constrained by values of +- 256, with negative numbers represented by darker greys and positive numbers by the lighter shades. The numbers relate only to the top-right hand corner of the image (indicated by the black rectangle), as they were originally acquired from magnetic data collected at a 4:1 ratio on the ground. The greyscale image is of a single 30 metre square of fluxgate gradiometer data, containing 3600 readings.

-40	-36	-53	-18	-11	-14	-24	0	3	-22	-55	-44	-48
-37	-34	-46	-11	-9	-4	-7	17	35	-2	-37	-37	-43
-23	-22	-29	0	0	19	19	35	71	30	-7	-29	-39
-6	0	-4	27	35	60	54	57	98	68	37	-21	-36
-2	23	24	52	64	85	55	60	63	70	59	-10	-39
14	43	53	73	84	90	44	44	33	55	65	1	-44
36	81	97	96	98	99	36	26	8	41	70	24	-26
41	106	96	106	100	84	20	17	-2	19	43	47	5
33	104	78	110	86	45	-2	0	-16	-8	19	64	34
34	108	68	80	36	9	-25	-19	-36	-24	8	94	77
43	106	48	49	2	-1	-31	-22	-33	-3	36	110	115
48	96	27	31	-12	-5	-36	-25	-28	26	67	110	127
52	78	-3	14	-21	-24	-53	-36	-24	68	98	92	105
68	59	-20	-6	-31	-36	-57	-40	-13	106	102	59	75
83	40	-27	-17	-38	-30	-50	-40	11	122	84	34	59

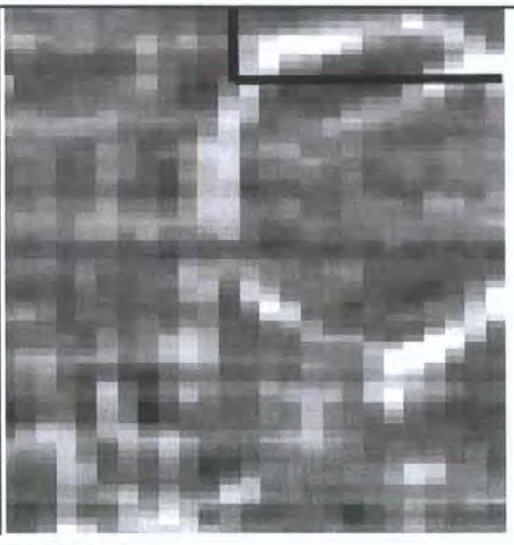

Figure 35 Numbers converted to greyscale

Image processing should not interfere with the raw data in any significant way, it is merely a stage to bring the data into a format that can be visualised. It is possible, though unlikely, that this processed data will be suitable for distribution without any further manipulation, although this is rarely the case.

Different types of manipulation can be applied to the processed images, in order to help bring out the particular parts of the image which are required to highlight an area or to demonstrate a specific point. This must be done in such a way that spurious or false values are not interpreted as valid data, or used to confirm or disprove hypotheses. To

this end, the raw data should always be archived and maintained, so that comparisons and checks with the processed data can be carried out, either by the researcher or by other interested parties (see Chapter 5 for an example why this is important). A number of different types of image manipulation can be carried out, depending on the quality of the initial data and the end result required.

4.1.3 Image enhancement

Image enhancement can be defined as a technique "to process an image so that the result is more suitable than the original image for a specific application" (Gonzalez and Woods, 1993, p.161). Enhancements can be applied in two main areas, the spatial domain and the frequency domain.

Spatial domain image enhancements

These enhancements primarily rely on changing or manipulating the pixel values which make up the image. The most common forms are discussed below.

Linear stretching

Linear stretching involves placing the actual pixel values into the full potential of the visual display device. For an 8-bit image the values would normally range from 0-255. The lowest value would be placed at 0, and the highest value at 255, with all of the intervening values stretched between, changing their values but maintaining their original relative distribution (Gonzalez and Woods, 1993, p.173-180; McManus, 2003, p.139).

Gaussian stretching is a form of linear stretch which performs an intensity transformation on the original data so that the histogram for the output data has a normal Gaussian distribution curve. It also allows for various parameters to be set, so that upper and lower limits for both the input and output images can be specified

(definition derived from Imagine 8.7 help files). It can use multi-pixel procession, that is it uses the pixels around itself to derive new values for the pixel, which can create a smoother look to the image.

Gamma corrections can be applied to images which have been produced by different hardware display drivers. If, for instance, a gamma value of 3 was applied to the input image (by a scanner, graphics card or other device driver), then a gamma correction of one third would be required to return the pixels to their original values.

Simple contrast stretching can be applied where the dynamic range of an image needs to be increased. The inverse of this function is dynamic range compression, where the range of values is too great to be displayed in a given device.

Histogram equalization

Histogram equalization applies a non-linear stretch which assigns pixel values so that each bin has roughly the same number of values. If we were using 255 bins, then the original values would be divided into 255 roughly equal ranges of values, and these values would then be used as a lookup table (LUT). This has the effect of increasing contrast at the peaks of the histogram (or where the data is densely populated), and reducing contrast at the tails (McManus, 2003, p.139).

Image restoration

Although similar to image enhancement in some of the techniques applied, image restoration can be defined as "a process that attempts to recover an image that has been degraded by using some a priori knowledge of the degradation phenomenon" (Gonzalez and Woods, 1993, p.253). For our purposes, this type of problem occurs in the night collected thermal data, which is prone to striping caused by across track illumination

effects (see Thermal data image restoration and geometric correction). A more usual example is the restoration of old and scratched photographs, where various algorithms have been devised to eliminate and "restore" damaged pixels with interpolated values.

4.1.4 Processing and georeferencing the gradiometer data

All fluxgate gradiometery data collected by the LRC has been processed and presented using the program G-Sys, a GIS which also deals with the processing of geophysical data.

After the data has been collected in the field, it is downloaded onto a computer, and a separate file is created for each 30 metre square grid. The number, operator, site number and local site origin (x and y) of each grid is entered into the file as the grids are downloaded. When completed, this allows the data to be viewed as a single image (see Figure 36).

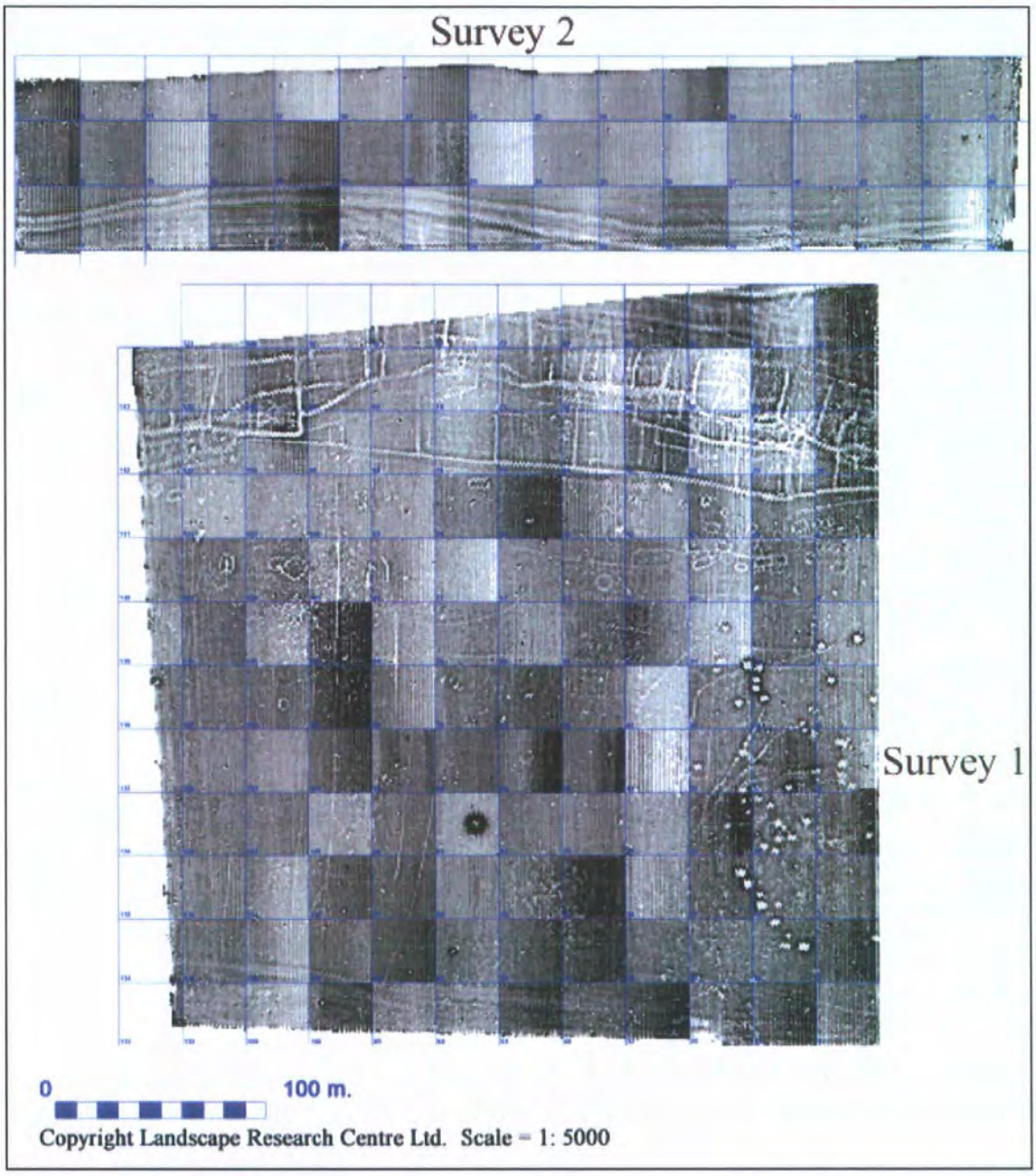

Figure 36 The raw gradiometer data from the two different surveyed areas carried out over Site 28

The survey (over site 28) was carried out using a Geoscan Research FM36 fluxgate gradiometer and utilised two different grids, with the southern half (survey area 1) surveyed in July and the northern half (survey area 2) surveyed in August, 2001.

The initial raw data from the survey 1 data grids are particularly affected by thermal drift and striping, indicated by the grids which begin grey and then change to either a lighter or darker average by the end of the grid (see Figure 36). This is partly because

the conditions were sunny with patchy cloud cover, giving rapid temperature variations, as well as being one of the two surveyor's first geophysical experiences. The northern survey grids (survey 2 in Figure 36) are also affected by thermal drift, although not to the same extent as in the southern survey.

Secondary data processing required a number of steps to be carried out. A zero drift correction was applied, followed by a general destriping algorithm (using a zero mean traverse function, which sets the background mean of each traverse to zero). Then a histogram tonal greyscale balance was applied, using a zero mean grid function, to even out the balance differences in the individual data grids. Many of the grids also required zigzag correction, using a destaggering routine. The data is displayed using 256 greys (with the cut-off points –12.8 nT represented by black and +12.8 nT by white).

To place the results for each survey onto the Ordnance Survey National grid, the processed image for each field needed to be rotated and moved (georeferenced) into "real" space based on measurements taken in the field by a differential GPS. However, for many of the earlier surveys, simple measurements to field boundaries at the corners of the surveyed area were taken in the field, and these were used to rotate the processed image. The base maps used for the georeferencing were the Ordnance Survey maps and latterly the Getmapping aerial photographic coverage of the area, itself rectified onto the OS grid.

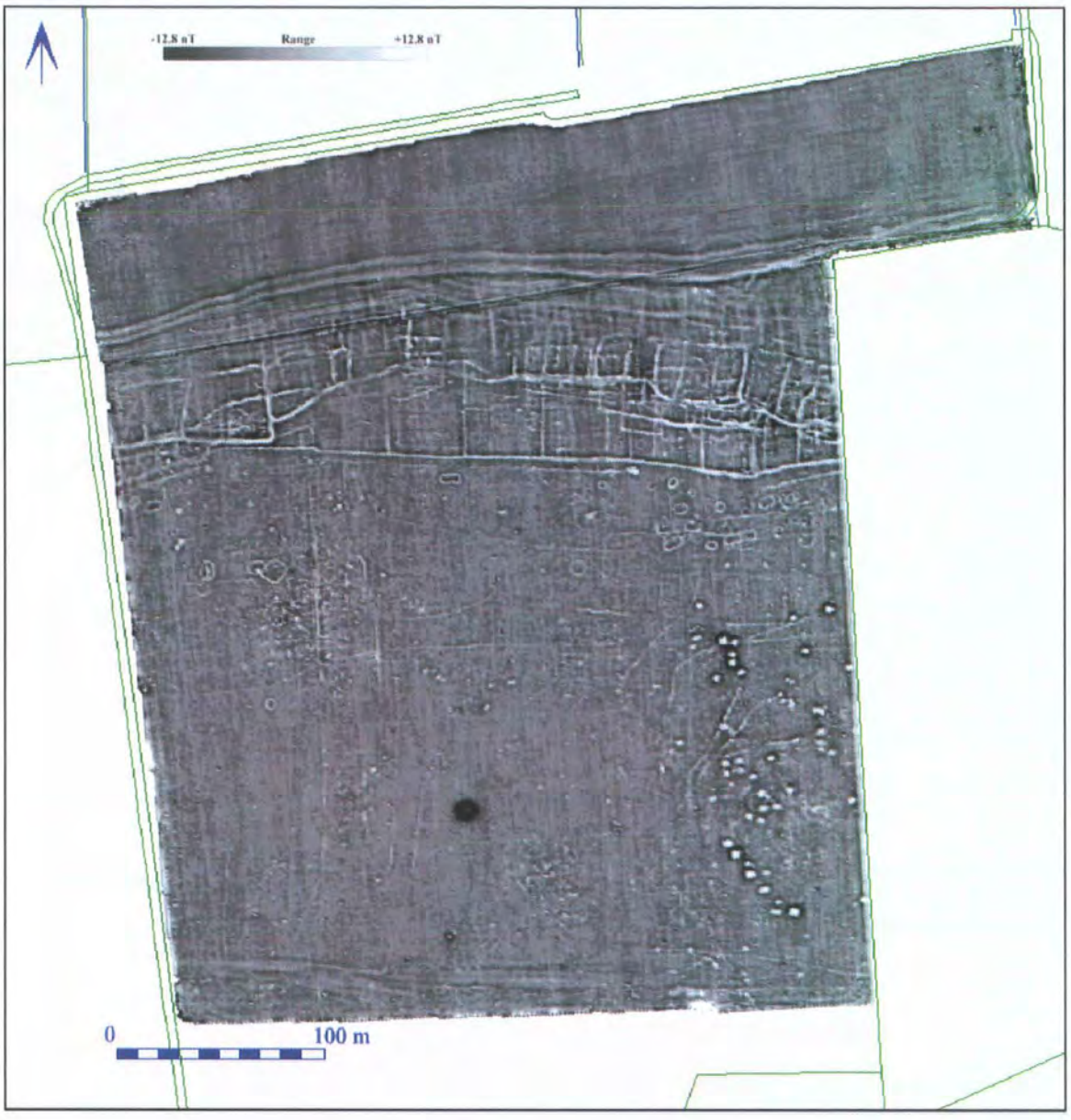

Figure 37 The processed and georeferenced gradiometer data from Site 28

Figure 37 shows the processed and georeferenced gradiometer data from the northern and southern surveys combined as a single image. Apart from initial machine drift correction and histogram grid balancing, further image enhancements were not required for this dataset. Four main archaeological areas were defined by the initial survey. The two most obvious are the Iron Age/Romano British ladder settlement in the north, and the western extent of the Grubenhäuser of an Anglian settlement in the south-eastern quadrant. Just to the south of the ladder settlement can be seen a number of round, ovate and rectangular anomalies. These have been noted at various places along the length of

the ladder settlement, and are currently interpreted as late Iron Age/early Romano British cremation cemeteries. Less visible are the number of discrete or localised anomalies which are prevalent in this area. These can be seen to cluster in two or three "zones of disturbance", and it is possible that at least one or more of these areas may be a flat grave cemetery. The most likely candidate is the area in the central west, which appears to have used an earlier Bronze Age round barrow as a focal point.

4.2 ATM Daedalus 1268 corrections

There are three main types of distortion which occur in airborne remotely sensed data: radiometric distortion, atmospheric distortion and geometric distortion.

4.2.1 Correcting radiometric distortion

Figure 38 Radiometric distortion in multispectral data

The radiometric response of the Daedalus 1268 instrument was not always standard. This is illustrated in Figure 38, where it can be clearly seen that the image shows a darker to a lighter response (left to right). This is caused by a drift over time of the instrument's calibration, and particularly affects thermal imagery. Normally this can be corrected by the use of a target with a known value (such a a white sheet) on the ground within the surveyed area, or by the use of internal sensor calibration (for instance recording the temperature and response of a blackbody during the data collection phase). Neither of these two options were possible for the 1992 data acquisition, although radiometric correction is relatively easily dealt with by modern software in the post -processing phase. All radiometric

calibration is now carried out by NERC Airborne Remote Sensing Facility, prior to the delivery of the data.

4.2.2 Correcting atmospheric distortion

The energy received by the remote sensor will not be the same as the energy which left the surface of the Earth, but will have become attenuated by a number of different atmospheric conditions. It is for this reason that it is better to have a clear sky when flying with ATM equipment, although even under these conditions atmospheric attenuation may still occur. It is important that any atmospheric distortions be corrected, particularly when datasets acquired at different times (either day-night or over a longer period) will be compared.

Image normalisation can be used to correct illumination variations over images collected at different times. This requires using one or more spectrally neutral targets, and an assumption is made that the response of these targets remains the same during the different flights (Warner and Chen, 2001). Empirical line calibration is the technique normally used for image normalisation, where a number of targets (for instance dark bodies like water, light bodies like concrete and a number of different types of vegetation) are measured on the ground with a spectroradiometer at the same time as the data collection flight.

As noted above, the techniques used for the correction of atmospheric distortion generally require a number of ground control radiance values to be acquired simultaneously with the data collection flight. Unfortunately, this was not possible in 1992, and so atmospheric distortion has not been corrected for in this dataset. An assumption has thus been made that any atmospheric distortion was minimised by the collection of the data under clear sky conditions.

4.2.3 Correcting geometric distortions (georeferencing the image files)

It was decided at the outset of the project that all raster image files would be georeferenced using a single data source, in this case the raster image *Getmapping* files.

Getmapping.com provide colour vertical photographs (see Figure 41 for an example area) of the entire mainland of Great Britain. Originally part of an ambitious millenium project (in the spirit of Domesday) to record the entire landscape of Britain at a given moment in time (in this case the year 2000), Getmapping can provide a colour vertical photographic image of any area on the British mainland, with the georeferencing of the images based on the Ordnance Survey maps. The LRC have obtained an academic license to use the Getmapping images of 500 square kilometres covering much of the eastern end of the Vale of Pickering and parts of the Yorkshire Wolds.

Initially the original tiled *Getmapping* files covering the project area were merged together into a single raster image using Photoshop. The resultant tif file was then imported into Imagine version 8.7. This reference image was placed into the United Kingdom National Grid Reference (NGS) co-ordinate system in Imagine, by using the change map model (see Figure 39 below) function, where the known pixel resolution and NGS grid coordinates for the top left hand corner of the image were entered.

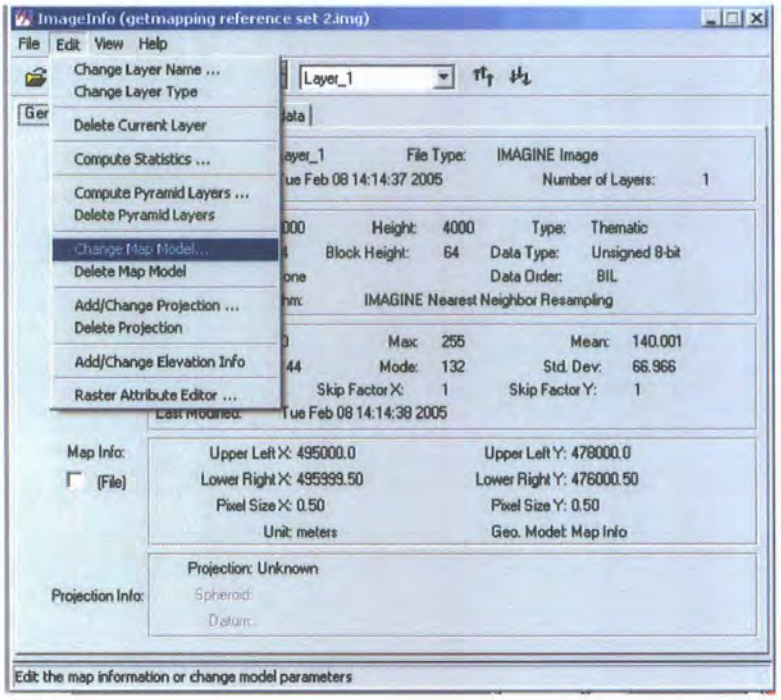

Figure 39 How to change the map model in Imagine

In the Viewer, the Utility menu/Layer Info provides access to the Change Map Model dialogue (Figure 39).

There were cases where additional information not present in the *Getmapping* coverage could be gained from aerial photographs taken at the same time as the multispectral imagery (ie where specific ground control points could be achieved when earlier field boundaries had been altered or removed, or where distinctive cropmarks were present). In these instances, the aerial photographs containing the information were georeferenced using the *Getmapping* files and then merged onto the main reference file. Georeferencing the June 1992 multispectral images provided a number of problems, not least the fact that at this time no navigational correction data was collected for the imagery. Also, some of the data were very distorted, particularly where the foot of the Wolds meets the Vale (see Figure 40). This was caused by a number of factors influenced by the attitude of the plane, including pitch, yaw and height above ground variation.

In addition, as the data was collected by the scanner in an across track swath mode, the pixels nearer the edge of the runs were more prone to distortion than those towards the centre of the image. This can clearly be seen in Figure 40 below, where the whole image, and in particular the eastern edge, is very distorted. The distortion was exacerbated as this is the point where the Wold scarp meets the Vale, and maintaining an even altitude becomes difficult.

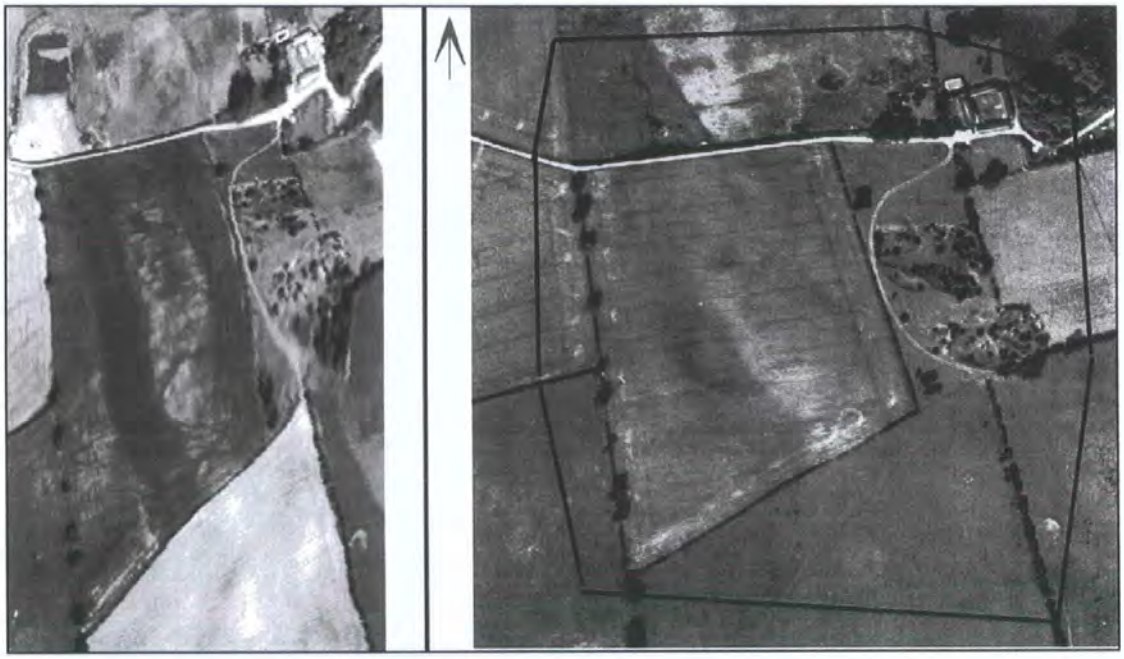

Figure 40 An unrectified multispectral image (Band 4) on the left, with the area covered indicated by the black line on the georeferenced *Getmapping* data on the right.

The central field in Figure 40 is 313 metres north to south. Note the extreme distortion in the central eastern area of the multispectral image. Distortion on this scale is difficult to correct without incurring loss of data from the original image.

While some of the ATM acquired data on the flatter Vale at first glance appeared reasonably easy to geometrically correct, it soon became apparent that the warping effect was also present here. This became more noticeable after an initial georeferencing was carried out, when comparison with the georeferenced aerial photographs taken at the same time showed a marked distortion in the centres of the fields. These distortions

were corrected by using the cropmark evidence from the georeferenced aerial photographs to warp the multispectral anomalies. This could only be done where there was no doubt that the anomalies in both images were definitely the same feature, and thus only distinctive or unusual features could be used to provide additional ground control points in this way.

A number of different warping facilities are possible using Imagine. These include polynomial and rubber sheet warps. Rubber sheet warping is recommended for datasets which are very distorted, and where a large number of ground control points, particularly around the edges, can be collected

After much testing, it was found that using the rubber sheet method of warping, combined with a nearest neighbour resampling method, provided the most accurate means of georeferencing the June 1992 multispectral dataset. Although bicubic spline resampling provided a smoother look to the image, no enhanced anomaly detection was derived from this method, and using the nearest neighbour resampling method has the advantage of not introducing new digital number (henceforth DN) values into the data. It is important not to let Imagine choose the pixel resolution at this point, as it tends to choose a higher resolution than the original data. The pixel resolution can be set in the final warping dialogue; for this dataset 1.5 metres per pixel. Due to the extreme image distortion in some of the runs, particularly near the edges, it was not always possible to get a perfect georeferenced match with the base map. However, although some of the features near the edges of the rectified images were up to seven metres away from the equivalent features visible on the georeferenced aerial photographs, within the central region of the warped image virtually all of the anomalies were within the original pixel resolution (ie less than a two metre difference) in terms of error, and many were virtually an exact match.

4.2.4 Ground control points

Ground control point geometric correction involves the use of two corresponding areas of interest. Normally, an image which requires correction will be warped onto an existing map or another image, which is already in the correct map reference projection. What is needed are easily defined points which exist both on the input image and on the reference map. These can be field boundaries, gate posts, road junctions, electricity pylons, ponds or the edges of structures and buildings. Because we were using image to image correction, it was sometimes possible to use hedges or trees in field boundaries where it could be ascertained that they were the same feature in both images. In order to completely cover the four case study areas, it was necessary to georeference parts of seven different runs. This involved the identification of a large number (2175) of ground control points (see Figure 41) for the entire image, varying from 79 for run 3b to 478 for run 2a (see Table 9 below). Altogether, 33.52 sq kilometres were georeferenced, which is just under 95% of the total 36.03 sq kilometres collected.

Figure 41 Ground control points on the reference Getmapping data

Run	Control Points	Date
1b	245	27/06/1992
2a	478	27/06/1992
3a	244	27/06/1992
3b	79	27/06/1992
3c_d	147	17/06/1992
4a_b	226	17/06/1992
4c	261	27/06/1992
5a	233	27/06/1992
6	262	27/06/1992

Table 9 The number of control points required to correct the 1992 multispectral runs

In addition, some of the original multispectral data files were originally split up in order to transfer the data in manageable chunks (back in 1992 large scale portable storage was not readily available). To facilitate georeferencing, these images were joined back together using the G-Sys GIS software package, and then imported into Imagine using the import generic binary file option (see Figure 42).

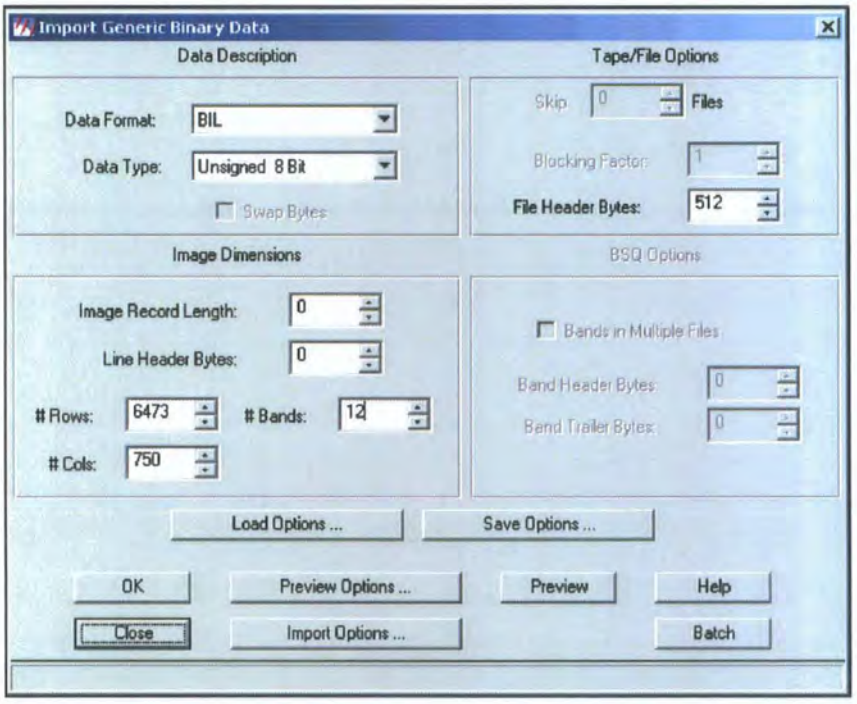

Figure 42 Import box for 1992 multispectral data using Imagine

This is the import dialog for the joined images originally named run3c and run3d, which are in a band interleaved (BIL) format.

4.3 Enhancing the georeferenced images

After the images were georeferenced, a method to enhance the visualisation of the anomalies was established.

The data range in the multispectral images was such that automatic or standard image enhancements were generally inappropriate, even within individual fields planted with the same crop. This is because the reflectance response is governed by a number of transient factors, and is also influenced by the underlying differences in geology and soils. It was necessary to define discrete areas within each field as required, because specific enhancements were needed in order to extract the maximum information from each dataset. The methodology used for enhancing the multispectral images is outlined below.

Initially, areas of interest requiring different treatment were defined. This was done using the polygon ouline tool to define each area that required a different stretch. This could be a number of adjacent fields, a single field, or discrete parts of fields which required different processing in order to enhance anomaly detection

Secondly, a technique for enhancing the images was developed. A sample of the enhancements applied to one dataset (run 5a) is given in Table 10 below. Although this general set of contrast stretching methods could be applied to other runs, each run had its own specific set of slightly different characteristics which made it necessary to try out a number of different techniques before the optimum method was established.

Band	Enhancement method	Notes for Run 5a
3	Gamma	A gamma scale of around 3.5 for most parts of the image.
4	Gamma	A gamma scale of 2 for the lighter, 3 for the medium and 4-5 for the darker parts of the image
5	Standard deviation	Generally 5 or 6 standard deviations
6	Gamma	A low gamma (scale 3 for darker parts of the image and 2 for lighter parts)
7	Gamma	A low gamma (scale 3 for darker parts of the image and 2 for lighter parts)
8	Gamma and Gaussian	Either a very low scale (2.2 gamma/scale 2) or a low (12-20) mean using a Gaussian stretch
10	Standard deviation	Generally 4 standard deviations
11	Standard deviation	2 to 3 SD's for lighter and 5 SD's for darker parts of the image
12	Gamma	A lower scale for lighter parts of the image

Table 10 Image enhancements for one of the multispectral runs

Experimentation proved that for bands 5 and 11, a standard deviation stretch was generally the most efficient for making the anomalies more visible, where these two bands responded particularly well to a stretch of between 2 and 5 standard deviations (depending on the specific run). Some areas in band 3 also responded well to standard deviation stretching, although this band required a stretch of between 5 and 8 standard deviations. Bands 6, 7 and 8 (the near infrared bands) generally did not respond well to data stretching, although a gamma adjustment was found to work quite well for some of the areas in these bands. When anomalies were visible but "muted", a linear stretch was applied. This was particularly useful for bands 3 and 4, and occasionally for areas in bands 10 and 12. However, some of the data was very "flat", and in these instances either a histogram equalisation or a Gaussian stretch was used. In other cases, the data was sufficiently rich that no enhancement was required. The reason that the various stretches are necessary for different bands is that the data range collected for each band alters, with the added complication that this data range will vary within a band, depending on the radiance values produced by the different crop types, which in turn depends on a number of factors, including availability of moisture and soil composition.

In order to view the different runs as one image, it was necessary to remove the very distorted fragments round the edges of parts of the georeferenced images. This was done by selecting the area which was to be retained using the area of interest (AOI) selection tool, and then creating a subset of the data using the AOI polygon. After all of the images were treated in this way, the mosaic tool was then used to combine the different runs into a single image.

Finally, the images were converted into tiff files, one for each enhanced band. It is important that after all of the enhancements have been made, a relevant scale (or zoom level) is chosen before saving the new images as tiffs. To obtain tiff files based on the original resolution of the data, use the zoom pulldown menu and choose 100%.

4.4 ATM AZ-16 and CASI corrections (2005 flight)

The initial flight was carried out on 20/06/2005, where six lines of ATM and CASI were flown. This flight was aborted because of sporadic cloud cover. Early the next morning (21/06/2005), the night time thermal band ATM data (5 lines) was collected. On the 23/06/2005, the second sortie was conducted in clear blue skies over the full project area, and 12 lines of both CASI and ATM data were collected.

4.4.1 Levels of processing

The ATM and CASI data files are delivered from NERC in an HDF (Hierarchical Data Format) file format, the various levels of which were defined by the National Centre for Supercomputing Applications. (See Table 11 or website at http://www.hdfgroup.org/).

Product	Definition
Level 0	Raw sensor format data at original resolution
Level 1a	Level 0 data reformatted to image files with ancillary files appended
Level 1b	Level 1a data to which radiometric calibration algorithms have been applied, to produce radiance or irradiance, and to which location and navigational information has been appended.
Level 2	Geophysical or environmental parameters derived from Level 1a or 1b data, may include atmospheric correction.
Level 3a	Level 1b or 2 data mapped to a geographic co-ordinate system using on-board attitude and positional information only.
Level 3b	Level 1b or 2 data mapped to a geographic co-ordinate system using on-board attitude and positional information with additional ground control points.
Level 4	Multi-temporal/multi-sensor gridded data products

Table 11 Hierarchical Data Format levels (From NERC azgcorr user maunual)

4.4.2 Using azgcorr

The data from the NERC 2005 campaign are delivered as level 1b HDF files, that is to say that the data have been radiometrically calibrated, and positional and navigational information is included with the file. However, in order to use the onboard GPS sensor logs to correct for aircraft heading (or yaw, which is deviation from a straight flight path due to wind effects), pitch (where the nose and tail rotate around the wing axis) and roll (where the wings move from a level flight position) errors, it is necessary to run the data through the azgcorr program, which is provided by the NERC. This geocorrects the level 1B data by using the onboard attitude sensors to produces a level 3a result. It runs under the Linux operating system, using a command line syntax, where a number of parameters can be set; critically the program will not run without the characters./ prefacing the command line. Two of the parameters are mandatory, the input file, which is prefaced with –1, and the output file, which is prefaced with –3. It was found that the pixel resolution, which is prefaced with –p was also required, or the program defaulted to a 5 metre resolution per pixel interpolation.

For the initial correction, the two mandatory parameters and an optional parameter –in were used, which indicates a nearest neighbour interpolation technique. If this is not set, the program defaults to a bicubic interpolation.

So, an example command line to correct the data from the provided hdf file would be

./azgcorr.455␣–1␣a171071b.hdf␣–3␣outputa171071b.hdf␣–p␣1.5␣1.5␣–in

where ␣ indicates a space, **-1** tells the program to expect an input file, **a171071.hdf**, **-3** tells the program to output file **outputa171071b.hdf, -p 1.5 1.5** indicates a nominal pixel resolution of 1.5 metres, and **–in** tells the correction software to use a nearest neighbour interpolation technique.

While either linear or cubic spline interpolations are possible, the nearest neighbour method is the most appropriate, as no new DN values are created. While the program is running the contents of the HDF header is shown onscreen, where the nominal pixel resolutions are displayed.

```
CASI CApsfov table from hdf file with: 512 entries
CASI  view angles port: -26.3117 star: 26.7592
CASI  view angles port: -26.2217 star: 26.7592

Site details...
  site nav  start x,y: 486460.5 477681.2  end x,y: 497970.3 477605.4
  line length: 11510  azimuth: 0.0  flight direction to: East
  pixel size  from centre average: 1.57  from ave height and fov: 1.77
  input lines: 7348  corrected image pixels : 7771  lines: 905

Correction init  interpolation: NeNe  pixel size X: 1.50 Y: 1.50

HDF image access...
  Image input HDF file: c174131b.hdf
  input  level1 image: CAimage   bands: 48 pix: 511 lines: 7348
  HDF output file: out_a174_013.hdf
  output level3 image: CAimage   bands: 48 pix: 7771 lines: 905
```

Figure 43 Screenshot showing the HDF file details while running azgcorr on a CASI file

If pixel resolutions are initially entered which are different from those calculated by the software (see Figure 43, nominal pixel size in yellow), it would be prudent to re-run the azgcorr program with the modified pixel resolutions in the command line. Resampling the data to different pixel resolutions is better carried out after the navigational corrections have been applied.

All of the ATM and CASI files were processed in this way, to provide an initially corrected set of images. However, certain parts of the images were still slightly warped, particularly towards the edges of the scanlines, so that these images still required further geometric rectifcation (or warping) onto the National Grid Reference system (see Figure 44).

4.4.3 Georeferencing the ATM and CASI images

In order to provide a directly comparable dataset, the georeferencing was done in the same way that the original Daedalus 1268 imagery was georeferenced, that is the new imagery was warped (using Imagine 8.7) onto the vertical aerial photographic mosaic provided by Getmapping.com.

Figure 44 shows the data at the different stages of geometric correction, with an OS base map in the bottom right as a reference. The 2005 data proved to be much easier to georeference than the 1992 data, although slight distortions were still visible near the edges of each run. However, there was enough of an overlap between the runs to allow a nearly perfect edge match to be carried out. As before, a rubber sheeting method of correction was used, because many (1138) ground control points were required, particularly towards the edges of each run. The south-eastern quadrant shown in Figure 44 also covers the same location as Figure 40, allowing a direct comparison to be made between the raw data from the 1992 and the 2005 ATM flights.

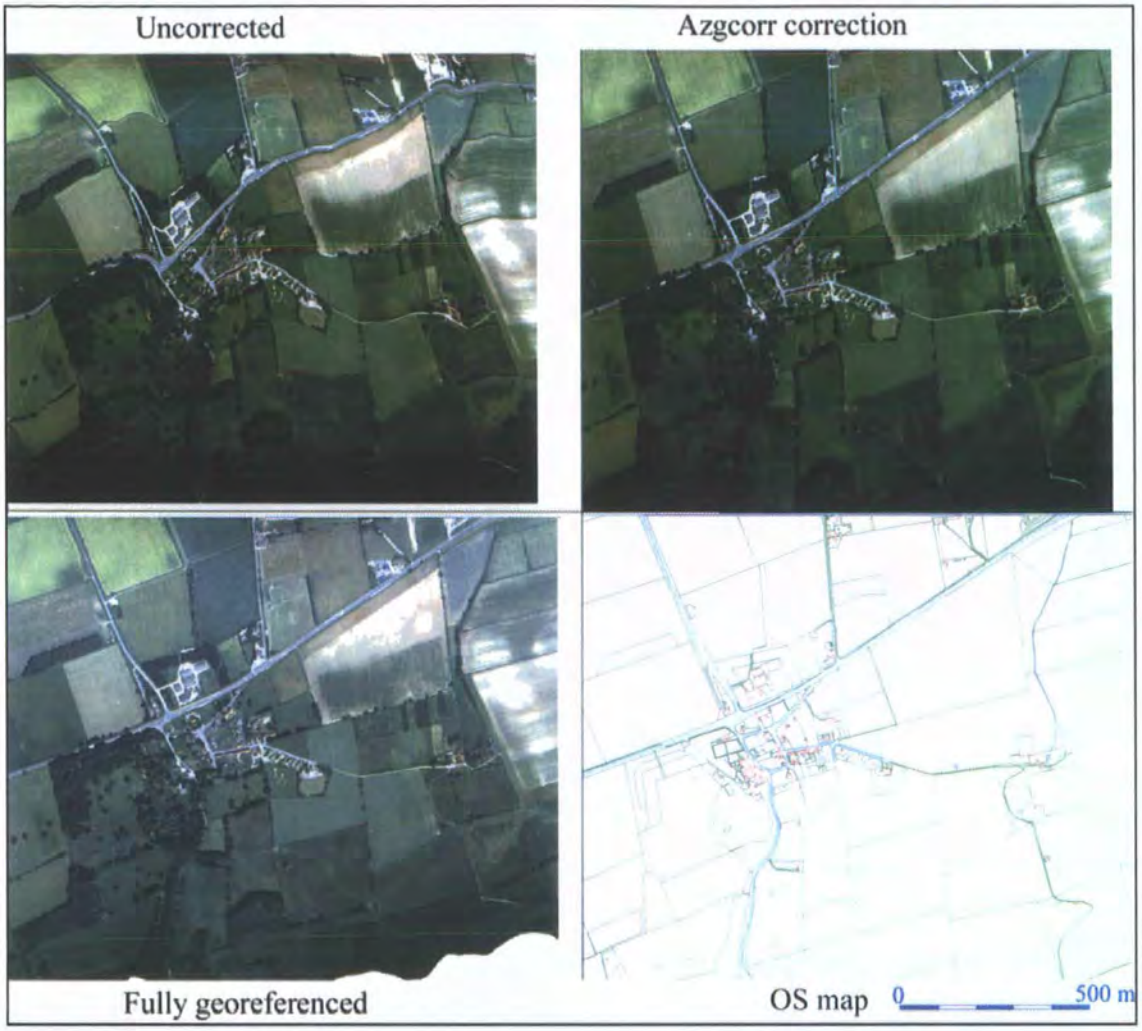

Figure 44 The phases of geometric corrction applied to the ATM AZ-16 data

Run	Control Points	Date
ATM_174101b	108	23/06/2005
ATM_174121b	151	23/06/2005
ATM_174131b	58	23/06/2005
ATM_174151b	79	23/06/2005
ATM_174171b	197	23/06/2005
ATM_174191b	158	23/06/2005
ATM_174201b	99	23/06/2005
Thermal_172021b	73	21/06/2005
Thermal_172031b	92	21/06/2005
Casi_174141b	123	23/06/2005

Table 12 The number of control points for the 2005 multispectral run

After the full georeferencing of seven lines of AZ-16 data, it was necessary to mosaic the lines together so that a single image could be created. This was achieved by creating a number of area of interest (AOI) files with shared cut lines along field boundaries

where each of the scanlines overlapped. This was necessary to avoid histogram balancing problems occurring towards the edges of the georeferenced files.

Thermal data image restoration and geometric correction

The night time thermal band collection was carried out in the early hours (between 2.09 and 2.36am) of 21/06/2005. The data was processed in the same way as the other ATM data, that is initially being run through the azgcorr program and then georeferencing onto the Getmapping base map. However, it quickly became clear that the thermal data from this early morning flight had a number of across track signal to noise problems, which are manifested as lines running across the images (see Figure 45). These stripes are caused when the blackbodies (2 in the ATM) used to record the thermal data are not set to exactly the same temperature, something which is difficult to achieve in practice. The problem is also present on the day time thermal data, but is not as prominent. This would make the comparison of apparent thermal inertia between the day and night time thermal collections very difficult, with only the most major of features being visible in the night time data. This interference problem can be resolved using a notch filter to define an area where an inverse Fourier transform can eliminate the lines across the image (Gonzalez and Woods, 1993, p.296-298).

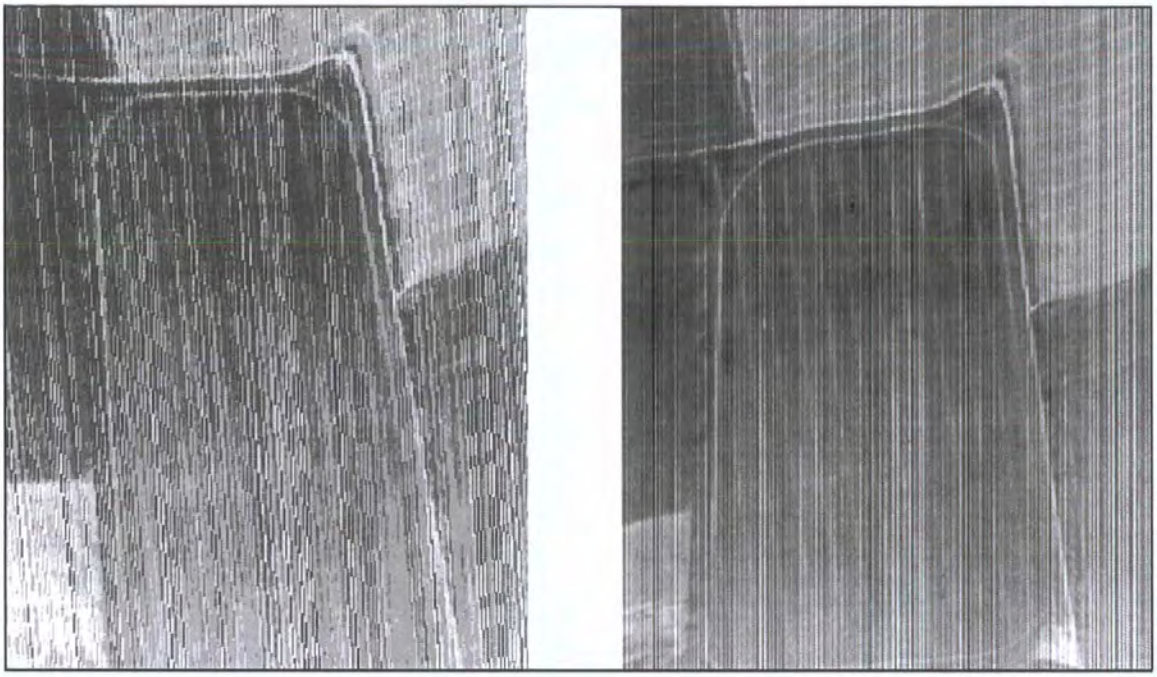

Figure 45 Georeferenced thermal image on the left and uncorrected image on the right, showing signal to noise problem from night collected data

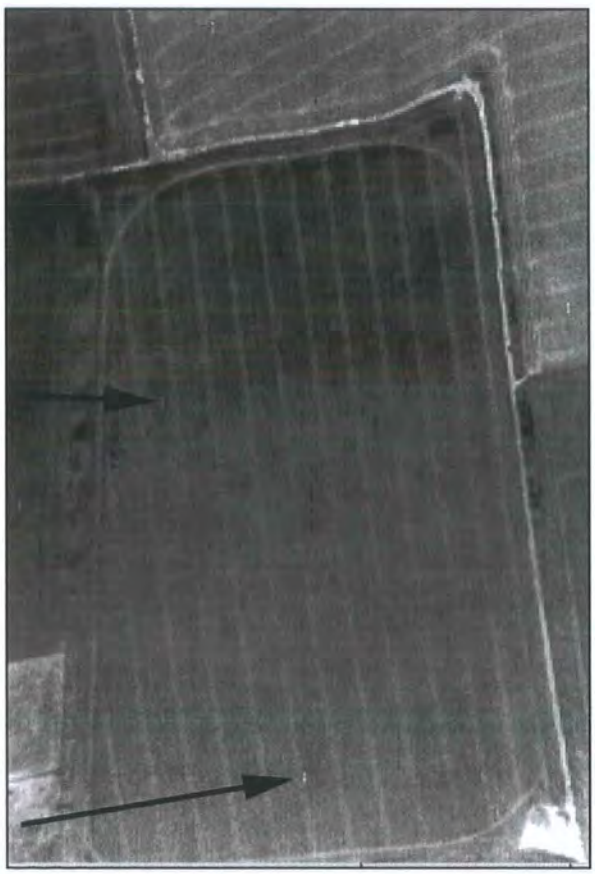

However, a simpler solution was found by using the destripe TMdata function in Imagine, which eliminates the striping very effectively. The result of this destriping algorithm can be seen in Figure 46, which demonstrates that almost all of the across track striping has been eliminated, while the tractor lines in the field remain clearly visible.

Figure 46 Uncorrected night time thermal data after destriping algorithm has been applied

Only a small number of residual lighter lines remain in the image (indicated by arrows). The main problem using this method is that it will not work on the geocorrected data, and must be applied before running the azgcorr program, which uses an HDF file with inbuilt navigational data to correct for aircraft pitch and yaw. As Imagine will currently not output HDF files, it is necessary to output the file as a band interleaved file (or BIL), which can then be run through the azgcorr program, using the original HDF file to obtain the navigational correction details. Because the new file is exactly the same size in terms of the rows and columns of pixels as the original file which had already been geocorrected, the destriped data can then be run through the georeferencing routine using the same ground control points, allowing for an exact match between the first 10 bands and the newly processed thermal data. The new file can be kept as a separate image, or can be merged in with the existing georeferenced data as an extra band.

As stated above, the same across track scan line problem also occurred on the day acquired thermal images, so in order to prepare the images for thermal inertia calculations, the same destriping algorithm was carried out. The stripes across the image were corrected, but at the same time thermal "shadows" were created by the destriping algorithm. They did not occur across the whole image, but only where very light (hot) areas were found next to relatively dark (cold) areas. It was felt that as the shadowing was so obvious, this was not an insurmountable problem, and the benefit of having destriped thermal data for day and night thermal inertia comparison outweighed the cost of adding potentially spurious data to the imagery.

Figure 47 Thermal "shadows" caused by destriping the day time thermal raw ATM data

The use of azgcorr to correct the data in a BIL file is slightly different to the normal command line correction. So, an example command line to correct the data from the BIL file using the original NERC provided hdf file would be

./azgcorr.455□–1□a171071b.hdf□-B□7389□1□0□1.0□0.0□0□Bi□171_017b.bil□–3□outputa171071b.hdf□–p□1.5□1.5□–in

where □ indicates a space, **-1** tells the program to expect an input file named **a171071.hdf**, **-B** tells azgcorr that the parameters of the BIL file are as follows; **7389** lines, **1** is the number of bands in the BIL file, **0** indicates that the pixels have unsigned 16 bit values (this would be **1** if the values were in floating point integers), **1.0** indicates that the pixel scale is the same, **0.0** shows there is no pixel offset-and **0** tells the program not to fill in bad pixel values. **Bi** tells the program that the second input file is named **171_071b.bil**, **-3** tells the program to output the new values as file

outputa171071b.hdf, -p 1.5 1.5 indicates a nominal pixel resolution of 1.5 metres, and **-in** tells the correction software to use a nearest neighbour interpolation technique.

Note that the returns shown by azgcorr are different (see Figure 48) from those displayed when running a stright HDF correction. Also note that azgcorr creates an output file of 11 bands, even if the BIL file only contained a single band.

```
Site details...
  site nav  start x,y: 499040.1 477530.7  end x,y: 488352.1 477512.2
  line length: 10688  azimuth: 0.0  flight direction to: West
  pixel size  from centre average: 1.45  from ave height and fov: 1.56
  input lines: 7390  corrected image pixels : 7174  lines: 1581

Correction init  interpolation: NeNe  pixel size X: 1.50 Y: 1.50

HDF image access...
  HDF output file: 172031_out.hdf
  output level3 image: ATdata   bands: 11 pix: 7174 lines: 1581
Correcting bands:   1start line: 7389 lnsz: 1876 bfsksz: -3752 skip: 13861764 wa
y: 1
 2start line: 7389 lnsz: 1876 bfsksz: -3752 skip: 13863640 way: 1
 3start line: 7389 lnsz: 1876 bfsksz: -3752 skip: 13865516 way: 1
 4start line: 7389 lnsz: 1876 bfsksz: -3752 skip: 13867392 way: 1
 5start line: 7389 lnsz: 1876 bfsksz: -3752 skip: 13869268 way: 1
 6start line: 7389 lnsz: 1876 bfsksz: -3752 skip: 13871144 way: 1
 7start line: 7389 lnsz: 1876 bfsksz: -3752 skip: 13873020 way: 1
 8start line: 7389 lnsz: 1876 bfsksz: -3752 skip: 13874896 way: 1
 9start line: 7389 lnsz: 1876 bfsksz: -3752 skip: 13876772 way: 1
 10start line: 7389 lnsz: 1876 bfsksz: -3752 skip: 13878648 way: 1
 11
     start line: 7389 lnsz: 1876 bfsksz: -3752 skip: 13880524 way: 1
```

Figure 48 Screenshot showing the HDF file details while running azgcorr on a BIL file

After both the day and night collected thermal datasets were destriped, they were geocorrected in the usual way, that is run through the azgcorr program to apply navigational corrections and then warped onto the Getmapping reference data using Imagine.

Apparent thermal inertia

There are a number of ways of calculating apparent thermal inertia. The simplest method is to subtract the values obtained from the night acquired data from the day acquired data. This results in an image of the difference (in DN values) between the two datasets. The resultant image contained a median value of -1373. Figure 49 shows the

difference expressed as a greyscale image, with the lighter areas indicating a smaller difference and the darker areas indicating greater differences.

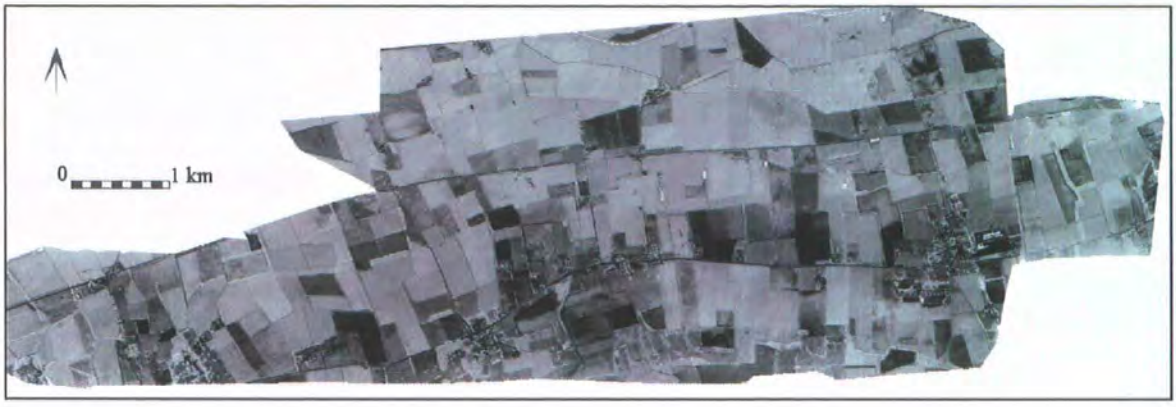

Figure 49 Difference between day and night thermal data expressed as a greyscale image

Figure 50 shows the difference between the two datasets expressed as a colour around a single value, that is if the DN difference was greater than 1464, then the pixel is coloured violet, otherwise the pixel was coloured black.

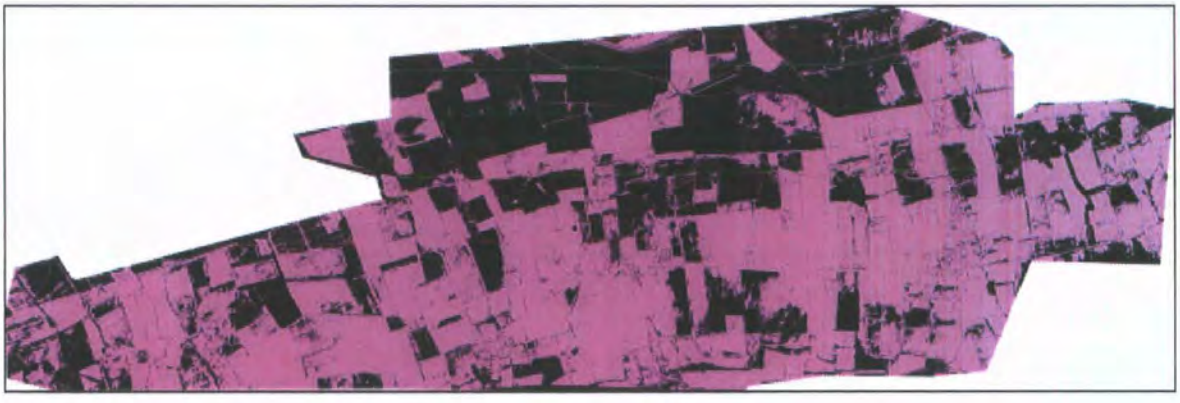

Figure 50 The difference between day and night thermal data, based around a single value

The overall trend of the difference is that the fields to the north (in the alluvial sands and silicaceous gravel zone) are showing less of a thermal difference, with the fields to the south (sand and calcareous gravel with windblown sand) showing a greater difference between day and night.

4.4.4 Aerial photographic geometric correction

At the same time that the 2005 ATM and CASI data was collected, a set of high resolution digital photographs was taken, using the Rollei medium format digital camera.

These digital photographs were very near vertical, and only required a very slight geometric correction. This was done by warping the selected photographs onto the Getmapping base map, so that direct comparison between the returns from the aerial photographs and the two multispectral scanners could be carried out. However, it soon became apparent that getting an exact match between the adjacent photographs would be quite difficult for some of the runs, as some of the areas where only a small overlap was present had no ground control points available near the edges. Where possible, this was overcome by using the technique developed for the 1992 multispectral data, that is by rewarping the problem photographs onto a previously georeferenced aerial photograph, using specific cropmarks in the centre of the fields to provide the lacking ground control points.

4.5 Hobo thermal logger processing

The data was downloaded from the Hobos as a TXT file in a comma separated format, with headings being date, time, and temperature in Centigrade from each of the 4 sensors. These files were read into an Excel spreadsheet, and all charts were generated using Excel.

4.6 LiDAR data

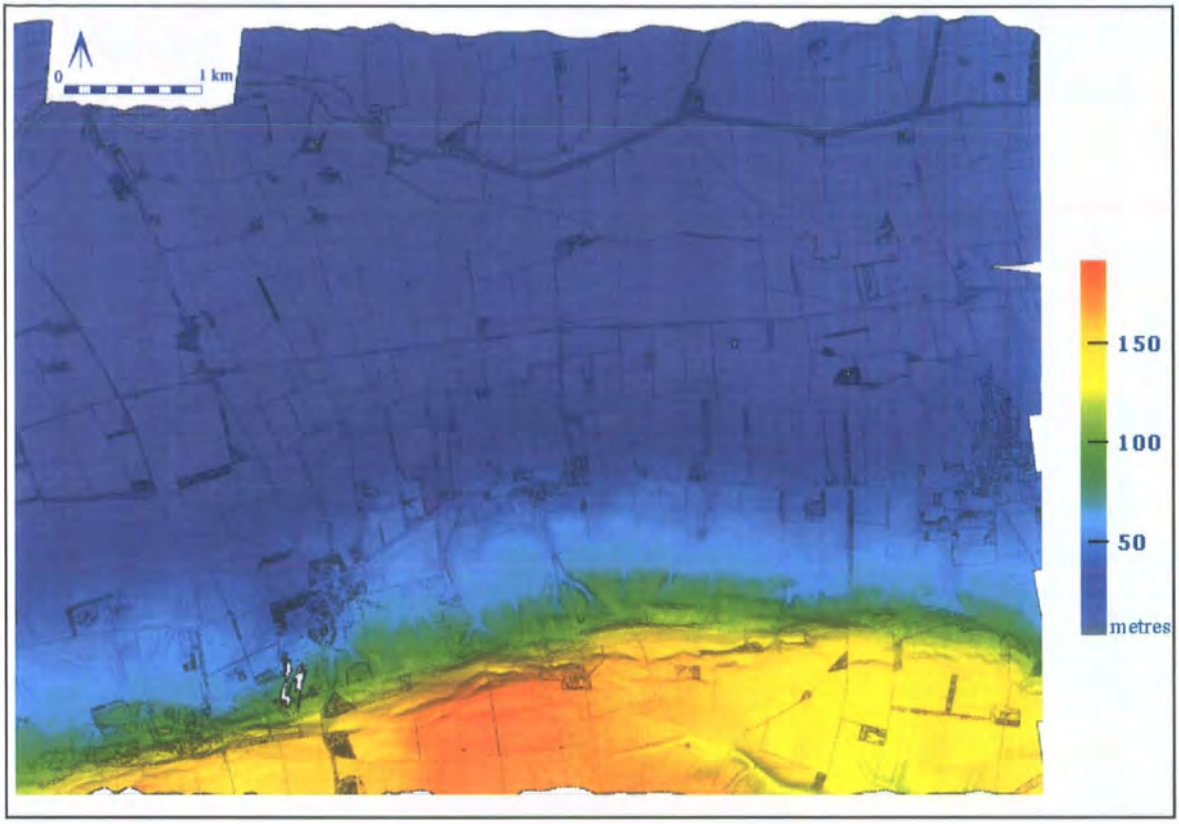

Figure 51 The extent of the LiDAR coverage

The LiDAR data covered an area of 41.03 sq kilometres, roughly 7.5 km east-west and 5.5 kilometres north-south. Figure 51 shows the area colour coded according to elevation in metres.

The data was gathered by the ULM at Cambridge, on behalf of NERC, and provided in a format which included first and last pulse data, both sets of points comprising of easting, northing, elevation and intensity data. The first and last pulse data was separated out into two files, and the last pulse data was then used to create a digital elevation model. In all 34410930 points were present in the last pulse data, although the eventual gridded file, processed using an OpenGL utility within G-Sys, at a spatial resolution of 2.1 metres contained just over 9 million points.

The LiDAR data has been employed to drape the processed MSS and magnetic data for visualisation purposes (see Figure 158 and Figure 159) and for examining the relict stream channels and gravel spurs in the centre of the wetland (see Figure 160).

Chapter 5 Interpretation and data integration

5.1 Raw data checking

As stated above in Chapter 4, it is vital that the raw data is maintained and checked, particularly before any interpretations are made. If this is not done, the possibility arises that any errors in the raw data may be interpreted as anomalies in processed data. An example from the CASI multispectral dataset illustrates this problem, but the principle applies equally to all other forms of remote sensing.

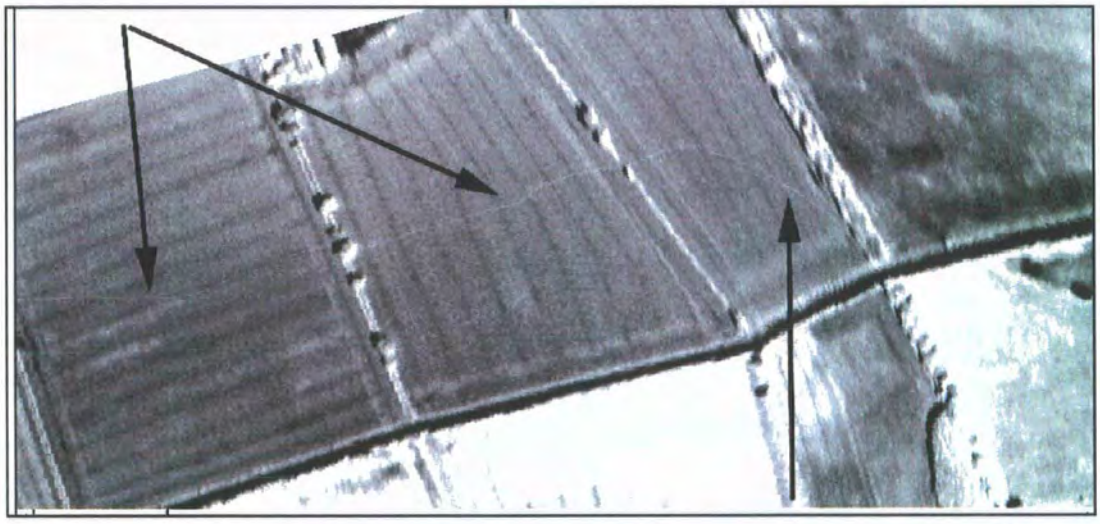

Figure 52 Geocorrected image showing CASI data (band 48)

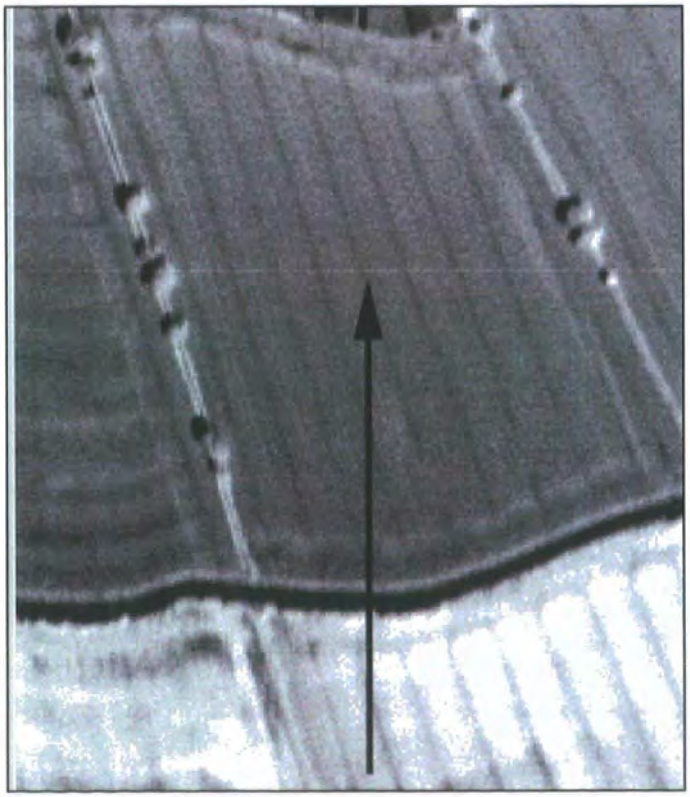

Figure 53 CASI raw data for band 48

Figure 52 shows the fully georeferenced data from the CASI instrument, in this case band 48, displayed as a greyscale image. Note the thin lighter line which wiggles across the fields (arrowed). It would be all too easy to interpret this either as an

archaeological (i.e. old field boundary) or a modern (i.e. footpath) feature, even though its path is somewhat erratic.

However, the real explanation is much more prosaic. A perusal of the raw data for band 48 immediately reveals that the "anomaly" is in fact the result of an instrument error, right down the centre of the image. This problem only occurred in band 48, and could easily have been misinterpreted had the raw data not been checked.

5.2 Integrating the remotely sensed data

As an archaeologist, my primary interest remains the quest to understand how past human societies lived and operated within the landscape. I believe that the use of multiple forms of remote sensing will allow great advances to be made in this field, but that the techniques and methodologies of analysis to achieve this are still in their infancy. Currently the collection and processing of remote sensing data is primarily within the remit of the "scientist", while the archaeological interpretation of the processed data is believed to be a much more "subjective" or theoretical process. By using digital vector drawings of remote sensing anomalies combined with a relational database which allows for different levels of interpretation, the aim is to marry the two processes in a more coherent fashion. The methodology adopted for this technique is discussed below.

One of the problems of integrating and quantifying various forms of remote sensing imagery is that by their very nature, they are designed to collect different types of data. It is possible to use complex mathematical algorithms to combine, add, subtract or multiply different raster images with each other. Kvamme uses a number of discrete and continuous integration methods to combine the returns from up to six different ground based geophysical survey results in a number of different ways (Kvamme, 2006, pp.62). While his results are valid, they are not readily applicable to the various datasets used in this research, for two reasons. The first is that combining images requires that each pixel is exactly mapped to the same point for each of the different datasets. Although this is possible using gridded ground based geophysical techniques, it is not so easy to achieve when using airborne remote sensing, where data was acquired on different occasions, and with different ground resolutions. Even after scrupulous georeferencing and resampling to the same ground resolution, it cannot be guaranteed that the pixels from

each dataset will be covering exactly the same area on the ground (see Figure 57 and Figure 58 for examples). The second reason is that the study area that Kvamme used was a well-known, relatively modern site (a World War One town established to provide entertainment for the troops stationed at the nearby army base of Camp Funston, USA). The site consisted of a grid pattern of streets with associated houses and shops. The geophysical data produced by this type of site is reasonably unambiguous, unlike the Vale of Pickering research area, where the relatively ephemeral traces of prehistoric occupation are masked by the results of millennia of agricultural activity. In addition, because the area has been utilised from at least the Mesolithic period onwards, a palimpsest of the traces of occupation occurs, with each cultural shift providing evidence which overlies the earlier activity.

Although composite images are of value for the visualisation of different aspects of complex imagery (see Figure 54), they do not help in quantifying the returns from different methods of remote sensing.

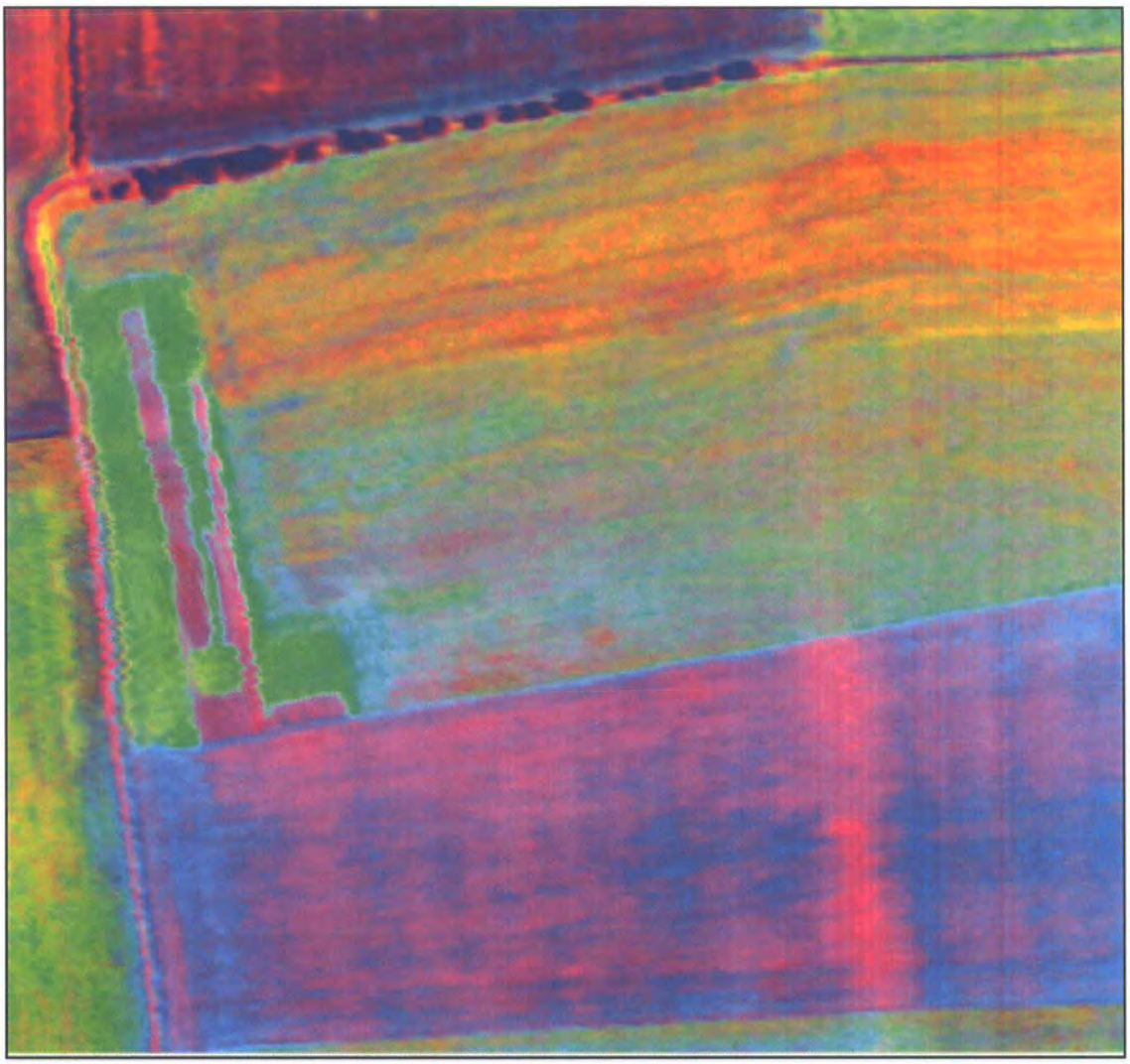

Figure 54 A principal components analysis (all bands) of the north-western corner of site 28 (1992 multispectral data).

5.2.1 Vectorising the remotely sensed data

The digitisation of geophysical and remotely sensed data is nothing new (Buteax et al 2000, 77: Buteaux et al, 2000). These techniques involve analysing the data in a subjective and interpretative way, creating vectorised polygons or lines of the anomalies from the various data sources. These can then be combined in an eclectic map of all of the potential features discovered. What this research attempts to do is to take this one

stage further, by allowing different interpretative overlays to be applied to the vectorised drawings using a linked database, as well as creating a correlation database, which would allow the returns from the different datasets to be analysed and displayed.

A new methodology was thus developed to allow the quantification of the returns from multiple methods of remote sensing. In order to ensure compatiblity and integration, the design followed the basic vector drawing structure already established by the LRC for the excavation data, with specific modifications for each set of remotely sensed data. Initially, an individual vectorised polygon for each anomaly was digitised. These are digital interpretations of remotely sensed data, and each polygon was attributed with a Key_ID which distinguishes it by type, site and anomaly number. The origin of the data can also be included in the polygon attributes, so that when interrogated, it is immediately clear which type of remotely sensed data is being viewed (see Figure 55 below).

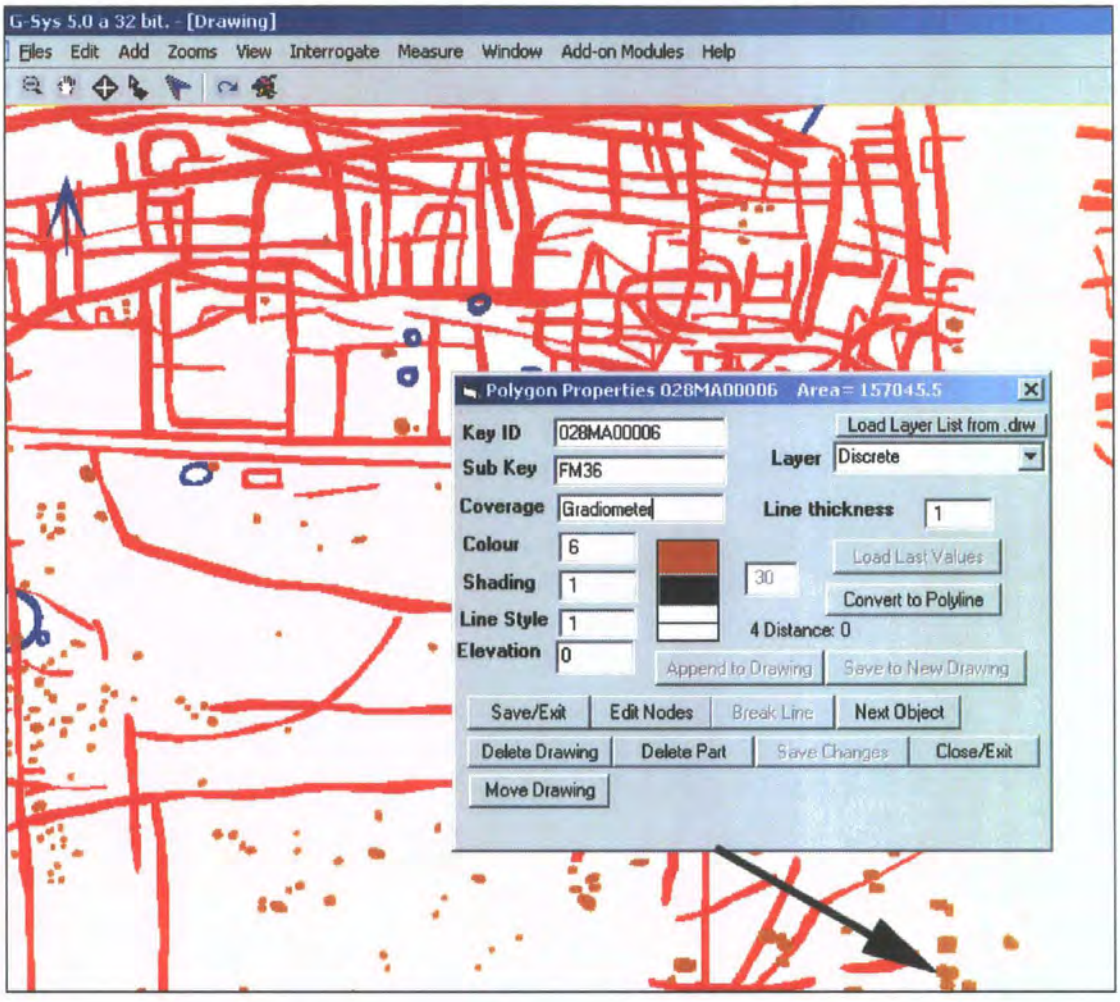

Figure 55 The attributes of a G-Sys vector drawing

In Figure 55 the polygon being interrogated is shown by the black arrow. The interrogation box indicates the nine different attributes attached to the individual polygon. The Key_ID field identifies the site number (028) followed by the anomaly type (MA= magnetic anomaly) and then the anomaly number (00006). Note that this numbering system closely follows the Key_ID used in the excavation database.

One of the most important aspects in this process is the ability to attach a number of attributes to each polygon. Initially, the vectors derived from each form of imagery can be placed on their own named layer, which can be turned on or off as desired. In this way, the returns can quickly be visualised, compared and contrasted with other sets of digitised data, derived from the returns from other forms of remote sensing.

In addition, creating a digital drawing allows the returns from a given dataset to be quantified, as the vector polygons can be counted and measured (in terms of both area and length and breadth). Each layer can easily be turned on or off to see the relative proportions of anomaly type.

Attribute	Description
Key ID	Unique identifier which provides the link to the database entry for the anomaly
Sub Key	Name of instrument used to collect the data
Coverage	Type of instrument used to collect the data
Colour	Colour of the digitised polygon
Shading	Shading of the digitised polygon
Linestyle	Linestyle of the digitised polygon
Elevation	Elevation in this case 0, but pseudo elevation can be derived from a DEM
Layer	Description of the type of anomaly (in this case discrete)
Line Thickness	Thickness of the polygon outline in centimetres

Table 13 A description of the nine attributes which can be attached to a G-Sys polygon

Of course this process merely gives a relative quantification, as we normally have no idea of the actual total number of archaeological features in a given area (for further discussion see Actual archaeological remains in Chapter 7)

The primary advantage of this form of image interpretation is in allowing a direct visual comparison between many forms of imagery as well as with the existing datasets of digitised vector plots of aerial photographs (i.e. English Heritage NMP plots and County Sites and Monuments Records).

At the same time as the vector drawings were digitised, a database entry for each individual polygon was created.

5.2.2 Database Design

Over the past 25 years, the LRC has developed a data structure which allows all excavated data to be linked using relational data tables. These use the concept of an

identifier called the Key_ID, which consists of a combination of three fields, Site, Area and Context, which together provide a unique linking field allowing both one to one and one to many relationships to be expressed. The Key_ID field identifies the site number (028) followed by the area code (AA= trench one, AB = trench two etc) and then the context number (00006). The Key_ID also provides the link to the vector drawing (see Figure 66) of each feature.

When the original excavations at Heslerton generated large quantities of finds from many different features, it became necessary to design a database which would allow the analysis of multiple sets of excavation data. Initially, this was done by using a custom built proprietary database (GeoDB), designed by Dominic Powlesland. Moving to a Windows environment, the Microsoft database FoxPro was initially used, before the current porting into Microsoft Access, which allows relational datasets to be easily established and maintained.

In order to be able to apply different interpretations to the drawings, and to link the different datasets together, it was necessary to create a relational database which contains details on all of the remotely sensed anomaly polygons. Each vectorised polygon is linked by its Key_ID to a table in the database. The database contains interpretative fields which allow the drawing to be displayed and redefined in a number of different ways, for instance by phasing, anomaly type, signal strength or feature interpretation. The method described is of course simplified, as each form of remotely sensed imagery has many subtle nuances. For instance, a fluxgate gradiometer survey can generate both weakly or strongly negative and positive anomalies. A thermal image can generate cold, warm or hot anomalies. In order to take these differences into account, specific characteristics for each type of remotely sensed data can be identified and recorded within individual tables. For instance, the magnetic table contains a field

which indicates whether the anomaly is positive or negative, with another field which allows relative magnetic strength to be expressed (in values ranging from 1 to 5). Design views of all of the remote sensing databases can be found in Appendix four.

As well as interpreting the individual anomalies, it was important to be able to differentiate between different types of anomaly, and so each anomaly was placed into one of six groups (see Table 14 below). The groups were chosen to reflect the type of activity which was being interpreted.

Group	Title
1	Agricultural activity
2	Alluvial activity
3	Archaeological activity
4	Geological activity
5	Quarry activity
6	Post-medieval or modern activity

Table 14 The six groups into which all of the anomlies were categorised

This allowed the returns from each form of remote sensing to be analysed in a number different ways, rather than just relying on a simple anomaly count. Being able to do this becomes more important when looking at the wider landscape, where different returns of specific types of activity can be linked to changes in geology or to differences in landuse.

5.2.3 Vectorising the multispectral data

Initially, the band with the most archaeological information was chosen by eye, by looking at all 11 bands and choosing the one which contained the most anomalies believed to be of archaeological origin. Each anomaly present was digitised as a polygon, and a database entry was created. A printout of each band was then compared with the digitised drawings, and any additional anomalies not present in the initial band were then digitised. If anomalies already digitised were present in the second and

subsequent bands, they were not redigitised, but an entry in the database was created to indicate the presence of the anomaly in this band.

Multi-spectral Anomalies : Table

Fromdraw	Link_Key_Id	Streng	Dig	1992 Band 3	1992 Band 4	1992 Band 5	1992 Band 6	1992 Band 7	1992 Band 8	1992 Band 10	1992 Band 11
027MS00027	027RS02467	1	11	☐	☐	☐	☑	☑	☑	☐	☑
027MS00028	027RS02466	1	11	☐	☐	☑	☑	☑	☑	☑	☑
027MS00029	027RS02537	1	11	☐	☐	☑	☑	☑	☑	☑	☑
027MS00030	027RS02465	3	11	☐	☑	☑	☑	☑	☑	☑	☑
027MS00031	027RS02446	3	11	☑	☑	☐	☑	☑	☑	☐	☑
027MS00032	027RS02464	2	11	☐	☑	☑	☑	☑	☑	☑	☑
027MS00033	027RS02462	2	11	☐	☐	☐	☐	☐	☐	☑	☑
027MS00034	027RS02545	1	11	☐	☑	☐	☑	☑	☑	☑	☑
027MS00035	027RS02546	1	11	☐	☐	☐	☑	☑	☑	☑	☑
027MS00036	027RS02472	1	11	☐	☐	☐	☑	☑	☐	☑	☑
027MS00037	027RS02469	1	11	☐	☐	☐	☑	☑	☐	☑	☑

Figure 56 A view of the data contained within the multi-spectral data table

This is graphically shown in Figure 56, which shows part of the multi-spectral data table. Here we can see that all of these anomalies were originally digitised from the thermal band 11 (field heading Dig). It can also be seen that many of the anomalies detected in the thermal band were also present in the other bands, their presence indicated by a tick in the yes/no fields for each band. After going over all of the 1992 data for the four case study areas, the same process was carried out for the 2005 multi-spectral data. In this way, a picture of the complete return from both sets of multispectral data was accomplished. Anomalies visible in multiple bands could be displayed by using SQL queries to graphically display the results using the vector drawings (see Figure 57).

5.2.4 Vectorising the aerial photographs

The aerial photographs were georeferenced onto the *Getmapping* reference file using Irwin Scollar's Airphoto program. They were vectorised using a similar system to the multispectral data, in that even though the same cropmarks may have appeared in photographs taken at different times, only a cumulative or eclectic drawing was created, with multiple occurrences being logged in the aerial photographic database, rather than being vectorised for each individual photograph. For example, if an existing cropmark suddenly showed new detail, for instance a linear anomaly extending by 20 metres, then

only the new data would be vectorised, with the existing data indicated by a true/false field in the database.

5.3 Correlating the returns

The most time consuming part of setting up the new system was the correlation of the returns from each form of remote sensing. What this entailed was that after all of the anomalies for each set of data had been vectorised, the returns from each dataset were then visually compared with all of the others to establish which anomalies were the same and which were not detected by the other methods. This involved the creation of a correlation table in the database (see Figure 64). Initially, the gradiometer data was imported and a unique number issued for each anomaly. The gradiometer data was chosen as the starting dataset because it incorporated the vast majority of anomalies (17494) detected to date. The vectorised drawings from the other forms of remote sensing were then compared to the gradiometer drawings, and any correlations were entered into the database. If there was no correlation with the gradiometer data, then a new database entry was created. Each anomaly will appear only once in correlation table, no matter how many times it was detected by different remote sensing techniques. A link back to the Key_ID of each type of remote sensing is provided by a set of relevant field headings. Although it may seem like a relatively simple task to correlate the returns from multiple georeferenced sources, in practice this can be quite tricky, because slight differences in the location of anomalies causes some doubt as to whether they are the same feature or a different one. The different locations of the anomalies depend on the original data source. For instance, the Daedalus 1268 data was very warped to begin with, and even after georeferencing it was not always possible to be confident of the exact positioning of anomalies from this source (Figure 57).

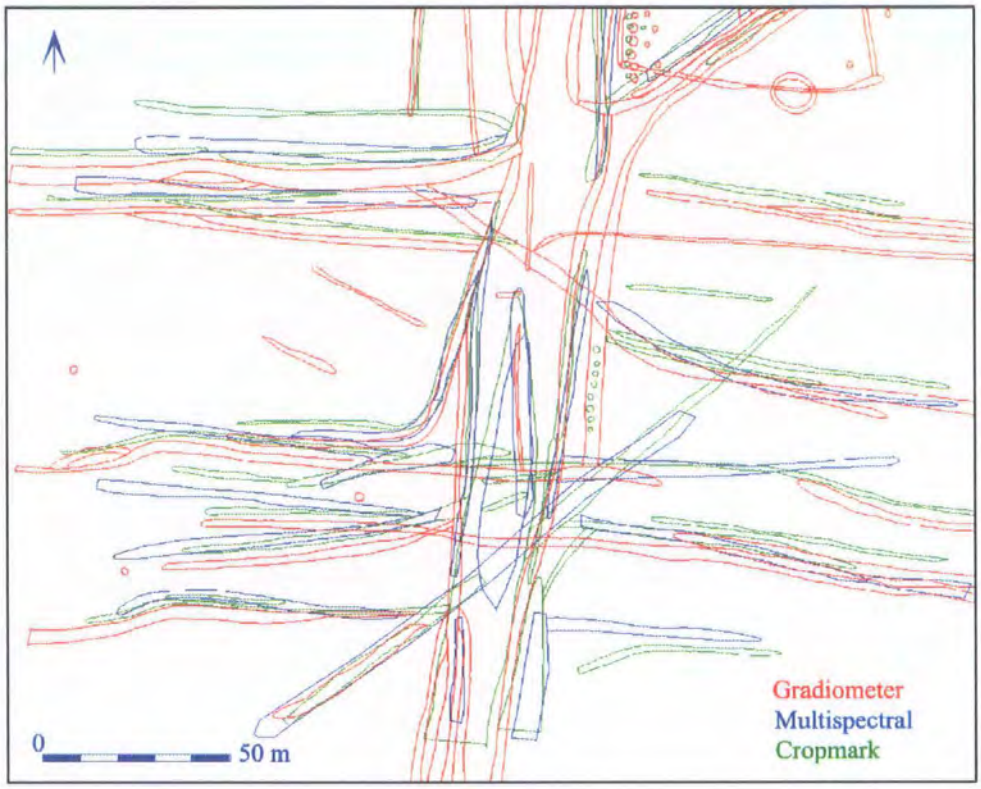

Figure 57 A view of the interpreted returns from three types of remote sensing superimposed (linear anomalies)

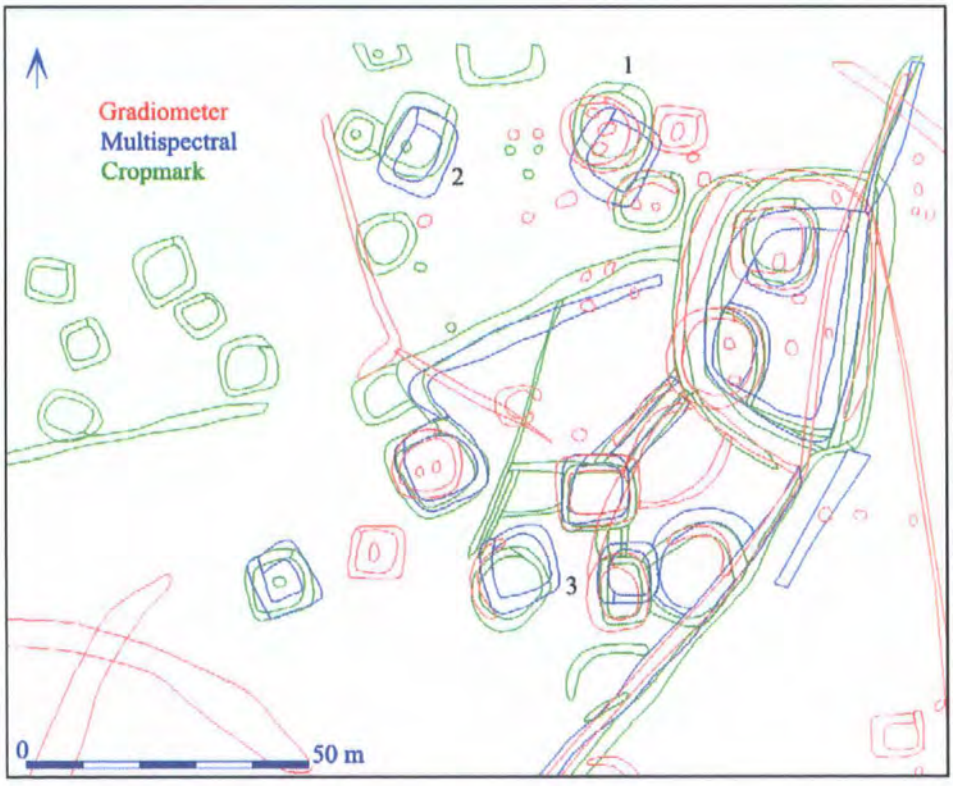

Figure 58 A view of the interpreted returns from three types of remote sensing superimposed (square barrows)

While it is obvious that some of the anomalies are the same features detected in each form of remote sensing, a number of linear anomalies may represent different features, and must be represented as such in the correlation database.

Where it is clear that the same features are being detected, even though they do not have an exact match between the different georeferenced datasets, then they are recorded as such, with a note in the description field indicating how much the offset distance was (see numbers 2 and 3 in Figure 58). Where there is ambiguity (number 1) then the anomaly must be recorded as a separate feature, although again the description field can indicate that the anomaly could be correlated.

5.4 Data integration - a case study

Two forms of structure occur in Anglo-Saxon settlements, the post hole structure (or hall) and the *Grubenhaus* (also known as the sunken featured building or SFB). Post hole structures are generally rectangular in shape, with a number of posts providing the basic construction or frame onto which the main superstructure was attached. Grubenhäuser use a completely different technique, initially created by digging a large rectangular hole in the ground, before inserting two (or more) posts at either end, on which at least part of the superstructure was erected. It is probable that the post hole buildings were timber-framed structures with raised floors and were held together using a tie beam construction (Clemence, 1993, p.59), while the Grubenhäuser had timber floors laid across the cavity (with both structure types using floor plates). Both forms of structure were made of wood, although there is some evidence that turf was also used in the construction of Grubenhäuser (Tipper, 2004, p.80)

In order to demonstrate how all of the different datasets can be linked together, an Anglo-Saxon *Grubenhaus* has been chosen as an example. This is mainly because it is very difficult for any type of remote sensing to find the ephemeral remains of post hole structures, while Grubenhäuser respond well to some techniques, particularly magnetic prospection. In this instance, a bottom-up approach is used, where we will follow a data link through the system, beginning at the micro level (a single find), up through the context, feature and site stages, eventually finishing at the macro level (remote sensing landscape analysis). However, a top-down method, beginning with the remotely sensed data is equally applicable, and would perhaps be the more common route for an archaeologist. Indeed, that is how this feature came to be excavated, as the site was

initially recognised through aerial photography and multispectral survey, which prompted a magnetic survey (see Figure 63). This survey identified a specific group of four Grubenhäuser, three of which were excavated.

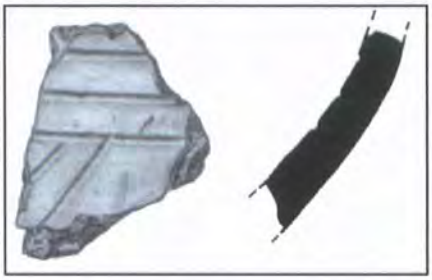

Figure 59 A drawing of find number 028AA00034LW

An extract from the finds database is shown in Figure 60 below, which tells us that the find illustrated in Figure 59 is an Anglian potsherd, with sand and mica temper. It is a decorated sherd, with three horizontal incised neck lines above two parallel diagonal lines. The important field here is the object field, where the first ten digits provide the link back to the fill in which the object was originally found. In this case, the context is number 028AA00034, with the suffix LW providing the unique find identifier (the finds are given this suffix when the initial analysis on them is carried out, beginning with AA, AB and so on). Just out of interest, a further 390 finds were associated with this fill.

OBJECT	FABRIC	INC1	INC2	WAL	WEIGHT	PERIOD1	COMMENTS
028AA00034LO		ABS.CALCITE		7	3	R-B	
028AA00034LP		ABS.CALCITE	CHALK	8	3.5	IRON AGE	
028AA00034LQ	LIMES A	LIMESTONE		7	4.5	ANGLIAN	
028AA00034LR		SAND		5.5	6	ROMAN	
028AA00034LS		ABS.CALCITE		10	5	IRON AGE	
028AA00034LT		ABS.CALCITE		8	4.5	IRON AGE	
028AA00034LU		ABS.CALCITE		12	7.5	IRON AGE	
028AA00034LV	LIMES A	LIMESTONE		6	3	ANGLIAN	
028AA00034LW	SST G	SAND	MICA	6	4.5	ANGLIAN	THREE HORIZ. INCISED NECK-LINES ABOVE TWO-PARALLEL
028AA00034LX	CALCT A	ABS.CALCITE	CALCITE	9	1.5	IRON AGE	
028AA00034LY	SST A	SAND	CHALK	8	37.5	ANGLIAN	?STRAIGHT-SIDED VESSEL
028AA00034LZ		ABS.CALCITE		7	5	IRON AGE	
028AA00034MA						ROMAN	
028AA00034MB							
028AA00034MC							
028AA00034MD							
028AA00034ME							

Figure 60 A view showing find 028AA00034LW in the finds database

The context database provides the following information about fill number 028AA00034. "This number was issued after the removal of three spits of fill number 028AA00027, although it was not substantially different from the upper fill. It was present in all four quadrants, and its main defining characteristic was the perceived

increase in the density of animal bones, both large and small. Pottery was also present in small quantities, both abraded and well preserved. Two Anglian glass beads were recovered, both from the north-eastern quadrant."

KEY_ID	MASTER	FROMDRAW	TYPE	PHASE	SHAPE	XCOORD	YCOORD	ZCOORD	LENG	BRE	DEPTH	NOTES
028AA00027	028AA00022	028AA00036	GRUB FILL	ANGLIAN	SUB-RECTANGULAR	49377477	47713793	3156	425	369	7	This was the initial layer across the entirety of Gru
028AA00028	028AA00024	028AA00039	GRUB FILL	ANGLIAN	SUB-RECTANGULAR	49378101	47713342	3146	210	260	3	Spit across top of Grubenhaus 28AA24 in order to
028AA00029	028AA00023	028AA00058	GRUB FILL	ANGLIAN	SUB RECTANGULAR	49377644	47713492	3163	396	275	30	Initial darker fill of grub 23. medium sandy deposit
028AA00030	028AA00024	028AA00039	GRUB FILL	ANGLIAN	SUB-RECTANGULAR	49378168	47713317	3145	400	280	15	Upper fill of Grubenhaus 28AA24, apparently within
028AA00031	028AA00024	028AA00039	GRUB FILL	ANGLIAN	IRREGULAR	49377961	47713341	3145	180	265	16	Fill of Grub 28AA24, defined below 28AA30 on we
028AA00032	028AA00024	028AA00039	GRUB FILL	ANGLIAN	IRREGULAR	49378224	47713231	3145	270	230	6	Fill of Grub 28AA24, defined below 28AA30 aroun
028AA00033	028AA00022	028AA00036	GRUB FILL	ANGLIAN	SUB-RECTANGULAR	49377628	47713931	3142	376	61	11	This was a sandy fill, with quite a high percentage
028AA00034	028AA00022	028AA00036	GRUB FILL	ANGLIAN		49377628	47713833	3143	325	240	11	This number was issued after the removal of three
028AA00035	028AA00022	028AA00036	GRUB FILL	ANGLIAN		49377620	47713654	3143	170	58	14	A lighter, more sandy fill first seen in the south-ea
028AA00036	028AA00022	028AA00036	GRUB CUT	ANGLIAN	SUB-RECTANGULAR	49377622	47713776	3117	436	349	38	Cut of grubenhaus. The cavity was cut into natural
028AA00037	028AA00024	028AA00039	GRUB FILL	ANGLIAN	IRREGULAR	49378268	47713193	3141	150	270	7	Fill of Grubenhaus 28AA24, sealed below layer 28
028AA00038	028AA00024	028AA00039	GRUB FILL	ANGLIAN	SUB-RECTANGULAR	49378221	47713243	3141	200	260	11	Fill of Grubenhaus 28AA24, sealed below stone de
028AA00039	028AA00024	028AA00039	GRUB CUT	ANGLIAN	SUB-RECTANGULAR	49378130	47713322	3109	400	300	36	Cut of Grubenhaus 28AA24, located in SE part of
028AA00040	028AA00023	028AA00058	GRUB FILL	ANGLIAN	SUB-RECTANGULAR	49377672	47713413	3145	136	120	14	Lower fill 28AA 0023. sandy deposit of mottled, m
028AA00041	028AA00023	028AA00058	GRUB FILL	ANGLIAN	UNCLEAR	49377755	47713564	3145	90	70	12	Small patch of lighter sand in SE corner of 28AA0

Figure 61 Context number 028AA00034 in the context database

Figure 61 shows the first few fields of the context database, including two which allow different types of data analysis to be carried out. The first is the Fromdraw field, which links the data table to the vectorised drawing, allowing the database to "drive" the drawing through queries (as a simple example, the drawing could be coloured according to the phase field in the database). The second is the Master field, which links a number of related contexts together. This could be all the post hole fills and cuts of a timber structure, or, as in this case, all of the fills contained within the cut of the *Grubenhaus*. Using the master number, it is possible to group together all of the finds from the different fills. The results of this are shown in Figure 62, where a query has been written to plot all of the finds from *Grubenhaus* master number 028AA00022, which contained fill number 028AA00034. The distribution of the 1301 finds from this feature can thus be graphically displayed. The location of our sherd of Anglian pot (find number 028AA00034LW) is indicated by the red arrow. Note that this is a two dimensional plan view of the finds distribution. It is also possible to view this three dimensionally, as each find is logged in the field using a total station.

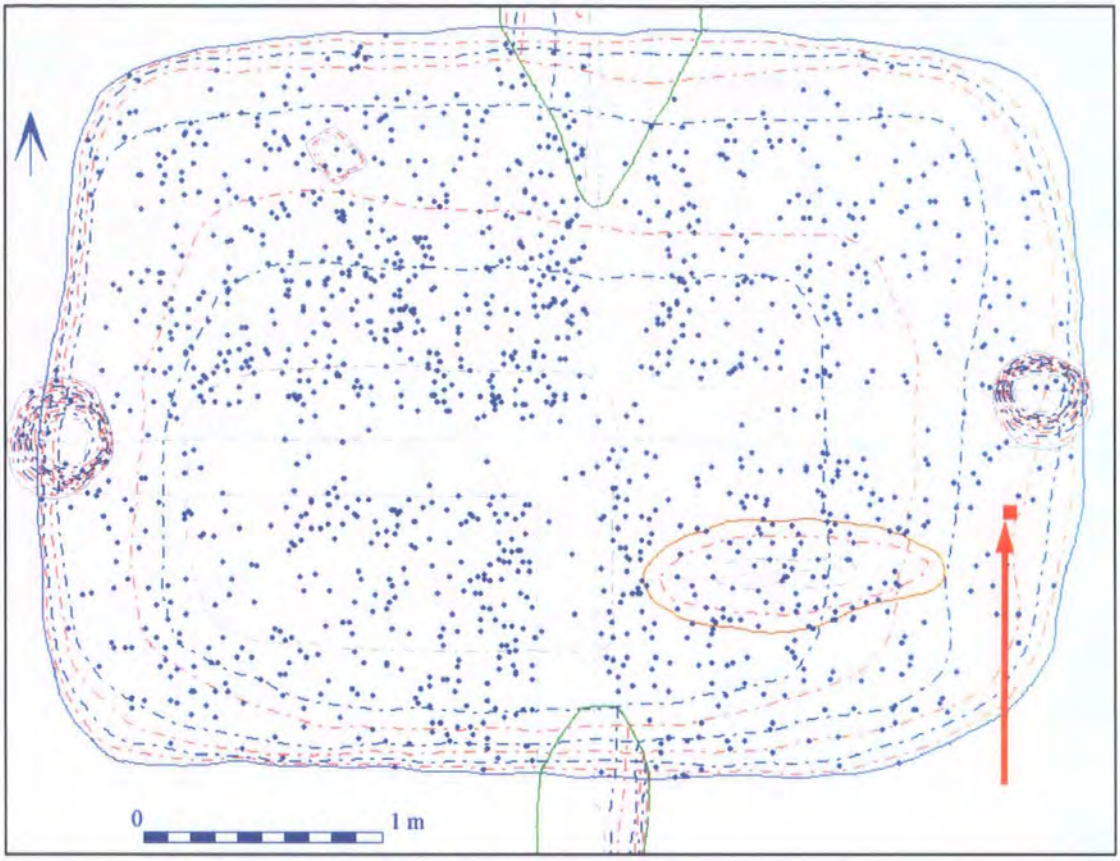

Figure 62 *Grubenhaus* Master number 028AA00022 with all finds distribution

Up to this point, we have been investigating a single feature and its related contexts and finds. However, the *Grubenhaus*, although defined and excavated as a separate entity, is of course part of a greater whole, in this case an Anglian settlement (see Figure 66).

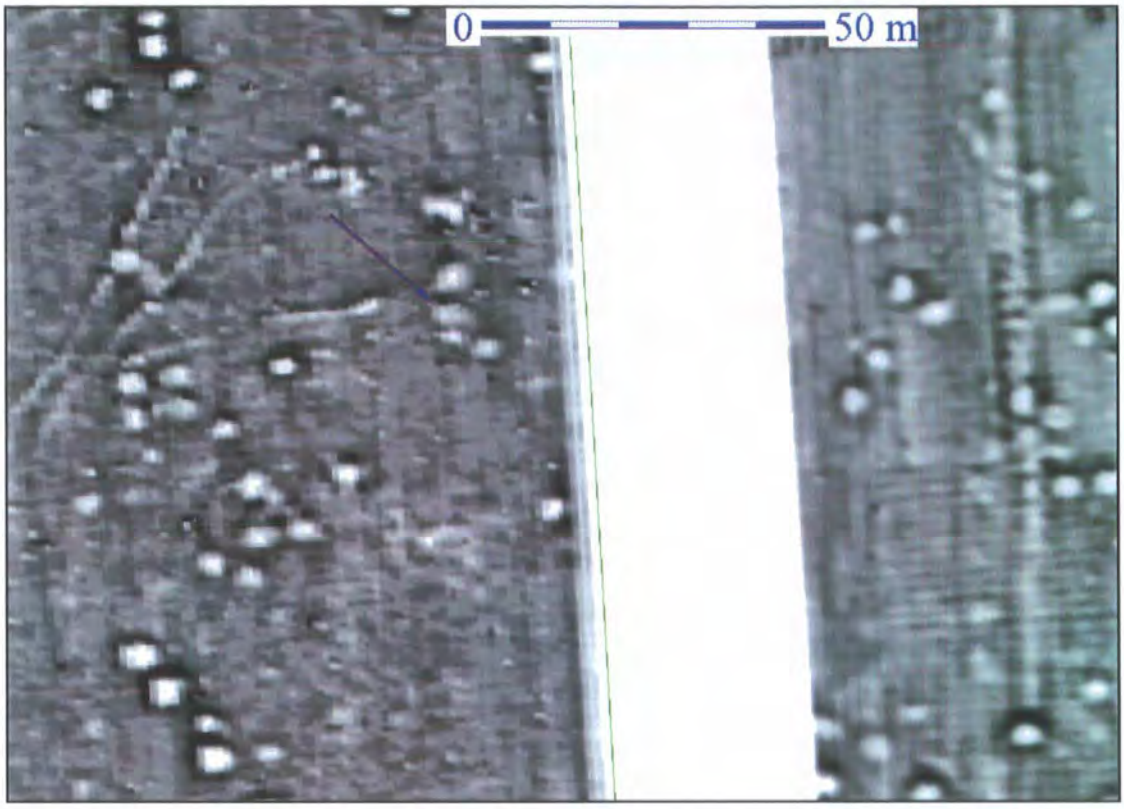

Figure 63 Fluxgate gradiometer survey showing location of the excavated *Grubenhaus* in relation to the surrounding *Grubenhäuser*

The system continues to operate using the LRC numbering technique, in this case our *Grubenhaus* has been issued with the identifier 028RS02893. The first three numbers indicate the site (028), with the second two letters (RS) indicating that it is a Remotely Sensed anomaly. The final five numbers (02893) are a unique sequence, which will not occur again in the table.

Remote Sensing Correlation Table : Table

Link_Key_ID	Fluxgate	AP	MSS_1992	Resistance	GPR	Master1	Interpretation	Group	xcoord	ycoord
028RS02891	028MA00004					028AA00024	Grubenhaus	Archaeological Activity	49378151	47713308
028RS02892	028MA00005					028AA00023	Grubenhaus	Archaeological Activity	49377629	47713473
028RS02893	028MA00006		028MS00051			028AA00022	Grubenhaus	Archaeological Activity	49377627	47713796
028RS02963	028MA00076					028AB00077	Barrowlet	Archaeological Activity	49377683	47726099
028RS03457	028MA00570					028AC00111	Trackway	Archaeological Activity	49376066	47729481
028RS03458	028MA00571		028MS00014			028AC00055	Enclosure Ditch	Archaeological Activity	49361187	47727055
028RS03475	028MA00588					028AC00071	Enclosure Ditch	Archaeological Activity	49377490	47729609
028RS03543	028MA00656					028AC00027	Enclosure Ditch	Archaeological Activity	49377617	47728582
028RS03544	028MA00657					028AC00049	Enclosure Ditch	Archaeological Activity	49378155	47728789
028RS03625	028MA00738					028AB00120	Barrowlet	Archaeological Activity	49378113	47725590

Figure 64 An extract from the remote sensing correlation database

In Figure 64, the Master1 field indicates that the feature has been excavated, and provides the link into the excavation data tables, as well as into the main correlation data table, so that it is possible to see whether the excavated feature was detected by any

form of remote sensing. It can be seen that anomaly number 028RS02893 is present in both the fluxgate gradiometer record and in the multispectral data, but was not represented by a cropmark (AP). Neither resistivity nor ground penetrating radar was carried out over this area, so there is no correlation data for these techniques.

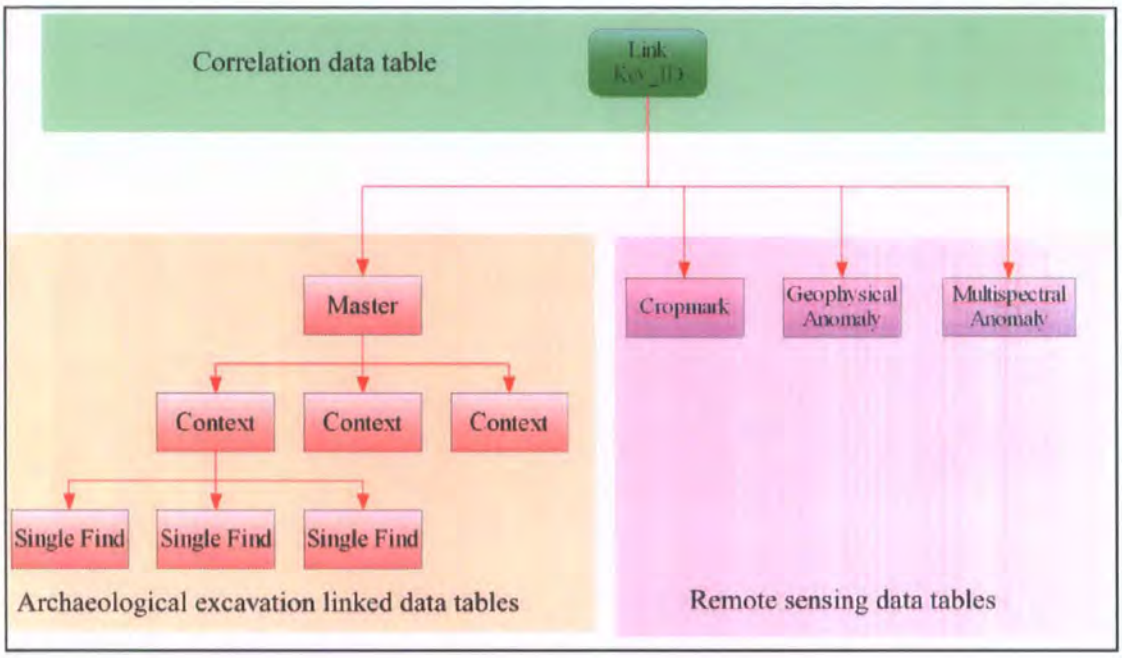

Figure 65 Flowchart indicating one to many links from related data tables

The links between the related data tables is graphically illustrated in Figure 65, where the unique Link Key_ID has a one to one relationship with the Master number in the excavation data table and a one to one link to the Key_ID fields in each of the remotely sensed data tables. The Master number in the excavation data table has a one to many relationship with the context field, which in turn has a one to many relationship with the object record table.

In order to allow large groups of related features to be viewed as a single entity, a master group number field was created. This allows features or anomalies which occur over multiple sites, but which are obviously related (in this case study the 224 *Grubenhäuser* from the Anglian settlement) to be grouped together. This permits all of the related features to be displayed as a unit, as in Figure 66. Note that this allows a

different type of analysis to be undertaken, where our *Grubenhaus* can now be seen to be part of a coherent and spatially limited whole, with the potential for localised or site-based study.

At first glance, all of the *Grubenhäuser* may appear to be spread at random across the area, but closer inspection reveals that some of them are grouped in small clusters, either linear (towards the western edge of the settlement) or in small localised groups. A few outliers can be seen to the north of the main grouping, within a late Iron Age/Romano-British ladder settlement, and these may indicate that the earliest *Grubenhäuser* were established within a later Romano-British context. Note that by stepping out a level we are now able to imply that the location of the Anglian settlement is referenced to an earlier settlement type, which was probably still in existence in some form when the first of the distinctively different *Grubenhäuser* structures were constructed.

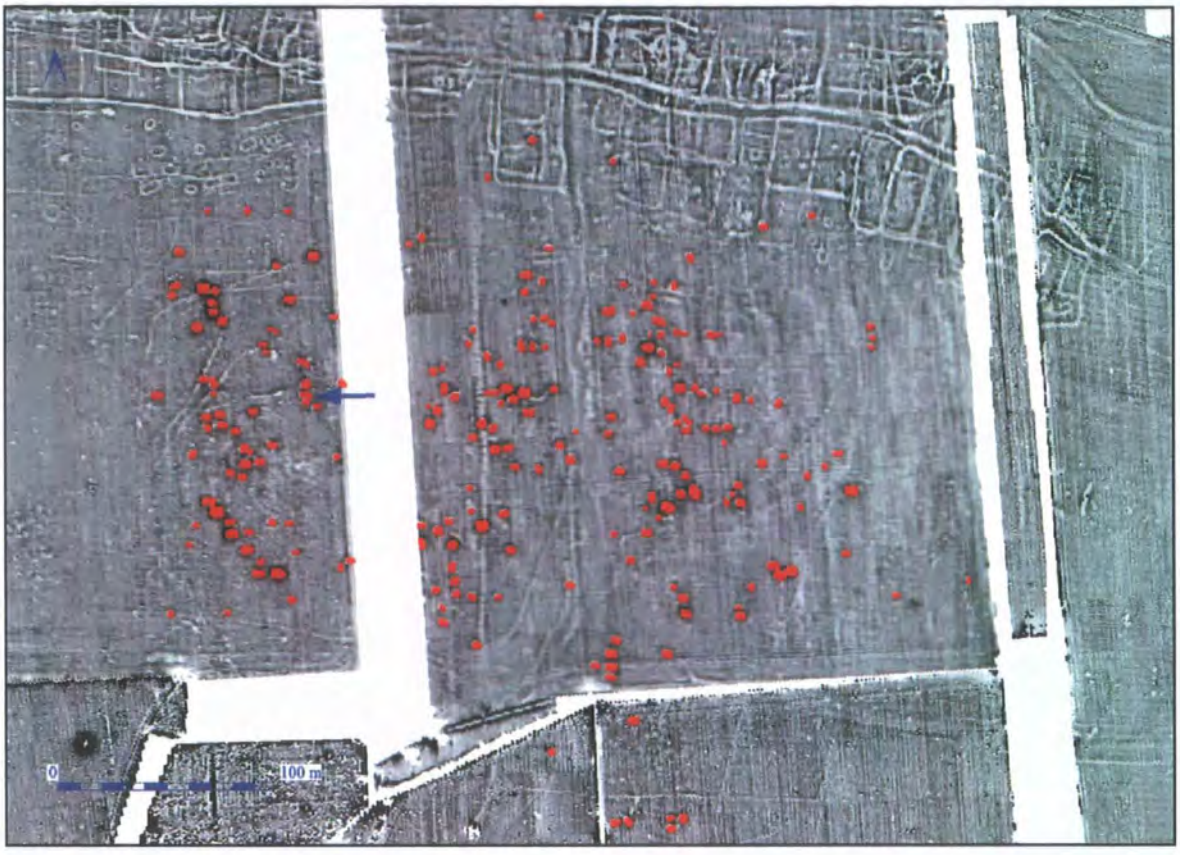

Figure 66 An Anglian settlement grouped together using a Master grouping field

One of the most important reasons for maintaining a strong link with the excavation data is to allow this data to feed back into the remote sensing data tables.

All of the initial interpretation of remotely sensed data is hypothetical to a greater or lesser degree, depending on the anomaly being analysed, and the type of interpretation being attempted. The interpretation of archaeological feature type is primarily based on the morphology of the anomaly, although its context (i.e. its relationship to nearby anomalies) is also of importance in the early interpretative stages. Therefore, the ability to tie in phasing data from targeted excavations across the area is essential, either to help confirm or deny any initial hypotheses, as well as in allowing a certain amount of extrapolation to be applied to other anomalies which appear similar in character to the excavated examples.

Figure 67 Three *Grubenhäuser* fully excavated

In our test case, the excavated features all proved to be fairly typical *Grubenhäuser* in their shape and form (Figure 67), with all three having two post holes in the eastern and western shorter ends. Anglian material (including glass beads, pottery and bone comb fragments) was recovered from each of the features. This confirmed the initial interpretation, and allows the extrapolation of the feature classification to be extended to the others in this master group. However, although this helps to increase the confidence in the interpretation, the possibility must always remain that some of the anomalies, while having the same magnetic (or spectral, or electrical, depending on the original dataset) characteristics of their surrounding partners, may have a totally different archaeological origin.

In order to understand the Anglian settlement in its local context, we need to extend our area of investigation by a factor of two or three. Anglian settlements invariably have an associated cemetery, which in many cases are deliberately located on (situated, referenced to) older monuments, including Neolithic henges, Bronze Age round barrow cemeteries and Iron Age square barrow cemeteries (Haughton and Powlesland, 1999, p.3). By their nature, cemeteries are usually difficult to detect using remote sensing techniques, as after the interment of the body, grave pits tend to be quickly backfilled with the same material which has just been removed from them. Most forms of remote

sensing (or at least those used for archaeological prospection) work by finding a difference in the general background readings and those which fill a specific feature, so graves are usually invisible, especially to magnetic techniques. However, the older monuments which form the focus for the Anglian cemeteries tend to be detectable using different remote sensing techniques, and so a scan through the data can, if not pinpointing the exact position, at least provide a number of locations which are the most likely to contain the cemetery.

Figure 68 Potential locations for the Anglian cemetery associated with the settlement

Figure 68 demonstrates that at least two locations are possible for the Anglian cemetery related to our settlement. The first is some 630 metres to the south-west of the settlement, and is centred on a hengiform monument, probably established some time in the middle Neolithic period. Although no evidence for this monument exists on the ground surface today, it would certainly still have been visible during the Anglian

period. At the excavated Anglian settlement and associated cemetery of West Heslerton located 3.2 km to the south-east, exactly this situation occurred, where another Neolithic henge monument also provided the focus for a later Bronze Age round barrow burial complex. The Anglian cemetery used these earlier prehistoric monuments as a means of expressing a form of continuity with an older system, breaking away from Roman and Romano-British burial tradition.

The second possible location for the Anglian cemetery is some 445 metres to the south of the settlement, and is a complex set of Bronze Age funerary monuments, including round barrows and other more enigmatic features. Again, although no remains are now visible above the ground surface, the round barrows would have stood perhaps over one metre tall when the Anglian settlement was originally founded. A third option could be that both of these areas were used.

Up to this point, we have been treating a set of archaeological features as belonging to a specific "site". However, Anglian settlements did not exist in isolation, and it is here that remote sensing techniques come into their own, allowing an analysis of the wider landscape to define the settlement patterns within a given area. In a magnetic survey which covered more than 8km by 1km, it was possible to begin to see these patterns emerging. It should be restated here that these settlements are defined purely by the identification of magnetic anomalies interpreted as *Grubenhäuser*, as neither graves nor post hole structures can normally be found using this technique. In addition to the excavated settlement at West Heslerton (numbered 1 in Figure 69), two more major Anglian settlements were discovered, each just over 2.1 kilometres apart (numbered 2 and 3 in Figure 69). The *Grubenhaus* used in this case study is located near the western edge of settlement 2. What was even more unexpected was the discovery of at least 10

smaller settlements (numbered 4 to 13 in Figure 69), located between the larger settlements.

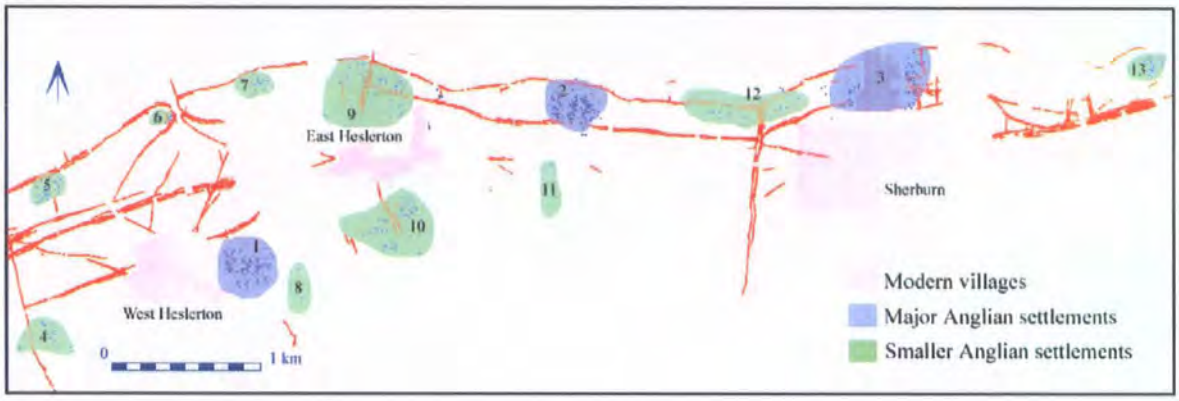

Figure 69 Major and minor Anglian settlements in relation to the modern villages

These were not necessarily all the same type or even the same phase of Anglian settlement, as the numbers of *Grubenhäuser* within them varied from 8 to 117 (see Table 15).

Master Type	No	Grubs	Excavated	Density per Ha	Area
Major Anglian settlement	1	136	133	12.91	10.535
Major Anglian settlement	2	224	3	25.67	8.726
Major Anglian settlement	3	153		19.08	8.02
Dispersed Anglian Settlement	4	35		17.17	1.98
Dispersed Anglian Settlement	5	62		21.38	2.9
Dispersed Anglian Settlement	6	25	2	40.3	0.62
Dispersed Anglian Settlement	7	37		21.76	1.7
Dispersed Anglian Settlement	8	8		11.9	0.67
Dispersed Anglian Settlement	9	117		6.08	19.23
Dispersed Anglian Settlement	10	81		8.2	9.87
Dispersed Anglian Settlement	11	12		5.66	2.12
Dispersed Anglian Settlement	12	45	1	3.24	13.87
Dispersed Anglian Settlement	13	67		33	2.03

Table 15 The relative numbers of *Grubenhäuser* as defined by settlement type

The definition of settlement as either major or dispersed was not based solely upon the number of *Grubenhäuser* detected, although this was the major criterion, but also on the relative density of the features, with the major settlements having a large number of *Grubenhäuser* within a relatively confined area, and the dispersed settlements having less *Grubenhäuser* spread over a wider area. Even so, there is no hard and fast rule, as

dispersed settlements 5, 6 and 7 were all quite densely packed within their relatively small areas. Conversely, settlement 9, while containing 117 anomalies interpreted as *Grubenhäuser*, was spread over a much more extensive area. The remote sensing evidence points to a much more populated landscape than has heretofore been imagined, and the different settlement types hint at a more complex social structure, even in the early Anglian period. Settlement number 10 is located to the south of the Medieval village of East Heslerton, and could belong to a Middle Saxon phase, rather than the immediate post-Roman period.

See Results (Case study area 2) for a more in depth analysis of the returns from different forms of remote sensing for the Anglian settlement, and Discussion (A new understanding of Anglian settlement patterns) for discussion on the impact of these discoveries.

5.5 Image Classification

The use of computer software programs to automatically classify images has developed from the need to utilise the immense resources provided by satellite imagery. Traditionally, the data from satellite images have been low resolution but covering vast areas, making scanning through the images extremely time consuming. To this end, a number of classification routines have been devised, primarily to assist the detection of geological (Haralick et al, 1973) and vegetation (Vuorela, 1997) differences in the data.

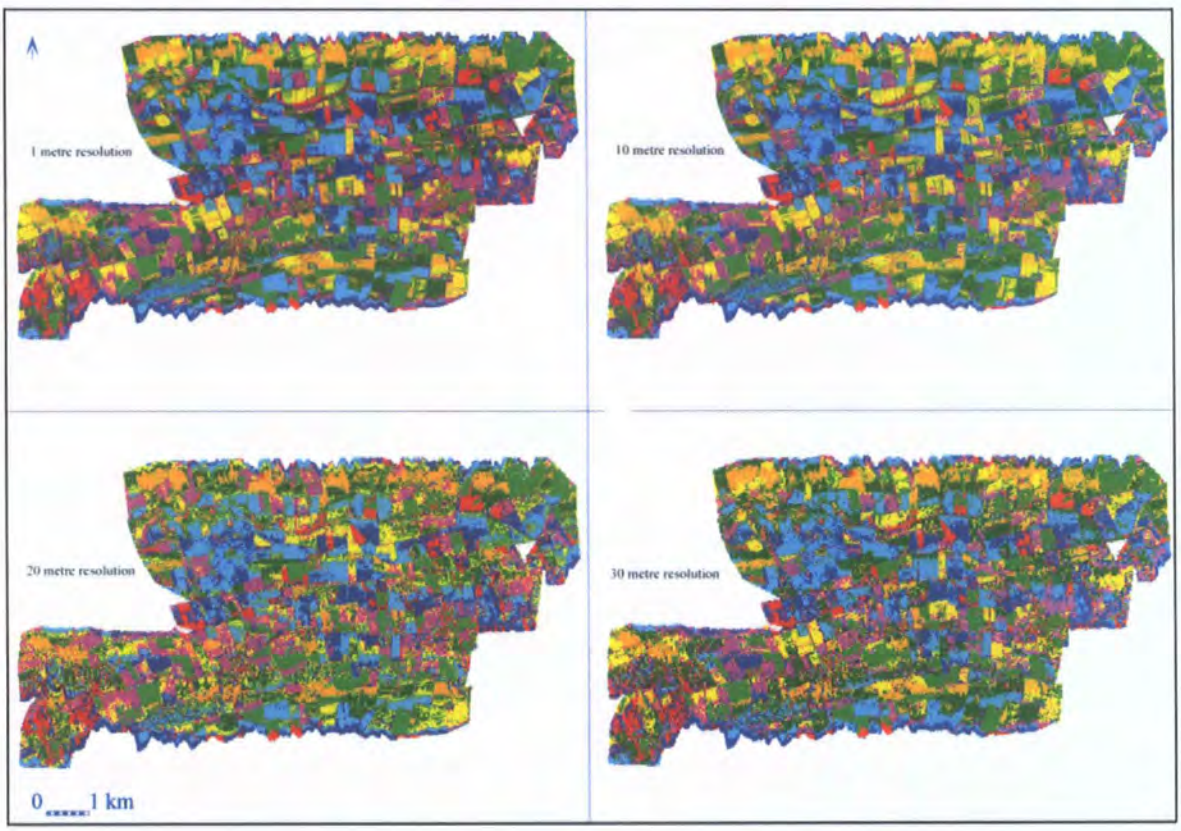

Figure 70 The returns from an unsupervised classification using different resolution data

The multi spectral data was prepared in Imagine, taking the original 1.5 metre AZ16 ATM data and then subsampling this to 10, 20 and 30 metre resolutions. The same unsupervised classification routine was then run on each of the images. In this case, the routine was set to extract only 8 classes from the image data, as we wanted to maximise the potential to extract different crop information.

The results of an unsupervised classification routine can be in Figure 70 and Figure 71, where the algorithm has been able to detect the different crop types with a reasonable degree of success. In general, the returns were very similar for each of the different resolutions, and it was possible to extract crop types with relative ease.

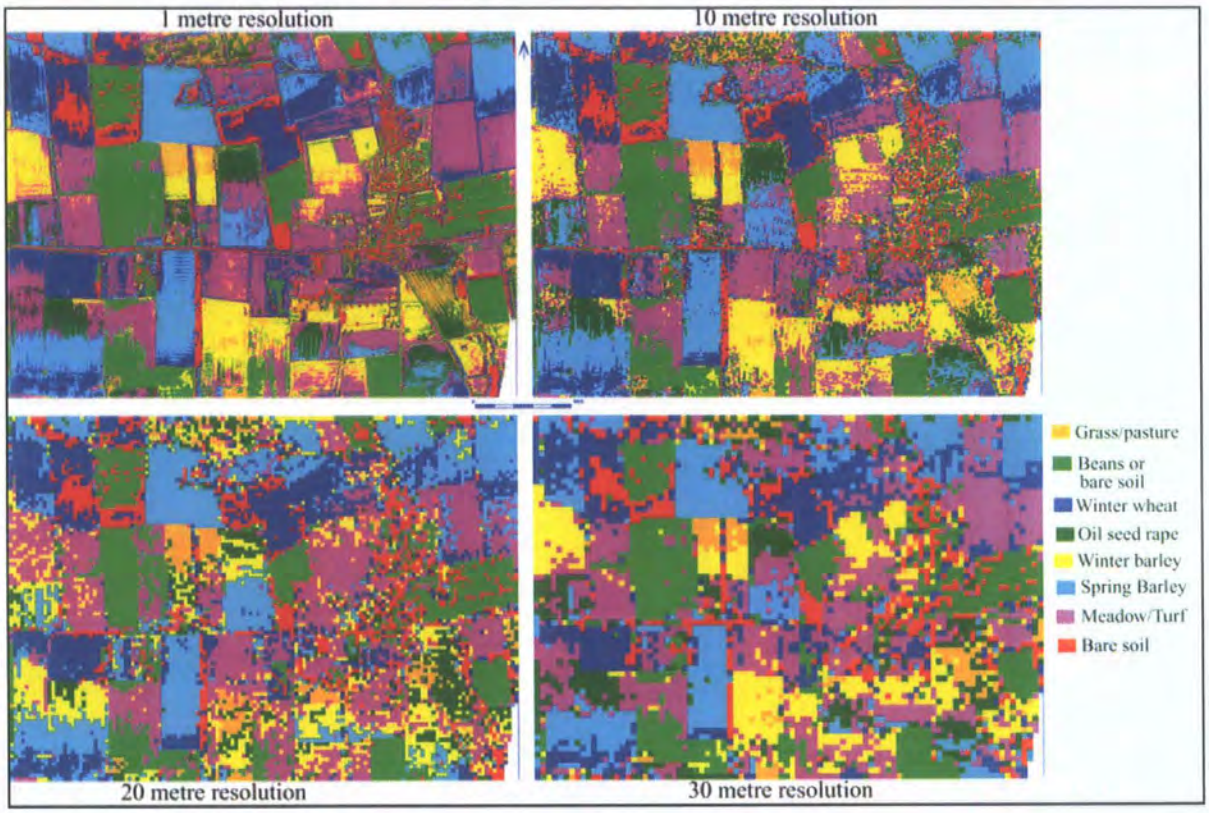

Figure 71 Zoomed view of unsupervised classification using different resolution data

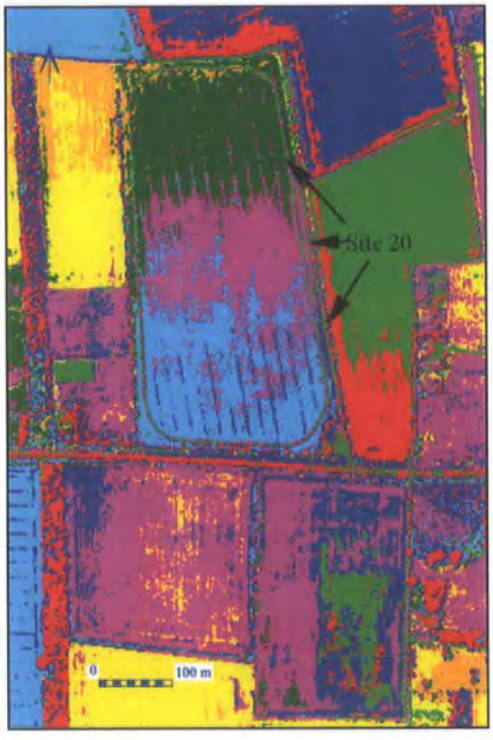

Figure 72 Site 20 showing anomalous crop classification

However, certain areas gave apparent classification errors, that is a number of different classes in the same field were generated even when it was known that the same crop was present. This can be seen clearly in Figure 72, which shows site 20 with three different classifications from south to north. This image can be directly compared with Figure 74, which

is an aerial photograph of the same area in 1992.

While classification routines can identify broad differences in underlying geology or the type of crop growing in a field, the classification of archaeological features presents a different set of problems. For a number of reasons most classification routines do not generally work well here in the highly agricultural temperate zones of the United Kingdom, and specifically not in areas with complex drift geology, as is the case in the Vale of Pickering. Firstly, anomalies of archaeological origins tend to have similar characteristics to the surrounding area, with differences smaller than those that classification routines are designed to look for. If all of these tiny differences were to be selected for classification, then the hundreds or thousands of classes which result become meaningless, at least for archaeological feature detection.

Secondly, the different drift geologies which interact at the foot of the Wolds mean that the response of both crops and cropmarks can vary considerably, even within the confines of a single field. These drift geologies can include pure sand (both soft and sharp varieties), sand and calcareous gravel, sand and silicaceous gravel, hillwash and clay, as well as combinations of any of these parent materials. Outcrops of chalk and relict stream channels are also present to further complicate matters. An example is shown in Figure 73 (part of the excavated area comprising sites 2, 11, 12 and 13), where it is possible to pass over six different drift geologies in less than 200 metres. The soil types shown in Figure 7 are indicated on the left in Figure 73.

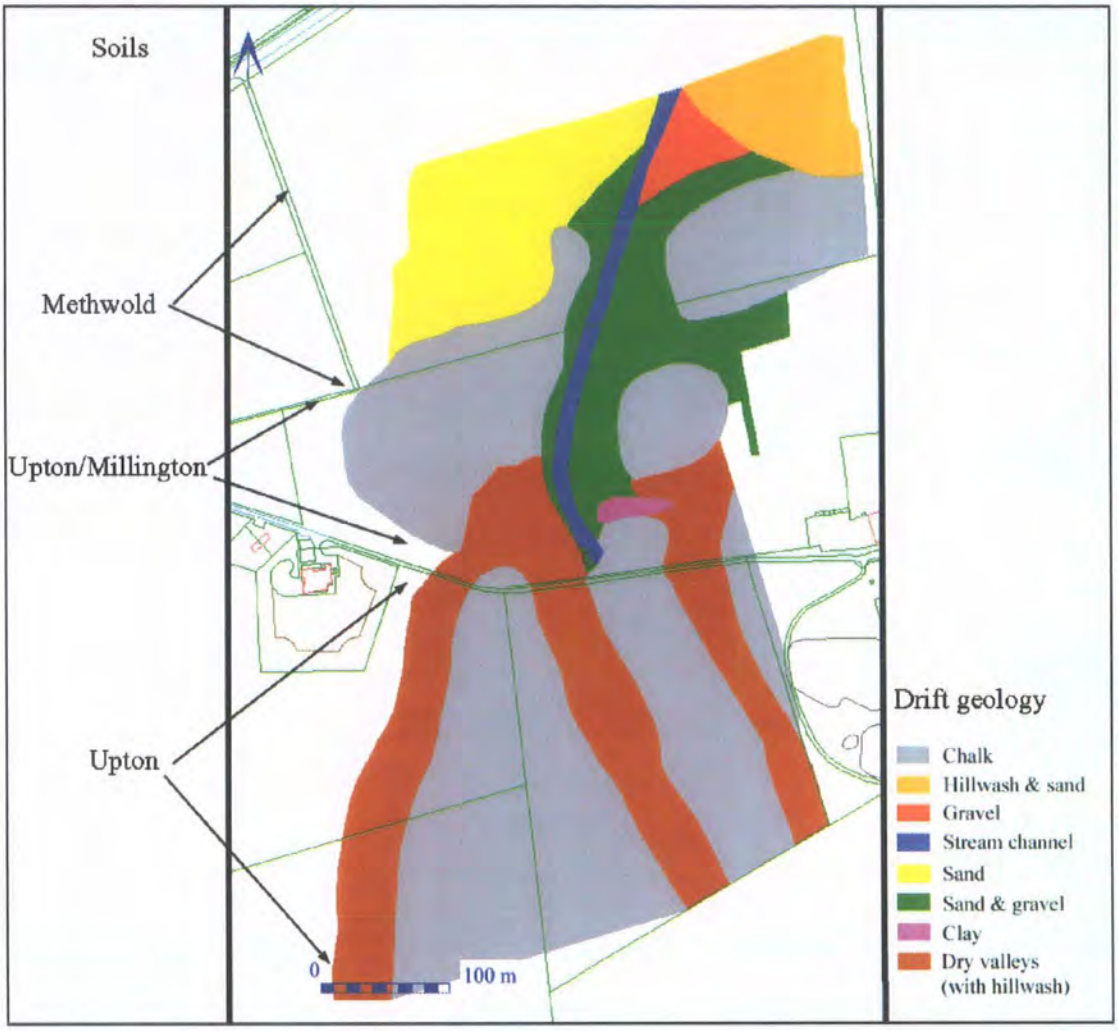

Figure 73 Drift geology changes over a small area

The effect of many different factors on cropmark formation is visually represented in Figure 74 (site 20, case study area 4), which shows that even though planted with the same crop, the field to the north of the road shows three areas of distinctly different crop response, with cropmarks relating to a trackway noted only in the southern part of the field. The trackway is known to continue northwards in this field, joining in to an east-west aligned ladder settlement. One of these factors relates to plough damage, and in this case the main plough damage to archaeological features has occurred in the south, thus providing readily visible cropmarks. Secondly, the crop response varies over the different underlying drift geology with windblown sand potentially inhibiting the early formation of cropmarks, and multiple flights would have been necessary to document these changes. The area in the north of the field is near the boundary of the sand and

calcareous gravel zone and the more organically enriched peaty zone to the north, and as such may retain moisture for longer, preventing crop stress and thus also preventing the development of cropmarks. The trackway can also be seen in the field to the south, again very clear in the northern part of the field, before fading towards the south.

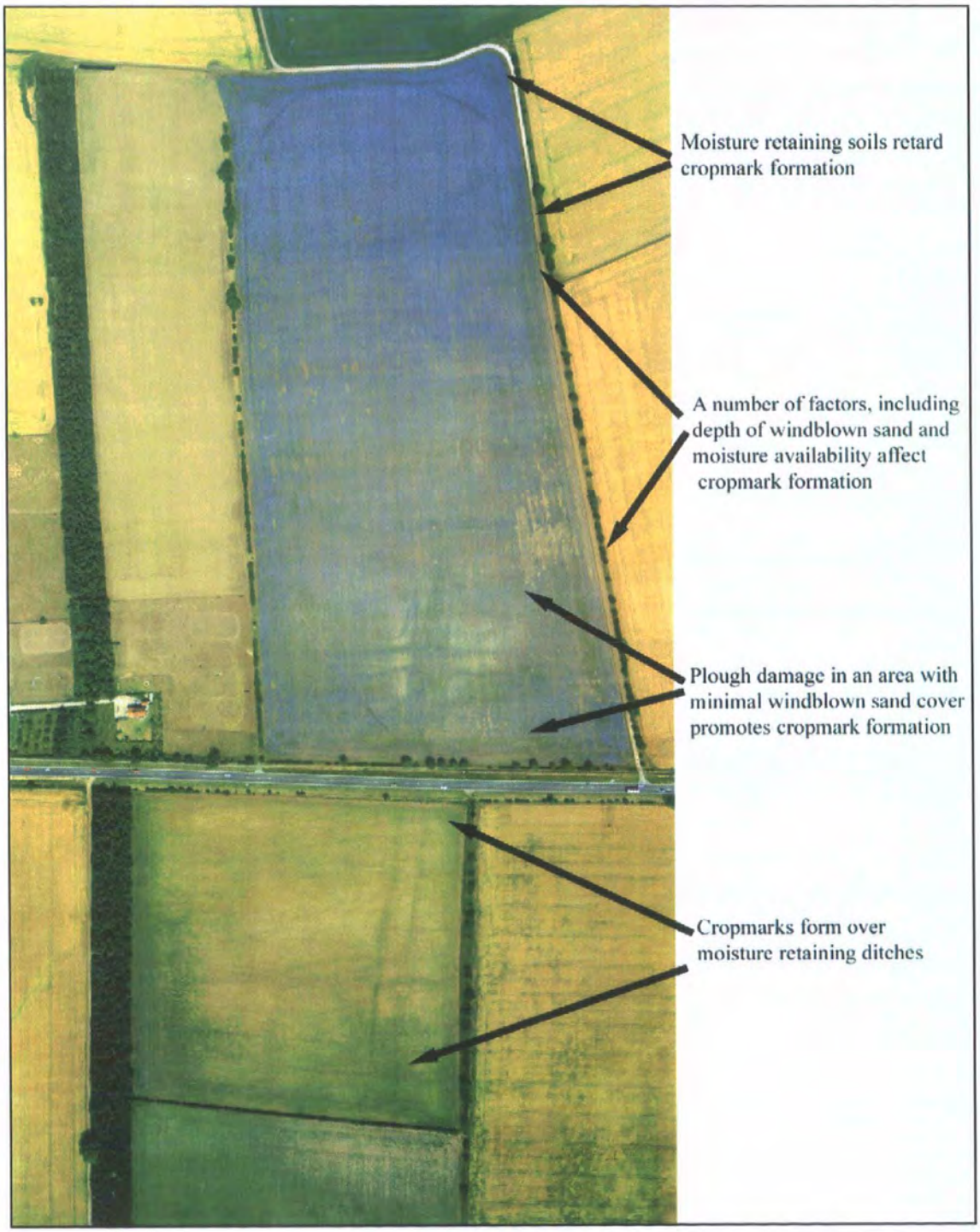

Figure 74 Different cropmark response under different soil conditions (source NERC June 1992)

5.6 Health Warnings

It is sometimes very easy to look at the returns from multispectral imagery and get that sudden feeling of elation at finding a "new" site. While this does happen, it is important to remember the limits of the data with which you are dealing. Two examples will be used to show how easy it is to be fooled into making false assumptions.

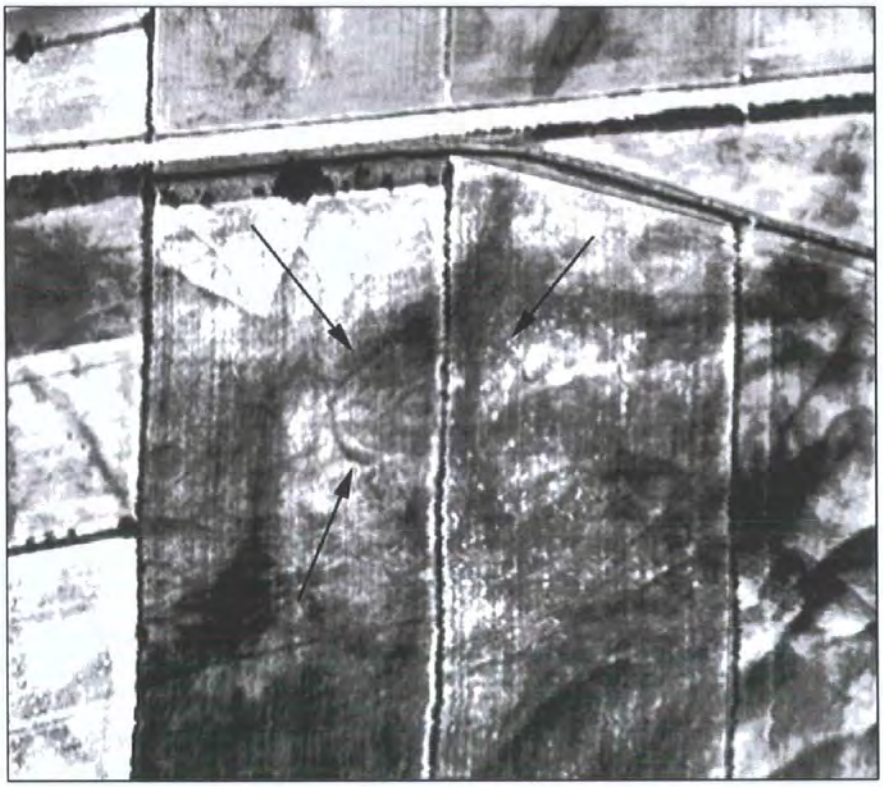

Figure 75 Arrows indicate the location of the putative hengiform feature (Thermal band 11 raw data)

Figure 75 shows a large, roughly circular feature (indicated by black arrows) in the thermal band of the ungeoreferenced 1992 ATM data. This was initially interpreted as a possible hengiform feature with a small internal circular anomaly, located in the alluvial sand and gravels (with desiccating peat deposits) of zone 5. The linear anomalies visible in the image are the result of glacial action. It was believed that full georeferencing would elucidate the true shape of the feature.

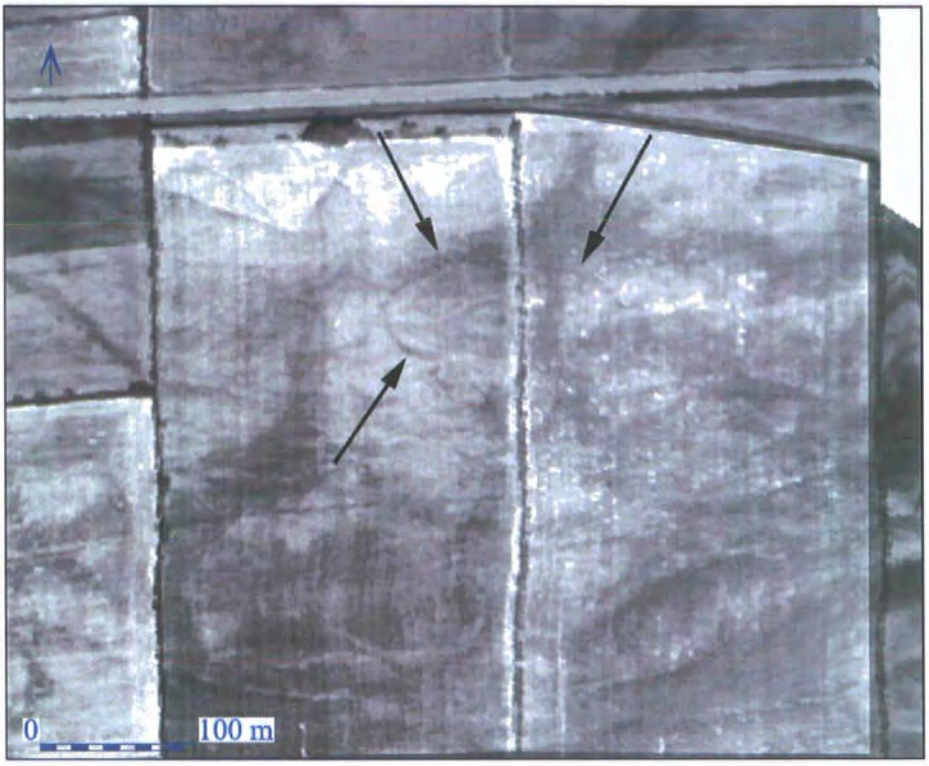

Figure 76 Georeferenced view of putative henge

However, when the image was georeferenced, a completely different picture becomes evident, where what appeared to be a roughly circular anomaly is now 151 metres long by 62 metres wide. While it remains an unusual feature in this area, and may well be of archaeological significance, its initial interpretation as a potential hengiform structure is now questionable.

The second example uses data collected in 2005. When analysing both the ATM and CASI data, this feature (see Figure 77) was visible, and was initially interpreted as a possible barrow.

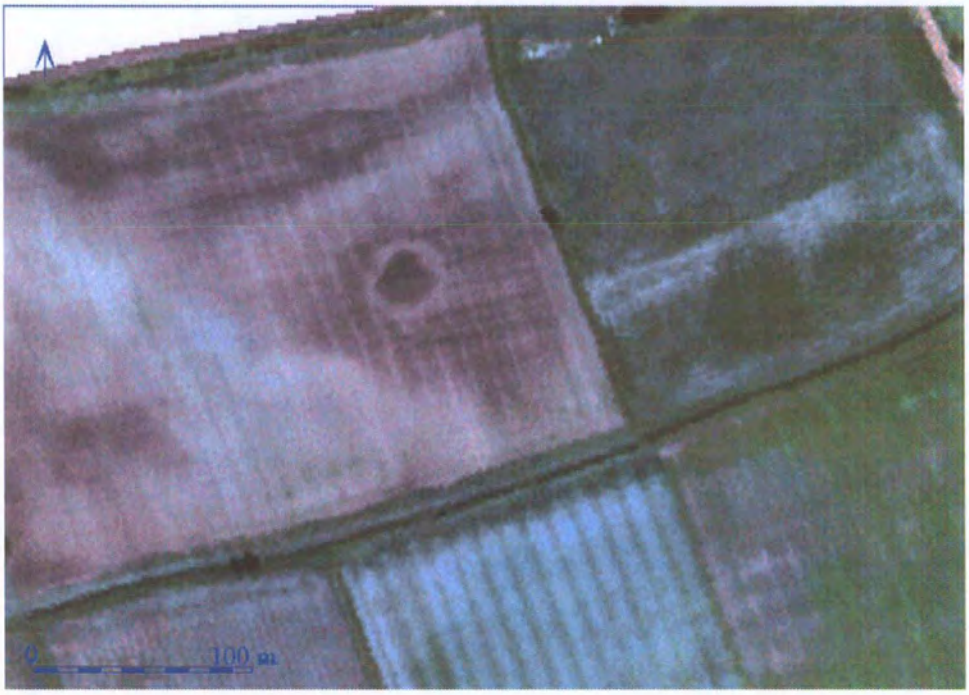

Figure 77 Possible barrow identified in ATM 2005 data (false colour image)

It was a slightly unusual shape, and appeared in virtually all of the bands from both the ATM and the CASI data.

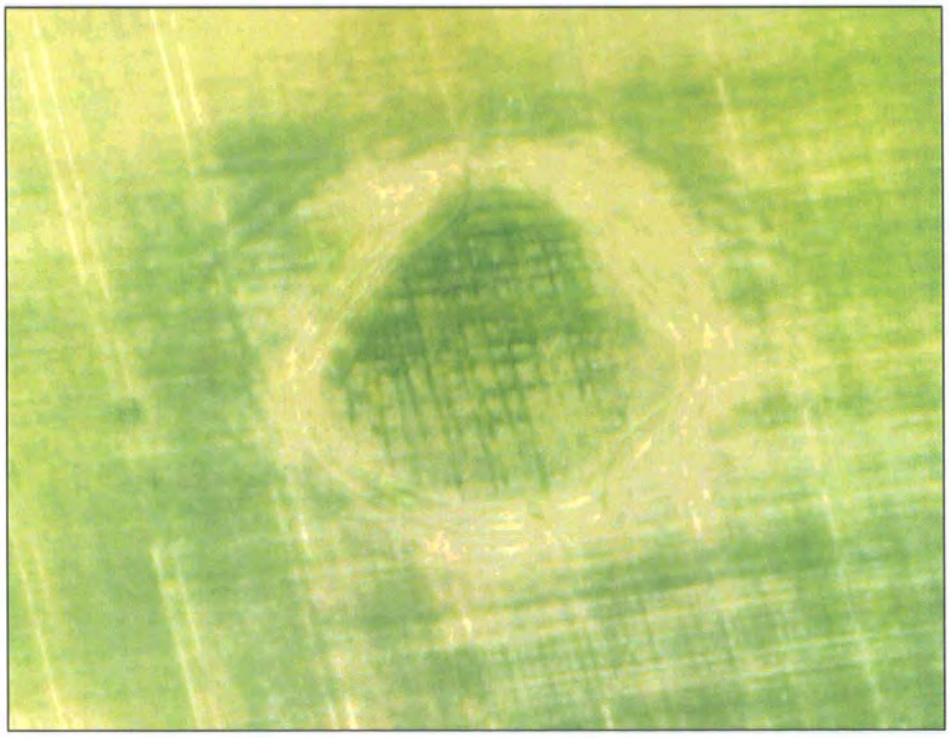

Figure 78 Possible barrow revealed as tractor tracks in the field

The true nature of the feature was revealed when looking at the higher resolution digital photographs taken at the same time. It was clear that the "feature" was nothing more than a series of tractor tracks flattening the crop.

Chapter 6 Results

6.1 The June 1992 multispectral results

It was immediately apparent that three of the bands from the 1992 multispectral image would be of very limited use in the detection of archaeological features. These were bands 1, 2 and 9 (see Figure 79), which uses the eastern part of case study area two (site 27) to demonstrate the differences in return. The grainy nature of the imagery from these three bands made any feature detection difficult, although the main anomalies can be seen in band 2, with some smaller anomalies also visible in band 9. However, all of these anomalies were present in the adjacent bands of the image, and so no quantitative data was lost by discarding these three bands.

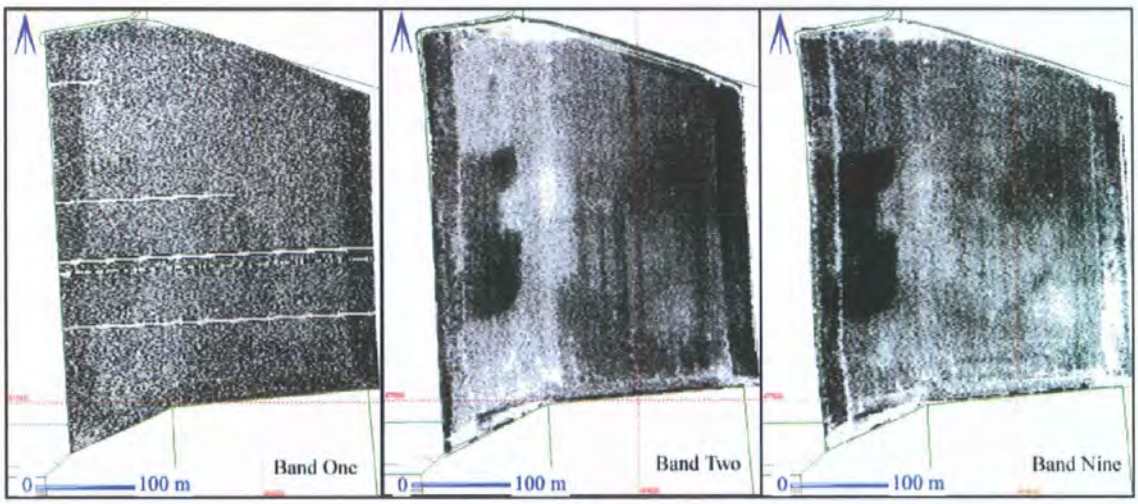

Figure 79 The three bands which were discarded centred on Site 27

Apart from georeferencing the image and giving each image a cursory inspection, no further work or enhancement was carried out on the images from these three bands.

Of the remaining visible bands, band 5 proved to be the most responsive, at least in terms of archaeological cropmark formation. As band 11 responded well to a standard deviation enhancement, this band was chosen to represent the thermal response. Band 12 (also thermal but with half of the gain settings on acquisition) could equally have

been chosen, but there was virtually no difference in the returns from these two thermal bands after enhancement of the images (see Figure 80).

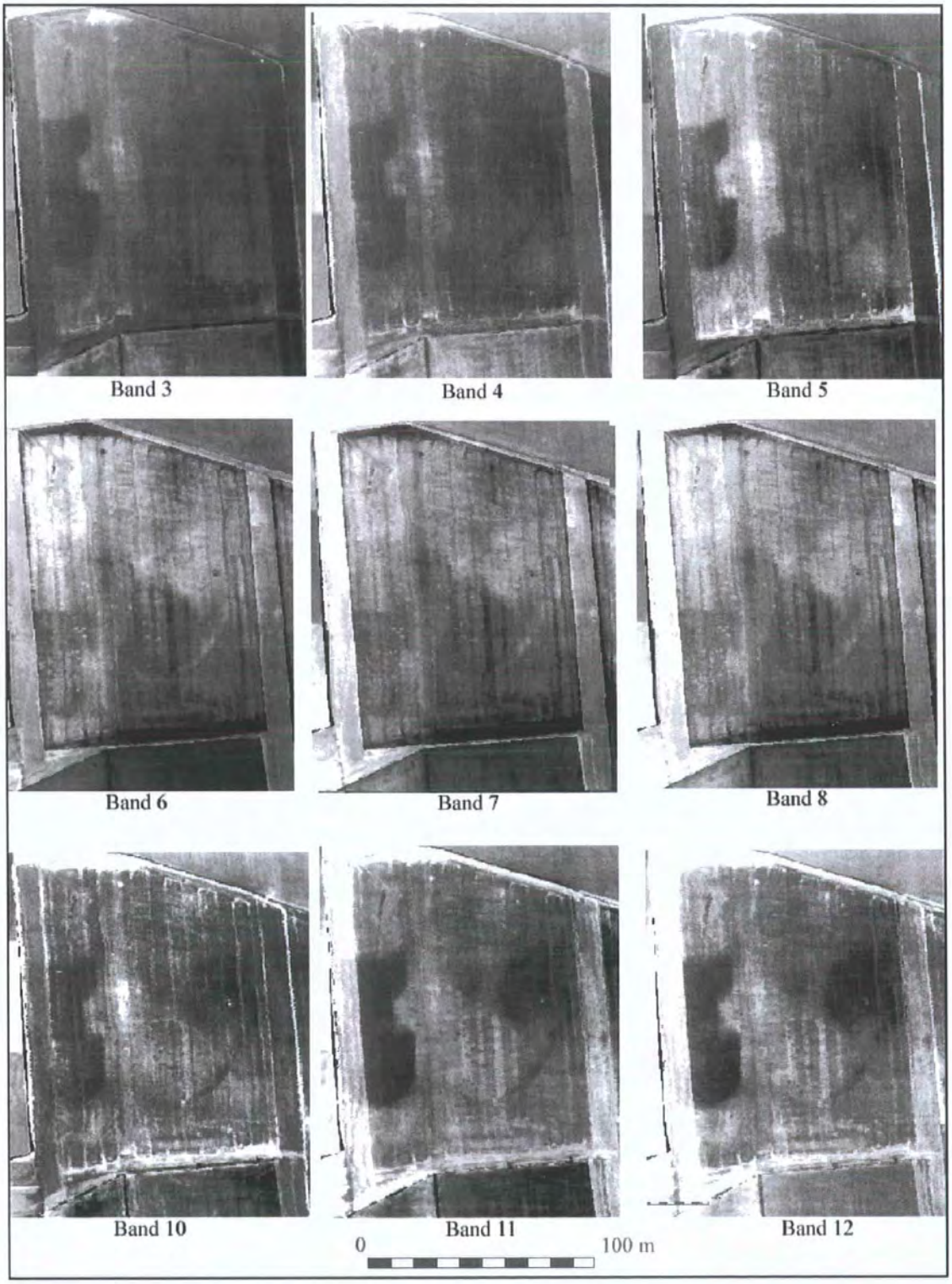

Figure 80 The remaining bands centred on Site 27

6.2 Timing of the data collection

It has long been known that cropmark formation is dependent on a number of factors, with probably the most important being the amount of water available to the root systems, both during the early stages, when strengthened root development will give greater access to water during times of deficit, and again as the crop approaches maturity. This becomes very apparent during times of crop stress, when the extra moisture available to crops located above pits and ditches leads to increased growth, denser foliage and a deeper green colour, relative to the plants unable to access the extra water. The best cropmarks develop at this time, and the same restraints are present for the visible wavelengths of the multispectral data.

However, it was thought that thermal data would not be quite so tied down to the same window of opportunity as the visible wavelengths. It was something of a shock therefore, to discover how much a 10 day difference made even to the returns in the thermal wavelengths (see Figure 81)

The first data acquisition flight (on 17/06/1992) was marred by sporadic cloud cover, and the mission was called off after only two runs. The second flight was carried out on the 27/06/1992, with no cloud cover. However, much of the data over the Vale from the first flight was not affected by cloud cover, and this allowed an opportunity to compare the returns from two flights with close chronological acquisition, at a time when cropmark formation is in a critical phase. This was done for site 27, the eastern part of case study area two.

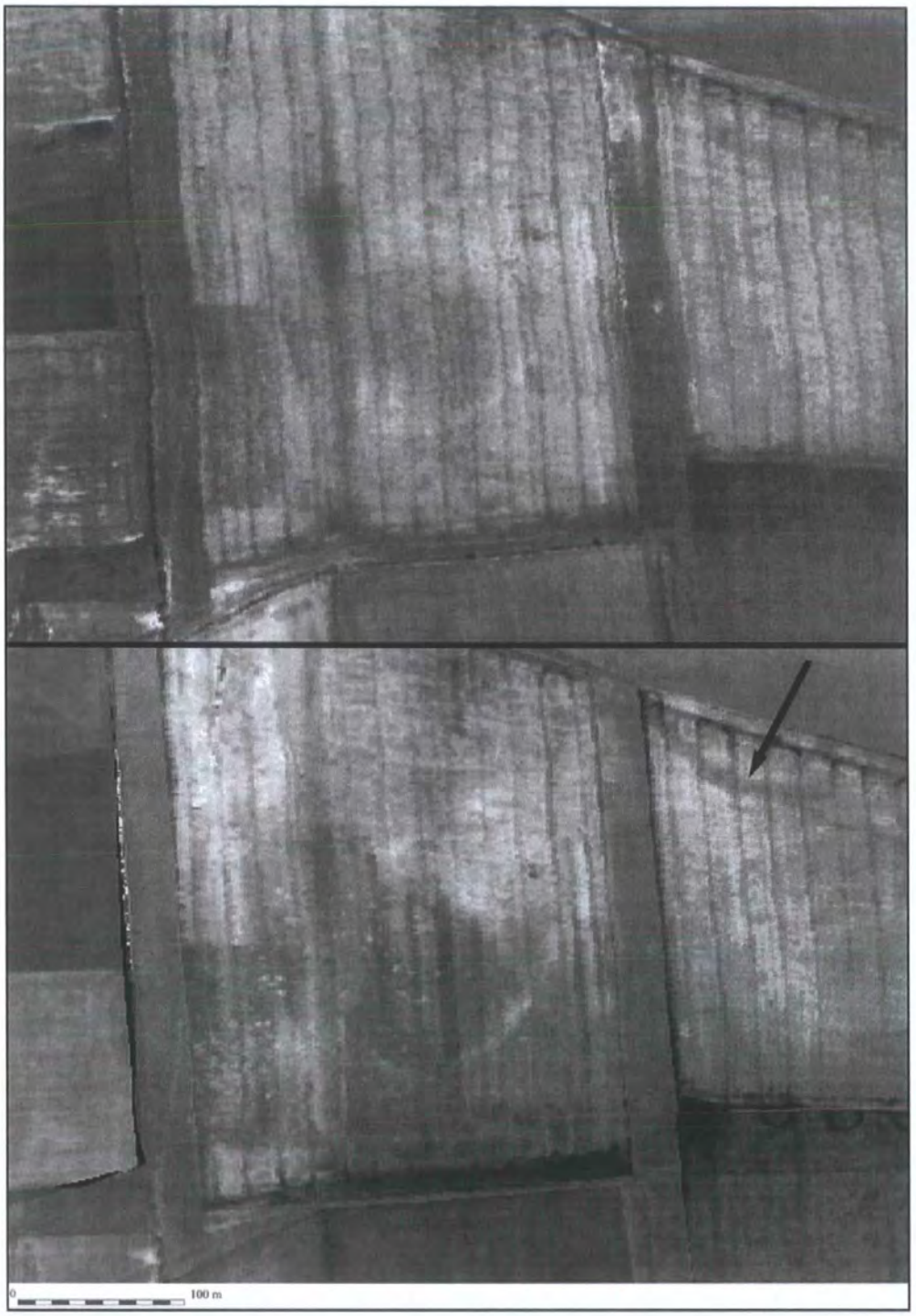

Figure 81 Data from band 7 (near infrared) collected on the 17/06/1992 above and on the 27/06/1992 below

Figure 81 clearly shows that in the crucial 10 days between the initial (upper) collection on the 17 June and the second (lower) collection on the 27th June that the crop response had changed markedly. Although atmospheric distortion has not been corrected for between the two images, it is unlikely that any significant anomalies would not be detected if they were present in the data. In the eastern part of the image (part of site

037), the late Roman drainage ditch located to the north of the ladder settlement is only just visible on the 17th June, but is clearly seen splitting (indicated by the arrow in Figure 81) into two parts (known to have this characteristic from the gradiometery data) on the data acquired on the 27th June.

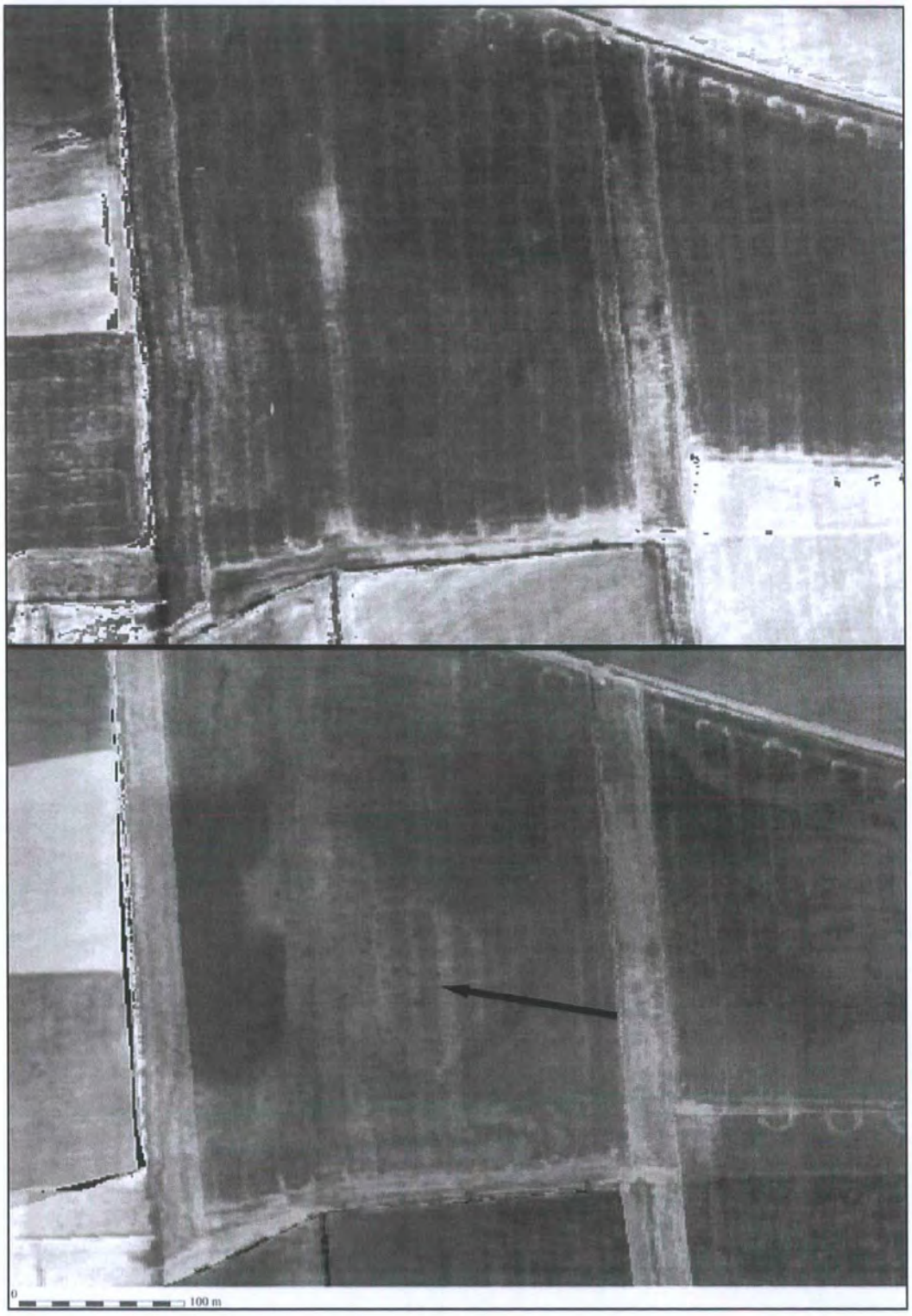

Figure 82 Data from band 11 (thermal) collected on the 17/06/1992 above and on the 27/06/1992 below.

Even the thermal band 11 (Figure 82) shows a completely different response over the 10 day period. The *Grubenhäuser* clearly visible in the 27 June data (a number of darker i.e. colder anomalies indicated by the arrow) are not detectable in the 17 June image. The ladder settlement linear anomalies show a similar difference, becoming much clearer over the short time frame. The broken water pipe (seen as a dark spread in the later image), is also not visible in the earlier data collection, again confirming that the cropmark formation is occurring between the two dates. The field immediately to the south-west however, gives a different response. Here, the detail is slightly clearer in the earlier dataset, particularly in the thermal band, indicating that the linseed crop in this field (the southern part of site 028) had reached maturity slightly earlier than the sugar beet in sites 027 and 037.

Thus the timing for the collection of both aerial photography and multi spectral imagery, at least for archaeological anomaly detection, is vital.

6.2.1 Timing of gradiometer data collection

Figure 83 The effect of different agricultural regimes on gradiometer surveys

The time of year for collecting magnetic data is not significant. However, during the course of carrying out the major gradiometer surveys, it has been noted that the surface condition of a field during magnetic survey plays a substantial role in quality of the data collected and the apparent strength of the magnetic signal.

For example, Figure 83 shows an enclosure system spread across two modern fields. The field on the left is a horse paddock under permanent pasture, whereas the field on the right had been ploughed, then harrowed and drilled some two weeks before the survey was conducted. The variable magnetic response as the anomalies cross the field boundary is obvious. The north-south aligned western edge of the enclosure is barely visible in the horse paddock to the west, whereas the remainder of the enclosure to the east could not be more pronounced. It is thought that the disturbance to the archaeological deposits caused by ploughing brings more magnetically enhanced material from the underlying features nearer to the surface, therefore making the anomalies more visible. In addition, the field to the west has a large deposit of blown sand along its eastern edge. This has the joint effect of masking the magnetic anomaly and protecting the archaeological feature. This situation is therefore analogous to the creation of cropmarks, where the features that are most visible are generally those which have been substantially damaged. The conclusion must be that although at first glance the field to the east looks archaeologically more interesting, it is the horse paddock to the west which will contain the best preserved archaeological deposits. This has ramifications for the scheduling of sites based on remote sensing evidence alone, as what tends to happen is that only the most obvious sites are scheduled, whereas the better preserved areas around the actively damaged fields which would be worth preserving, may well go unnoticed.

Some agricultural practices, such as disking, have a substantial effect on the data collected, but apparently only for a relatively short period of time. The implications for the timing of gradiometer surveys are demonstrated in Figure 84, which shows the same field re-surveyed under different agricultural conditions.

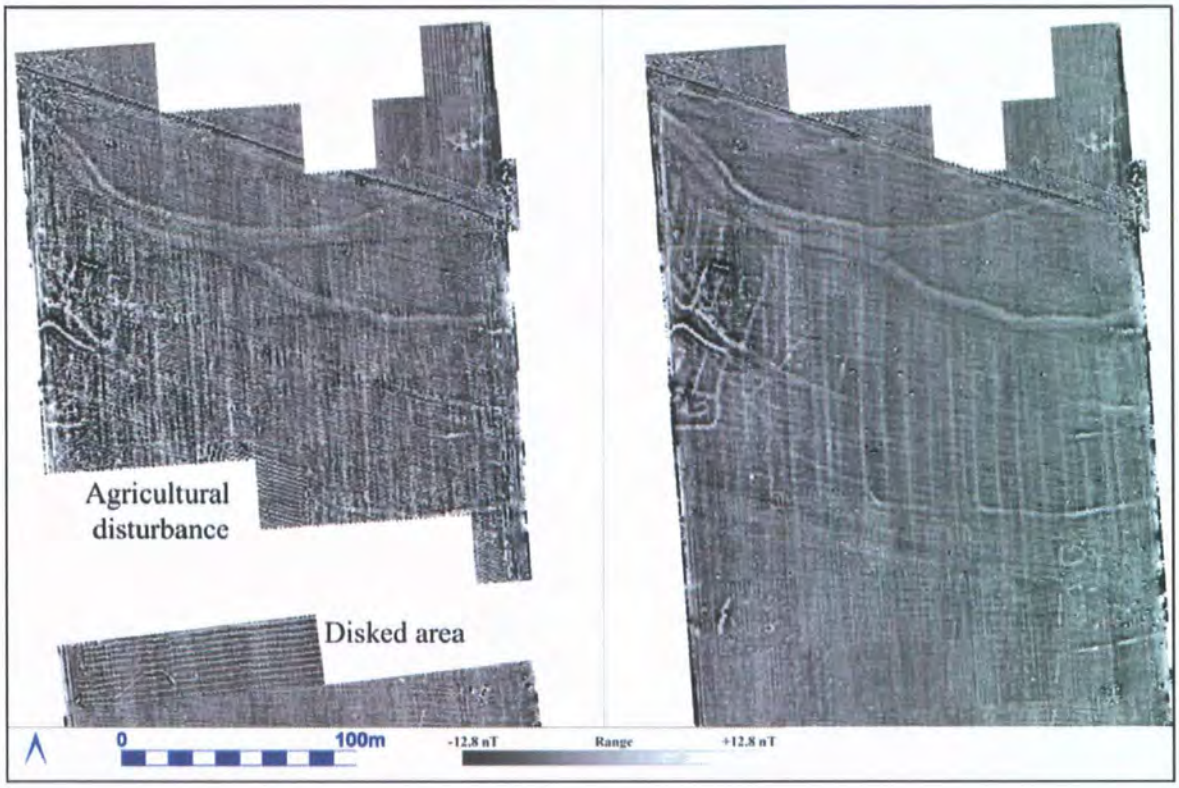

Figure 84 The impact of disking on a magnetic survey

The data displayed in the image on the left was collected when the northern area of the field was covered in straw and carrots, both of which had been partially turned into the surface. In addition, a number of deep ruts were present across the area. While the southern part of the site was being surveyed, the area was being disked, and four grids were surveyed immediately thereafter. The east-west anomalies caused by the disking are clearly visible. The data on the right is from a second survey of the same field some 6 months later, when it was under a turf crop. The change in data clarity is remarkable, with a number of archaeological anomalies now clearly defined. Also of note is the complete absence of any evidence for the disking. The ramifications for magnetic surveying are clear; that surveying using this method should not be carried out immediately after ploughing or any other intrusive agricultural practice, as time should be allowed for the soil to "settle" before attempting magnetic surveying. The exact time required for this "settling" needs to be assessed, which could be done by returning to an area affected by disking, and resurveying the same area on a weekly (or even daily)

basis until the effects were gone, although the time taken for the effects to dissipate could well vary depending on soil composition.

6.3 Temperature recorded by the Hobo loggers

The results from the temperature loggers were processed into graphs using Excel, and kept to a standard colour format so that all of the graphs could be directly compared. Hobo 5 was placed within an archaeological deposit (a trackway) and Hobo 4 just outside the trackway in an area of open sand and calcareous gravel some 4 metres to the north of Hobo 4. It was hypothesised that the redder, more compact sands in the fill of the trackway would absorb more heat than the lighter sand and gravel deposit. Initially, the data which covered the times of both the day and night acquired thermal imagery were extracted and graphed.

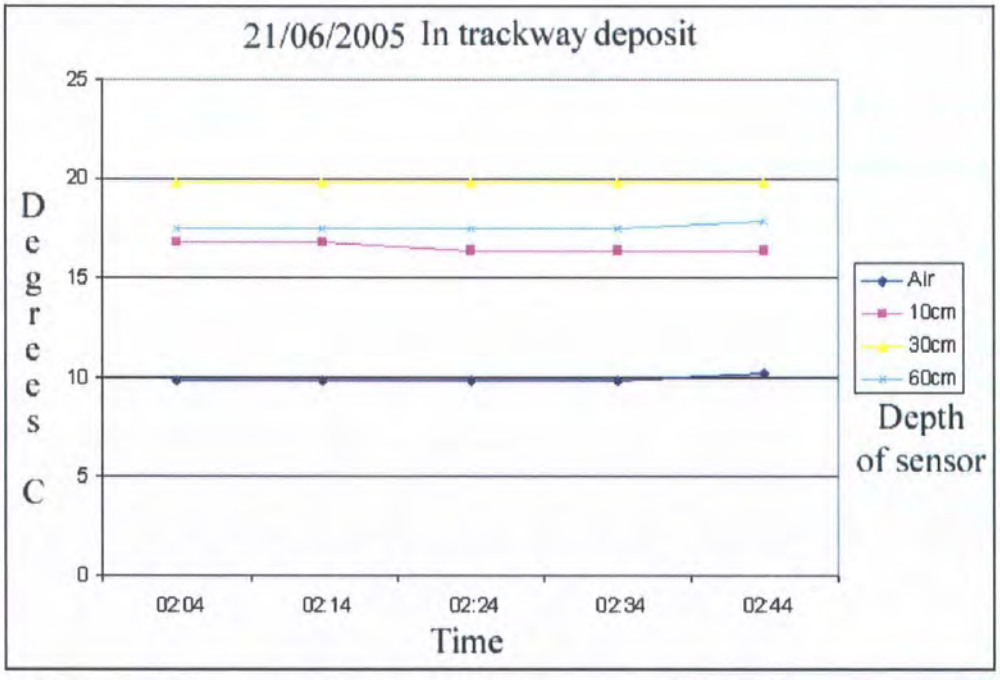

Figure 85 Temperature results from the logger buried within an archaeological deposit

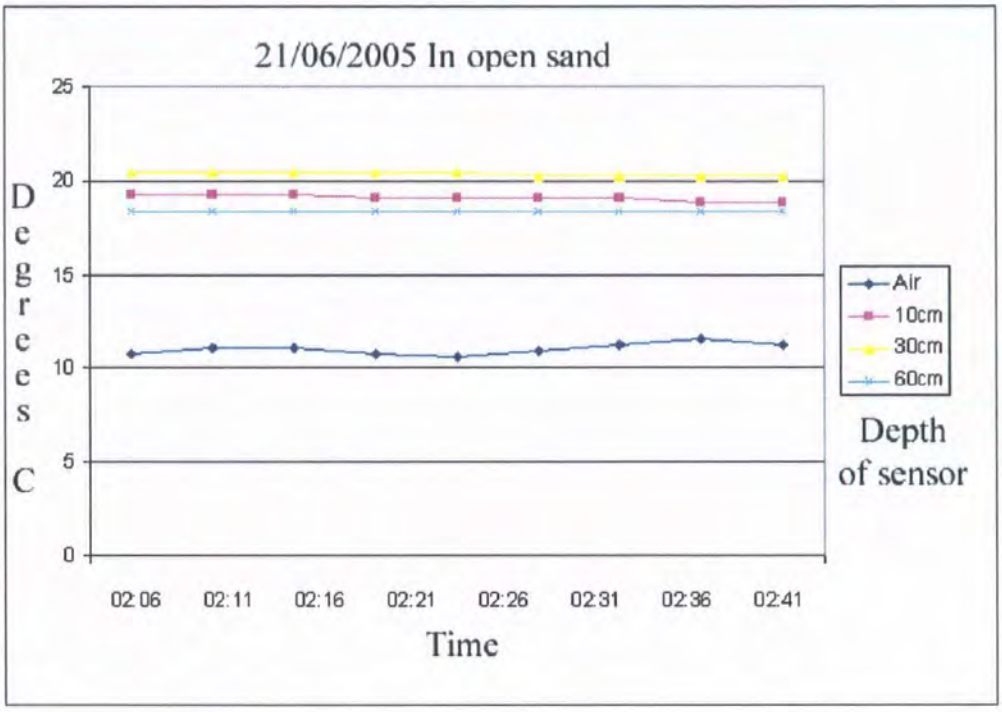

Figure 86 Temperature results from the logger buried within natural sand

Figure 85 and Figure 86 show the results of the two loggers at the time of the night acquired thermal data (2:09 to 2:36 on 21/06/2005). In both deposits, the 30cm sensor maintained a 20 degree C value, with the air sensor reading at just above 10 degrees C. The other sensor readings (see Table 17 and Table 16 for actual recorded values) for the different depths showed a difference in return between the two deposits. In the open sand deposit, the 10cm sensor gives a very similar return to the 30cm deposit, whereas in the trackway, the 10cm sensor is much colder than the 30cm temperature. This indicates that the upper trackway fills are radiating the heat away much faster than the open sand. The average temperature difference between the 10cm sensors at the time of the night flight was 2.47 degrees C). Figure 88 shows a similar set of readings for each night around the time of the ATM flights. For both night time locations, the 30cm sensor gave the warmest reading.

Time	Air	10cm	30cm	60cm
02:06	11.12	19.21	20.4	18.36
02:11	11.12	19.21	20.4	18.36
02:16	10.79	19.04	20.4	18.36
02:21	10.62	19.04	20.4	18.36
02:26	10.96	19.04	20.23	18.36
02:31	11.29	19.04	20.23	18.36
02:36	11.63	18.87	20.23	18.36
02:41	11.29	18.87	20.23	18.36

Table 16 Actual values recorded by Hobo 4 in the open sand deposit (night)

Time	Air	10cm	30cm	60cm
02:04	9.82	16.76	19.81	17.52
02:14	9.82	16.76	19.81	17.52
02:24	9.82	16.38	19.81	17.52
02:34	9.82	16.38	19.81	17.52
02:44	10.21	16.38	19.81	17.9

Table 17 Actual values recorded by Hobo 5 in the trackway deposit (night)

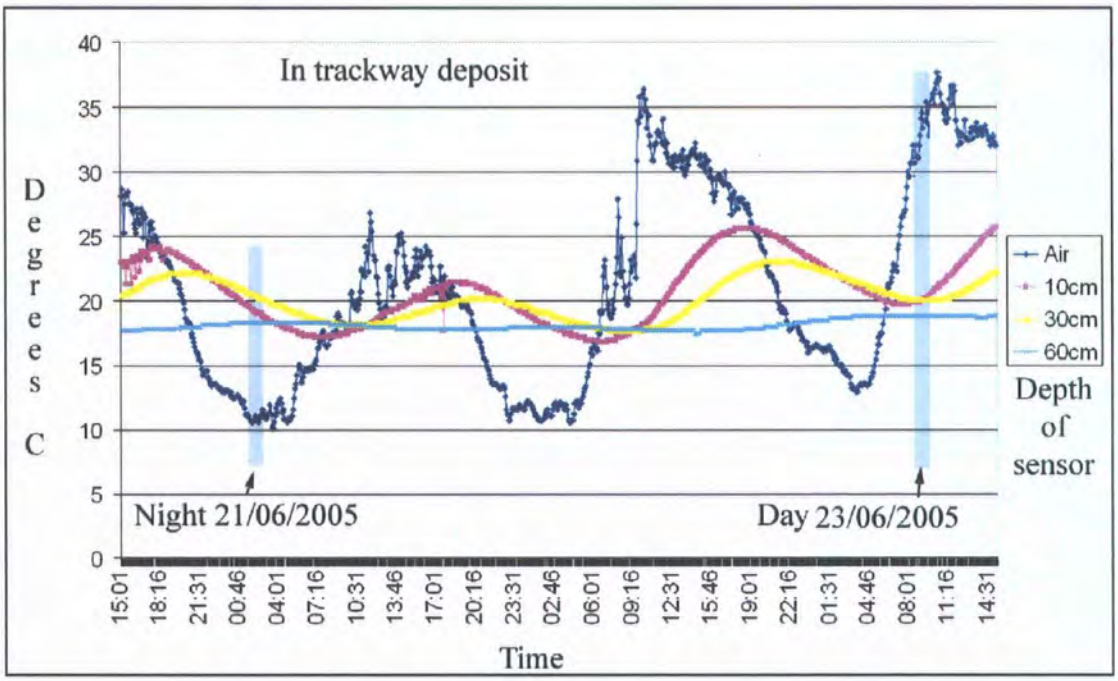

Figure 87 Temperature results (Hobo4) from 20/06/2005 to 23/06/2005

A number of other differences between the returns from the sensors at different depths can be seen in Figure 87 and Figure 88 (time of flights indicated by the light blue columns). The 10cm sensor closely follows the open air sensor during the daytime in

the open sand location, but has a much smoother curve in the trackway deposit. This indicates that the darker, more compact sands filling the trackway absorb and hold on to the heat emitted of the day for much longer than the yellower, less compact natural sand, which reflects much more of the heat during the day. The 30cm and 60cm sensors follow a very similar curve for both deposits (with an average temperature difference of 0.5 degrees C for the 30cm sensors and 0.8 degrees C for the 60cm sensors).

In the open sand, the temperature drops off very quickly as the sun goes down, (Figure 88), whereas there is a more gradual decrease in temperature over the trackway deposit (Figure 87).

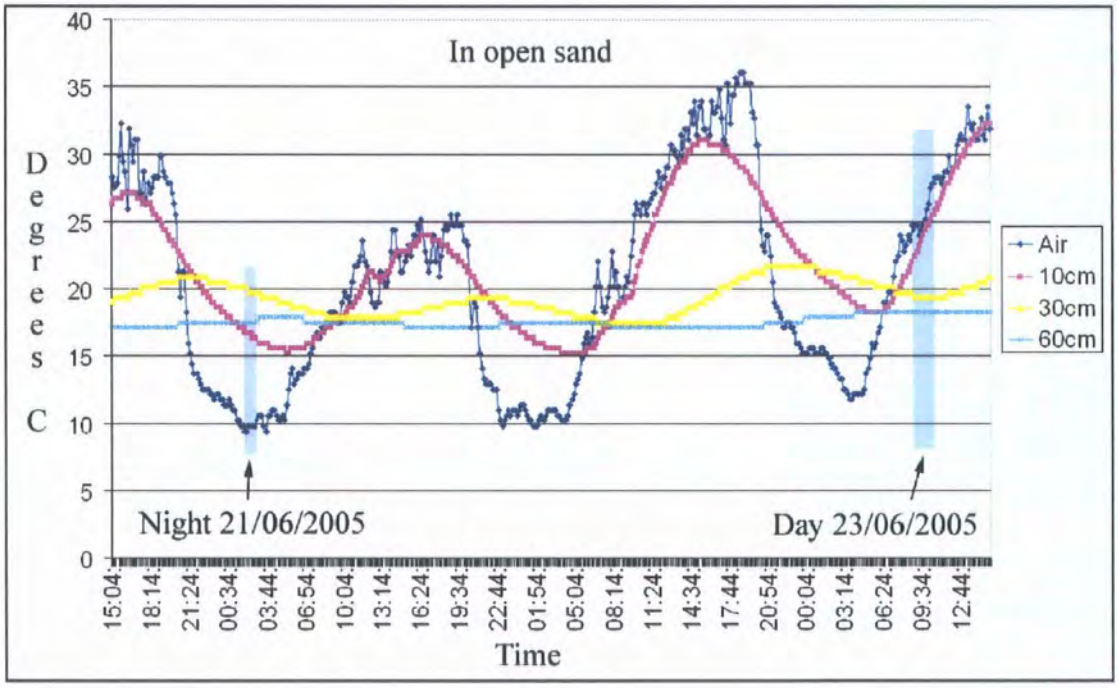

Figure 88 Temperature results (Hobo5) from 20/06/2005 to 23/06/2005

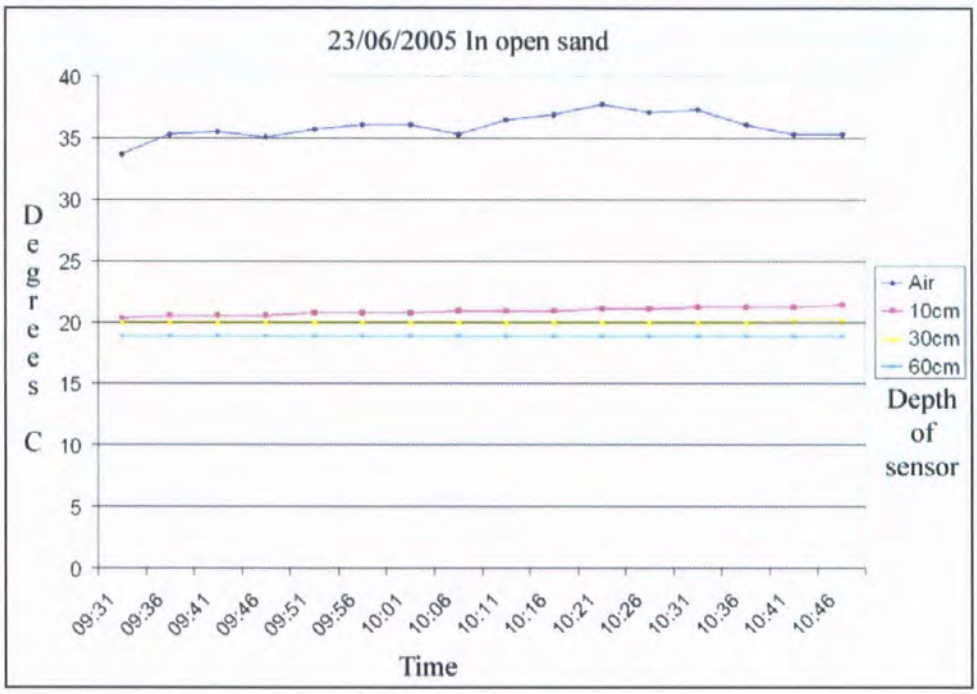

Figure 89 Temperature results from the logger buried within an archaeological deposit (day)

The daytime differences between the air sensors are even more marked, with the air sensors giving 9.9 degrees C difference. It is possible that the air sensors were being interfered with by rabbits, as the end cap of the open sand air sensor was missing when the Hobos were retrieved, but this did not affect the readings from the other sensors. The reading for the 10cm sensor in the trackway deposit confirms the hypothesis that this fill would absorb more heat than the more reflective yellow sand deposit, with a 3.7 degrees C difference. As with the night temperatures, the differences between the 30cm and 60cm sensors was slight, being 0.64 and 0.59 degrees C respectively. Note also that the temperature remains stable for these two sensors while the daytime data is being acquired, whereas the upper two sensors show a general increase in the trackway deposit, and fluctuations within the open sand deposit (see Table 18 and Table 19).

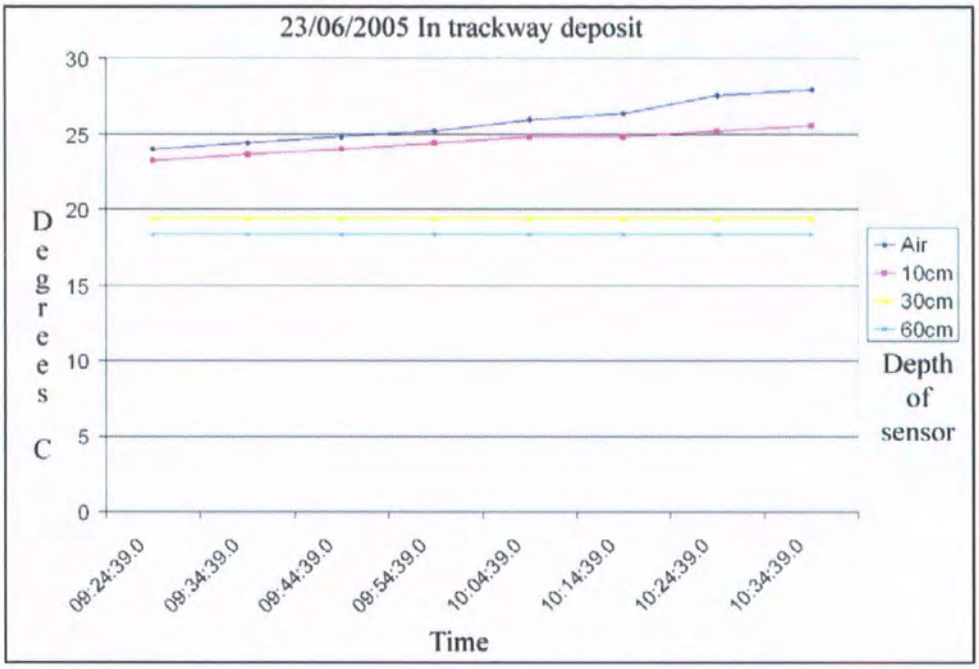

Figure 90 Temperature results from the logger buried within the open sand deposit (day)

Time	Air	10cm	30cm	60cm
09:31	33.64	20.4	20.06	18.87
09:36	35.24	20.57	20.06	18.87
09:41	35.44	20.57	20.06	18.87
09:46	35.04	20.57	20.06	18.87
09:51	35.64	20.74	20.06	18.87
09:56	36.05	20.74	20.06	18.87
10:01	36.05	20.74	20.06	18.87
10:06	35.24	20.91	20.06	18.87
10:11	36.46	20.91	20.06	18.87
10:16	36.88	20.91	20.06	18.87
10:21	37.71	21.08	20.06	18.87
10:26	37.08	21.08	20.06	18.87
10:31	37.29	21.26	20.06	18.87
10:36	36.05	21.26	20.06	18.87
10:41	35.24	21.26	20.23	18.87
10:46	35.24	21.43	20.23	18.87

Table 18 Actual values recorded by Hobo4 in the open sand deposit (day)

Time	Air	10cm	30cm	60cm
09:24	24.01	23.24	19.42	18.28
09:34	24.4	23.63	19.42	18.28
09:44	24.79	24.01	19.42	18.28
09:54	25.17	24.4	19.42	18.28
10:04	25.95	24.79	19.42	18.28
10:14	26.34	24.79	19.42	18.28
10:24	27.52	25.17	19.42	18.28
10:34	27.91	25.56	19.42	18.28

Table 19 Actual values recorded by Hobo5 in the trackway deposit (day)

The returns from both sensors confirm McManus's findings (McManus, 2003, p.341) that solar heat variation (diurnal patterning) penetrates only to a depth of between 20cm and 50cm, despite the fact that the current research used sensors in open sand deposits with no vegetation cover.

6.4 Geological information

As well as archaeological features, a number of features of geological interest were detected by the 1992 and 2005 ATM data.

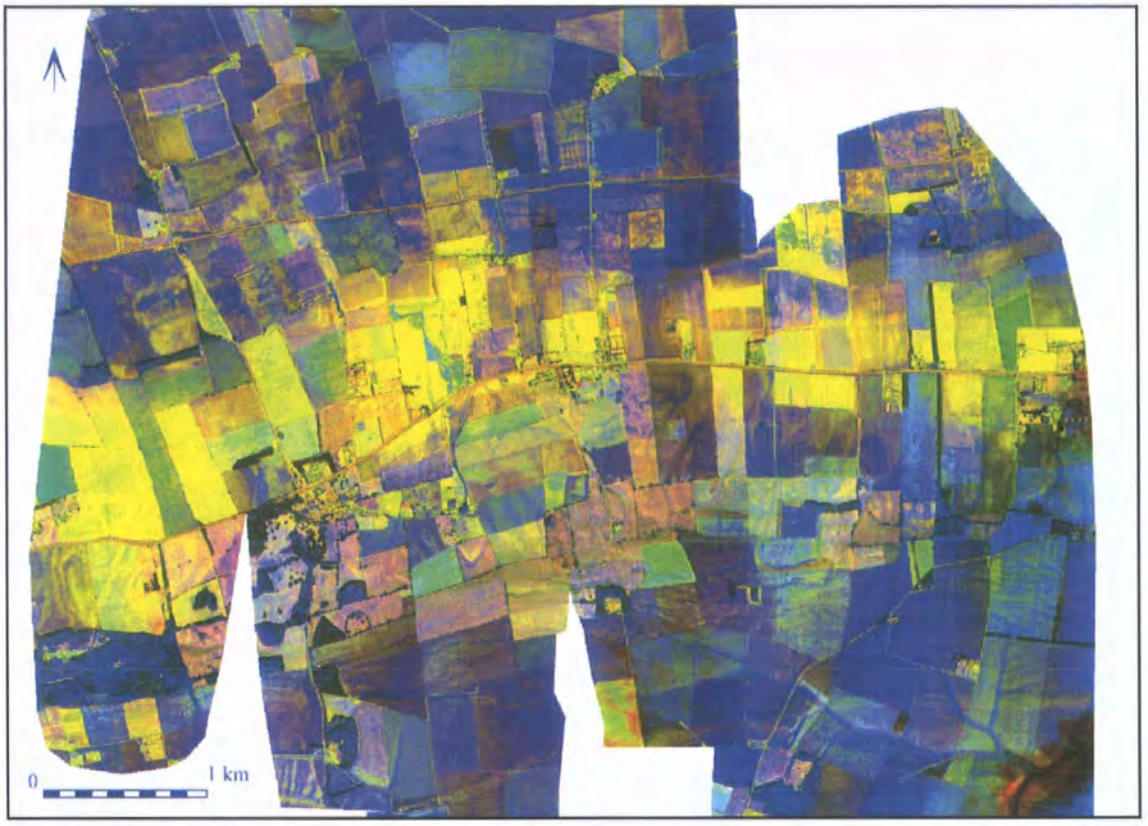

Figure 91 Combination of bands 11, 10 and 7 (1992 ATM data) clearly showing the extent of the blown sand deposits.

Figure 91 (1992 data) shows the extent of the blown sand deposits as a yellow band stretching across the surveyed area. This was derived by using a combination of bands 11 (red), 10 (green) and 7 (blue). The resultant image was then histogram stretched to enhance the differences identified across the geological zones.

The same area is shown in Figure 94, but with the extent of the ladder settlement shown as a solid red band. This demonstrates quite clearly that the ladder settlement was located on the boundary of the sandy zone with the wetter areas to the north.

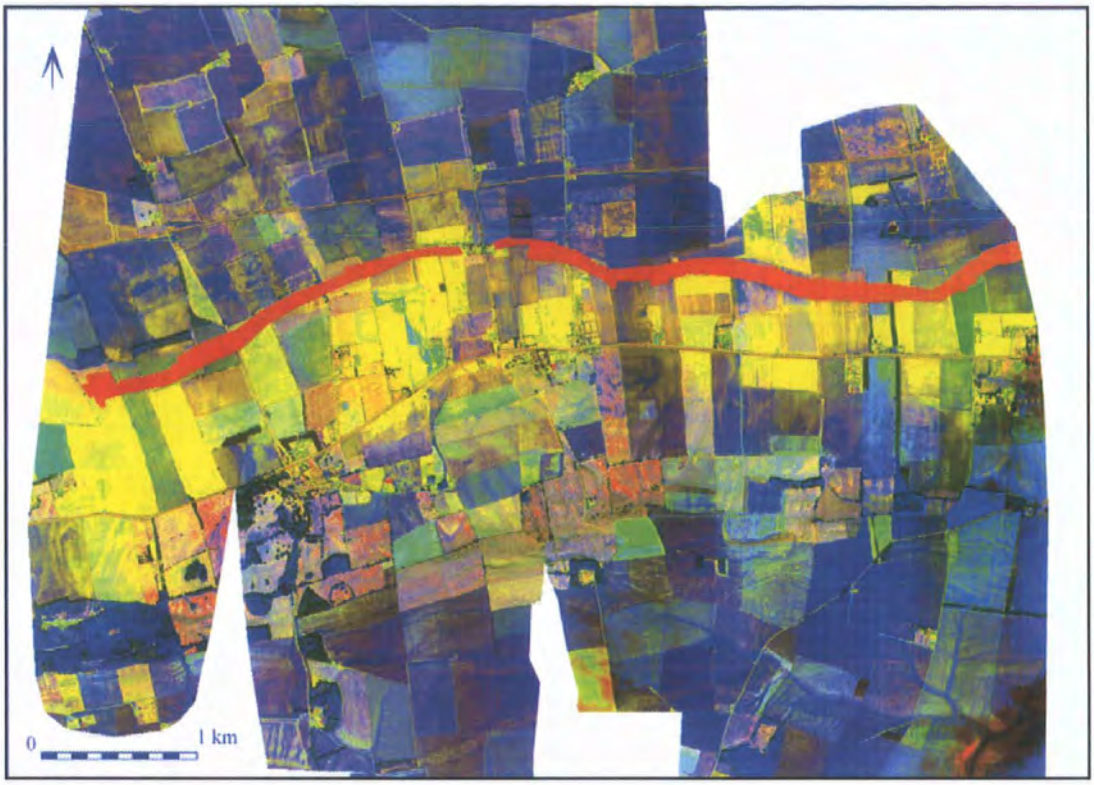

Figure 92 As Figure 91 with extent of ladder settlement superimposed

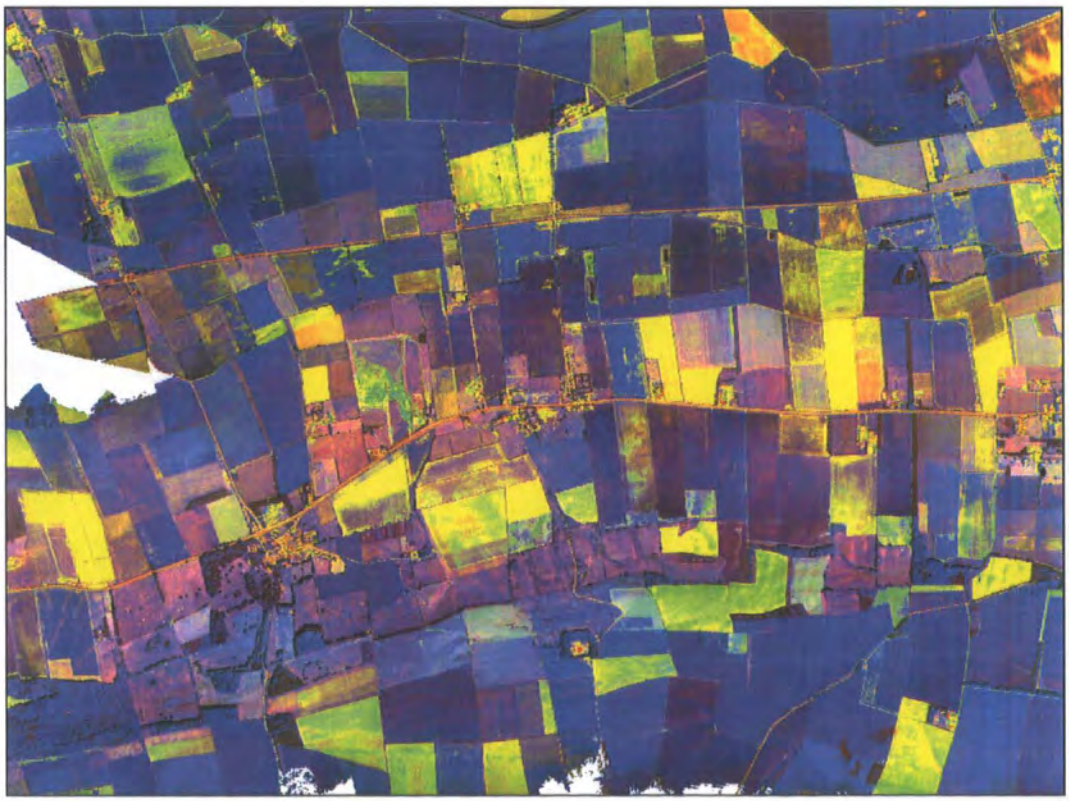

Figure 93 The AZ-16 2005 data for the same area displayed in Figures 91 and 92

This pattern is not as visible in the 2005 data (see Figure 93 for a comparison); the clarity of this phenomenon was much more apparent in the earlier ATM data, possibly due to the drier conditions leading up to the flight.

As well as the broad geological changes across the area, closer inspection reveals a number of smaller geological and alluvial features.

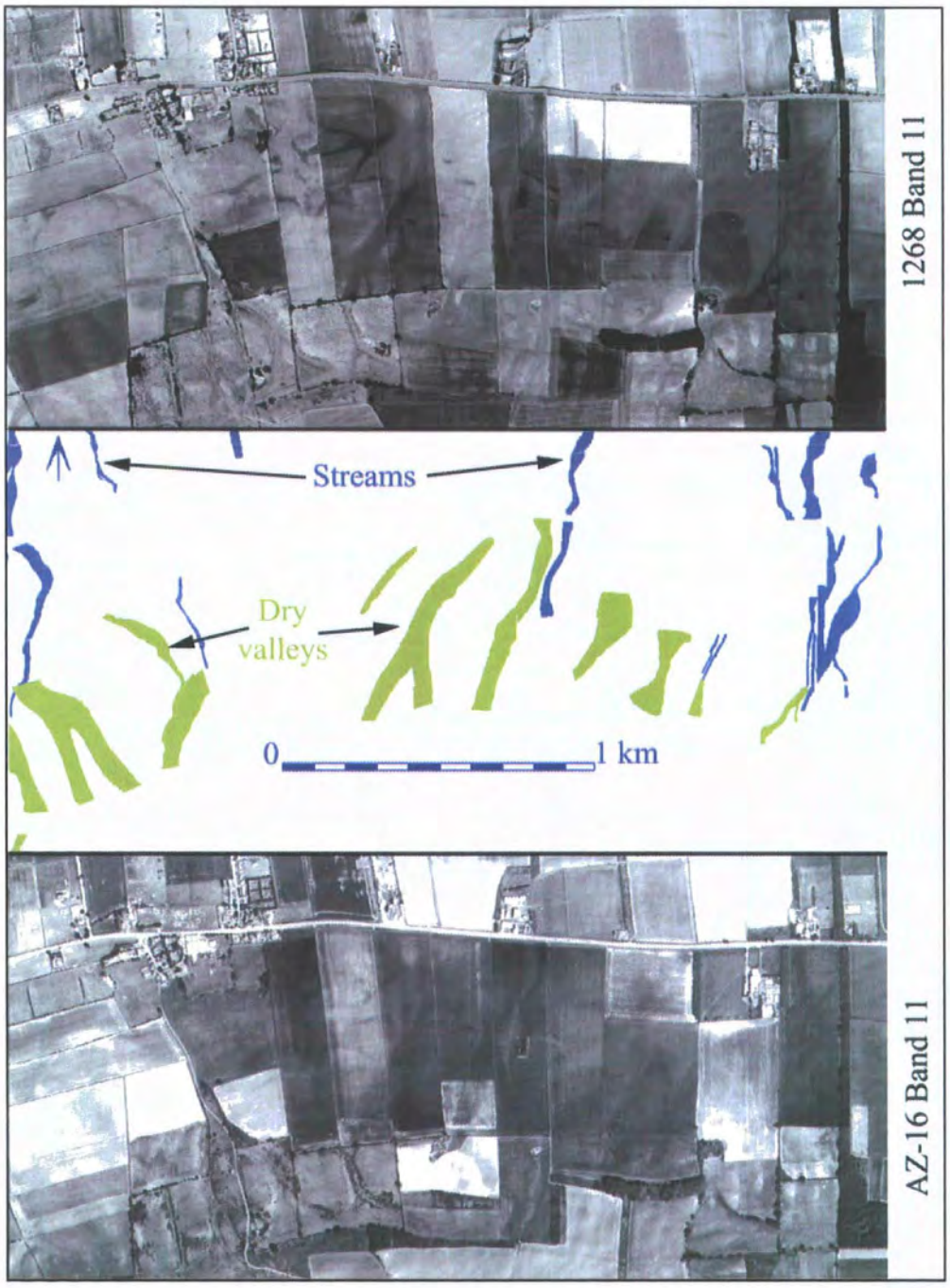

Figure 94 Geological features detected in the thermal band of ATM data.

At the foot of the Wolds is a spring line, which feed into stream channels, some still active and some now relict. The location of these is displayed in Figure 94, where the thermal band of the ATM has successfully detected nearly all of this class of feature. It has also detected the location of the dry valleys, which are small cuts through the chalk which are then filled in with colluvial material (hillwash), which is washed down from the upper slopes of the Wolds.

6.5 Comparison of different techniques

In order to compare the returns from three remote sensing techniques, four case study areas (see Figure 8 for the location of these areas) were selected. These were chosen so that the returns from the 1992 multispectral surveys could be quantatively measured against those from aerial photography and gradiometery; and to allow the returns from the 1992 and 2005 ATM multispectral surveys to be compared.

6.5.1 Case study area 1

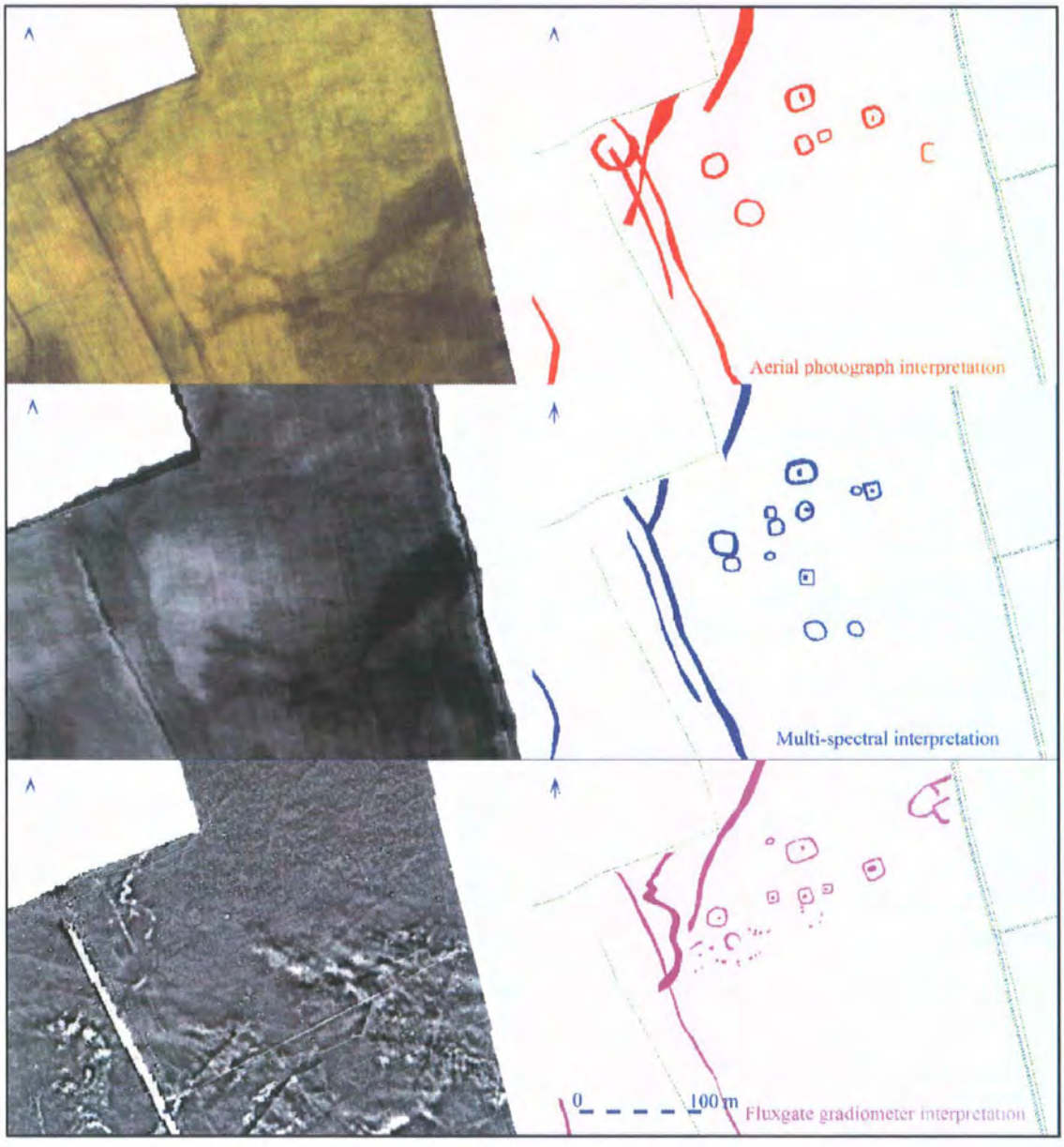

Figure 95 Comparison of three different remote sensing techniques (Site 174)

Case study area one was chosen as it was known to contain part of an Iron Age square barrow cemetery (site 174). The field contained spring barley on both multispectral flight dates. The area was located within the alluvial sand and silicaceous gravel zone in a previously organically enriched, peaty area (Zone 6), although modern drainage is causing the peat to shrink at an alarming level. Figure 95 shows the northern part of Site 174, with a colour oblique rectified aerial photograph above, Band 11 (thermal) of the June 1992 multispectral image in the centre and the fluxgate gradiometery survey below. The interpretative drawings on the right are of archaeological features only, with geological features and field drains removed.

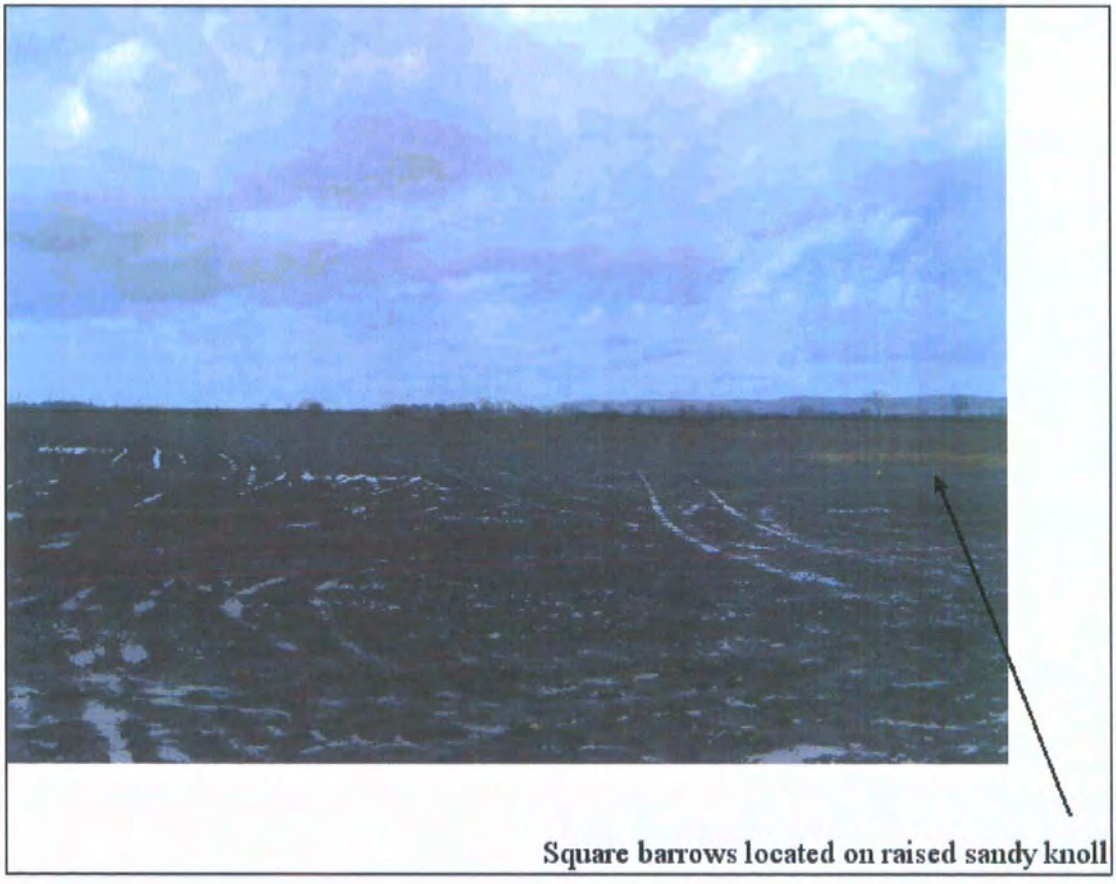

Figure 96 Site 174 from the north-western corner looking east

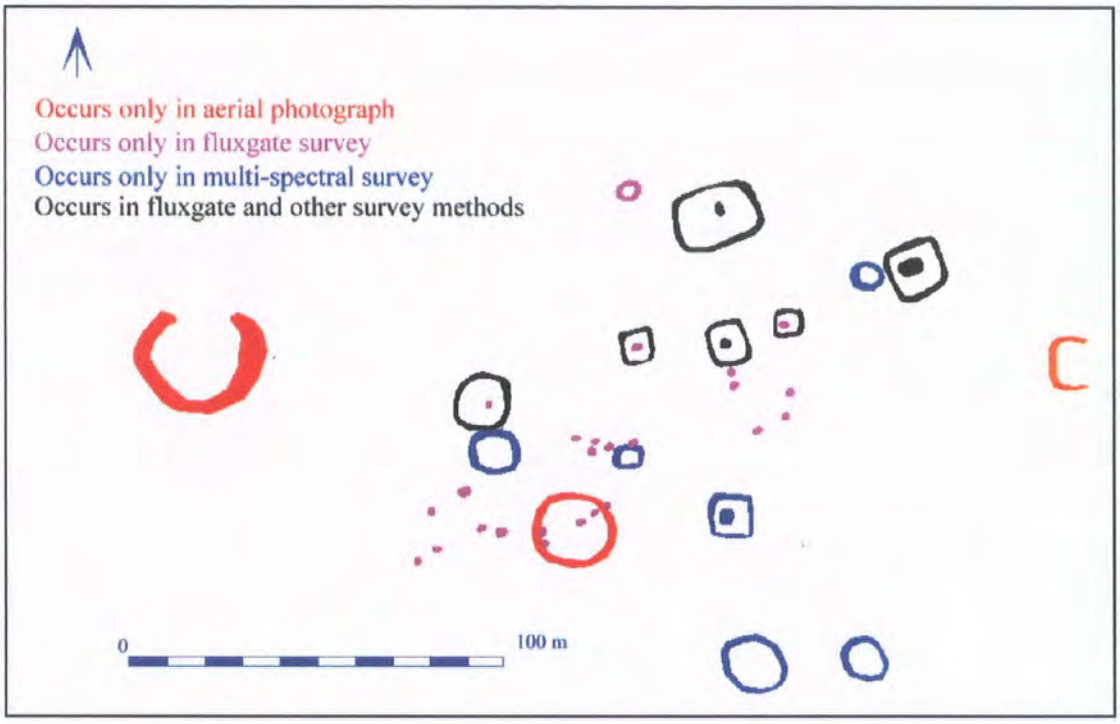

Figure 97 Showing the unique returns from three different forms of remote sensing

The barrow cemetery was previously known from aerial photographs, and occupies a low sandy knoll (see Figure 96), seen in the aerial photograph as a lighter zone near the centre of the area. A trackway is present, seen as two darker linear anomalies running parallel to the western field boundary, with the eastern ditch well defined in both the cropmark and multispectral image, less well defined in the gradiometer data. The western ditch is faint in both the cropmark and multispectral data, and is not detected by the gradiometer. A quick glance reveals that all three remote sensing techniques find the main five barrows, but also shows that each technique finds barrows which are not detected by the other methods. In order to visually display the different returns, a number of queries were applied to the remote sensing database, generating Figure 97.

The multispectral data detected more barrows to the south of the main cemetery area, where cropmark formation and magnetic contrasts are very subtle. The gradiometer also detected a number of localised anomalies on the sandy knoll, which may prove to be flat

inhumation graves next to the more prominent barrows. The aerial photograph shows a number of larger circular cropmarks which may be later Neolithic and thus both predate and provide the focus for the smaller and later round and square barrows in the area.

It can be seen from Table 20 that in the nine instances where more then one form of remote sensing detected either a square barrow ditch or grave, the fluxgate gradiometer detected all nine, with the multispectral imagery detecting eight and aerial photography detecting seven. Six of the nine anomalies were detected by all three methods.

Link_Key_ID	Fluxgate	Aerial Photo	MSS_1992	Interpretation
174RS13950	174MA00048	174AP00004		Square Barrow
174RS13946	174MA00044	174AP00006	174MS00012	Barrow
174RS13947	174MA00045	174AP00001	174MS00009	Square Barrow
174RS13948	174MA00046	174AP00005	174MS00011	Square Barrow
174RS13949	174MA00047	174AP00007	174MS00016	Square Barrow
174RS13952	174MA00050	174AP00025	174MS00013	Square Barrow Grave Pit?
174RS13953	174MA00051	174AP00002	174MS00010	Square Barrow Grave Pit
174RS13951	174MA00049		174MS00019	Square Barrow
174RS13956	174MA00054		174MS00022	Square Barrow Grave Pit

Table 20 Showing the barrow anomalies detected by more than one type of remote sensing

Link_Key_ID	Fluxgate	Aerial Photo	MSS_1992	Interpretation
174RS13945	174MA00043			Barrowlet
174RS13954	174MA00052			Square Barrow Grave Pit
174RS13955	174MA00053			Square Barrow Grave Pit
174RS13957	174MA00055			Square Barrow Grave Pit
174RS13958	174MA00056			Square Barrow Grave Pit
174RS14037			174MS00014	Square Barrow
174RS14038			174MS00015	Square Barrow Grave Pit
174RS14039			174MS00018	Square Barrow
174RS14040			174MS00020	Square Barrow
174RS14041			174MS00021	Barrowlet?
174RS14042			174MS00023	Barrow?
174RS14043			174MS00024	Barrow?
174RS14044		174AP00003		Square Barrow
174RS14045		174AP00012		Round Barrow?
174RS14046		174AP00016		Round Barrow?

Table 21 Showing the barrow anomalies detected by a single type of remote sensing

Table 21 demonstrates in a tabular form that where only a single form of remote sensing detected an anomaly, the fluxgate gradiometer was much more likely to detect the grave pits in the centre of the barrow. The cropmarks detected in the aerial photographs and no other method were all barrow ditches, although it should be pointed out that two of these were round barrows, and thus of a much earlier date than the square barrow cemetery. The anomalies detected only by the multispectral imagery were a mixture of square barrows, a square barrow grave pit and a smaller barrow ditch.

Thermal difference (case study area 1)

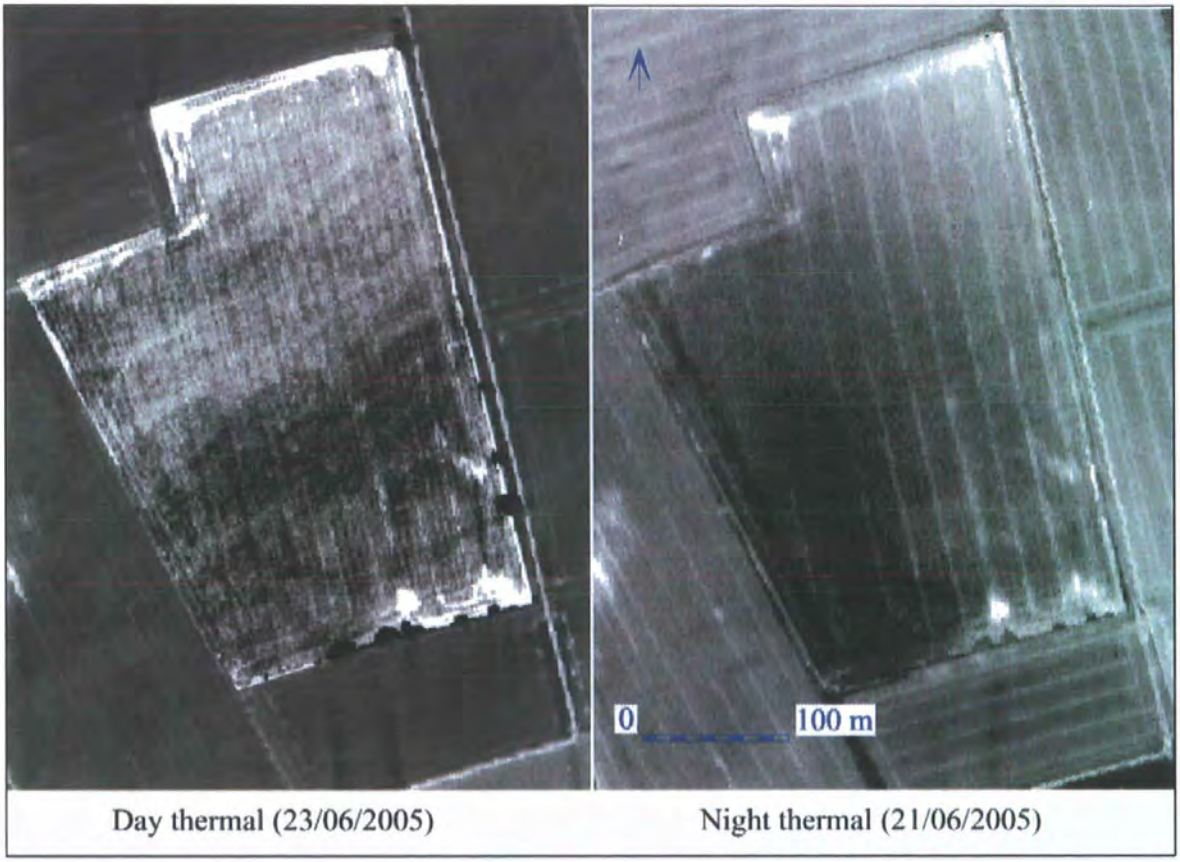

Figure 98 Thermal difference between night and day flights (AZ-16 ATM). Case study area 1 spring barley

As can be seen in Figure 98, the difference in returns between the day and night flights is extreme for this area. The day time flight provides the most contrast, with the geological differences clearly defined, (note the sandy island showing as a lighter, thus slightly warmer, zone in the north of the area. However, no discrete anomalies that

could be equated with the known square barrows were identified in the 2005 multispectral data. The night acquired thermal is much quieter, showing a general east-west trend, with the western half of the field slightly colder than the eastern half. However, the trackway which runs parallel to the modern field boundary is very well defined as a dark linear anomaly, with its location indicating that this is the western half of the trackway, that is the half which was ill-defined in the previous (1992) flight.

6.5.2 Case study area 2

This area comprises site 28 to the west and site 27 to the east. The underlying drift geology is of different thicknesses of aeolian sand, lying on a mainly sand and gravel base (Zone 4). The features of particular interest in site 27 had been noted from the air in the past, although it was the 1992 flight which demonstrated that the size and grouping of these cropmarks indicated the potential location of an Anglian settlement, and led us to carry out the geophysical survey. The area was particularly responsive to the fluxgate gradiometer, and a total of 218 (151 in Site 27) anomalies which were interpreted as *Grubenhäuser* were detected. The total number of anomalies for each remote sensing technique is displayed in Table 22.

Type	Site 27	Site 28	Total
Fluxgate	152	66	218
Multispectral	80	9	89
Cropmark	28	8	36

Table 22 Numbers of *Grubenhäuser* detected by the different remote sensing technique

However, these numbers cannot just be added together to give us the total number of *Grubenhäuser* associated with the Anglian settlement, as a number of the same anomalies are present in more than one form of remote sensing. This is where the correlation database previously discussed in chapter 5 allows the absolute number of *Grubenhäuser* found in each site to be established. Table 23 indicates that a total of 241 different *Grubenhäuser* were detected using the three different types of remote sensing.

Detected by	Site 27	Site 28
Fluxgate unique	89	55
Multispectral unique	20	0
Cropmark unique	0	3
Found by all 3	23	2
Found by fluxgate and multispectral	35	7
Found by fluxgate and cropmark	5	2
Actual *Grubenhaus* total	172	69

Table 23 Unique totals for each form of remote sensing

Figure 99 Site 27 from the north-east, looking south-west towards the Wolds.

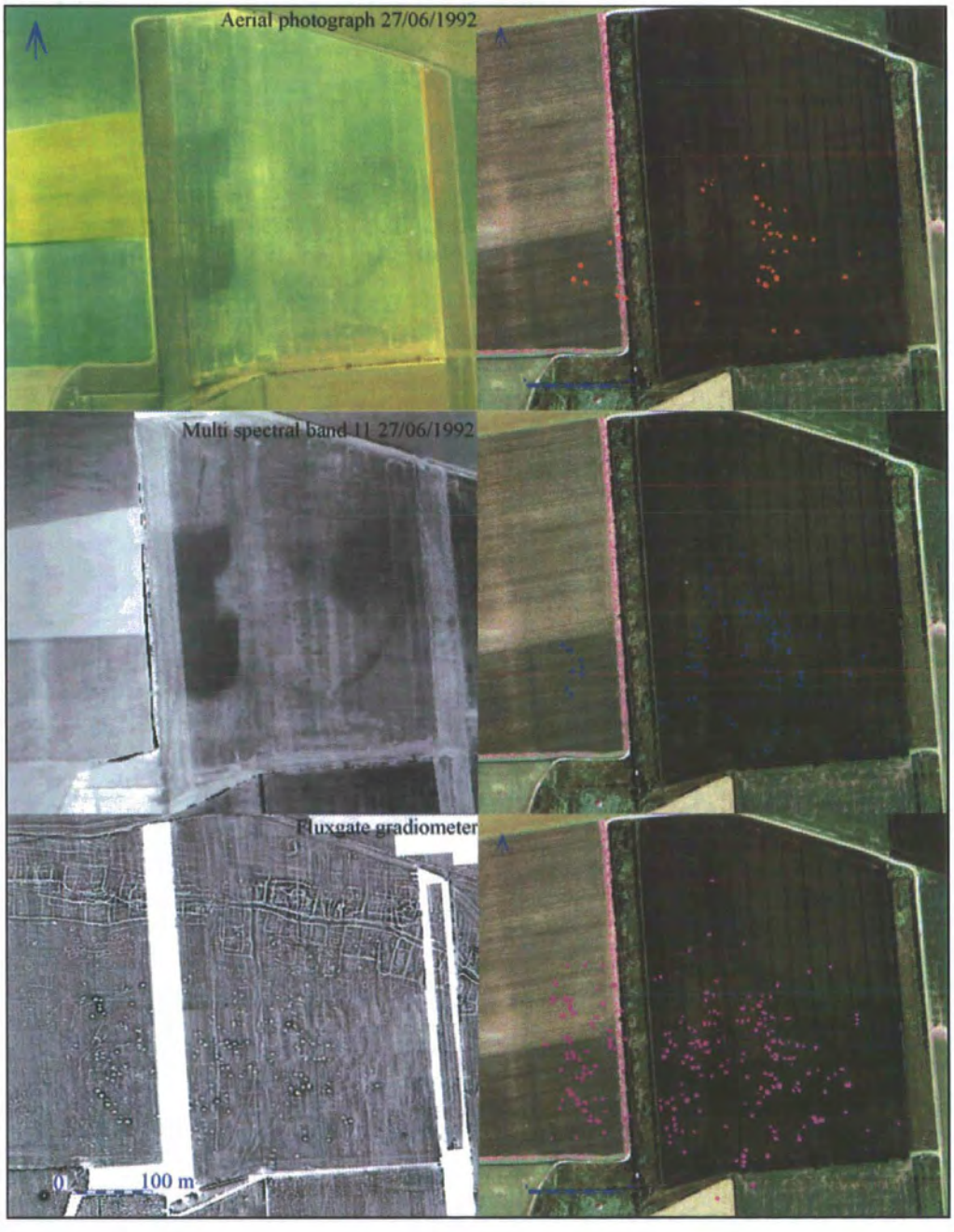

Figure 100 A comparison of three different forms of remote sensing (Site 27), with interpretative plots of *Grubenhäuser* only on the right (aerial photograph NERC 2005, *Grubenhäuser* on Getmapping data)

The left half of Figure 100 shows a comparison of the three types of remote sensing used on site 27 (linseed crop), with an interpretative plot of the *Grubenhäuser* on a background of the Getmapping data on the right. It can quickly be seen that the returns from each form of remote sensing vary considerably in this area.

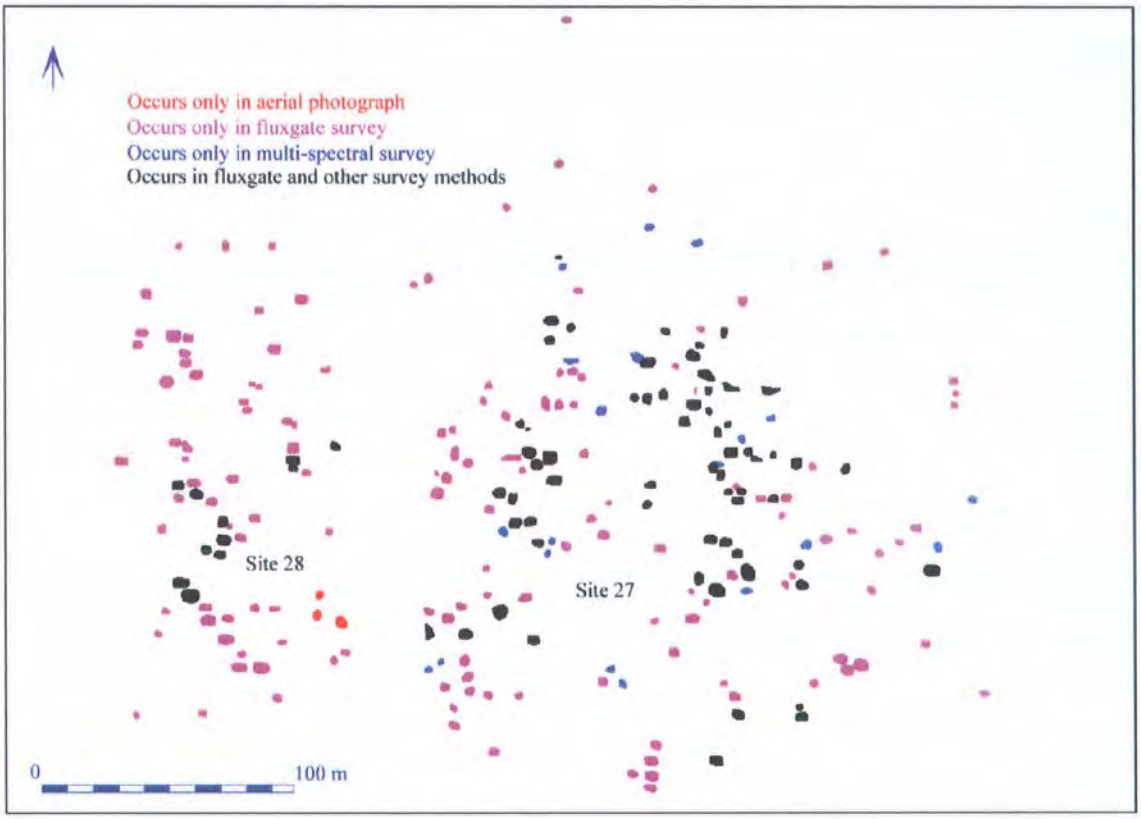

Figure 101 Showing the unique returns from three different forms of remote sensing (*Grubenhäuser* only)

Because this area responded particularly well to the fluxgate gradiometer, the difference in anomaly detection was not so marked in this second case study area. The returns from the magnetic data were so comprehensive that no new or different anomalies relating to the ladder settlement in the northern part of the field were detected by the multispectral imagery or the aerial photographs. However, in the Anglian settlement to the south, 23 possible *Grubenhäuser* not detected by the gradiometer were present in the multispectral data (see Table 23 and Figure 101).

In all, a total of 172 *Grubenhäuser* were discovered in Site 027, of which 58 were detected both by the fluxgate gradiometer and the multispectral imagery (see Table 23 and Figure 101). This means that if only the gradiometer data was available, then 20 *Grubenhäuser* would have gone undetected (see Figure 101), and if only the multispectral imagery was presented then 89 *Grubenhäuser* would remain unknown.

Band	No of grubs	Unique	% of Total
3	10	0	12.5
4	21	0	26.25
5	30	0	37.5
6	62	0	77.5
7	68	0	85
8	45	0	56.25
10	65	2	81.25
11	69	4	86.25

Table 24 *Grubenhaus* occurrence in multispectral bands

When looking at the multispectral data alone, two important points need to be made. The first is that the *Grubenhäuser* are not being detected equally across the different wavelengths of the EMS. Table 24 (graphically represented in Figure 102) show that the majority of the features are being detected in the near and short wave infrared and the thermal bands. In this case study area, none of the *Grubenhäuser* detected in the visible wavelengths were not also detected either by the infra-red or thermal bands. Only six *Grubenhäuser* were detected in a single band only, 4 from band 11 and 2 from band 10, and it was only the two from band 10 which were not detected by the other remote sensing techniques. This result emphasizes the potential value for archaeological feature detection of the infra-red and thermal bands over the visible bands of the multispectral data.

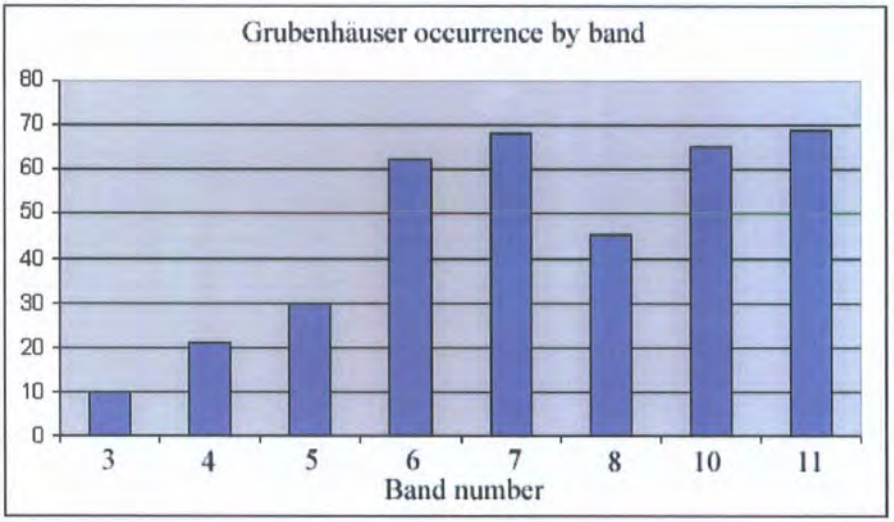

Figure 102 *Grubenhaus* occurrence in multispectral bands

Secondly, classification using a principal component analysis across all bands would not extract all of the features, because of the way that they are spread across the EMS. Only four *Grubenhäuser* were present in all of the bands. Unsurprisingly, these were also present in the gradiometer data and they all occurred as cropmarks. Figure 103 shows the number of *Grubenhäuser* present in various permutations of bands. This indicates that the *Grubenhäuser* found in different band combinations were fairly evenly distributed, and any subset classification would be unlikely to extract all of the features from the imagery. In this case, the only way to be sure that all of this type of anomaly was found was to go over each band by eye. "There is still no better, nor more sophisticated image interpreter than the human eye" (Winterbottom and Dawson, 2005, pp.212).

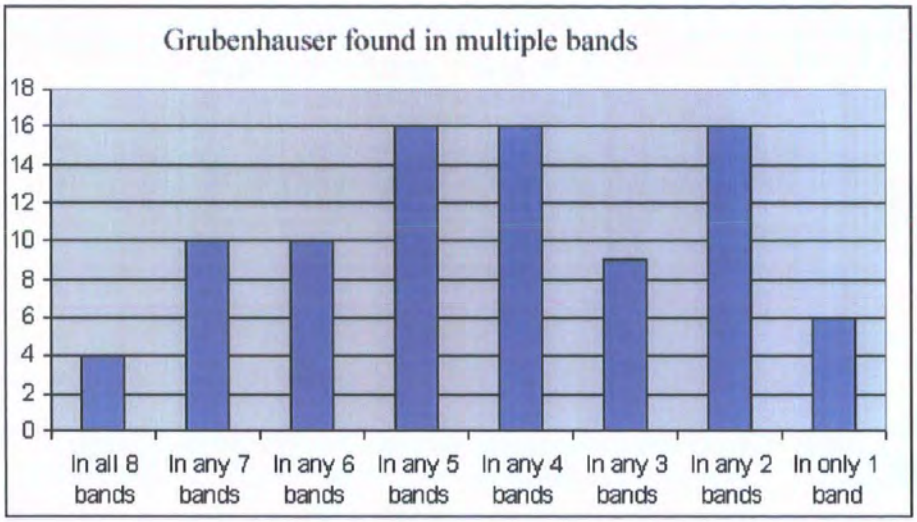

Figure 103 Total *Grubenhaus* occurrence in multiple multispectral bands

Thermal difference (case study area 2)

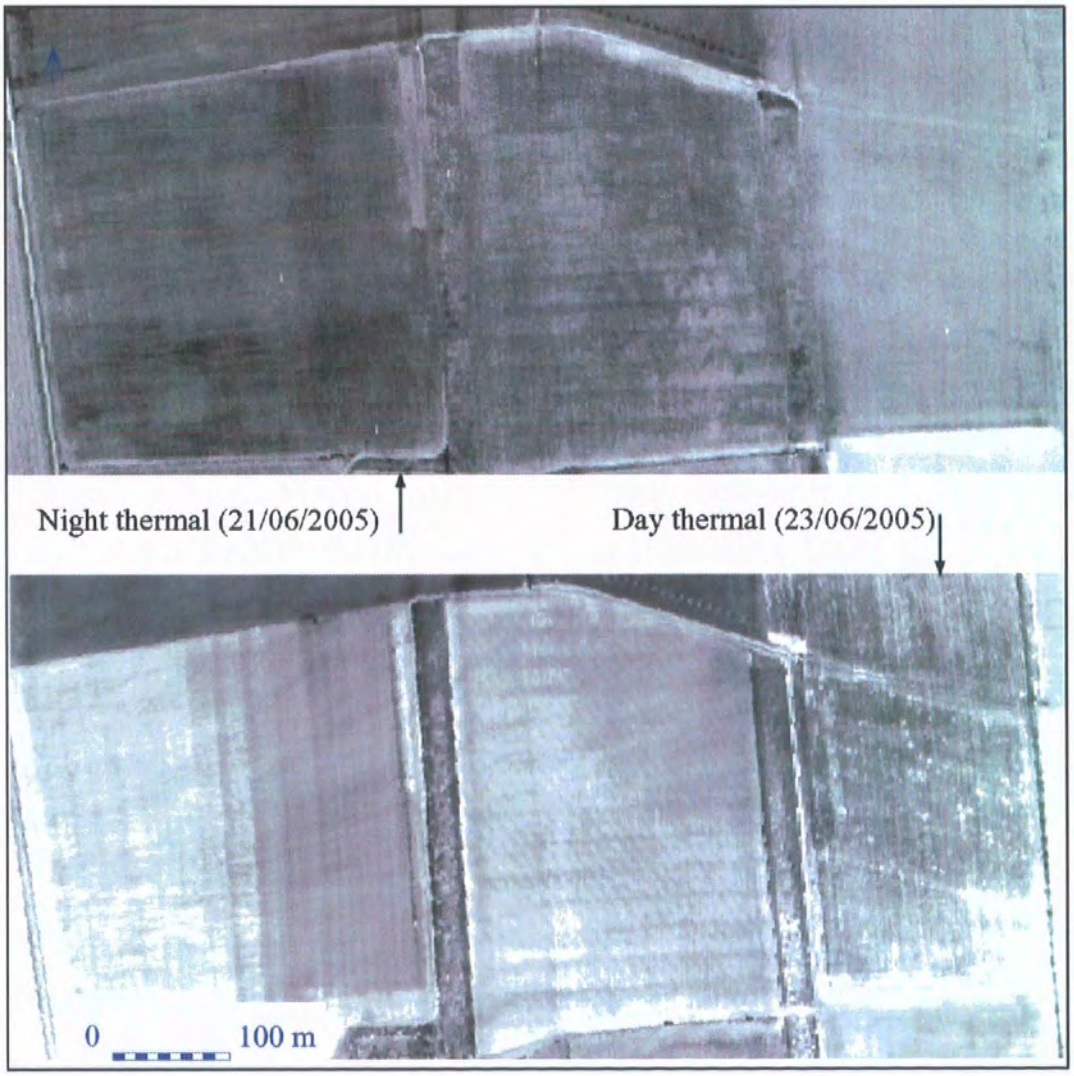

Figure 104 Thermal difference between night and day flights (AZ-16 ATM). Case study area 2

The fields which comprised case study area 2 did not provide good archaeological anomaly detection from the 2005 ATM flight (compare Figure 104 above with Figure 100). This is because both fields were under a low turf crop at the time of the 2005 flight, and the average rainfall figures for May and June meant that there was very little stress to the turf growth at this time (see Figure 21 for good cropmark formation on turf). There is a difference in the thermal difference returns, particularly in the field on the east, where the daytime thermal shows a number of hotspots, although these are caused by agricultural activity.

6.5.3 Case study area 3

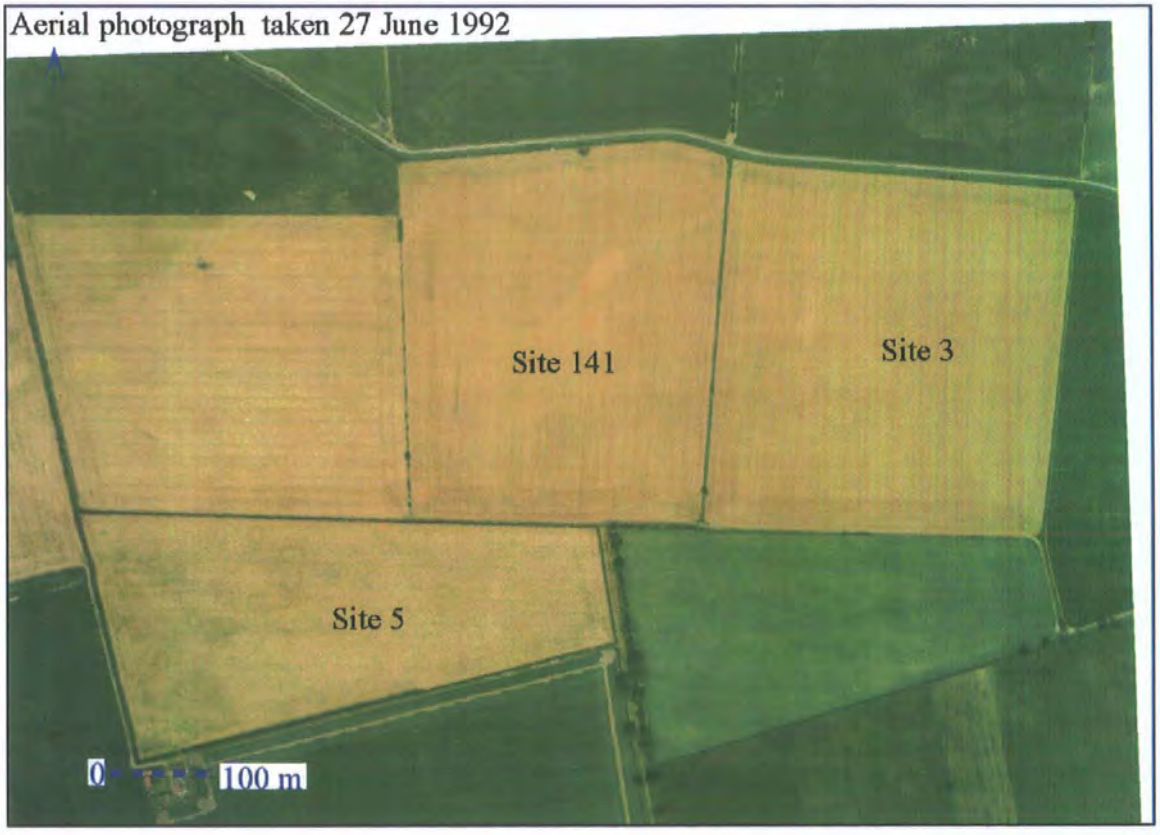

Figure 105 An aerial photograph of case study area 1 taken on 27 June 1992 (source NERC)

This area consists of site 3, site 5 and site 141, and is located within geomorphological Zone 6. Sites 3 (winter barley) and 141 (winter barley) were known to contain an enclosure system of uncertain date, which had shown particularly well in an early aerial photograph (see Figure 117 for cropmark plot), with different parts of the system

developing cropmarks in more recent times. Site 5 (spring barley) contains a square and round barrow cemetery, located on a small raised area. The field is known locally as Roundhills, probably because the field once contained small raised sandy gravel "bumps".

Figure 106 A montage aerial photograph of case study area 1 taken on 23 June 2005 (source NERC)

Two sets of vertical photographs have been taken by the NERC of the area, the first with the Wild RC10 on the 27 June 1992, and the second using the Rollei medium format digital camera on 23 June 2005. A direct comparison of Figure 105 with Figure 106 demonstrates that the cropmarks from the 23 June 2005 give a very detailed return, particularly of the cemetery in site 5. The crops in 2005 were winter wheat in sites 3 and 5, and spring barley in site 141.

This is shown in detail in Figure 107, where the fully georeferenced images have been enhanced using histogram stretches. A cursory initial inspection confirms that the clarity of the cropmarks from the 2005 photograph in comparison to the 1992 image is immediately apparent. However, there are a number of features on the 1992 photograph which either do not appear or are very faint on the 2005 image. The small black arrows at numbers 1 and 2 all indicate the location of square barrows which are only visible in the earlier image. Number 3 shows the much greater detail in the 2005 image, with more square barrows visible as well as two faint grave pits. Number 4 shows the rectilinear enclosure system, in great detail, and number five gives a very clear picture of the nature of the small enclosure on the edge of the cemetery, plainly showing the double ditch system on the western side of the enclosure.

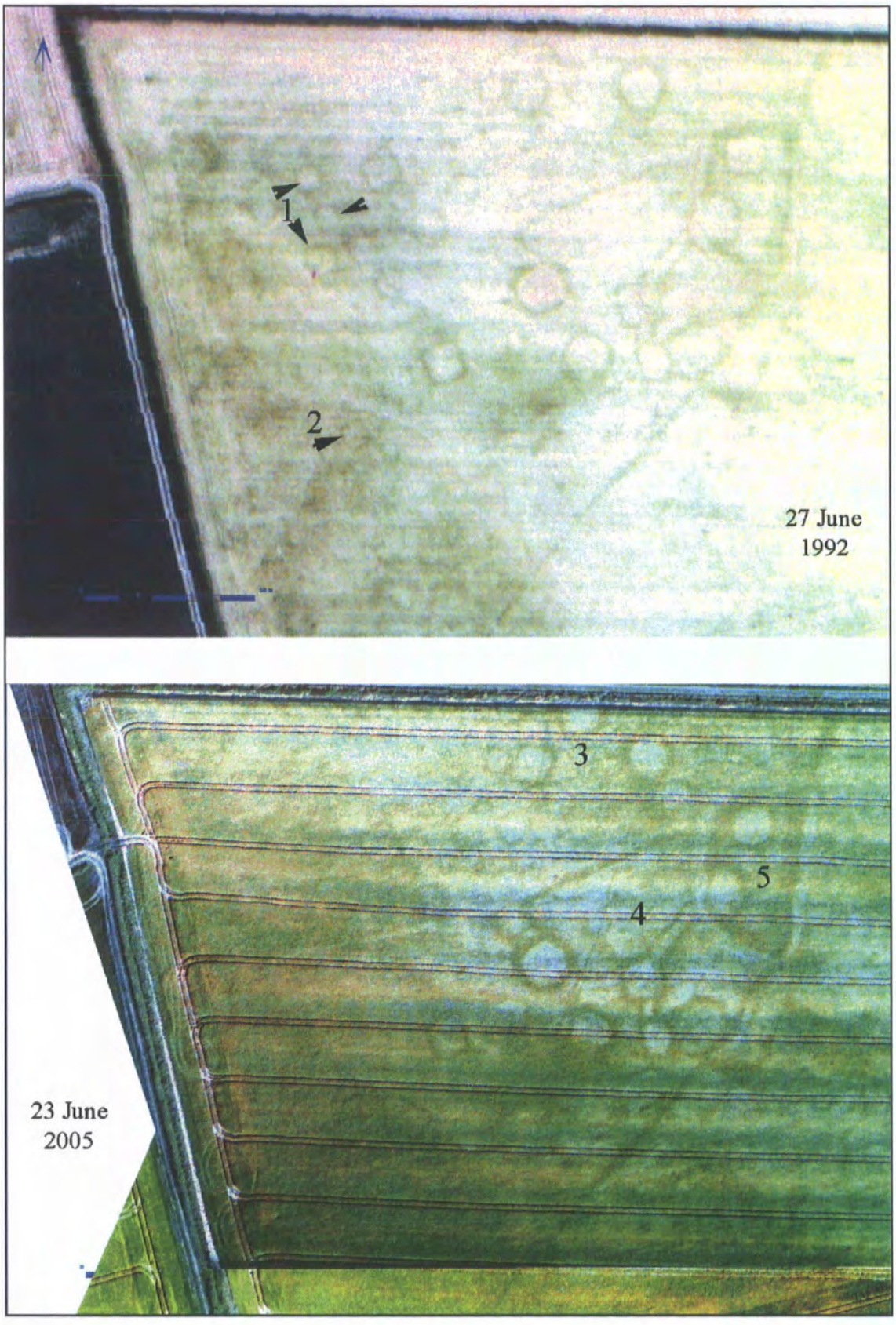

Figure 107 A comparison of the cropmark returns from 1992 (spring barley) and 2005 (winter wheat) (source NERC)

In order to visually show the different returns from the ATM flights, a number of georeferenced ATM images acquired on 27 June 1992 will be compared with the images acquired on 23 June 2005. Of course, the returns from these two sources are not directly comparable, mainly because different crops are present in the fields, but even if the same crop was present, the exact growing conditions for each season are in effect an unrepeatable experiment, generating a different result each year. Differences could include the sowing time of the crop, rainfall during the growing season, and whether fertilizers and/or weedkillers were applied to the crop.

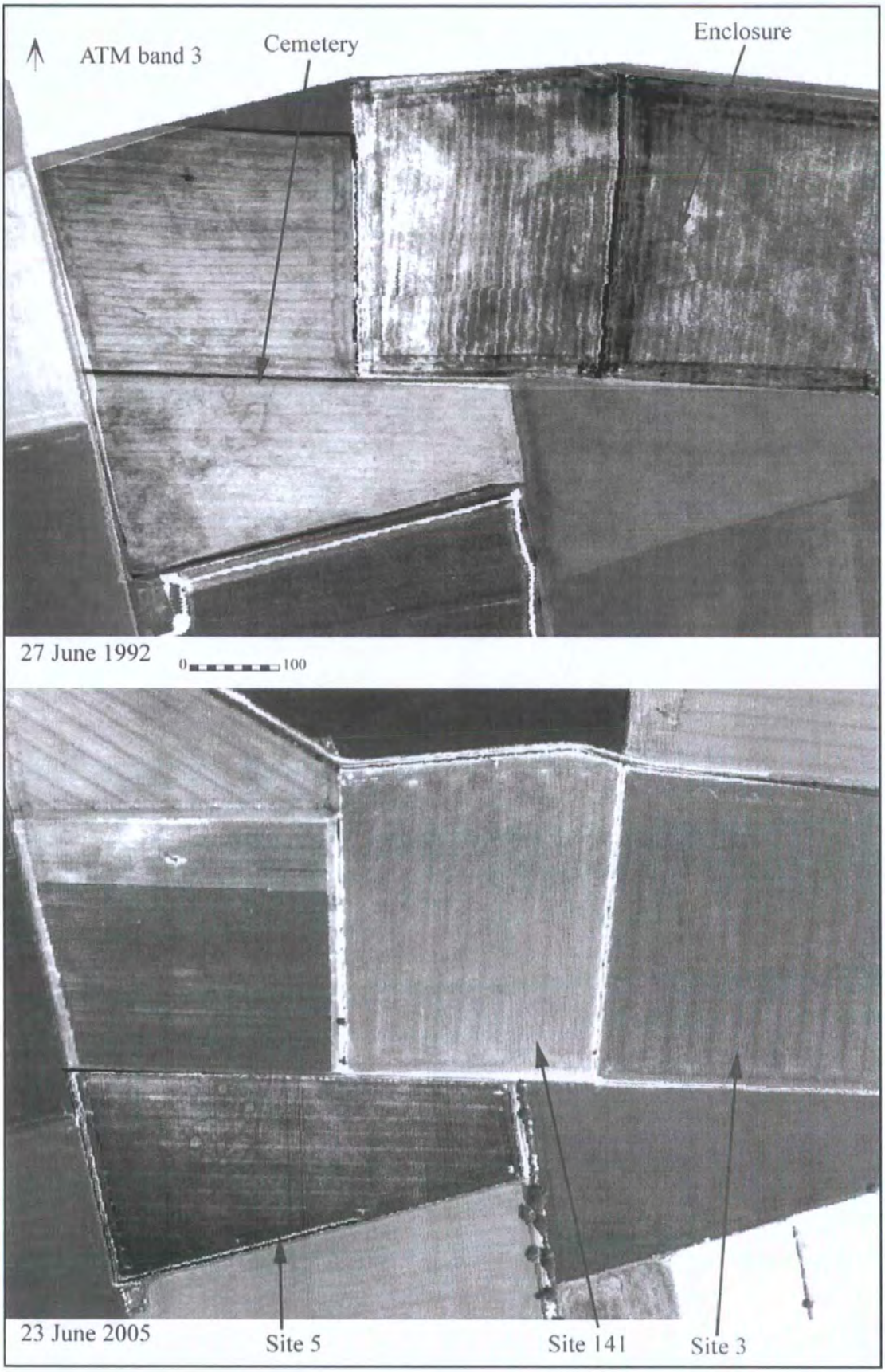

Figure 108 Comparison of ATM band 3 from June 1992 and June 2005

That being said, the comparison of the two datasets does allow us to see that different bands distinguish anomalies better in some crops than others, and it is only by looking at all of the bands that we can be sure of complete anomaly detection. The stage of development of a crop is of extreme importance for remote sensing purposes, and where the visible bands are more successful at detecting conventional cropmarks, the infra-red and thermal bands often find differences in areas where normal cropmarks are invisible. When looking at the comparison of the returns from band 3 (green) in Figure 108, it immediately becomes apparent that both flights have detected the cemetery in site 5, with the 2005 flight showing a greater return than the earlier flight. However, the 2005 flight shows nothing at all in sites 3 and 141, whereas the 1992 flight shows the small enclosure in site 3 with great clarity.

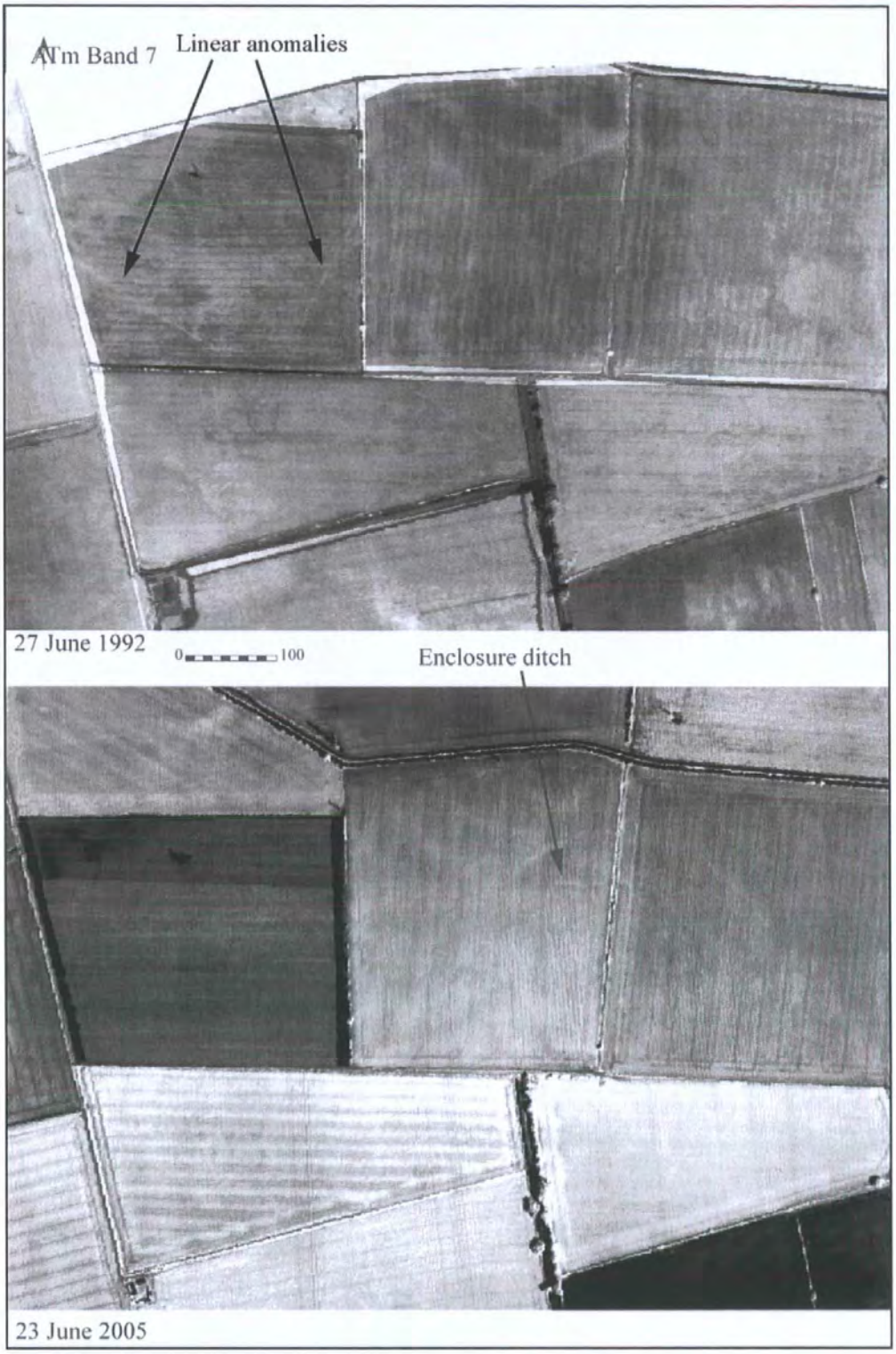

Figure 109 Comparison of ATM band 7 from June 1992 and June 2005

The returns from the near infra-red band 7 (see Figure 109) give us a completely different picture from band 3, with neither flight giving particularly good returns from the cemetery in site 5, although they are slightly clearer in the 1992 data. The 1992 data also shows us some detail in the field to the north of site 5, with two linear anomalies

extending outwards from the cemetery area. However, a further enclosure ditch can now be seen in site 141, visible in both flights, but clearer in the 2005 data.

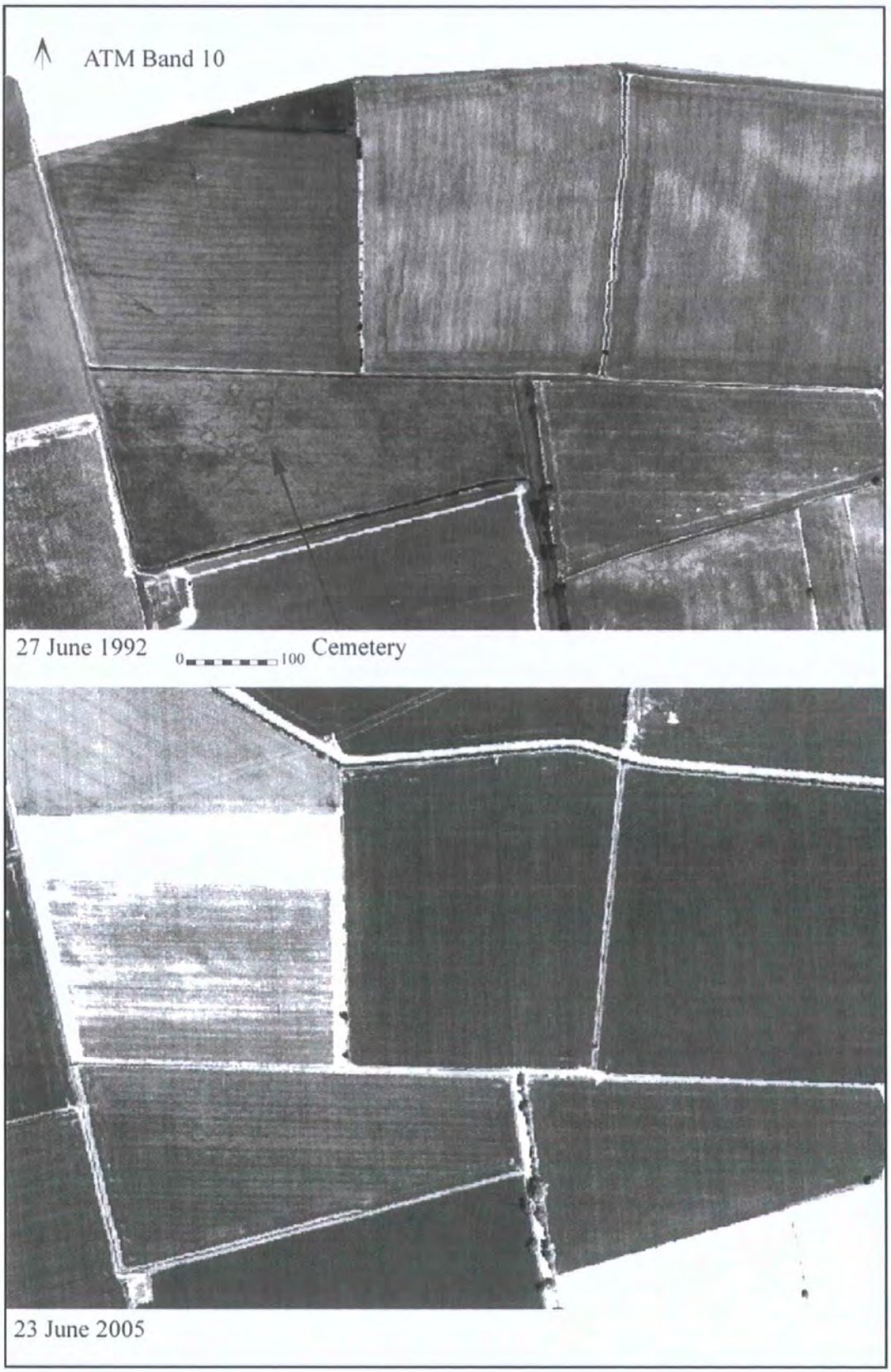

Figure 110 Comparison of ATM band 10 from June 1992 and June 2005

The short wave infra-red, (2.08-2.35um) band 10 gives us the clearest indication of the combined effects of different crops and changed growing conditions, as virtually no archaeological anomalies can be seen in the 2005 data (the cemetery in site 5 is just visible, see Figure 110). However, the 1992 returns from band 10 give the best result of all the bands for site 5, with a greater level of structural detail visible within the cemetery zone.

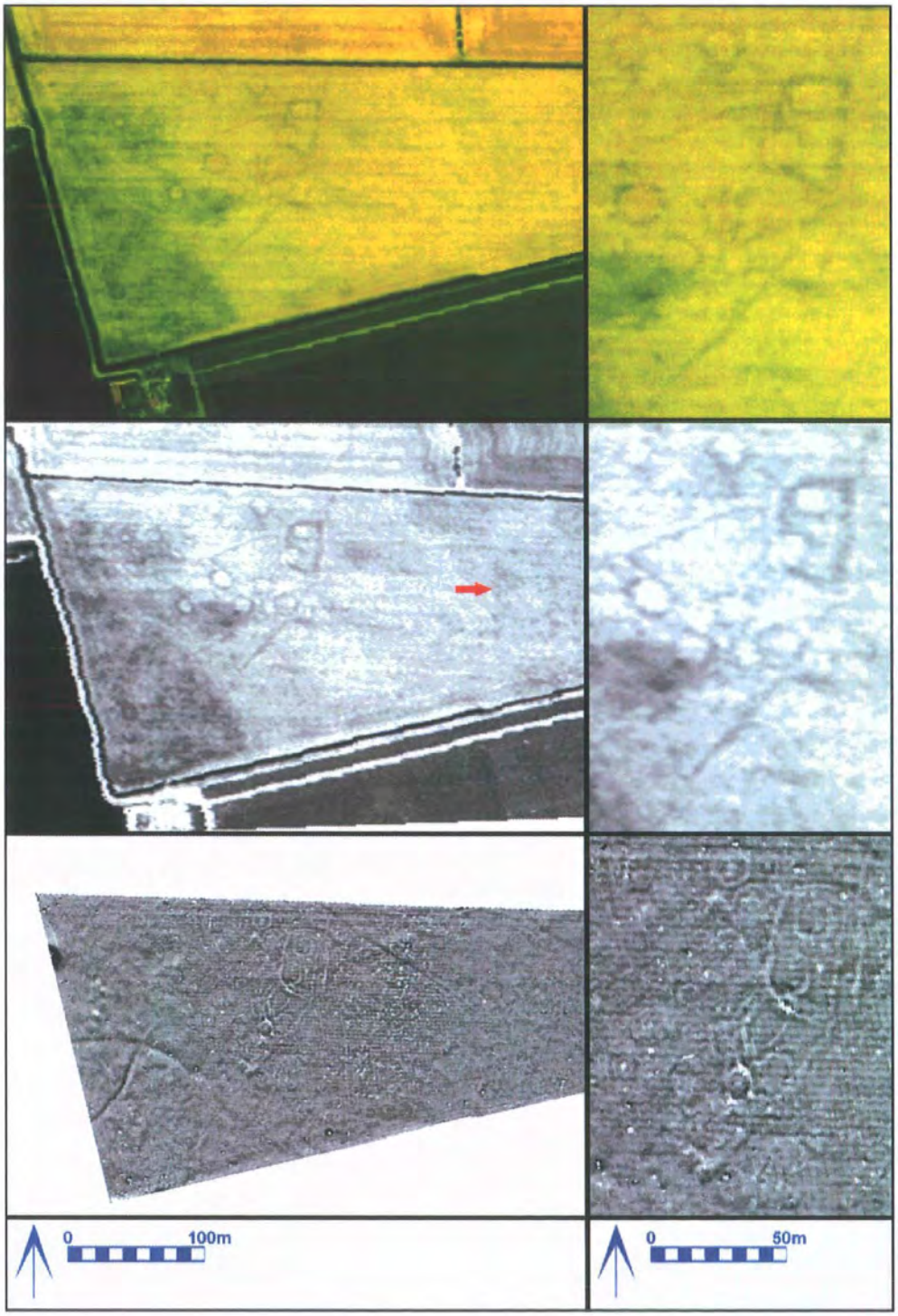

Figure 111 Complementary data sources

This is further demonstrated in Figure 111, which gives a comparison of three different remote sensing techniques. The upper image is the aerial photograph taken by the NERC in 1992 showing an area of square barrows; the central image is the same area from the 1992 multispectral data (band 10: short wave infra-red); the lower image is the geophysical data collected in 2003. On the right is an enlarged view of the central area.

The aerial photograph gives a reasonable overall picture of the archaeological deposits; which include round barrows, a trackway with attached enclosures and a number of associated square barrows. The detail is good, particularly in the south-western corner where features are visible that are not readily seen in the other remote sensing images.

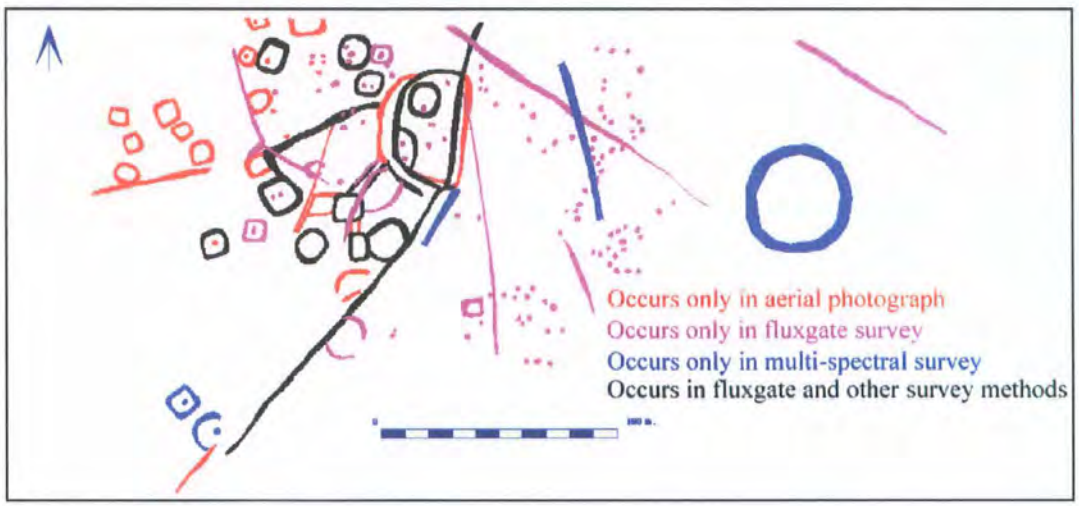

Figure 112 Showing the unique returns from three forms of remote sensing

The multispectral survey data from band 10 confirms the presence of all of these features, with greater detail in some and less in others. Of particular note is the faint circular anomaly in the eastern part of the image (the location is indicated by a red arrow in Figure 111), a feature which is not known from any other remote sensing source, and was seen only in band 10 of the 1992 ATM data.

The geophysical results show some of the barrows, but by no means the numbers detected using the other methods. However, more detail on the geological change in the

south-western part of the field was gained, as well as the discovery of a zone of localised anomalies situated to the east of the main barrow zone. It had long been thought that the wetland deposits would be less susceptible to magnetometry than the zones to the south. This does appear to be the case, though the extent of the loss of signal was less than anticipated. Further surveys to the north and west of the area are planned.

The unique returns from each of the three forms of remote sensing are displayed in Figure 112, together with the anomalies which occurred in more than one technique.

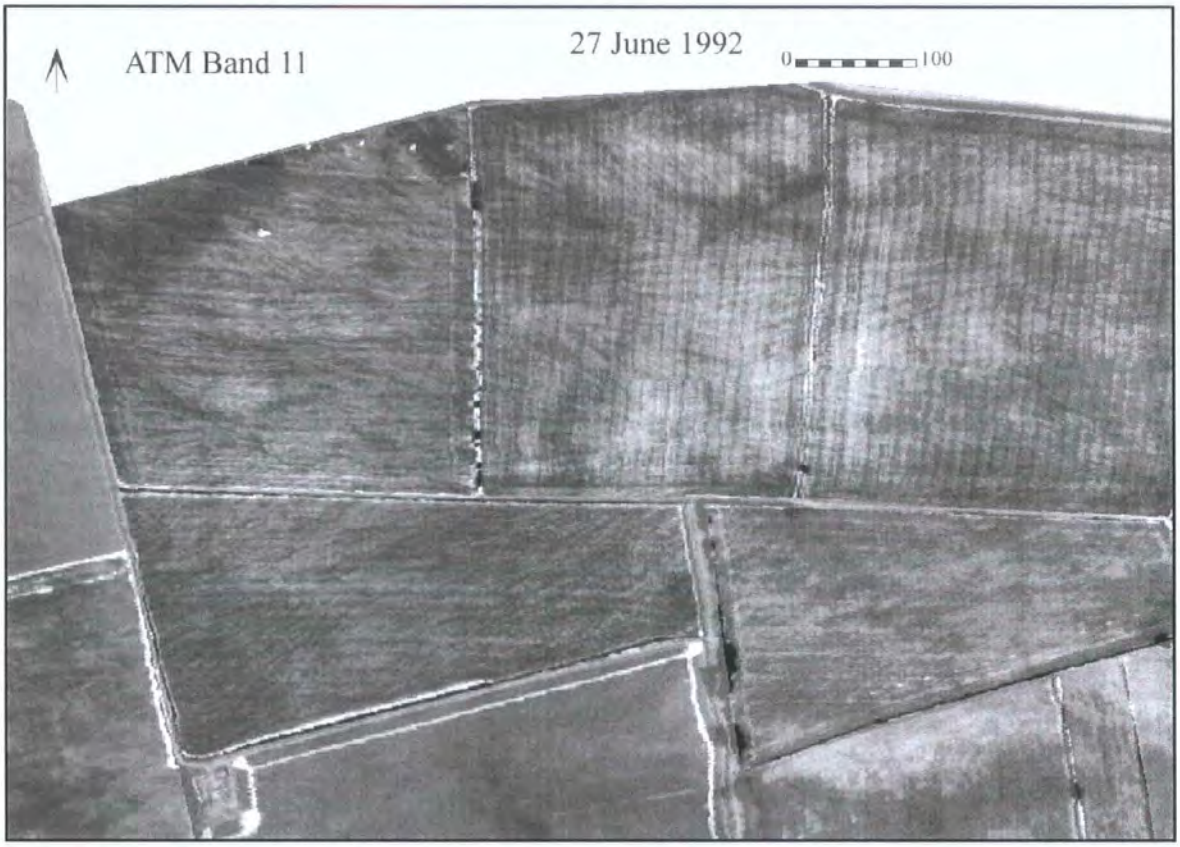

Figure 113 Thermal band 11 (June 1992 data) showing the effects of wind shear on thermal data

Figure 113 shows the effect of wind shear on thermal data, where a slight breeze blowing across the top of the crops causes a thermal ripple effect (combining emitted radiation from the soil and vegetation with thermal convection currents) which almost completely masks the underlying archaeological anomalies. With the eye of faith, it

would be just about possible to see a part of the cemetery in site 5, but without knowing it was there beforehand, it would be unlikely to be interpreted as an archaeological site from the thermal data alone.

Thermal difference (case study area 3)

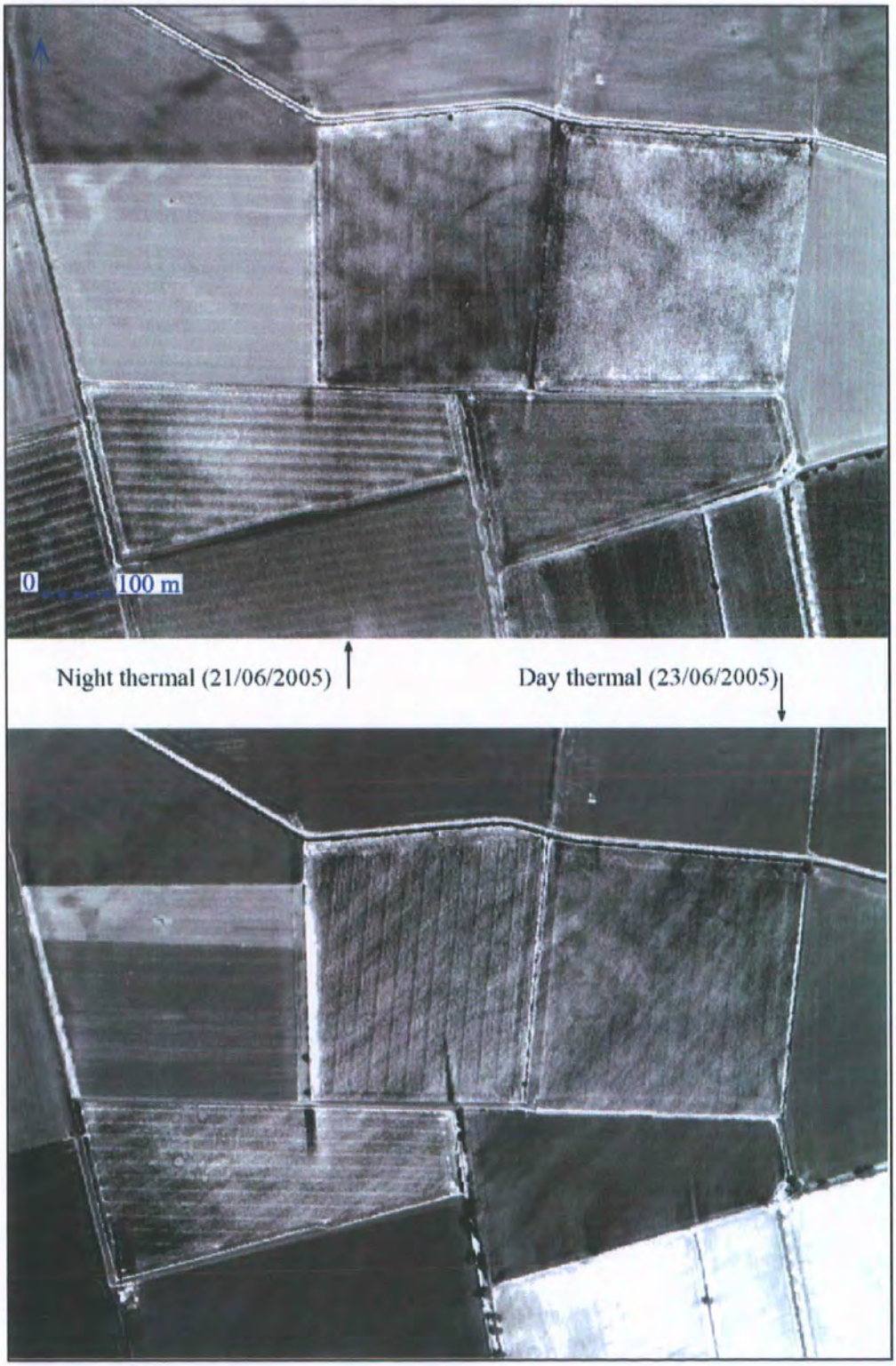

Figure 114 Thermal difference between night and day flights (AZ-16 ATM). Case study area 2

The thermal differences between night and day acquisition are very marked in this area. For instance, the cemetery zone in site 5 is clearly visible in the daytime data, but is completely missing from the night acquired data, where it shows only as a lighter (slightly warmer) part of the image (see Figure 114).

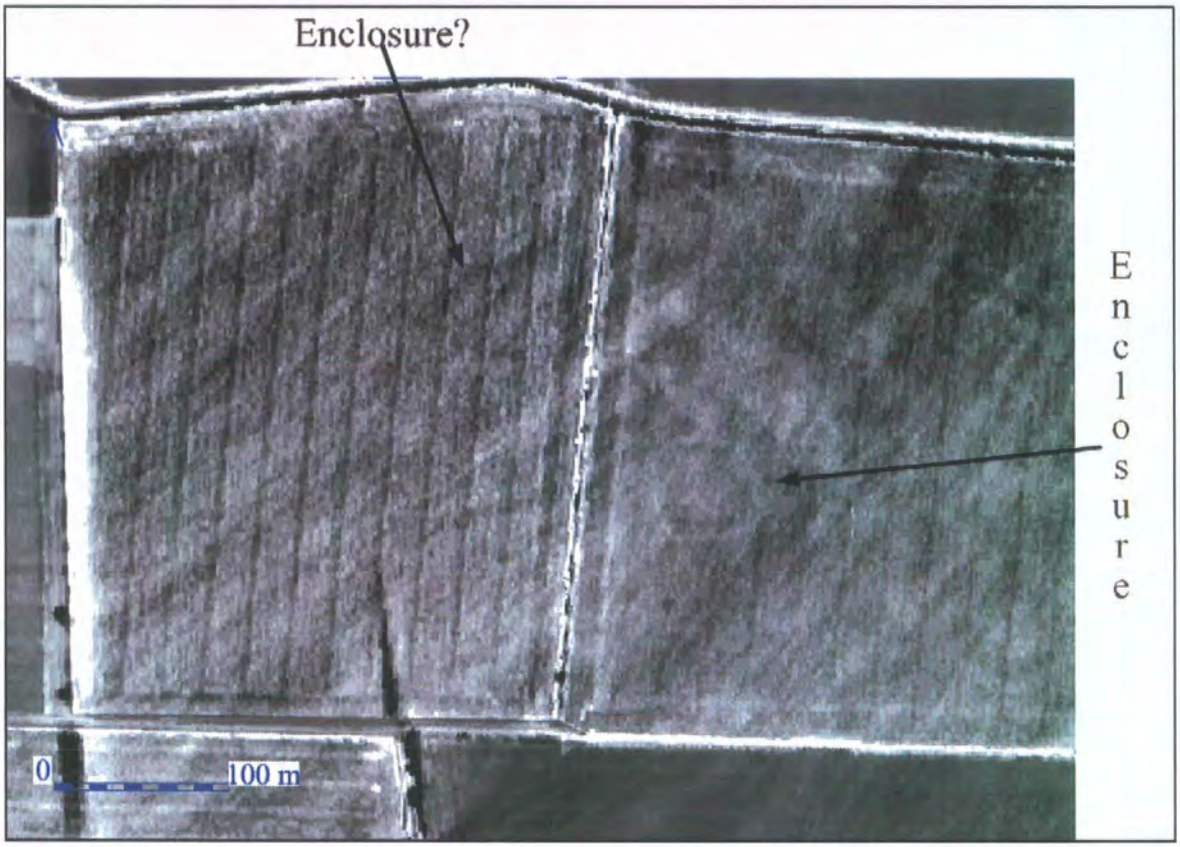

Figure 115 Day acquired thermal ATM data (23/06/2005)

For the eastern part of case study area 3, the difference between the day and night returns is equally apparent. In the eastern field, the square enclosure can be clearly seen in the daytime thermal (Figure 115), while it is virtually undetectable in the night time image (Figure 116). In addition, a possible small rectangular enclosure can be seen in the daytime data in the western field, but again is undetected in the night acquired data. It may be of note that the square enclosure is detected as a warmer anomaly, whereas the small rectangular enclosure is a colder (darker) anomaly.

It is in the western field where the night time data detects the western part of a large enclosure ditch, which is invisible in the daytime data. This enclosure was also known from an earlier cropmark plot (indicated in red in Figure 117), although the internal divisions seen in the cropmark plot are not detected as thermal anomalies.

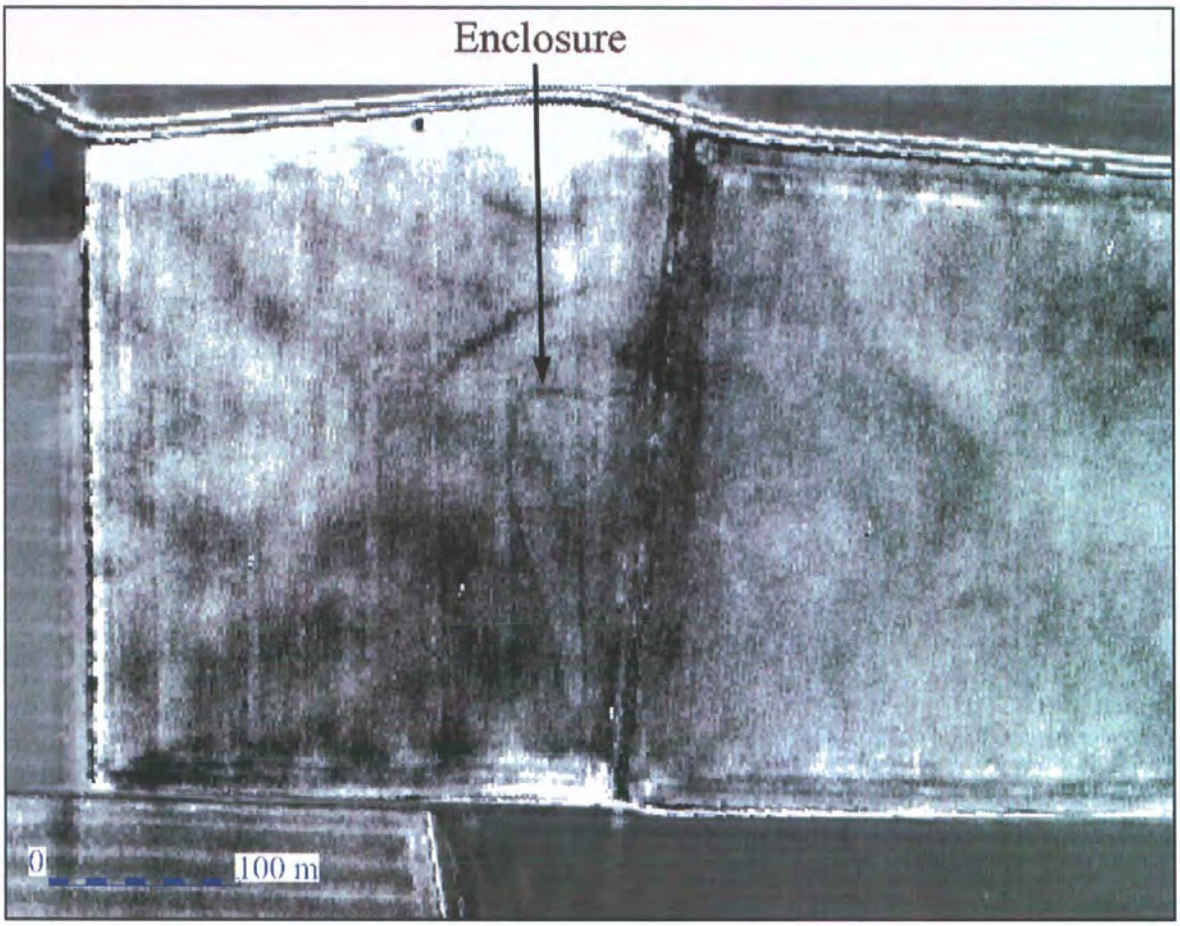

Figure 116 Night acquired thermal ATM data (21/06/2005)

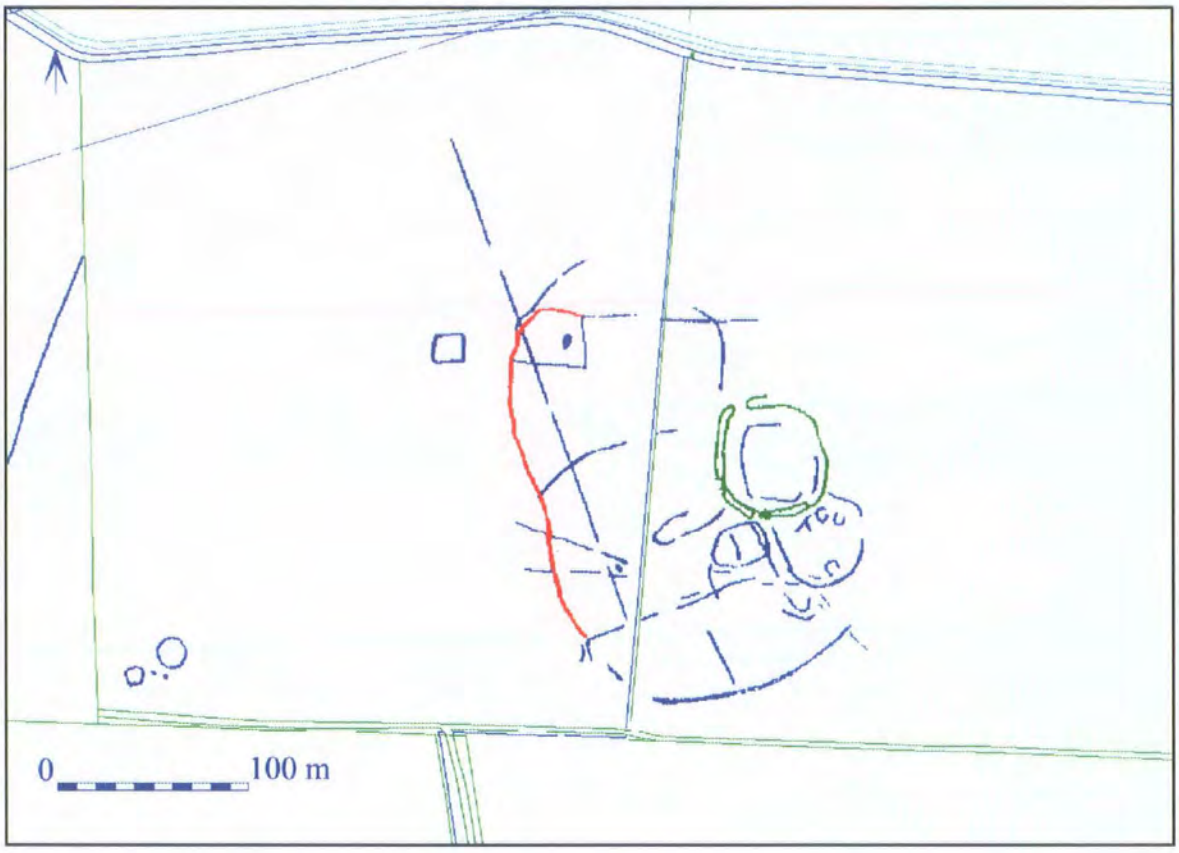

Figure 117 Cropmark plot of case study area 3 (eastern zone)

Figure 117 is a cropmark plot (in blue) of an aerial photograph taken in 1975. The anomalies detected by the thermal imagery have been coloured red (night acquired) and green (day acquired) for reference.

Note the increased level of internal structure within the large enclosure ditch which is only visible in the cropmark plot.

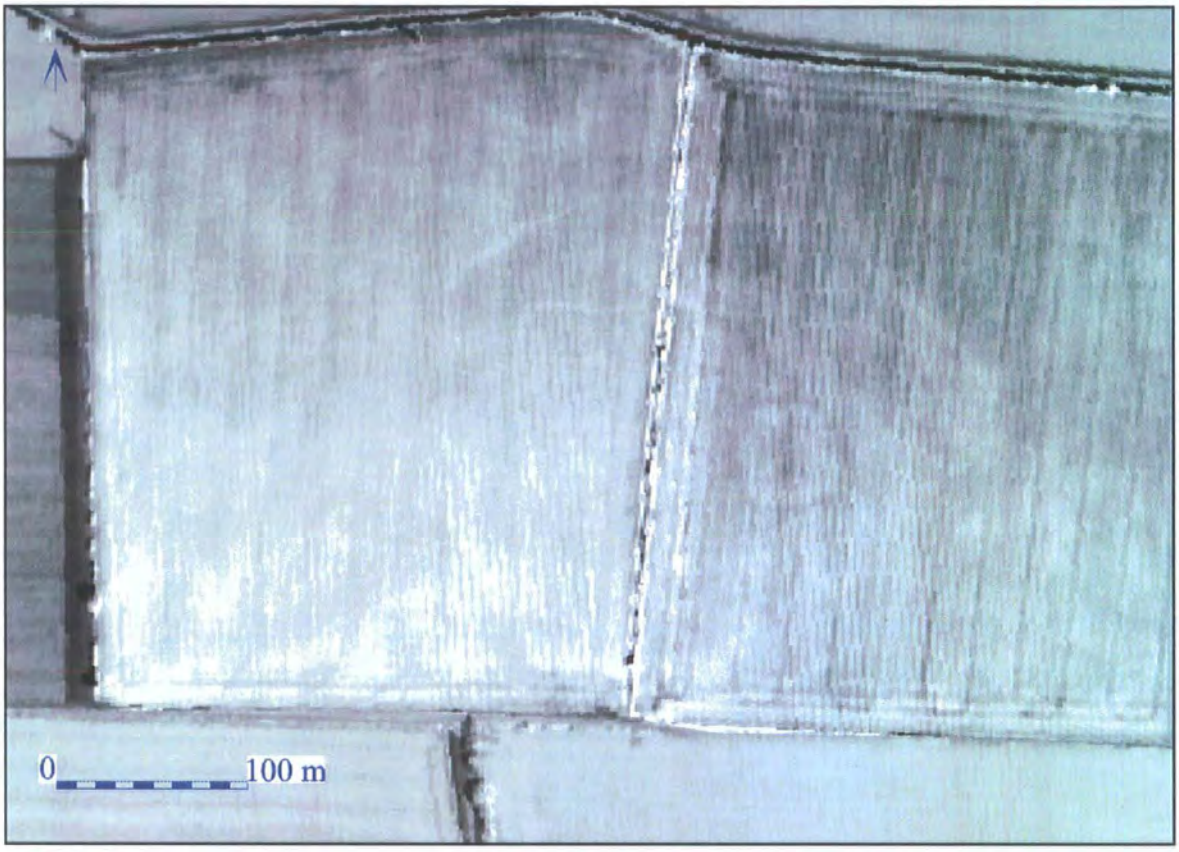

Figure 118 Band 7 (infrared) ATM image of case study area 3 (acquired 23/06/2005)

The infrared band 7 (Figure 118) contained evidence for both the square enclosure and the larger ditched enclosure, although the possible small rectangular enclosure was only visible in the daytime thermal band. The visible bands of the AZ-16 ATM 2005 imagery contained no evidence for any of these anomalies.

6.5.4 Case study area 4

This area was chosen because it covered the aeolian sands in the north (zone 4), the spring line and basal red chalk in the centre (zone 3), and solid chalk to the south (zone 2). It comprises sites 20 to the north of the A64, and sites 52 and 54 to the south. Site 20 contains a ladder settlement in the north and a sequence of trackways and pit alignments in the south. The trackway continues across the A64 to the south, first through site 52 and then site 54, although it becomes less visible as it climbs the slopes of the Wold scarp.

Site 20 gradiometer results

The full range of the archaeological remains can be seen in Figure 119, which also shows the relative positions of sites 20 and 52, bisected by the A64 trunk road. Although the site was long known from aerial photographs, the gradiometer survey has again enhanced the level of archaeological knowledge.

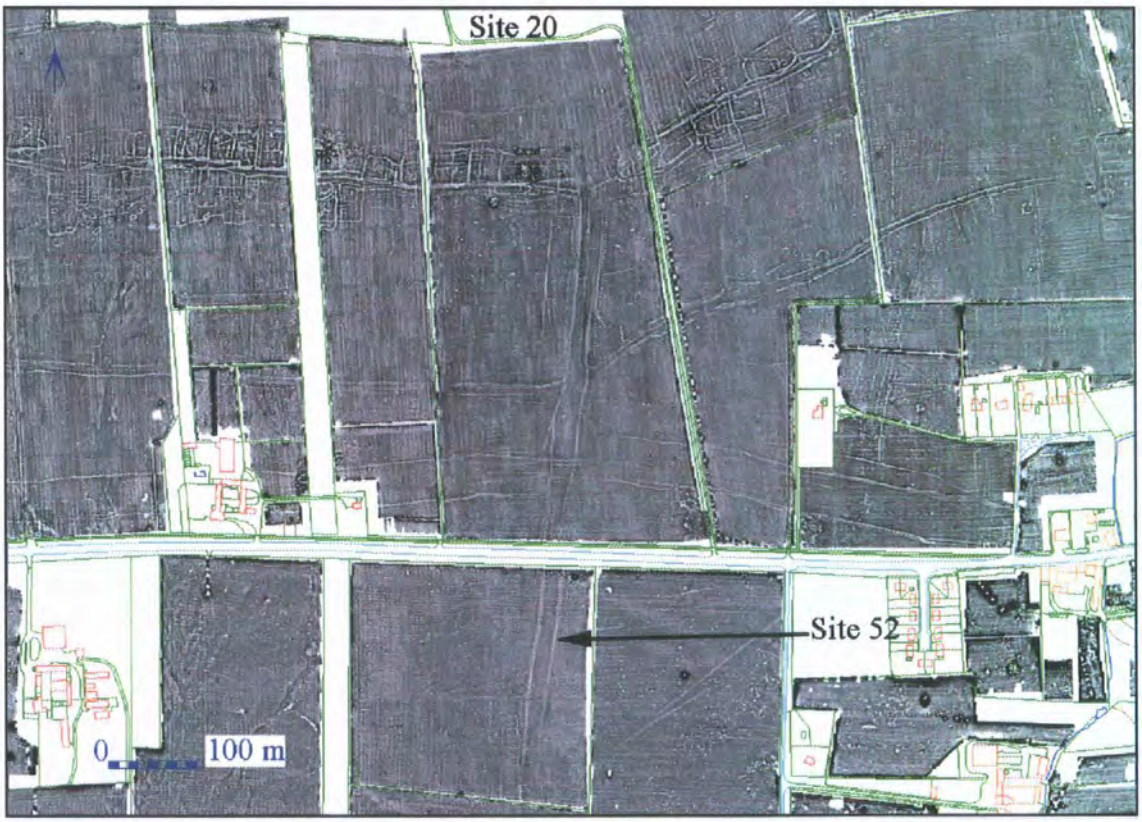

Figure 119 Sites 20 and 52 and surrounding area: fluxgate gradiometer survey

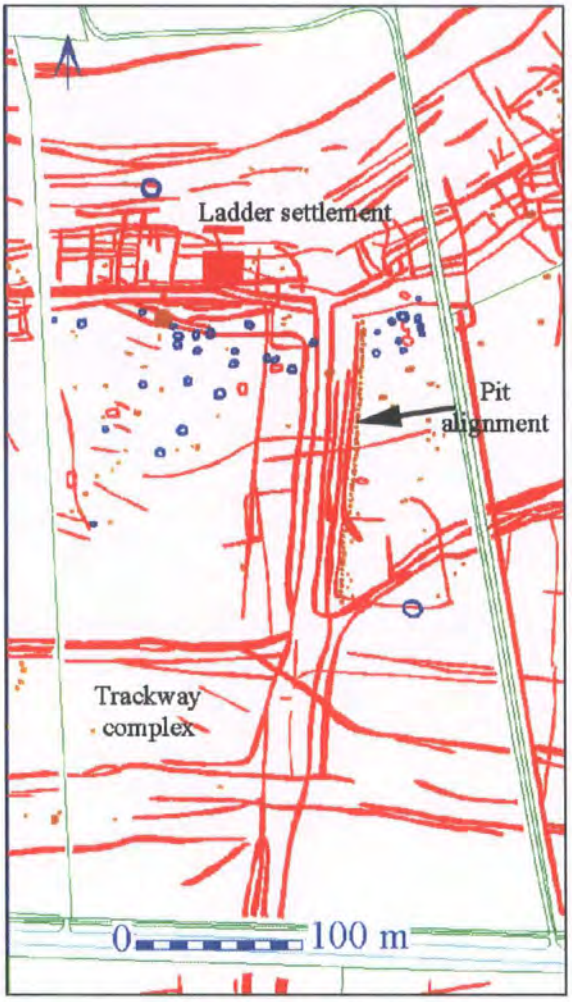

The ladder settlement itself is once again clearly delineated, with a number of ditches exhibiting enhanced magnetic signals. The level of activity appears to lessen slightly where the settlement meets the main trackway.

Figure 120 Interpreted gradiometer anomalies

The strong magnetic dipoles in the centre of the northern half of the area (see Figure 126) mark the position of the iron grid pegs left by sample excavations carried out in 1984. Just to the south-west of these is a large, powerful anomaly which almost certainly marks the location of a metal working furnace (fragments of iron bloom were found in the fill of the ditches during the excavation). A number of the round and ovate anomalies (believed to be part of a cremation cemetery) are also present, located as always to the south of the main east-west trackway in the centre of the ladder settlement. As the furnace appears to be in the centre of these barrowlets, it is unlikely that they were of a contemporary date. A potential round barrow can be seen to the central east of the area, although this is a very faint magnetic signal. A more definite round barrow is indicated to the north of the ladder settlement.

The main north-south trackway which leads down from the Wolds is clearly visible, indicated by a number of linear anomalies and a pit alignment down the eastern side. This is the southern extent of this trackway, which is known from the aerial photographic evidence to extend up onto the Wolds, before widening out into a funnel shape. A number of east-west aligned trackways and ditches extend off from the main north-south line. Some of these were pit alignments in their earlier phases, although by their final phase all of them had been converted into linear features in this area. Interestingly, some of the aerial photographs show pit alignments where the gradiometer has only detected ditches (see Figure 124 and Figure 125). A dispersed Anglian component was also found in the survey, with eight anomalies being interpreted as *Grubenhäuser*.

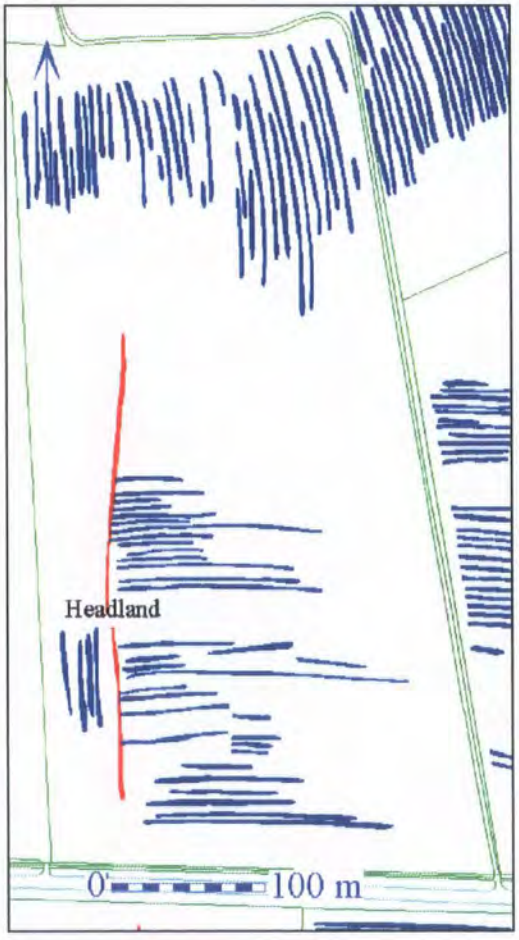

Medieval rig and furrow plough lines can be seen across the northern part of the field, in a rough north-south orientation. They appear to stop just before the faint linear anomaly near the northern part of the surveyed area (in line with current field boundaries to the west and east) indicating the presence of a medieval headland at this point. A second headland is indicated (in red) in the southern part of the area, where the alignment of the rig and furrow changes from a north-south to an east-west orientation.

Figure 121 Interpreted rig and furrow ploughmarks

Very little or no evidence from either the aerial photographs or the multispectral imagery for rig and furrow has been found in the sandy zone in the Vale of Pickering. This is not a phenomenon which is confined to site 20, but is found throughout the area so far covered by geophysical survey. A comparison between the collected returns for all oblique and vertical photographs in the project zone with the geophysical survey plots demonstrates this difference in returns in an emphatic way. Only five cropmarks interpreted as furrows were found in the area covered by the geophysical survey, where 2022 anomalies identified as Medieval furrows have been detected.

The location of theses five cropmarks is indicated by the pink square in Figure 122.

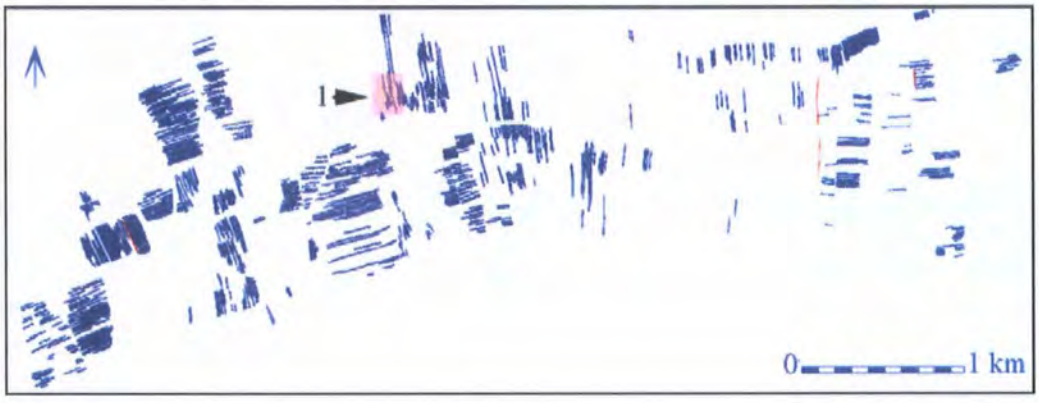

Figure 122 Comparison of interpreted rig and furrow ploughmarks from gradiometery and aerial photography

Site 20 aerial photography

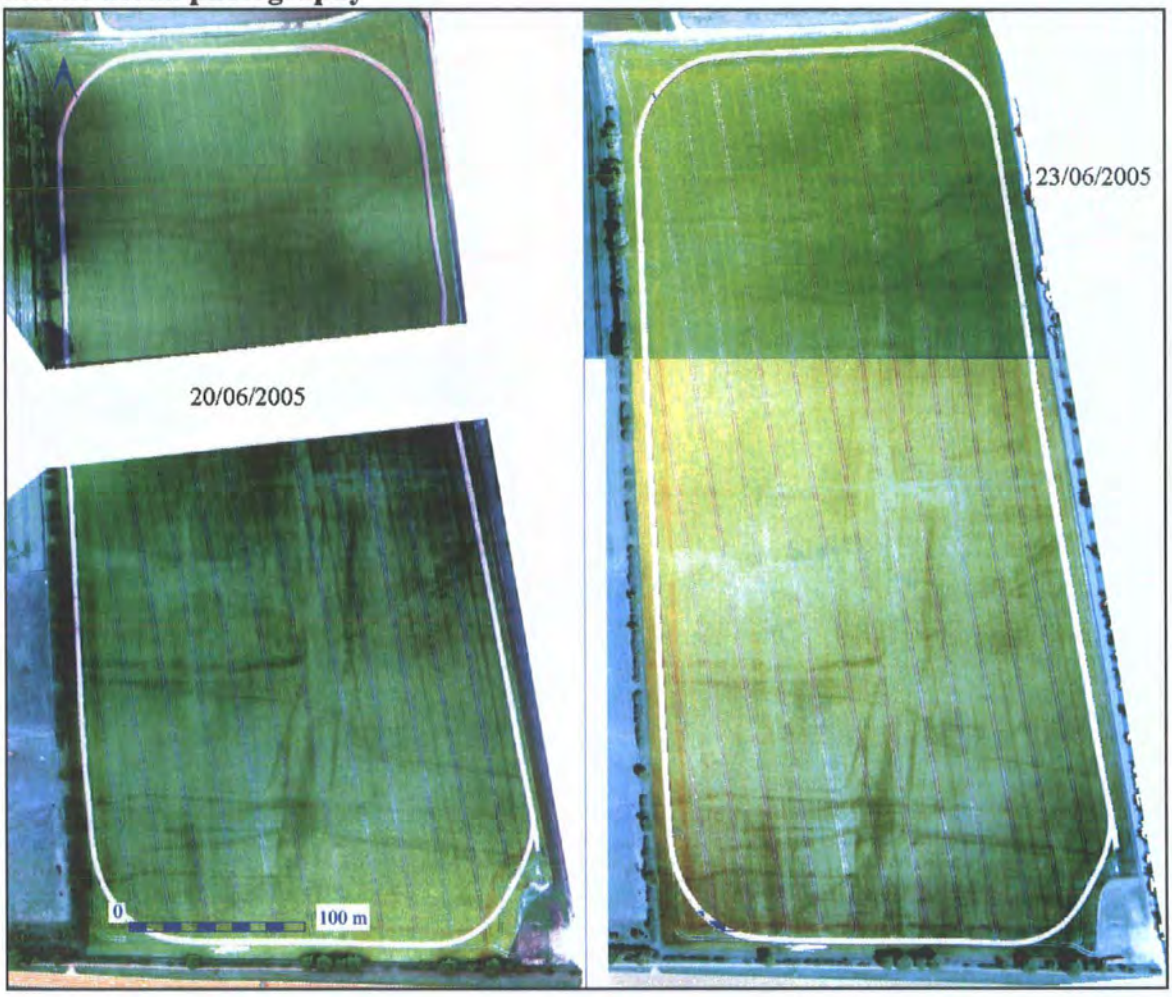

Figure 123 Site 20 showing change in cropmarks over a three day period (source NERC 2005)

As with the first ATM acquisition flight in 1992, the initial flight of the 2005 campaign was marred by cloud cover, and the mission was called off after 6 lines of data (approximately half of the area to be covered) had been collected. Once again this allowed for a comparison of data collected at a close chronological interval to be compared, although with only a 3 day difference (20/06/2005 to the 23/06/2005, see Figure 123, where overlapping georeferenced images have been individually enhanced to maximise the cropmark returns, hence the different colours across the figure) as opposed to the 10 day difference in 1992. The gap in the centre of the earlier flight is where there was no overlap between the consecutive runs. Unsurprisingly, the differences noted in return over a 3 day difference were not as pronounced as those noted in the 10 day difference 1992 data, but subtle changes can still be demonstrated

by using the georeferenced digital images from the two flights. Two smaller areas from the main case study area will be used to demonstrate this point, using the gradiometer results to provide a base map of potential archaeological anomalies.

Example area one looks at the southern half of site 20, at a point where the main north-south aligned trackway is met by a number of east-west trackways. All of the main features associated with the trackways are present in both of the images, although the contrast difference between the cropmarks and the crop is slightly greater in the later photograph. However, it is the pit alignment present to the east of the main trackway where a slight difference in cropmark return can be seen. The pit alignment to the north of the image (arrowed in Figure 124) is visible in both images. This pit alignment can be seen to continue to the south along the eastern side of the trackway, but the individual pits are much clearer in the later of the two images

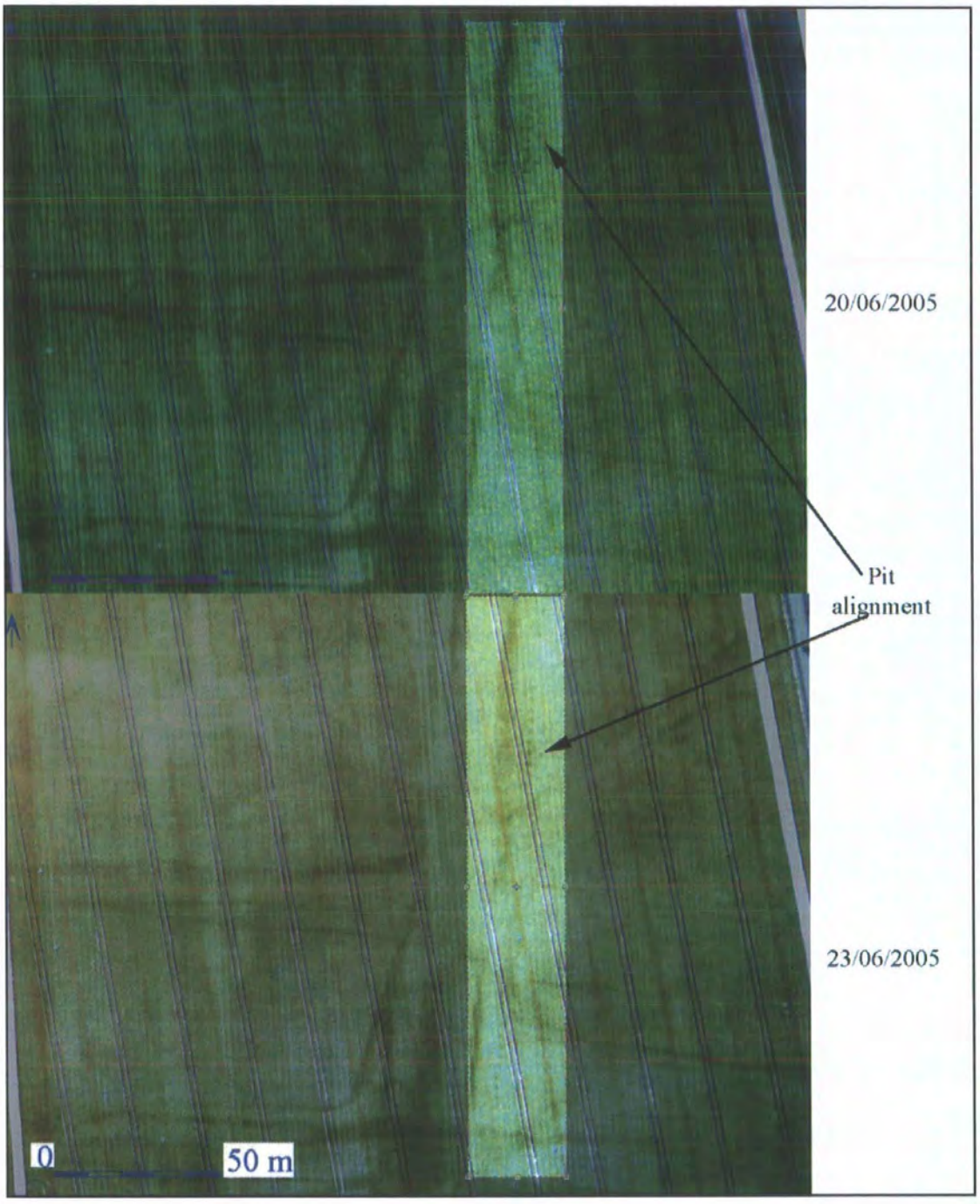

Figure 124 Detail view of aerial photographs over the southern half of site 20 showing highlighted pit alignment (source NERC 2005)

Figure 125 shows the same area covered by the gradiometer data, where all of the main trackways are immediately apparent, with some enhancement of detail in the centre of the area. Not visible on the aerial photographs are the east-west aligned Medieval rig and furrow ploughmarks. It is important to note that the aerial photographs clearly indicate that the pit alignment survives all of the way along the eastern edge of the trackway. They are also clearly visible as individual pits in the northern part of the

gradiometer survey, but appear only as a faint linear anomaly in the southern part. The magnetic constituent of the pits evidently changes after passing to the south of the trackway which branches off to the north-east, indicating a change of function in the area enclosed by the two trackways. This demonstrates once again the importance of using multiple remote sensing datasets to analyse areas. Both aerial photography and gradiometery gave good returns for this area, but only by studying both sets of data were more subtle differences noticed.

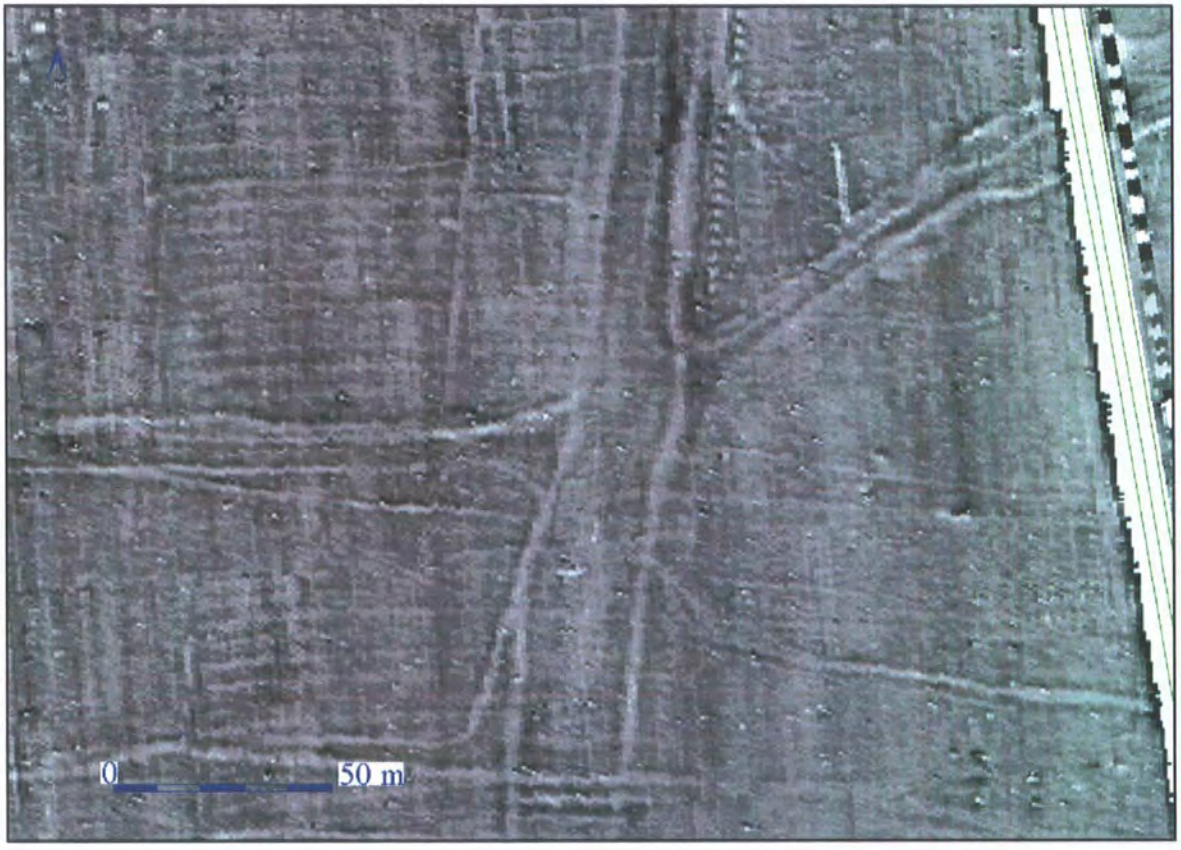

Figure 125 Gradiometer survey of southern part of site 20

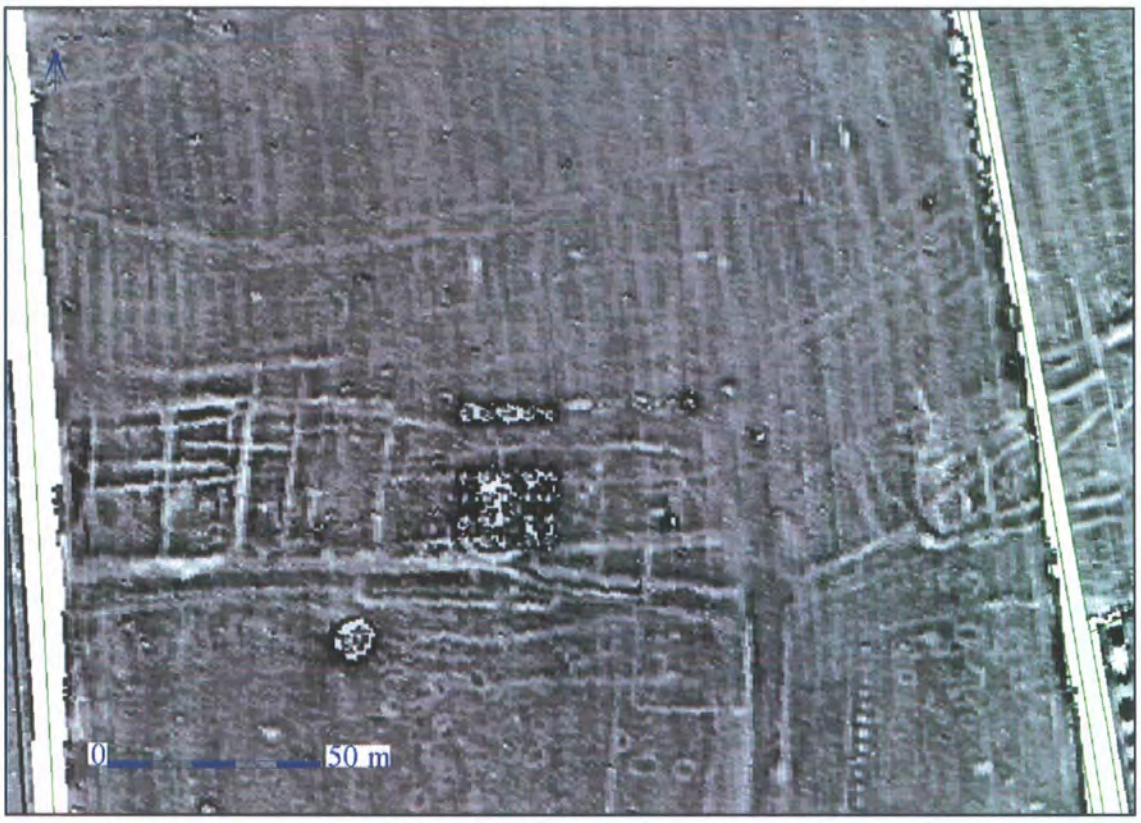

Figure 126 Gradiometer survey of northern part of site 20

Example area two is located in the northern part of site 20, where the main north-south trackway meets the ladder settlement, which at this point is east-west aligned. The northern end of the pit alignment discussed in example area one can be seen in the gradiometer data, coming up to the main trackway around which the ladder settlement is based (see Figure 126). A number of overlapping rectangular enclosures can be seen to the east and west of the area where the trackways meet, as well as a number of barrowlets to the south of the settlement.

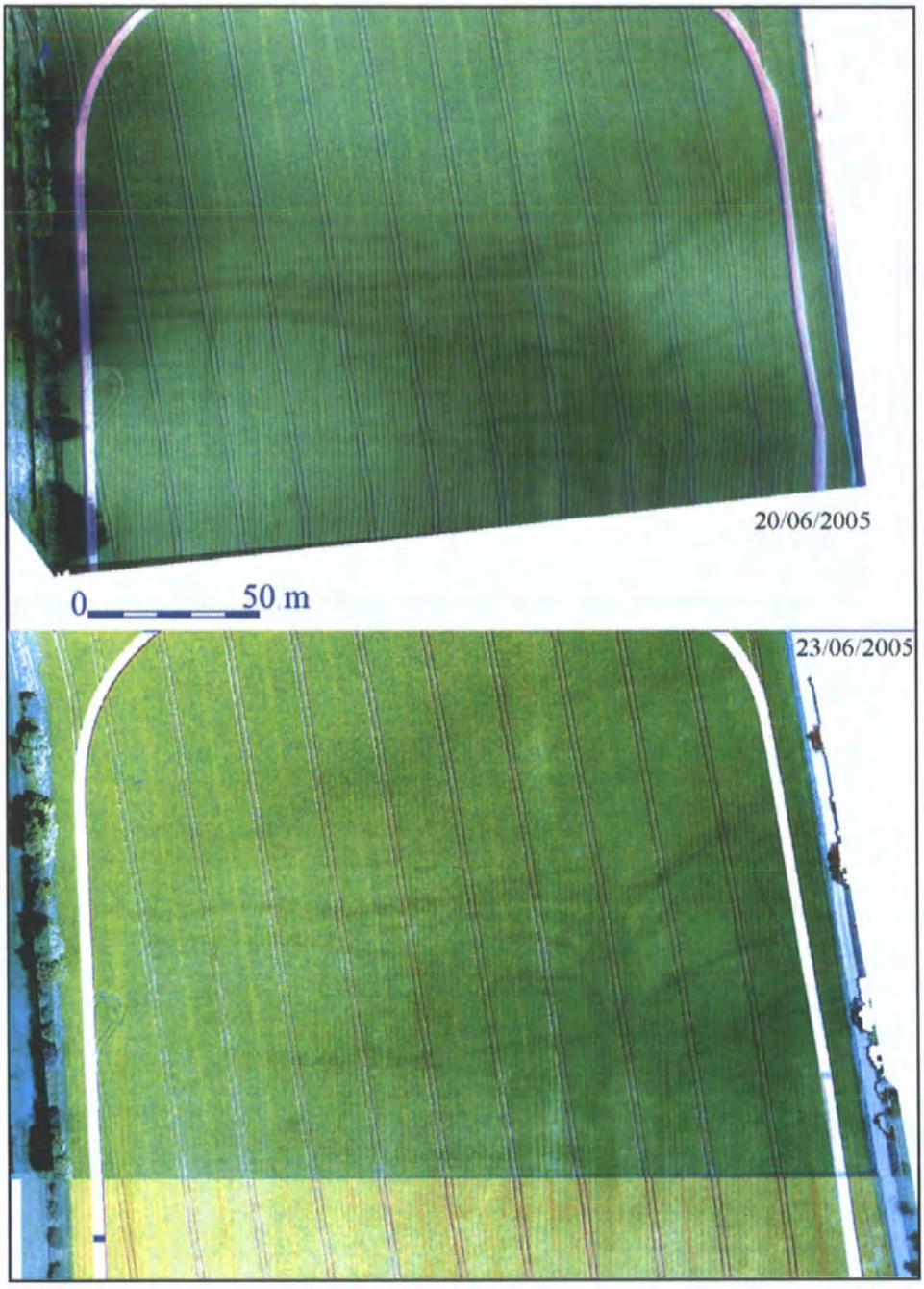

Figure 127 Detail view of aerial photographs over the northern half of site 20 showing ladder settlement (source NERC 2005)

Also visible as a faint lighter (positive) linear anomaly following the line of the ladder settlement to the north is what has been interpreted as the late Roman flood defences, a sequence of deep ditches which run along the length of the system, sometimes two or more ditches with a combined width of up to 15 metres.

The aerial photographs (see Figure 127) do not show the same level of detail, with the differences between the two photographs being very subtle. Most cropmarks are evident in both images, although once again the contrast between the cropmarks and the surrounding crop is greater in the later of the two images. It is certain that had this area been flown again a few days later, that the cropmark evidence would have been greatly increased. However, even with the just developing cropmarks, it is clear that the area where the main north-south trackway turns to the east and the west (to the north of the enclosures) is more clearly defined than the gradiometer data.

Site 20 ATM data

Figure 128 Visible bands (4, 3 and 2) of ATM data

Intriguingly, the ladder settlement which is clearly visible in the digital photographs is indistinguishable in the visible bands of the ATM image. This is shown in Figure 128, where the bands 4, 3 and 2 have been assigned red, green and blue respectively, giving a near normal colour range. Even after site 20 has been enhanced using contrast stretching, there is still no evidence of the cropmarks in the northern part of the field seen in the high resolution photographs. The ladder settlement does show up in a number of the remainder of the ATM bands, although it is also not detected in bands 5, 6, 8 and 10. It is just visible in bands 7 and 9, but is most clearly seen in the thermal band 11 (see Figure 129).

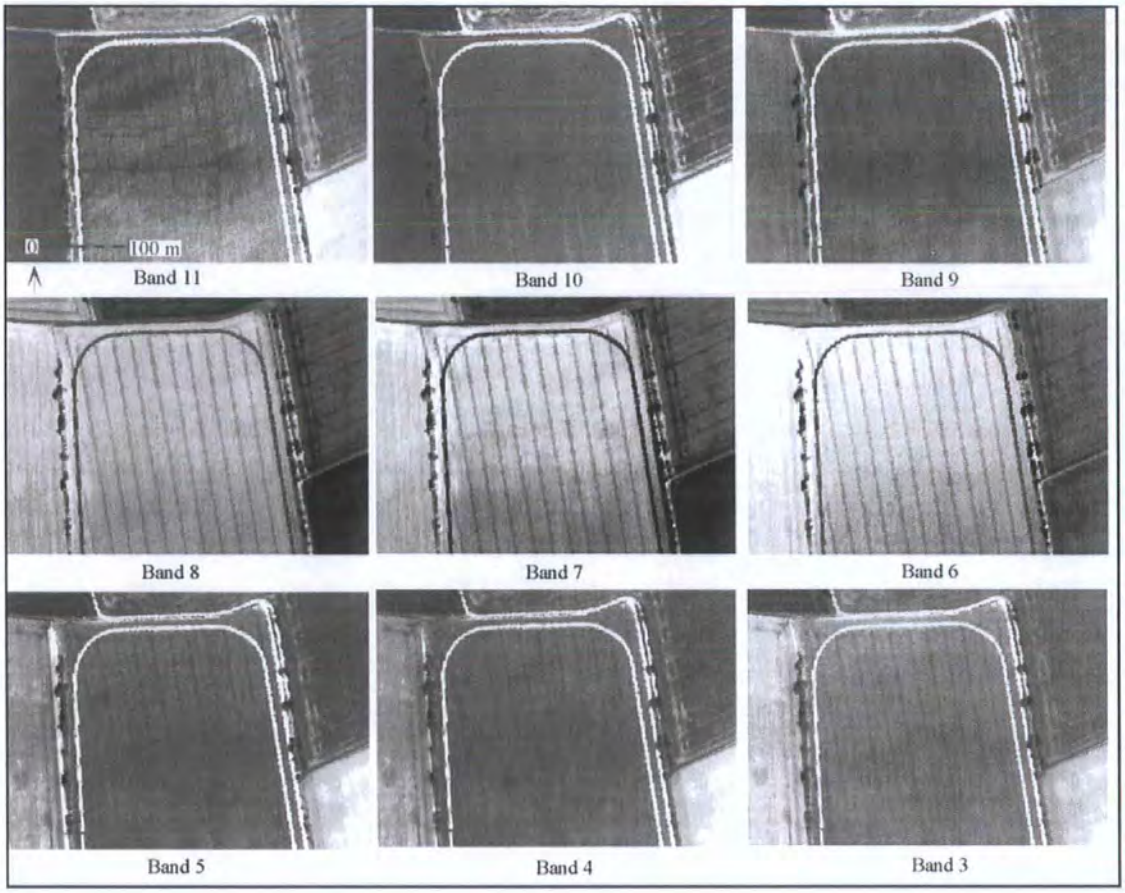

Figure 129 Comparison of 9 bands of ATM data

6.6 Pixel resolution and feature detection

There are two possible explanations for the fact that the visible wavelengths from the ATM data are not detecting the same cropmarks as the digital photographs taken at the same time. The first is the scan angle of the instrument. This is discussed in more detail below (see CASI data comparison). The second is the pixel resolution of the relative data sources. The apparent inability of the multi-spectral scanner to provide similar results in the visible wavelengths as those obtained by the aerial photographs is partially due to the disparity in ground resolution between these two techniques.

However, pixel resolution is not the only factor determining the response of multispectral data. It is the average radiance value of the target area which is collected, and this means that at times there are anomalies which are much smaller than the

ground pixel resolution which will be detected, because they are the dominant radiance value in the immediate vicinity.

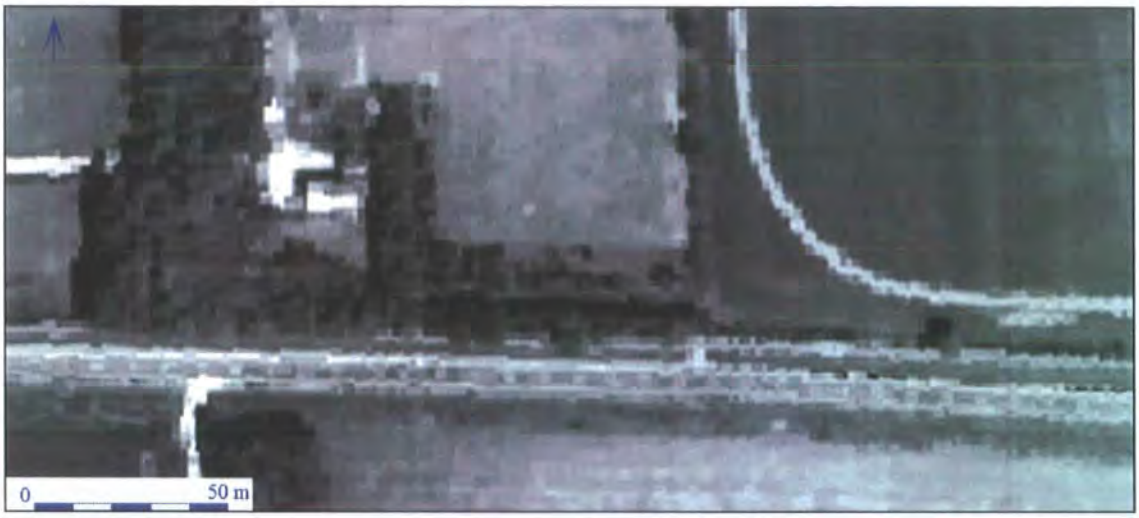

Figure 130 Showing the white lines on the road detected by band 5 of the AZ-16 data

This is demonstrated in Figure 130, where the white lines on the road are visible despite the fact that they are much narrower than the nominal pixel resolution (in this case 1.5 metre data). The radiance value of the white lines (which are designed to be reflective) is such that, if they were in the centre of the scan area, their value will be recorded for that pixel. If they were located towards the edge of the scan area, then the radiance value of the road is recorded, and this is why not all of the white lines are visible in the multispectral data. Of course, we now have an image which apparently contains a series of 1.5 metre wide white lines of varying lengths running down the centre of the road, obviously not a true representation of the actual ground conditions. This has a bearing on what we may term feature contrast in this dataset. The reason that anomalies are detected is that the radiance value is different from the surrounding pixels, but smaller, more dominant radiance values may mask subtle archaeological features.

In order to test what the returns from the aerial photographic data would have been had they been at the same pixel resolution as the multispectral data, the digital photographs of site 20 were georeferenced and then subsampled down to both 1 metre and 1.5 metre

resolution pixels, using a nearest neighbour technique to avoid introducing new data into the images. This allows us to directly compare the returns from both techniques.

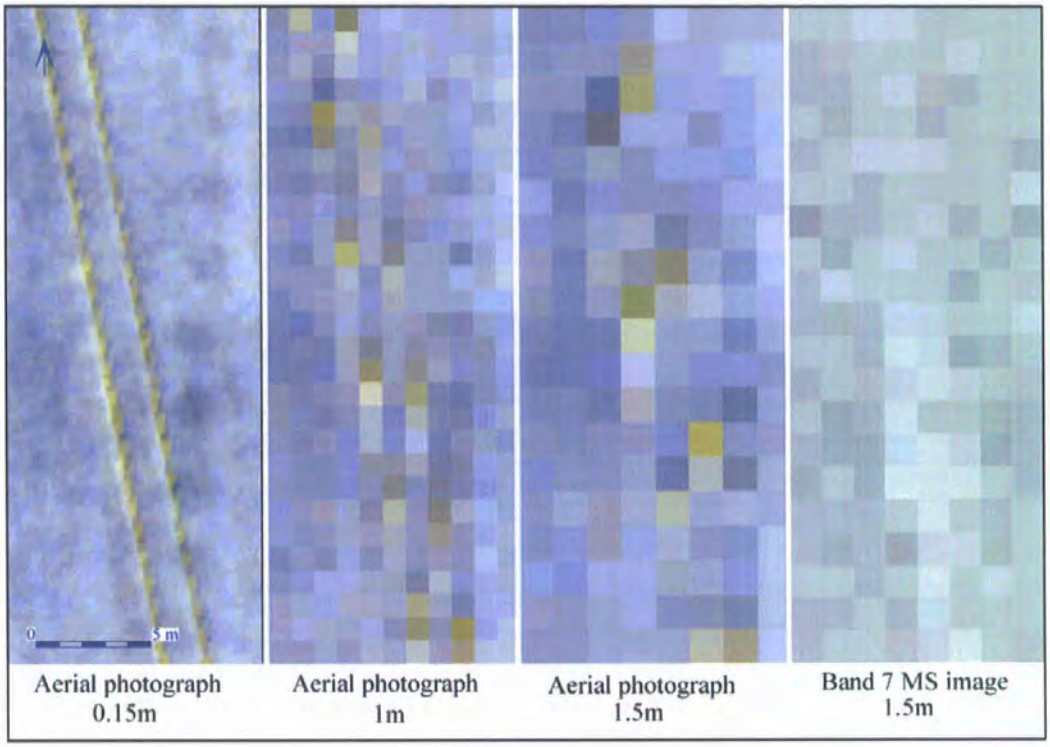

Figure 131 Subsampled aerial photograph at three different resolutions compared with band 7

The first thing to note (see Figure 131) is that the pit alignment which can be clearly seen in the high resolution 0.15 metre data is already lost in the subsampled 1 metre data. By the time the data has been reduced to 1.5 metre pixels, even the tramlines from the tractor are difficult to discern. The same area from the multi-spectral data has been included for reference. However, when viewing the larger linear cropmarks (see Figure 132), most of the features remained visible, even in the 1.5 metre subsampled data. While subsampling the data in this way does not give an exact representation of what may have been returned had the data been collected at that resolution (for instance features which are parallel to the sides of the image could become lost using this method), the implication is that smaller features will not be distinguished using remote sensing data which is of a pixel resolution greater than 1 or 1.5 metres, whereas the larger ditched features will be detected, given the correct conditions

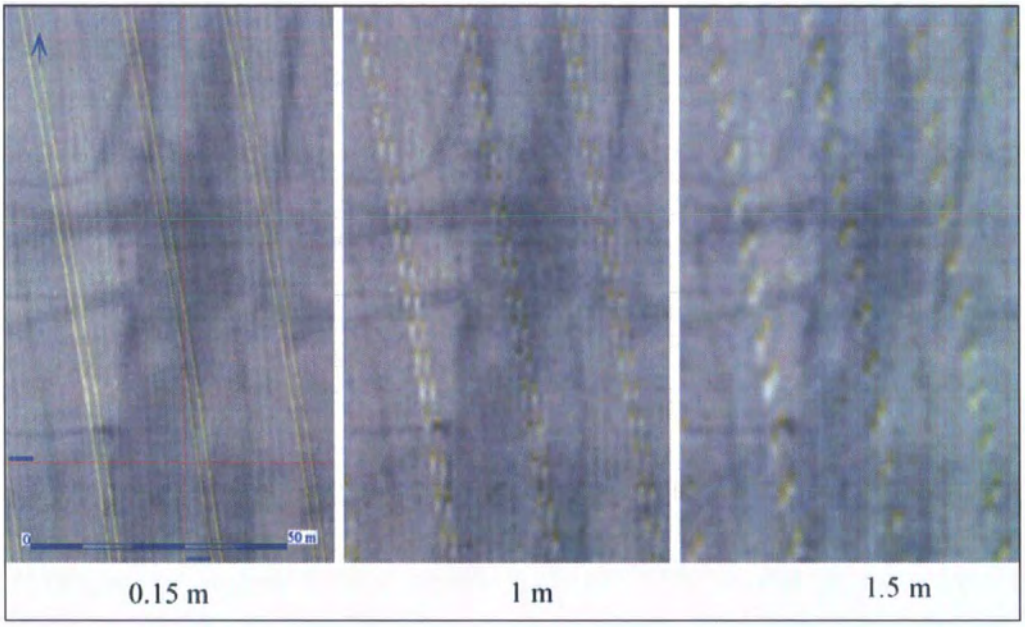

Figure 132 Subsampled aerial photograph at three different resolutions

Sites 52 and 54 gradiometer results

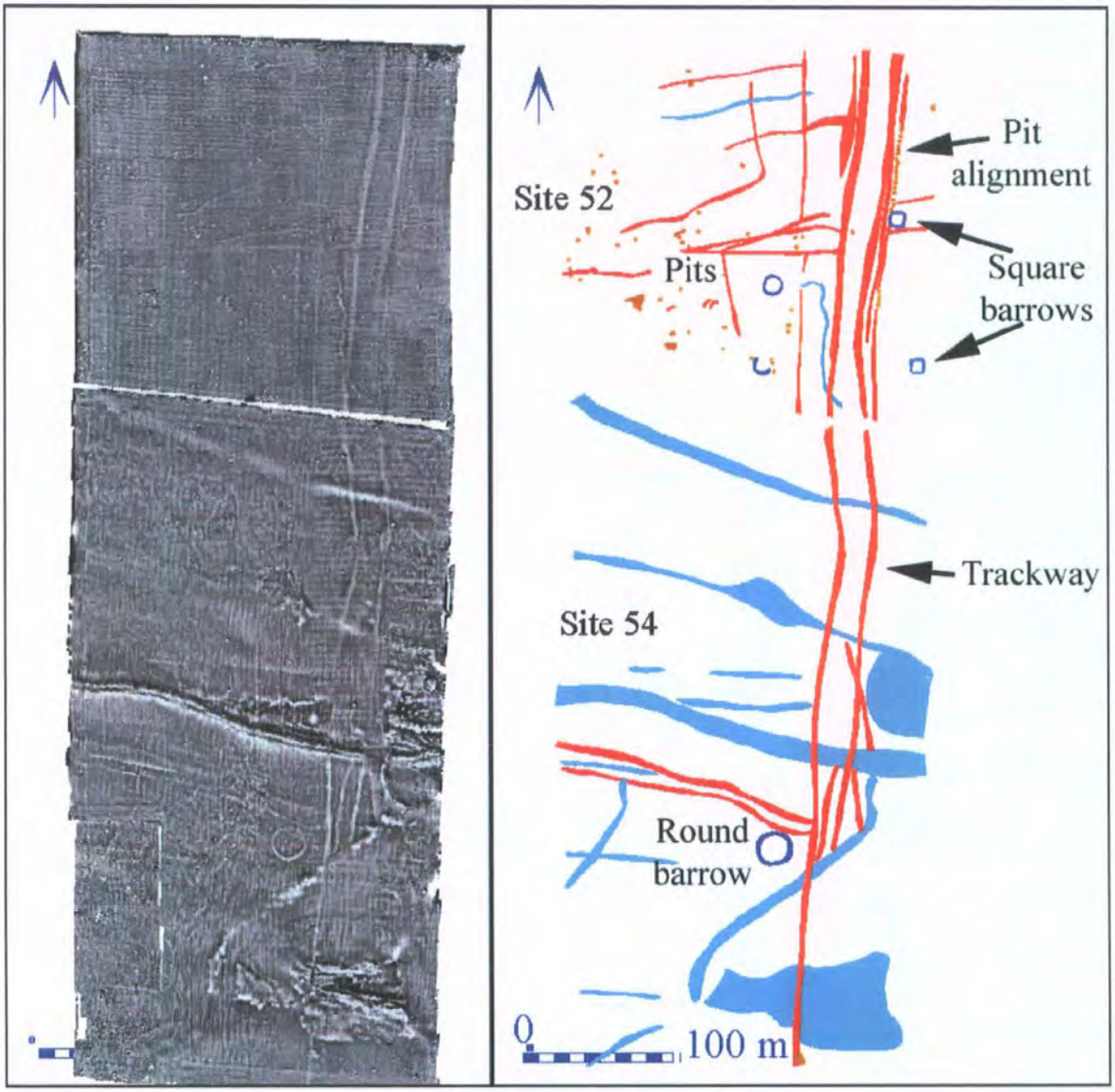

Figure 133 Gradiometer data and interpretation of sites 52 and 54

The main anomaly of archaeological interest on site 52 is the north-south aligned trackway in the eastern part of the area (see Figure 133). The pit alignment adjacent to the eastern trackway ditch is a continuation of that noted above in site 20. Pit alignments are extensive landscape features which generally (though not exclusively) run east-west or north-south in this region. Where they have been excavated, they are often of Bronze Age/early Iron Age origin. Pit alignments tend to be the earliest form of landscape boundary in this zone, often being replaced by a ditch on the same alignment,

sometimes adjacent to the pits and sometimes cutting through them (Powlesland, Haughton and Hanson, 1986). This is clearly the case on site 052, where the individual pits fade into a linear feature towards the south.

Two other significant anomalies lie in close proximity to the trackway and pit alignment. The earliest of these anomalies is probably the one to the west of the trackway. Its circular form indicates that it is a round barrow, which is likely to be of Early Bronze Age date. The two anomalies to the east of the trackway are of a very characteristic form and indicate the presence of square barrows. Several pits can be seen in the western part of the field. The linear anomalies to the west of the trackway are probably fault lines of geological origin. The amorphous discrete anomaly in the south-west of the field relates to a localised area of burning which was visible on the ground at the time of surveying. The faint linear roughly east-west aligned anomalies are not so easy to interpret. They continue into the field to the east, and could be some form of glacial scarring.

The gradiometer data for site 54 shows the trackway continuing up the slope to the south, at one point showing 3 clear ditches, before it becomes a single feature which disappears into a stand of trees (see Figure 133). A large (24 metre diameter) round barrow is also clearly visible. Just to the north of the barrow is a set of parallel anomalies which may indicate a trackway leading off to the west. The very strong anomalies running in a roughly east-west direction indicate the presence of red chalk, which has a much higher magnetic susceptibility than the surrounding white chalk.

Sites 52 and 54 aerial photography results

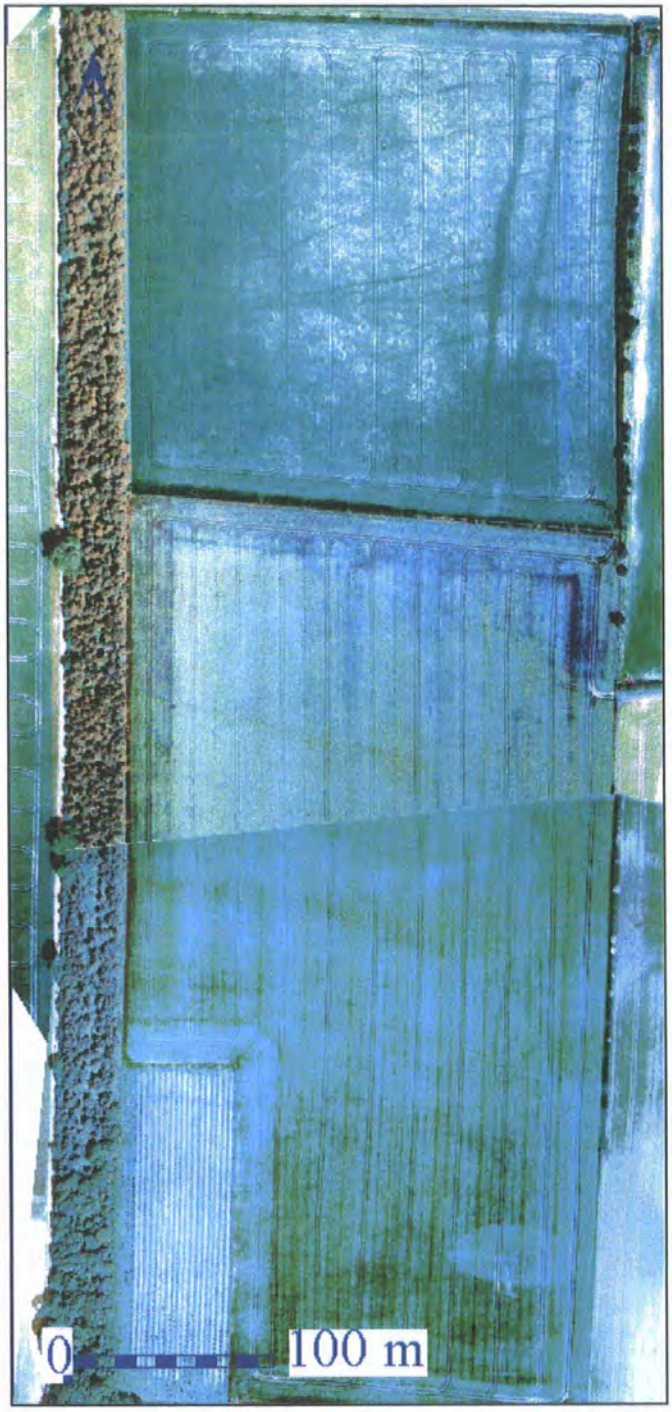

The aerial photograph for site 52 clearly shows the main north-south aligned trackway, as well as a number of the linear "scars" (see Figure 134) previously noted in the gradiometer survey. However, the detail of pits, pit alignment and barrows seen in the gradiometer data is not visible on this aerial photograph, although the square barrow had been noted on earlier aerial photographs.

Figure 134 Enhanced aerial photograph montage (source NERC 23/06/2005)

Likewise, the trackway is only visible as a faint cropmark in the southern part of site 54, before merging in with the tramlines of the tractor to the south. There is no evidence of the large round barrow in the centre of the field, although once again this is known from earlier photographs. The unusual ovate (lighter green) area in the south-east of the image is probably not archaeological. It is located on raised chalk knoll, and may be an area cleared of vegetation in order to facilitate the positioning of stands for shooting (the field is sometimes used for pheasant shooting parties).

Sites 52 and 54 ATM data

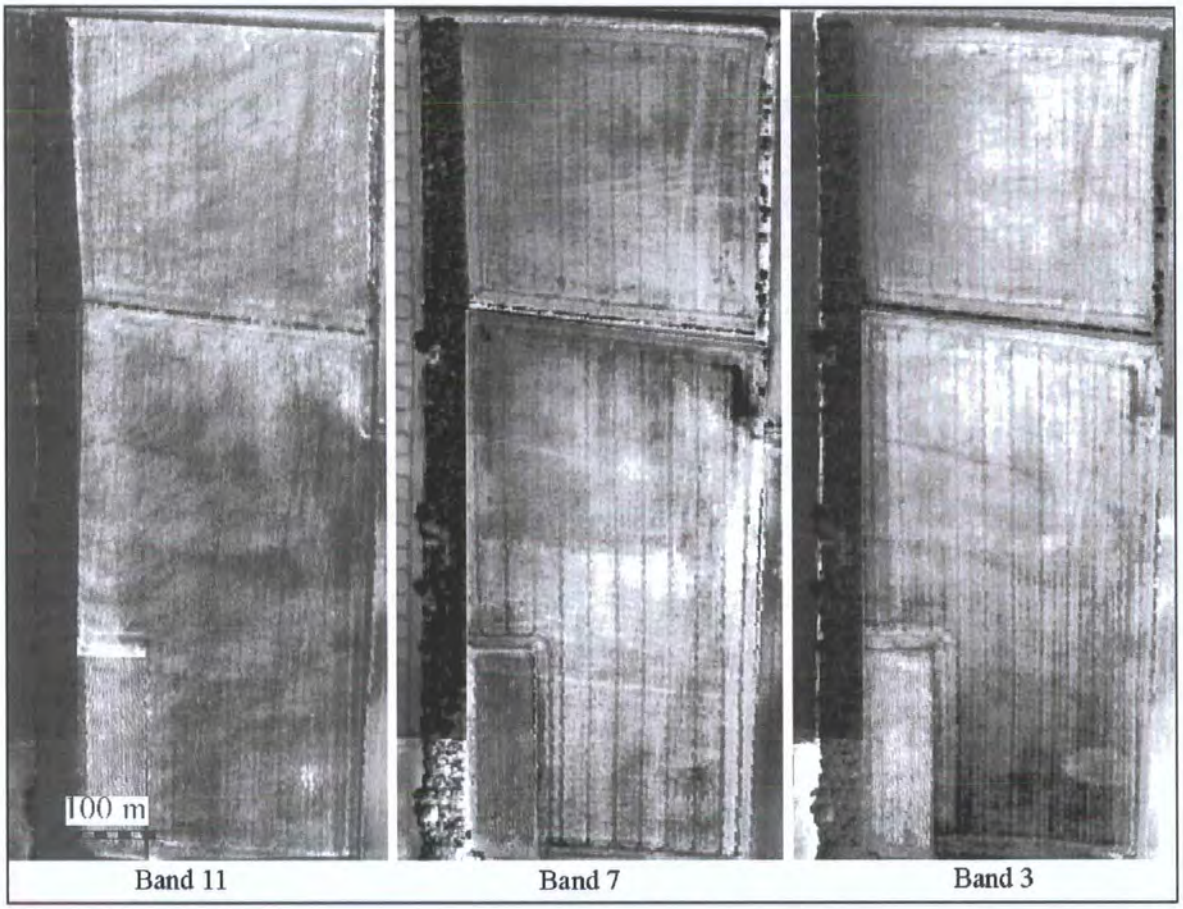

Figure 135 Sites 52 and 54 showing three bands of ATM data

There was very little difference in the returns from the ATM data for sites 52 and 54, so a representative sample of three bands (band 3, visible, band 7, infra-red and band 11, thermal) has been chosen to indicate the range of returns from this source (see Figure 135). Like the aerial photograph, the trackway is clearly visible in almost all of the bands, although it is only in the thermal band that it can be traced into site 54 as it heads upslope to the south. Band 7 clearly shows the remains of an earlier field boundary in the southern third of the image, a feature which is unclear in the other bands. The flattened area in the south-eastern part of the image, evident in the aerial photograph and the visible bands of the ATM data, cannot be seen in either the infra-red or the thermal imagery.

Thermal difference (case study area 4)

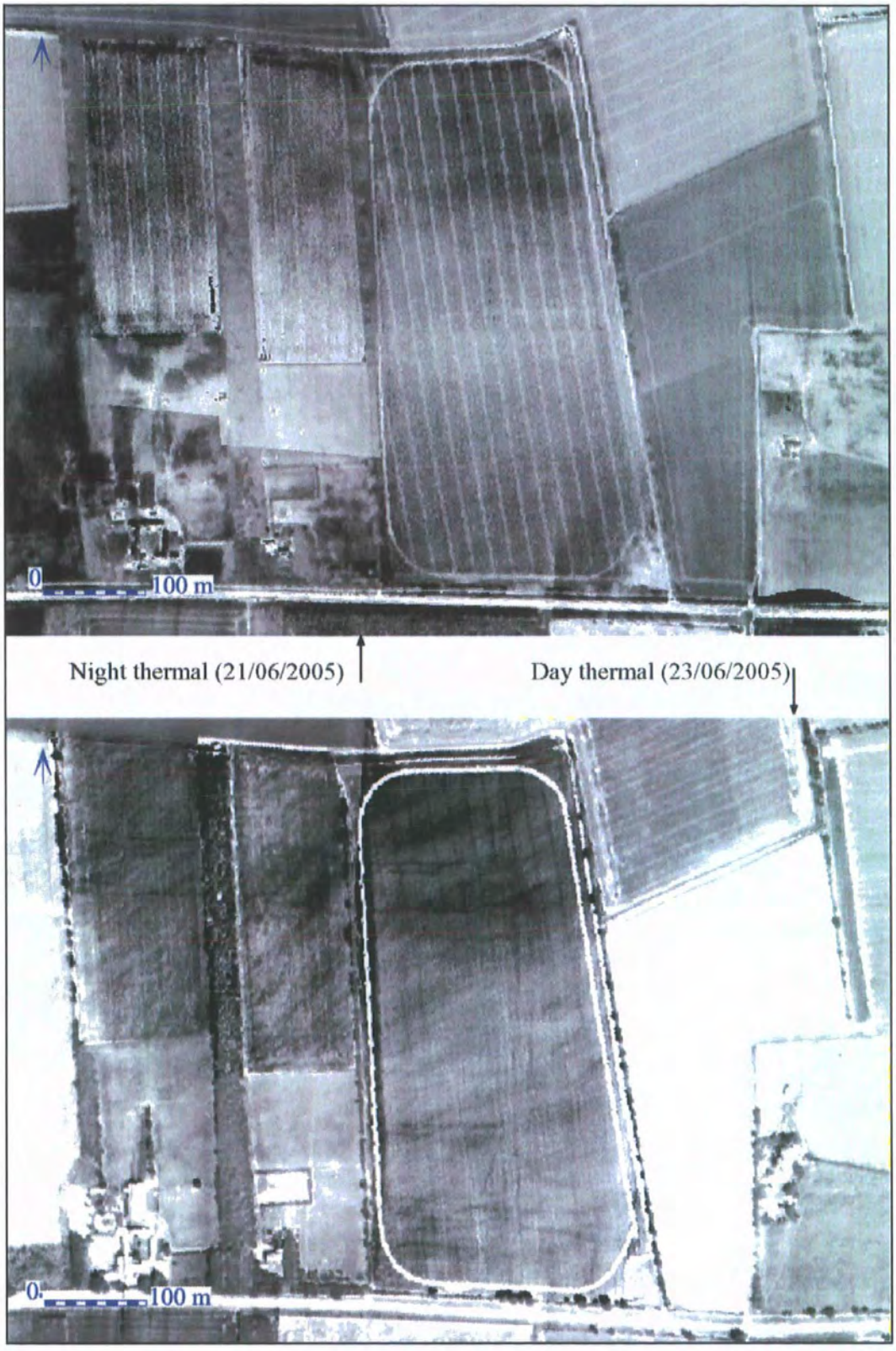

Figure 136 Thermal difference between night and day flights (AZ-16 ATM). Case study area 4 (north)

The difference between the day and night flights for the northern part of the area is striking (see Figure 136). In essence, the night thermal data has detected virtually no trace of the ladder settlement.

The day acquired imagery has detected virtually all of the main north-south trackway (although the individual pits in the pit alignment were not resolved). The main line of the ladder settlement is clear in the north, and the ditches which bound the ladder in the north and south have also been detected in the fields to the west.

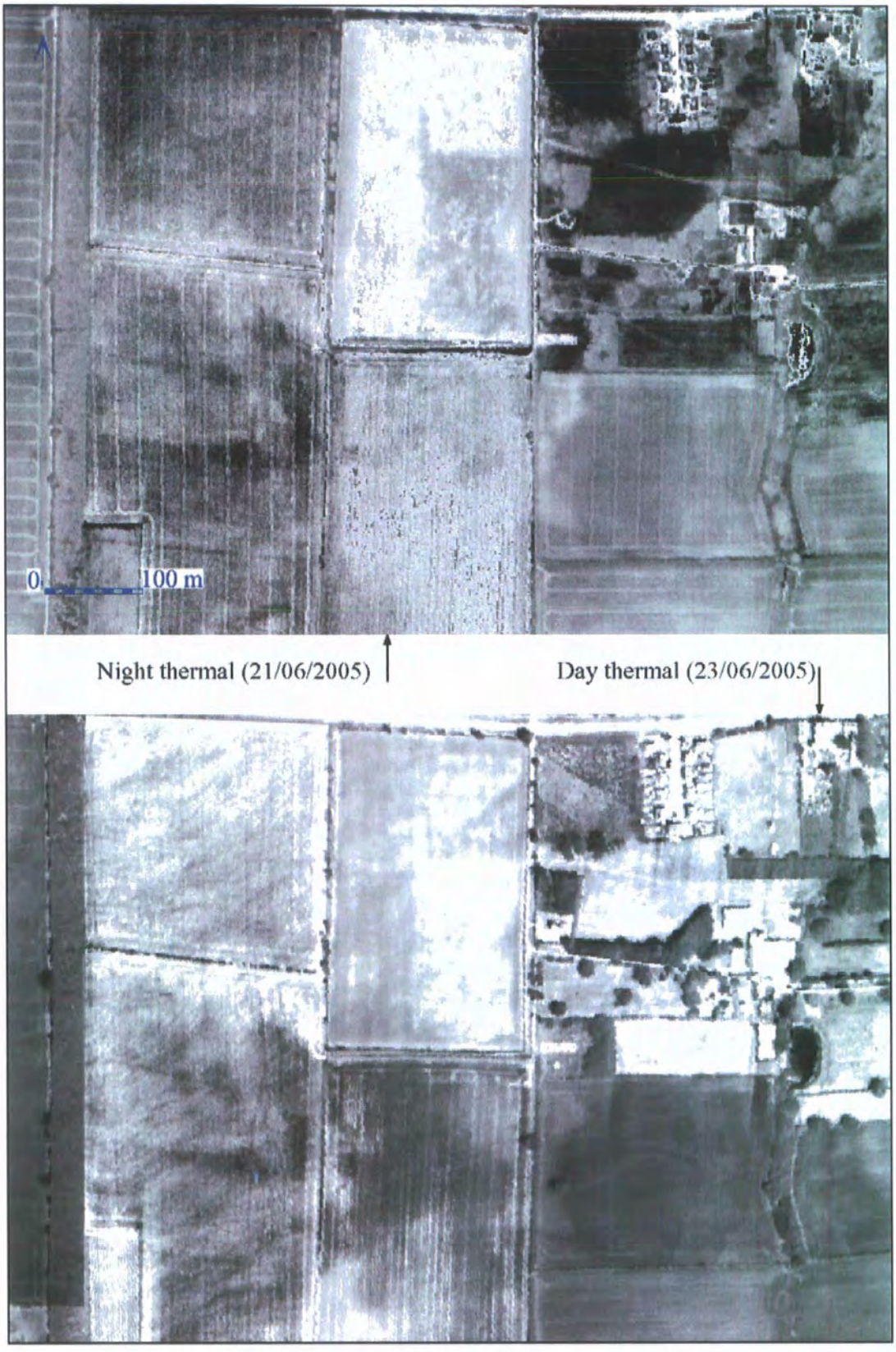

Figure 137 Thermal difference between night and day flights (AZ-16 ATM). Case study area 4 (south)

In the southern part of case study area 4, the main north-south trackway can be seen in the daytime thermal, as two linear anomalies in the north and then one anomaly towards

the south, which is as the geophysical survey indicated The round barrow (see Figure 133) located to the west of the trackway is not visible in either the day or the night imagery (see Figure 137).

6.7 Night thermal characteristics

The night thermal data also had different visual characteristics when compared to the day thermal. This was best seen over forested areas, where the canopy of the trees (Figure 138) showed very different thermal properties when compared to the surrounding field, in that they appeared to be slightly warmer (that is lighter) against the colder (darker) background of the fields.

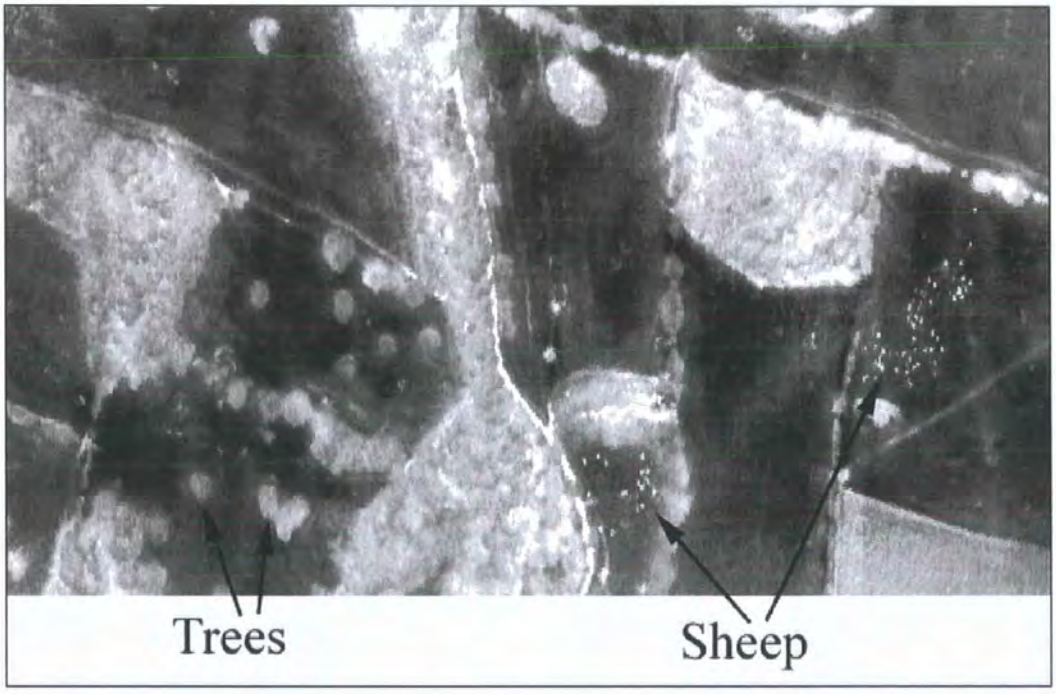

Figure 138 Night thermal data (ungeoreferenced) showing trees and sheep in pasture fields

Another interesting feature is that the night thermal is very adept at detecting the thermal properties of animals, in this case sheep. These can be seen in Figure 138 as clusters of hotspots within two pasture fields.

6.8 CASI data comparison

When analysing the CASI data for Site 20, data from two runs had to be looked at, as only half of the field was present in the first run. This led to an unexpected discovery.

The ladder settlement in the northern part of the field was visible in the first run (line 14) but was not visible in the second run (line 15). Band 15 (0.562-0.568 μm) gave the best response for these anomalies (Figure 139). The time differential between the two runs was only six minutes (10:28:30 to 10:34:30), and as the flight was under clear sky conditions, there is unlikely to have been any significant change in the spectral response of the area.

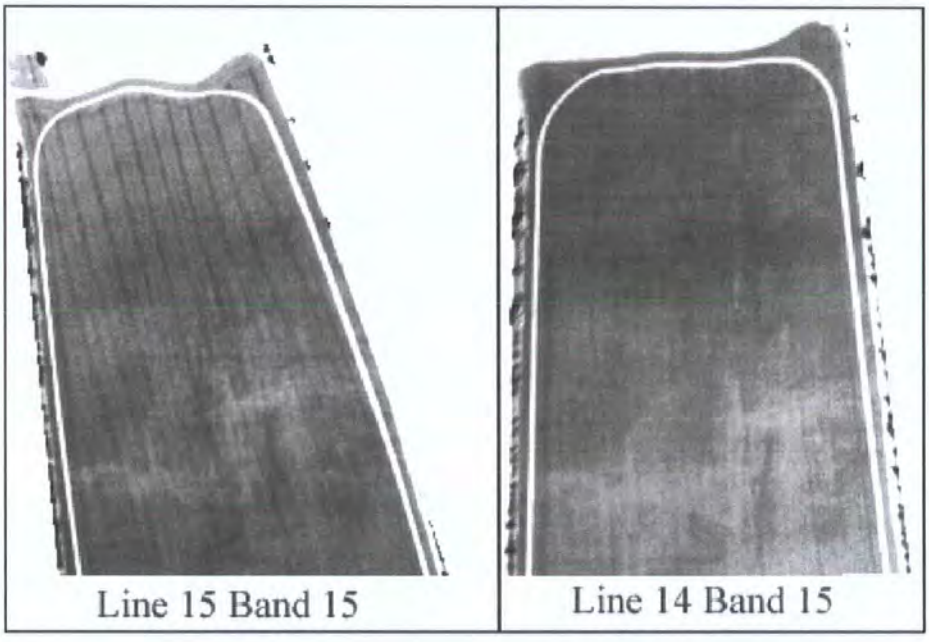

Figure 139 Different responses between the same sensor array (CASI data band 15) ungeoreferenced data

The same response was present in the georeferenced data (Figure 141). This figure also shows the returns from the AZ-16 over the same area, with a comparative bandwidth (in the centre of the green part of the EMS). All of the images have been contrast stretched to enhance the area of the field in question. Note that the AZ-16 band three data only finds a slight linear anomaly towards the southern part of the ladder settlement. The CASI line 15 data shows absolutely no evidence for the ladder, but it is clearly visible in the line 14 data.

An explanation for this phenomenon needs to be found. Two related factors could be affecting the returns recorded by the sensor. The first is how the cropmark is being

detected. It is possible that some early cropmarks are only seen from a vertical position because they initially form lower down in the crop canopy. In effect, there is no visible difference at the top of the crop, but the leaves lower down may be darker and/or greener. If this is the case, then oblique views will not detect this type of cropmark, and the location of the anomalies relative to the position of the scanhead becomes much more important. This leads directly on to where the anomalies are located on the across track scan line If they are at the positions marked A or B on Figure 140, then it would be likely that only the top of the canopy would be providing the returns. If they were located at position C, however, it is possible that the returns could be from deeper within the canopy.

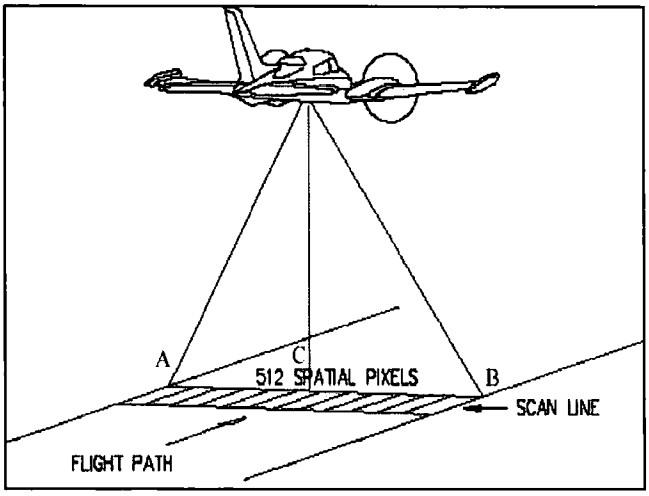

Figure 140 Imaging concept of the casi-2 CCD pushbroom spectrograph (adapted from ITRES user manual)

The location of the anomalies in relation to the centre of the scan line is shown in Figure 142, where it is marked as a black line through both images. This is a plot of the uncorrected level 1B HDF data, prior to azg correction and further georeferencing. Line 14 was collected travelling from the west to the east, with the returning line 15 collected from the east to the west, although line 15 has been flipped so that both lines are in more or less the same orientation, with north roughly to the left of the page.

What is clear is that in line 14, where the ladder settlement has been detected, the anomalies are close to the centre of the scan line, whereas in line 15, the same area is out towards the edge of the scan line.

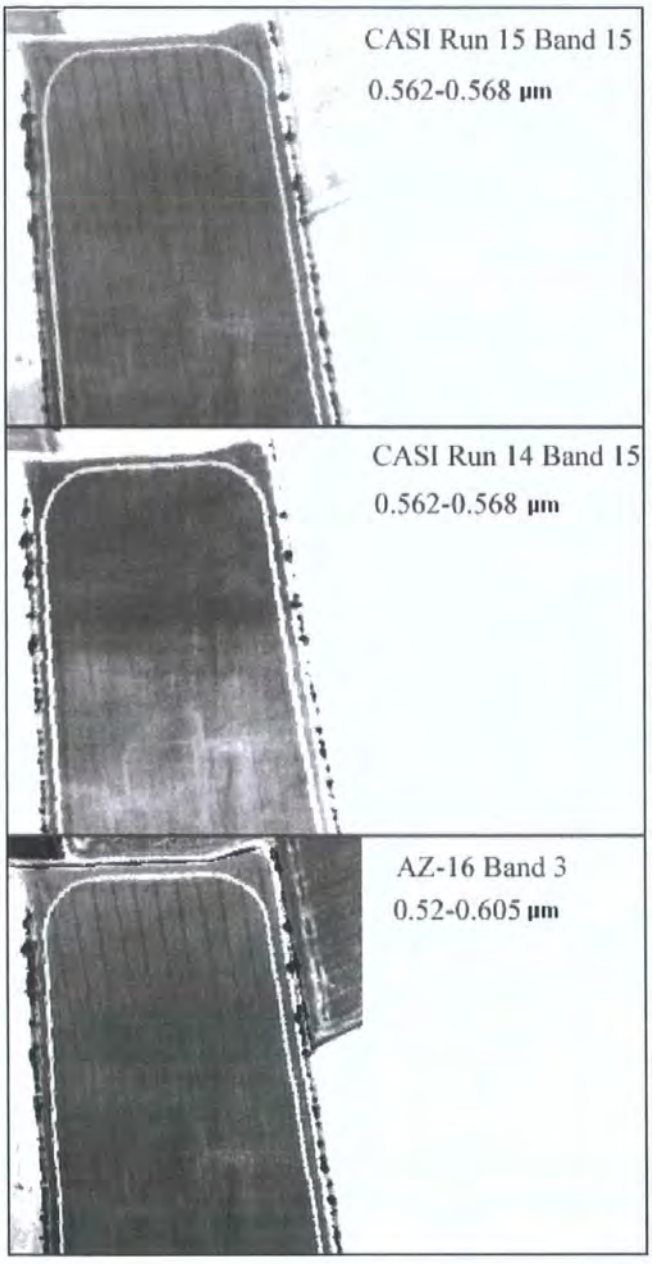

Figure 141 Comparison of two different airborne multispectral sensors

A second consideration is the attitude of the aeroplane at the time of the data collection. In line 14, it appears as if the plane is flying reasonably straight and level, with little pitch or yaw, as the raw data needed only a small correction to be fully georeferenced. In line 15, however (Figure 142), it is clear that there is a significant distortion visible in the raw data, which has affected both the ends (compare Figure 139 with Figure 141) and the centre of the scan line. For instance, the wiggly white line running through the right (south) side of line 15 is in fact A64 trunk road (see Figure 136 for georeferenced view of the A64). This also demonstrates how different the returns along each scan line can be. Although both lines 14 and 15 have a scan line of 512 pixels, the actual distance on the ground is 797 metres for line 14 and 819 metres for line 15. This alters the nominal ground resolution by a small but nonetheless significant amount of 5cm per pixel (1.55m for line 14 and 1.60m for line 15). It is important to remember that this may not extend across the whole image equally, that is there may be parts of the image which are at a resolution of 1.5m per pixel, and other (very distorted) parts of the image where this could be anything up to 1.8 or even 1.9m per pixel.

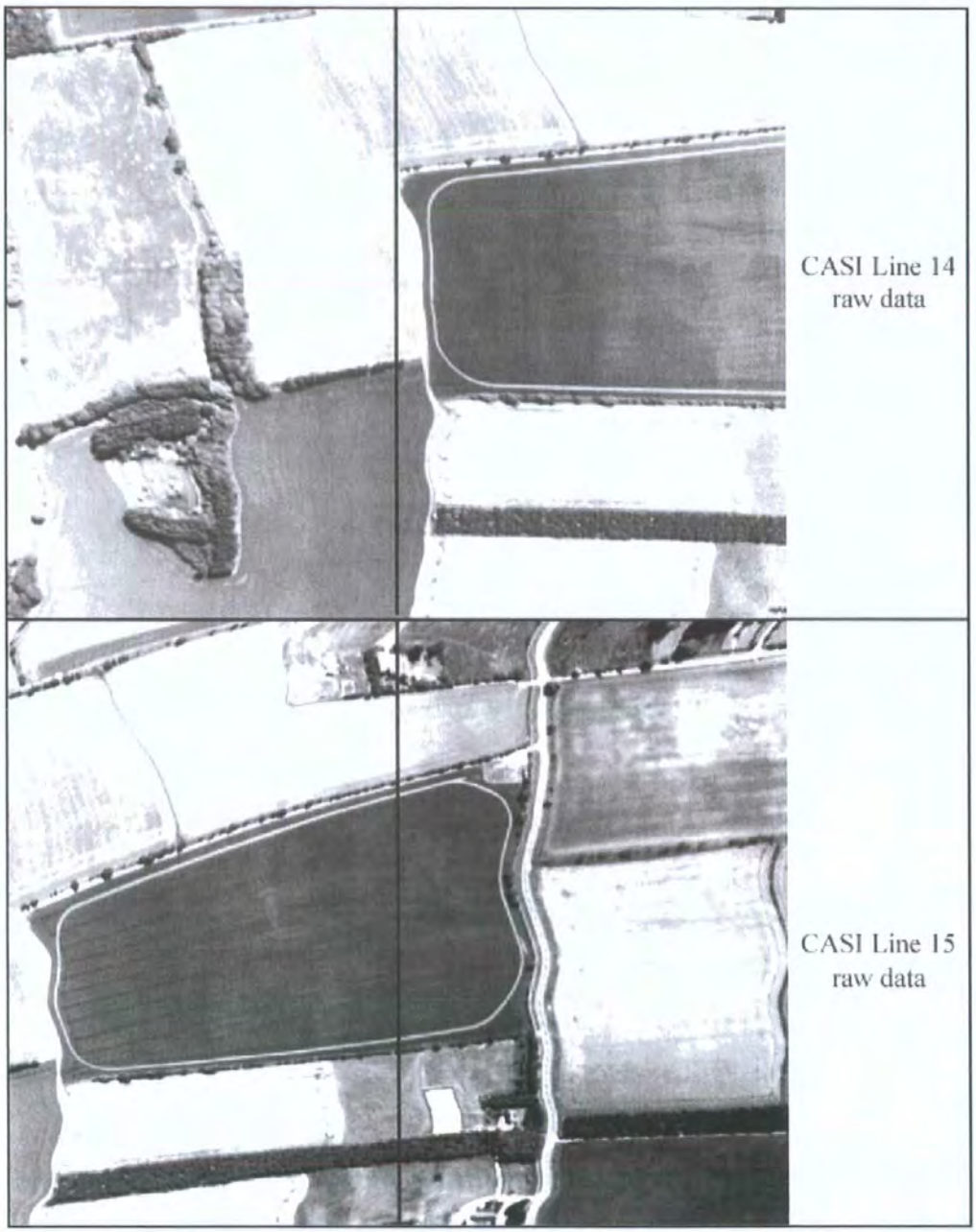

Figure 142 Centre line of the raw data for the two CASI runs (ungeoreferenced) covering site 20.

If the hypothesis about early cropmark formation is correct, it has important implications for exactly when to expect good returns from airborne remotely sensed data. It is likely that the cropmarks in this part of the field were in an early stage of development, and thus were not visible at the top of the crop canopy. This being the case, they were only detected when the scanhead was vertically above the cropmarks. This discovery will have ramifications for any further multispectral imagery obtained early on in the cropmark formation season.

Chapter 7 Discussion

This chapter will discuss how the aims and objectives of the research were achieved, and how the results from the different remote sensing techniques have considerably enhanced our archaeological knowledge of the area.

7.1 Research Aim

The primary aim of the research, to evaluate the returns from a number of remote sensing and geophysical surveying techniques across different aggregate geologies, was successfully achieved by developing a methodology which combined vectorised drawings linked to a relational database. This has allowed a number of questions to be posited and answered, in a way which would not have been possible only a few years ago.

Using remote sensing techniques in this way allows us to move away from a site-based mindset into seeing a landscape as a coherent entity, in which past societies operated. Even in the current archaeological climate of "landscape archaeology", most archaeological work is carried out on small sites, generally excavated because they are part of a local authority planning permission rather than to answer specific research questions. The ability to place these small-scale excavations into their wider context is thus of paramount importance, and remote sensing techniques are the only way that this objective can realistically be achieved.

7.2 Testing the returns over different drift geologies

Although it was visually obvious that different types of remote sensing were producing different levels of return across the various geological zones, to quantify these differences required a slightly different methodology than that developed above. All of the techniques used showed differences in return across the zones, but as these

differences were most marked in the gradiometer data, I will use this dataset as an example. The surveyed area was divided into three zones, chalk in the south, the sand and calcareous chalk gravels from the foot of the Wolds to the edge of the windblown sand (dry Vale) in the centre, and the alluvial sand and silicaceous gravels with overlying peat deposits (wet Vale) to the north. The number of anomalies from each group were then totalled for each geological zone (displayed in Figure 143 and Table 25).

Group	Chalk	Dry Vale	Wet Vale	Total
		Sands and calcareous gravels	Sands and silicaceous gravels	
Agricultural Activity	534	1781	576	2891
Alluvial Activity	17	93	20	130
Geological Activity	322	72	256	650
Post-Med or modern Activity	47	276	7	330
Quarrying Activity	62	17	1	80
Archaeological Activity	716	12155	509	13380
Total	1698	14394	1369	17461

Table 25 Gradiometer anomaly groups by underlying drift geologies

Figure 143 Location of anomalies detected against geological zones

What is immediately clear is that the vast majority of the magnetic anomalies were detected in the central dry Vale zone. To a degree, this must be qualified, as a greater

area of this zone was surveyed, and the breakdown of anomaly density per hectare is shown in Table 26.

Description	Chalk	Dry Vale	Wet Vale
Area in hectares	290	520	190
Anomalies per hectare	5.86	27.68	7.21
Archaeological anomalies per hectare	2.47	23.38	2.68

Table 26 Gradiometer anomaly density by drift geology

Even taking into account that just over half of the area surveyed was in the central dry vale zone, the returns of nearly 83% off all magnetic anomalies is significant. This figure rises to nearly 91% when only archaeological anomalies are counted. This result needs to be clarified, in that specific environmental imperatives are operating here. The same level of settlement encountered in the dry Vale zone should not be expected in areas that we know were wet for much of antiquity (i.e. the wet Vale), nor on the steep slopes of the Wold scarp. Secondly, from our initial phase interpretation of the magnetic data, we also know that we are seeing virtually no Neolithic or early Bronze Age settlement evidence, even in the very responsive central windblown sand zone.

Bearing in mind the labour intensive method of data collection for geophysical survey, the level of return is so different that the conclusion must be that only in the dry Vale area is further blanket coverage using a gradiometer a sensible option. Gradiometer surveys in the wet Vale zone should only carried out to confirm and enhance detail over sites discovered using the other techniques. It should be noted that this caveat does not hold true for the Wolds chalk, as much of the surveyed area here was carried out over a steep slope, where human activity is likely to be reduced. Earlier surveys to the south on the Wolds proper have demonstrated that the chalk provides an excellent background against which magnetically enhanced anomalies are readily detected.

7.3 "New" types of monument

At least two "new" types of monument were discovered by the geophysical surveys. In retrospect, it is possible to go back to earlier aerial photographs and see that some of these features were present, but it is the geophysical surveys which have discovered them in sufficient numbers, drawn attention to them, and thus allowed their classification as novel types of feature.

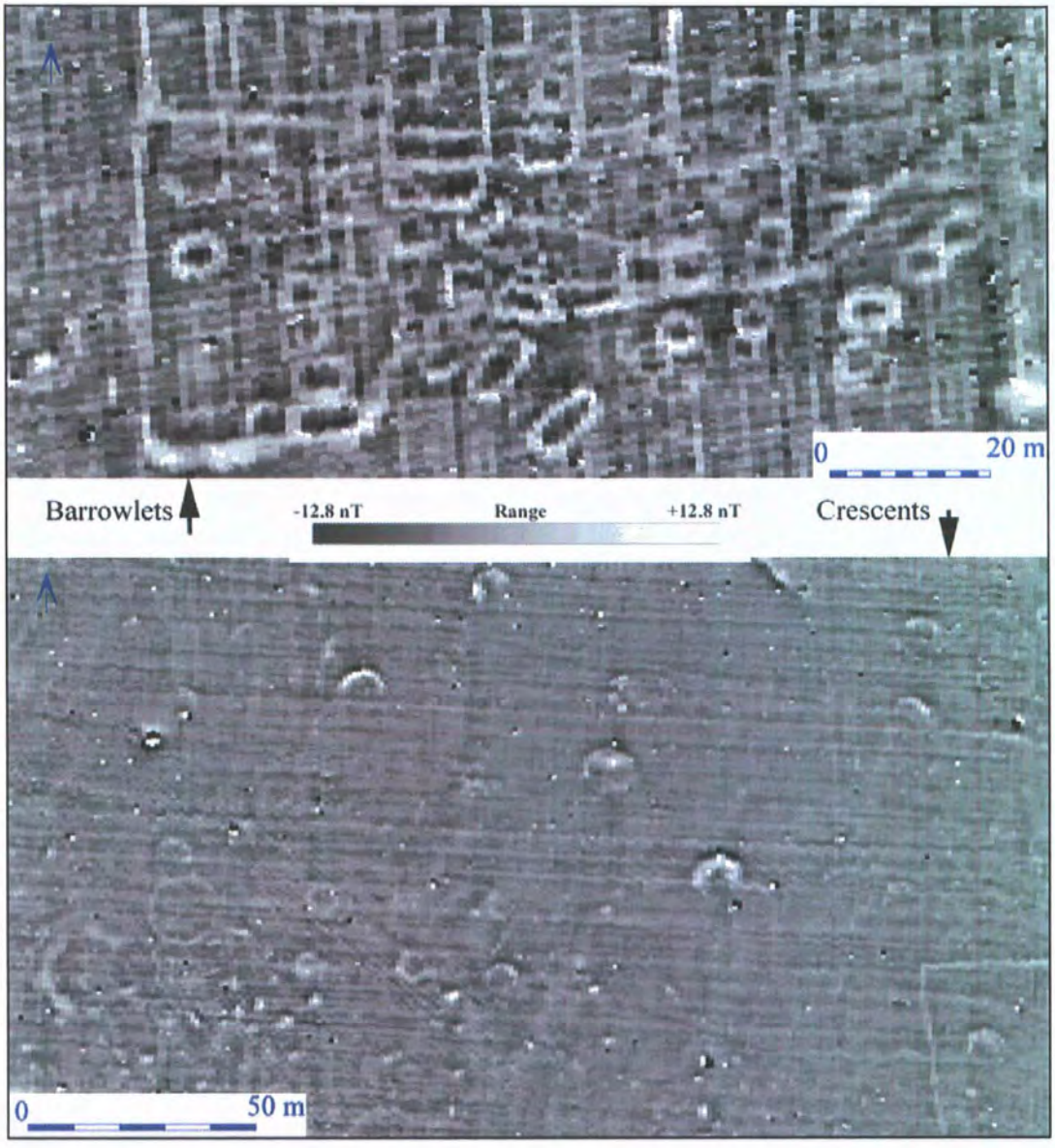

Figure 144 Barrowlets and crescents

These have been dubbed barrowlets and crescents (see Figure 144). The barrowlets are small ovate, circular and rectangular anomalies, the majority of which (97%) form discrete clusters to the south of the trackway which runs through the centre of the ladder

settlement. A total of 768 (see Figure 145) of these features have now been identified. See Figure 154 and Figure 157 for excavated examples and 8.2 Characterising the barrowlets for further research questions.

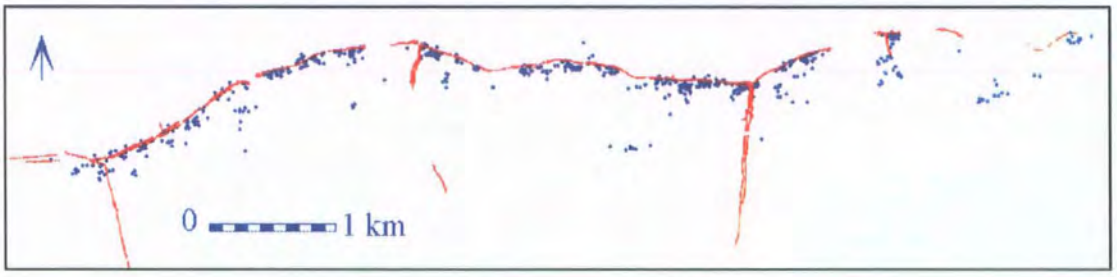

Figure 145 Distribution of barrowlets along ladder settlement trackway

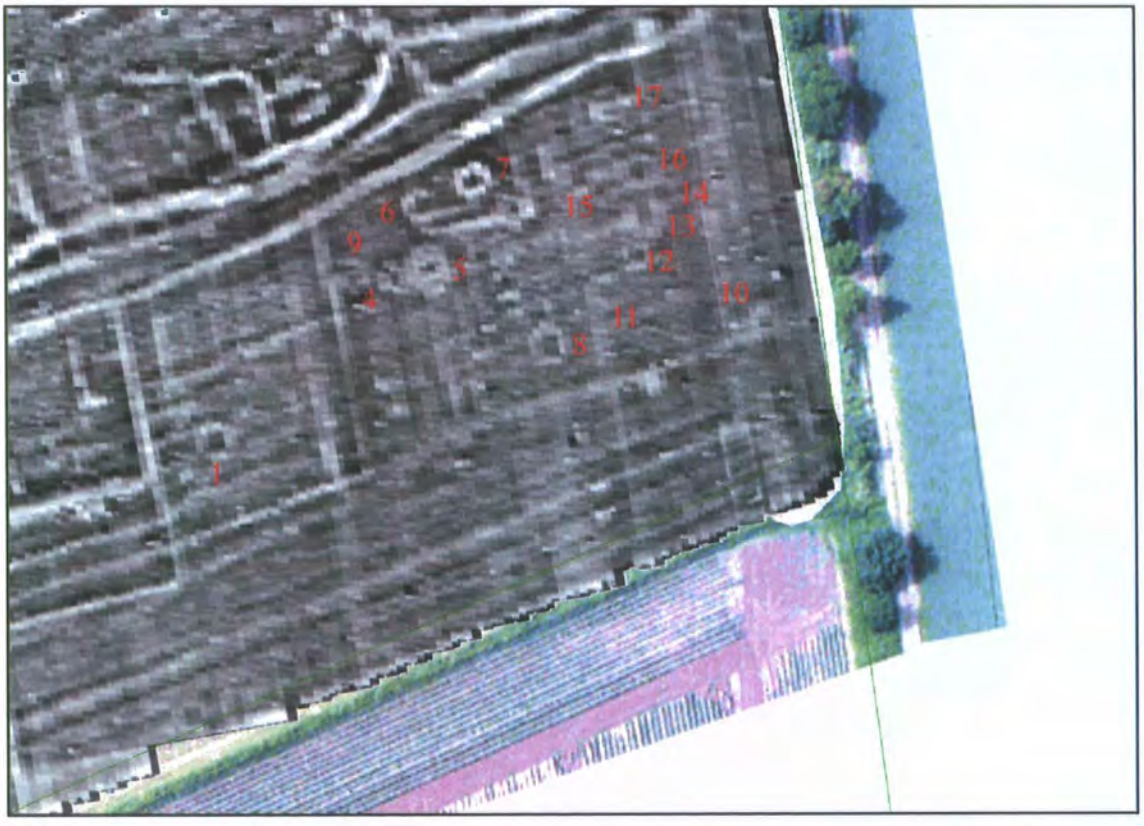

Figure 146 Magnetic survey showing a group of barrowlets to the south of the ladder settlement (Site 23)

The discovery of the barrowlets has come about almost exclusively by using magnetic surveying methods (see Figure 146). However, after they were characterised, it became possible to look at the other data sources for evidence of this feature type. Cropmarks visible on a recent aerial photograph (Figure 147, taken on 17/06/2006) clearly show the

location of 8 of these features. While they may have been seen on earlier aerial photographs, they tend to have been erroneously classified either as square barrows or round houses.

Comparing the 2 figures gives an indication of the returns which can be expected from these data sources. A total of 17 barrowlets are present, 15 of which are found in the magnetic survey and 8 in the aerial photograph. Only 6 of the features are present in both datasets (barrowlets 1, 4, 5, 6, 7 and 8). Barrowlets 2 and 3 are only seen as cropmarks, (the area was disturbed by ploughmarks at the time of the magnetic survey). Barrowlets 9 to 17 are only found in the magnetic data. Once again this demonstrates that remote sensing and geophysical surveys are complementary, and either method would have demonstrated that a site was present at this location. However, it is clear that the magnetic survey is giving a more comprehensive return at this point towards the northern edge of the blown sand zone.

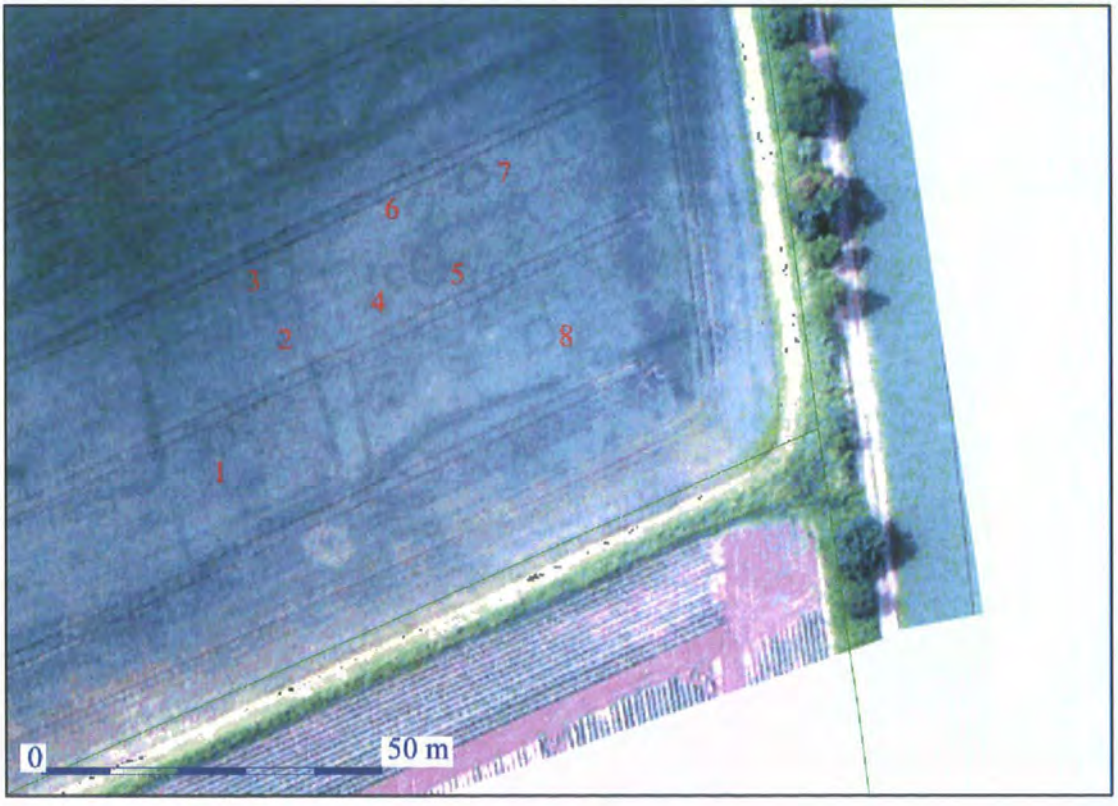

Figure 147 Aerial photograph taken on 17/06/2006 showing barrowlets (Site 23)

The second feature type discovered by the geophysical survey were the crescents. They are always found in association with prehistoric burial complexes. The location of the three main clusters are illustrated in Figure 148, at the same scale as the barrowlets in Figure 145. These are a much rarer feature type than the barrowlets, with only 48 so far discovered (7 in cluster 1, 26 in cluster 2 and 15 in cluster 3). In the enlargements of each cluster all of the o associated barrow types have also been plotted. Generally, the crescents are near to groups of barrowlets or slightly larger, somewhat misshapen barrows. Only in one instance (cluster 1) are they close to a full sized round barrow.

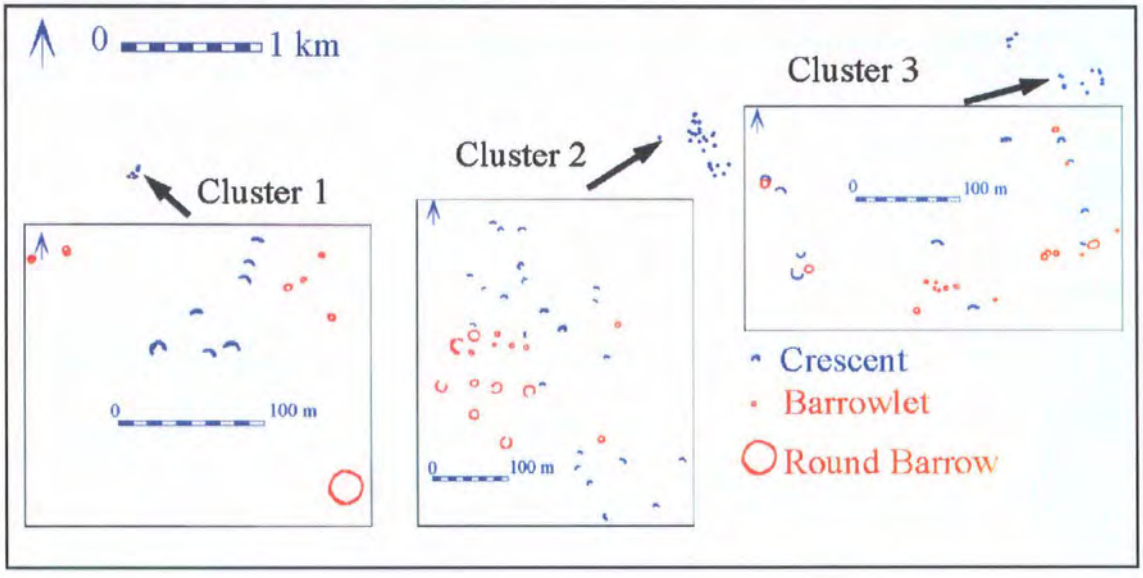

Figure 148 Distribution of crescents

7.4 Filling in the gaps in the ladder settlement

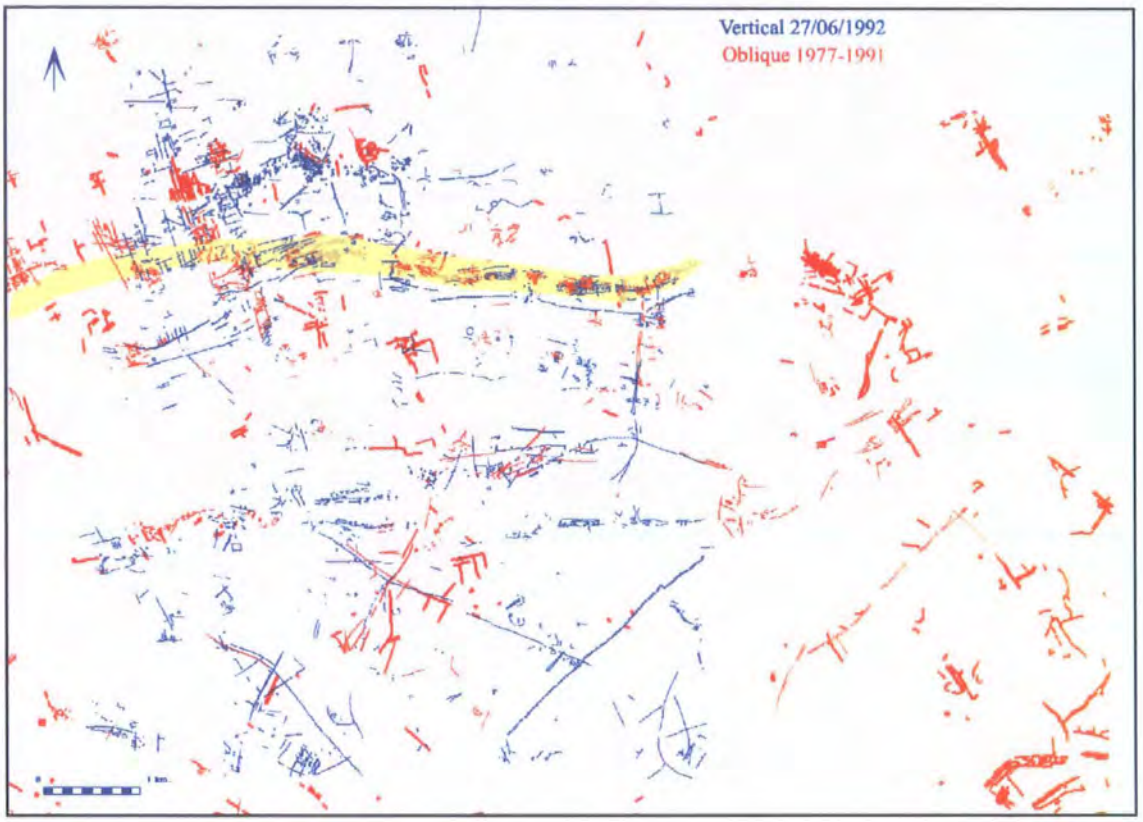

Figure 149 Combined vertical and oblique aerial photographic plot (ladder settlement highlighted)

Figure 149 shows what we knew from aerial photography about the project area before the first multi-spectral flight in 1992 (cropmarks derived from oblique aerial photographs shown in red). The vertical photographs taken in 1992 (shown in blue) both added detail to known sites and filled in areas where cropmarks had not been previously detected. A number of open areas remained, most notably along the length of the ladder settlement (indicated by the black arrows in Figure 150). However, we could not be certain that these gaps were real, as crop regimes may have ensured that the potential for cropmark formation was severely reduced. It was intuitively believed that the ladder would continue as a continuous linear feature, but this could not be proven at that time.

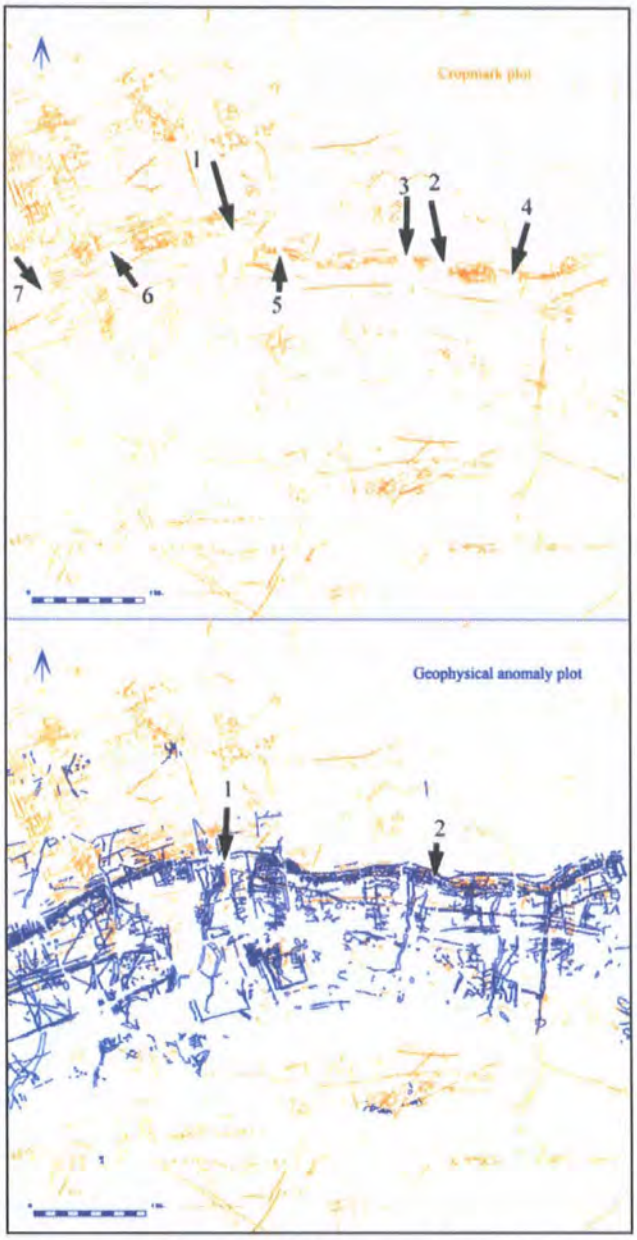

Figure 150 Cropmark and geophysical survey results compared

Figure 150 shows the central part of the project area. The upper part shows the combined cropmark returns from both oblique and vertical aerial photographs to 1994 (in orange). This shows that even after an extensive flying campaign which included the excellent cropmark year 1992, seven gaps in the ladder settlement remained. The lower part shows the geophysical anomalies from magnetic survey (in blue) superimposed onto the cropmark plot. It can immediately be seen that the central part of the project area (the windblown sand zone) responded exceptionally well to this form of survey, and that the five main gaps in the ladder settlement were filled in using gradiometery.

However, two gaps remained, approximately 2km from each other, and these are illustrated in Figure 150 and Figure 151. The first (gap one) appears to be a genuine break in the ladder, and is approximately 420 metres wide. It is certainly no coincidence that this occurs at a point where a major trackway extends southwards towards the Wolds. It is not a complete gap, in the sense that the major flood defence to the north of the settlement does not stop at this point, nor does the trackway through the centre of

the settlement, but there is certainly a change in the nature of the ladder here, with none of the characteristic rectangular enclosures present.

Gap two is different, in that it is only 117 metres wide. It is precisely at this point that the flood defences split into two, with one the northern ditch heading in an ENE direction, while the southern ditch appears to mark the northern boundary of the ladder enclosure system. Once again there is not a complete cessation of archaeological activity in the "gap", as a number of faint linear anomalies on the general line of the ladder settlement can still be seen. It is possible that this part of the ladder is sealed by a greater depth of topsoil and windblown sand, which could be muting the magnetic signals. If this is the case, then the ladder may be particularly well-preserved at this point.

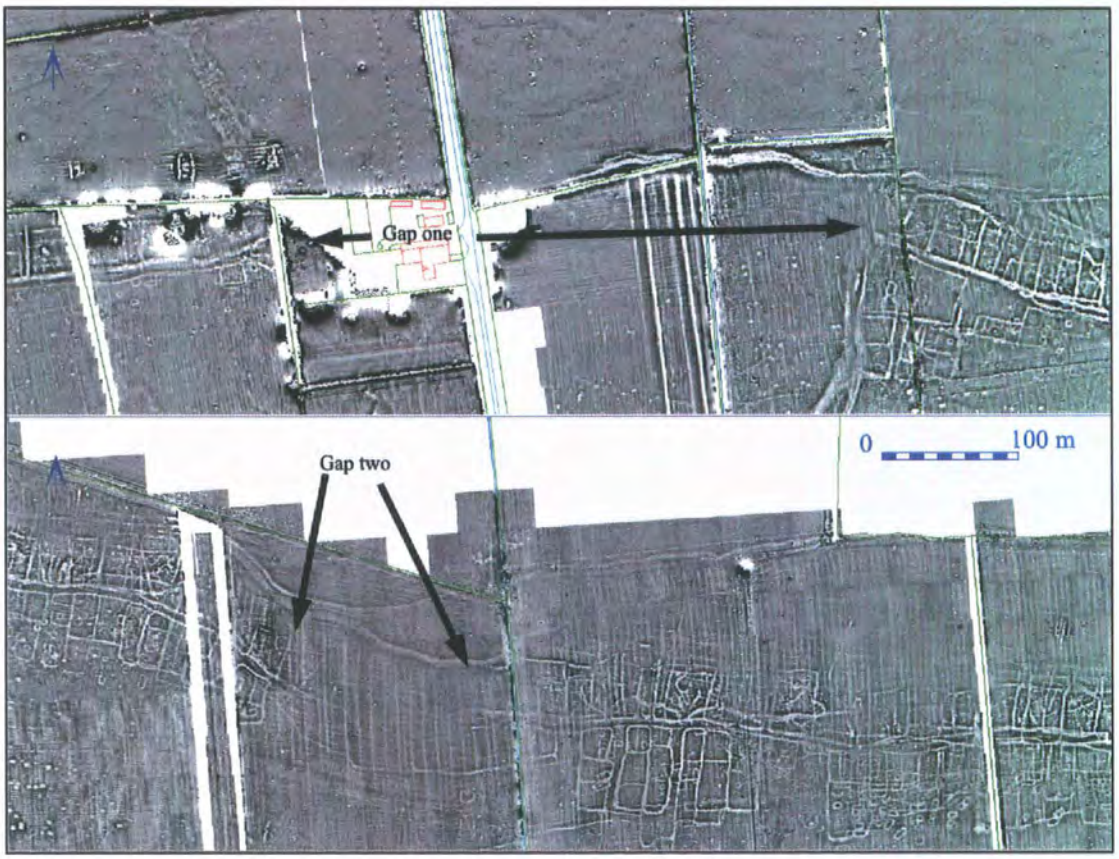

Figure 151 A greyscale image of the remaining gaps in the ladder settlement

It may be worth emphasising exactly how much more detail was being recovered by the magnetic survey in an area which had proven very unresponsive to cropmark formation. This was the western end of the ladder settlement, which occurs in soils dominated by the blown sand component. The upper part of Figure 152 shows the combined oblique and vertical photograph cropmark returns. The central trackway of the ladder is visible for part of its length, with a few linear cropmarks extending out from the trackway. The trackway appears to turn to the WNW at the western end, with a slight increase in archaeological activity at this point, including a small square barrow cemetery to the south.

The archaeological understanding of this area was completely transformed by the magnetic survey results (the lower part of Figure 152). The ladder settlement was shown to extend along the whole area, with an increase in activity at the western end. An overwhelming level of detail along the whole ladder was detected, including the potential for identifying different phases within the settlement enclosure systems.

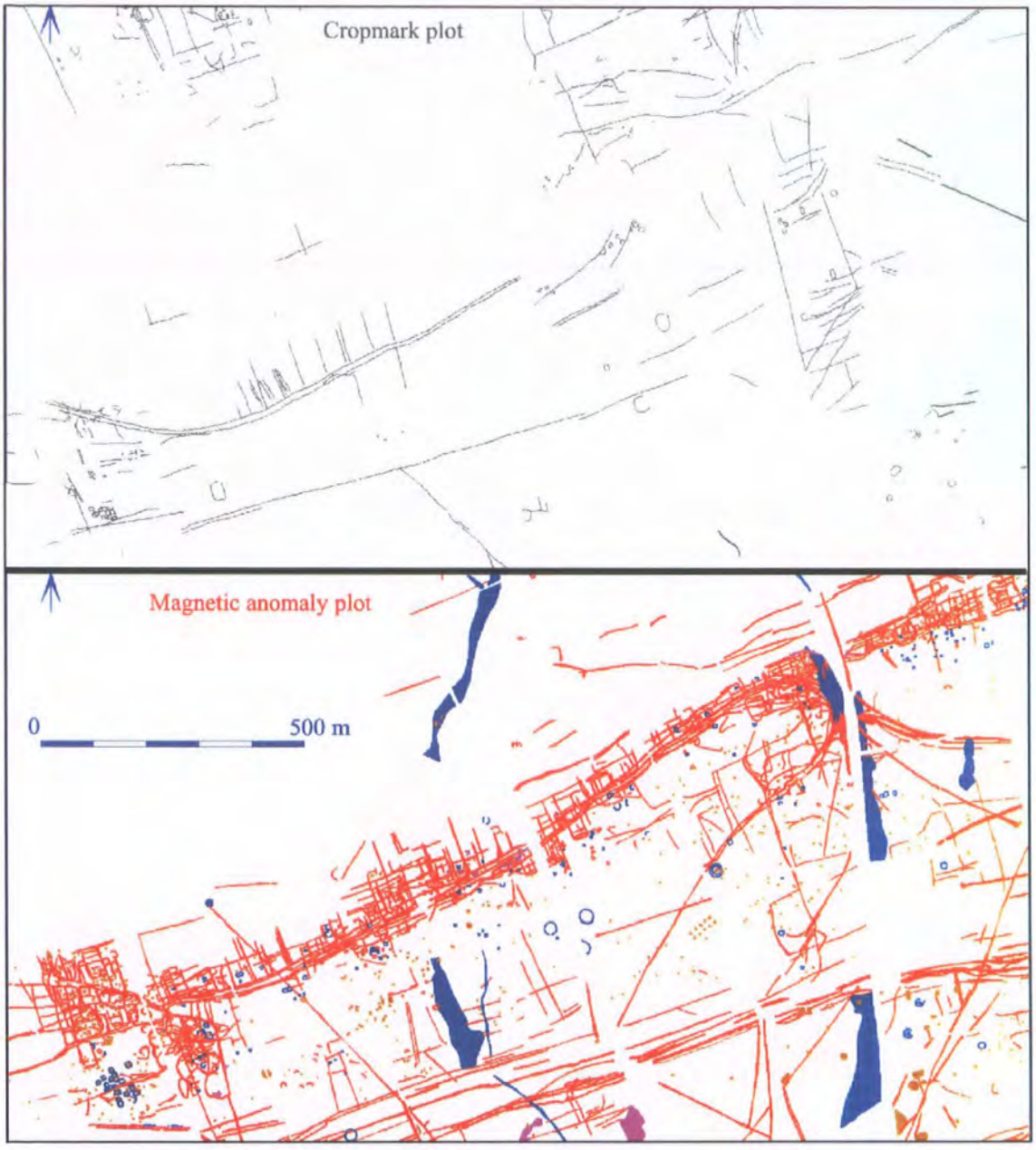

Figure 152 Comparison of returns (cropmarks upper and magnetic anomalies lower)

This difference in detection rate can be quantified using the relational database. Each anomaly and cropmark has a point assigned to it, and these points are plotted in different colours in Figure 153. There are a total of 373 different cropmarks, and 4024 different magnetic anomalies, more than a ten fold increase in feature detection. While this increase in detection rate is not consistent across the whole of the project area, it is reasonably consistent in the blown sand zone, where magnetic anomalies detected total

12088, and cropmarks 1830, giving an overall six fold increase in detection rate in this zone.

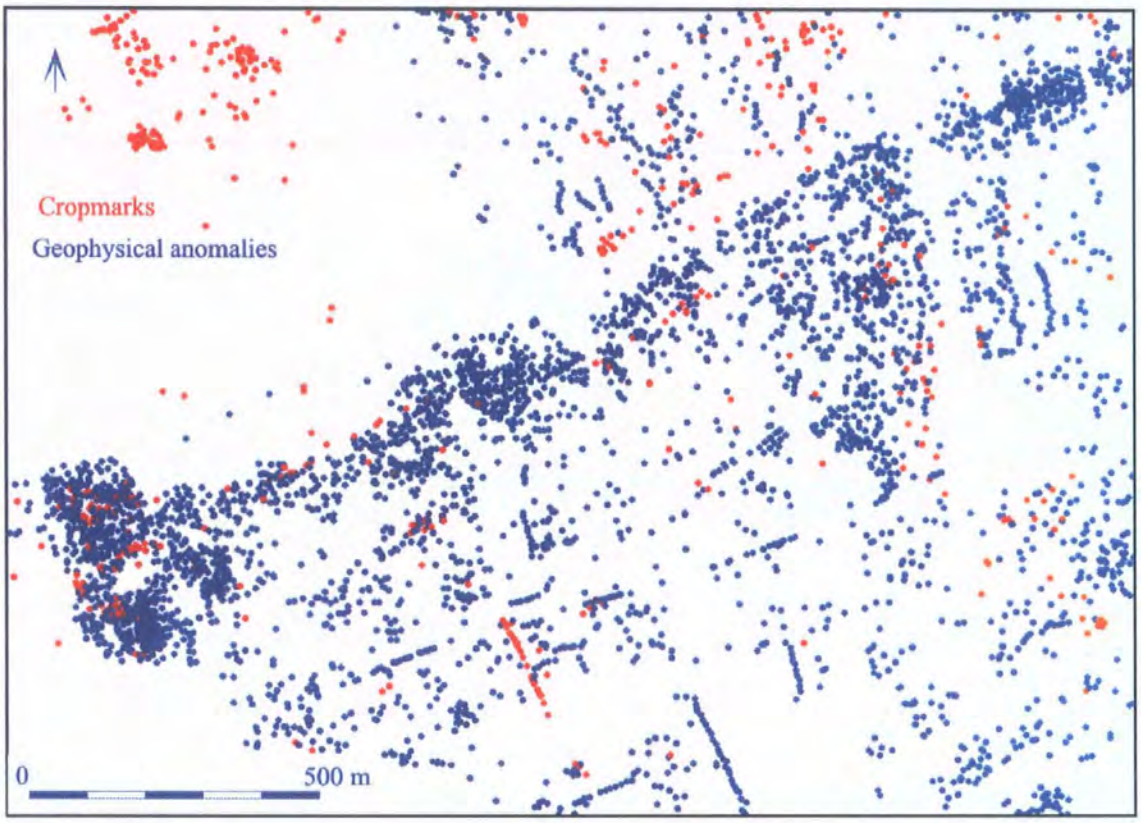

Figure 153 Showing number of anomalies and cropmarks detected using point data

7.5 A new understanding of Anglian settlement patterns

The full excavation of the Anglian cemetery and associated settlement of West Heslerton remains the only one of its kind in the north of England. The way in which settlements of this type have been interpreted has varied, with some writing that their size implied they were "centres of patronage" and consumption (Higham, 1992, p.126) The discovery of two more major settlements (see Figure 69) in the project area, both larger than the excavated example, certainly puts paid to the central point theory. The density of settlement revealed by these surveys is far greater than had been predicted for sites of this period, and the mechanisms which could cause such a widespread uptake of a new building (and burial) tradition need to be analysed (Powlesland et al, forthcoming).

7.6 Actual archaeological remains

It would be easy to look at the returns from the various forms of remote sensing and conclude that most of the underlying archaeological features had been detected, particularly where the returns were very good, as in the geophysical survey results or aerial photographic plots. However, this can only be verified by excavation. Wherever excavation has been carried out over previously surveyed areas, it has demonstrated that the actual density of archaeological features is almost invariably greater than those detected by any form of remote sensing.

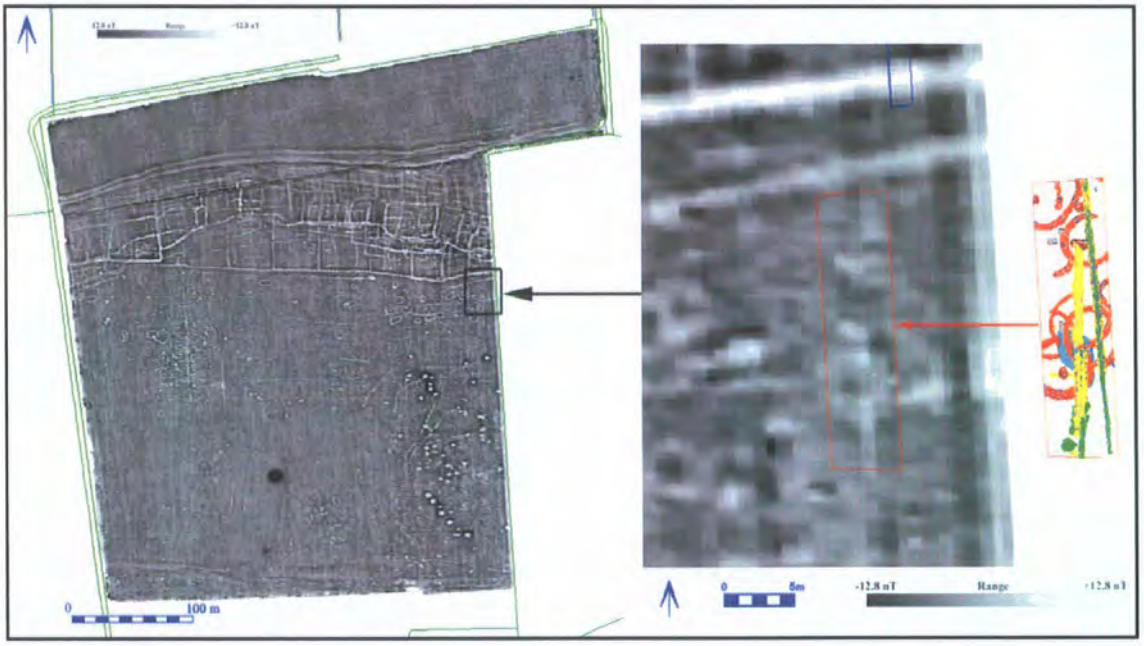

Figure 154 Comparison of returns from gradiometer data compared with actual archaeological remains (Site 28)

This is shown in Figure 154, which shows that where the geophysical survey indicates the location of two or three barrowlets, there are in fact at least eight of these features (either whole or partial) present in the excavated area (Site 28). While the difference between detected anomalies and actual archaeological remains is not always so pronounced, there will always be features which are not detected by remote sensing, either because they are too small to be detected, or because they are filled with a material which is not responsive to the technique being used.

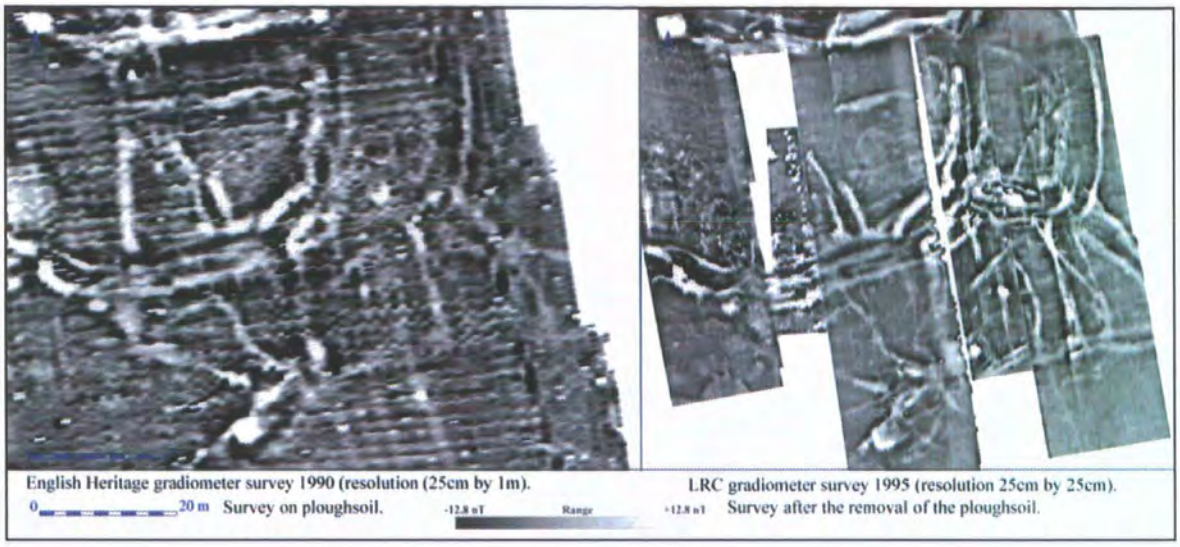

Figure 155 Comparison of different gradiometer survey resolutions (Site 12)

Using the same machine but adopting different techniques can also enhance the returns from a given area. Figure 155 (a close up of the eastern part of Figure 15) shows the difference in returns which can be achieved using a higher resolution magnetic surveying technique, which combined with the prior removal of the topsoil, generates a much more detailed result (Lyall and Powlesland, 1996).

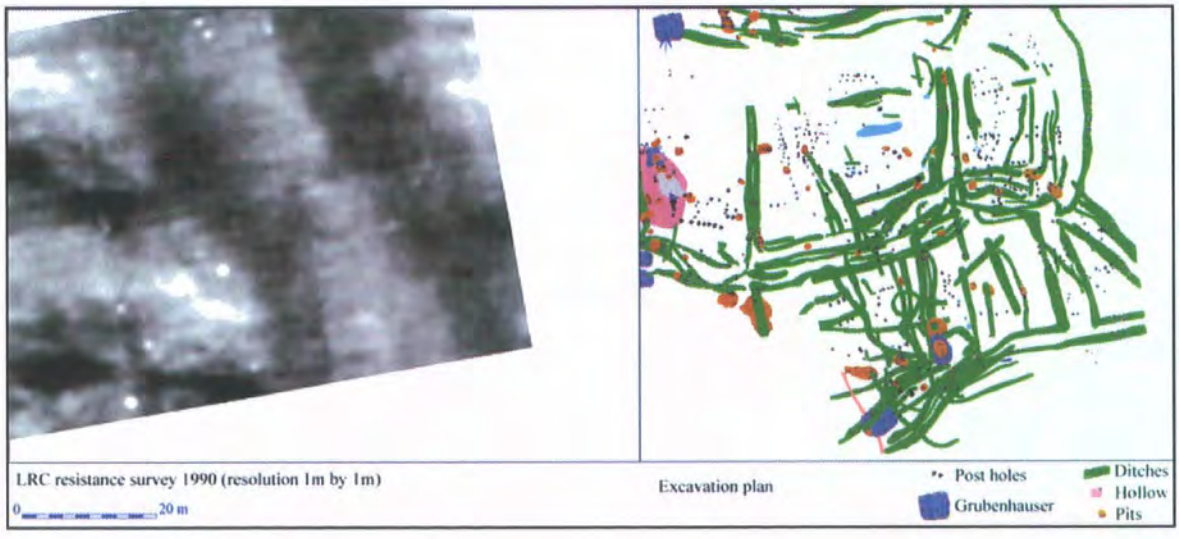

Figure 156 Comparison of returns from different techniques (Site 12)

A resistance survey (see Figure 156) of the same area carried out by the LRC in 1990 gives a completely different result, with only the geological anomalies being detected (a small dry valley in the east and a chalky knoll on the west). However, although the

returns from the high resolution survey do indicate that the area is highly archaeologically active, the complexity revealed by the fully excavated plan shows that not all features were being detected. There are a number of reasons for this. Firstly, the very strongly magnetic anomalies have the effect of masking some of the more subtle underlying anomalies, making them difficult, if not impossible to see in the survey data. Secondly, some of the features were filled with material which was not substantially different to the surrounding subsoil, which makes them virtually undetectable using this method. Thirdly, even though some of the post holes were detected, most cannot be seen in the gradiometer data, due mainly to the small size of most of these features, but also because of a combination of both of the above factors.

Chapter 8 Conclusions and recommendations

The main conclusion from the research is that remote sensing techniques are complementary, with the most comprehensive results often being obtained when using a number of different techniques over the same area. All of the remote sensing techniques investigated would have discovered the main archaeological sites known to exist in the project zone from previous aerial photographic campaigns. That being said, certain conditions favour one type of remote sensing over others, and once these conditions are known, the most responsive form of remote sensing can be applied with the expectation of a reasonable return.

8.1 Comparison of different techniques

This research has benefited jointly from the opportunity of accessing multiple data sources and the ability to assess the returns from these sources across different geological zones. This, combined with the use of vectorised drawings linked to a relational database, has allowed a comprehensive assessment of the different types of remote sensing to be conducted. Even after a campaign of over 25 years, the aerial photographic coverage still showed a number of gaps in the archaeological dataset. These gaps were to a large extent eliminated by the high resolution magnetic surveys. It has been demonstrated that on the chalk Wolds and the southern sandy zone of the Vale, magnetometry provides the most comprehensive results. Aerial photography can also provide very good returns in these zones, and the two techniques are complementary, that is aerial photography can produce results where magnetometry fails to detect anomalies, and vice versa.

Case study area two in the windblown sand zone demonstrated that even where magnetic surveys produced outstanding results, the multi-spectral data could still add detail to the overall picture. Of the 20 *Grubenhäuser* found only by the multi-spectral

survey, 11 were from band 11 (the thermal band) five were from band 10 and 4 from band 6 (both infra-red bands). In areas where geophysical survey produces poorer results, such as in case study areas one and three, both aerial photography and multi-spectral imagery have demonstrated the potential for discovering buried archaeological features. These areas demonstrated that magnetic survey, aerial photography and multi-spectral survey all provide different returns in the alluvial zone, and that although any of the individual methods would have identified that archaeological sites were present, a much more comprehensive view of the sites was gained when combining the returns from all of the different techniques employed.

However, of the total of 74 anomalies which were detected in these areas by the multi-spectral data alone, only 13 were in the visible spectrum, all from band 5. Of these, only one anomaly (a field drain) was not also detected by the infra-red and thermal bands. The implication for using multi-spectral data for feature detection is clear. The use of the visible wavelengths gave no apparent benefit over the aerial photographs taken at the same time. This is not surprising, as the aerial photographs have a much higher ground resolution than the multispectral data. Another significant factor was the timing of the flights, with both flights towards the end of June when cropmarks from nearly mature crops are the dominant type of visible archaeological feature. Further multi-spectral flights during the winter and early spring will be needed if the potential for using infra-red and thermal methods to detect soil marks is to be assessed. This could help to confirm the early results achieved at Morton Fen (Shennan and Donoghue, 1992, p.227), where flights in May produced infra-red evidence for germinating cropmarks which were not seen in the visible spectra.

The conclusion from the above is that while NERC continues to provide high resolution colour photographs of the area surveyed, or until the resolution of the multi-spectral

scanner is improved, when using the multi-spectral data for archaeological feature detection the emphasis must be placed on the infra-red and thermal bands.

8.2 Adding chronological depth

Collecting, processing and interpreting the data from a number of different forms of remote sensing can provide an unparalleled resource for mapping the hidden archaeological remains in a given area. However, this knowledge is two-dimensional; that is the extent of the preservation of the underlying features is not indicated on these maps. In order to provide chronological depth to the returns, as well as to assess the level of preservation of the remains, it will be necessary to undertake a number of targeted small-scale excavations, located to address these and other research questions.

Characterising the barrowlets

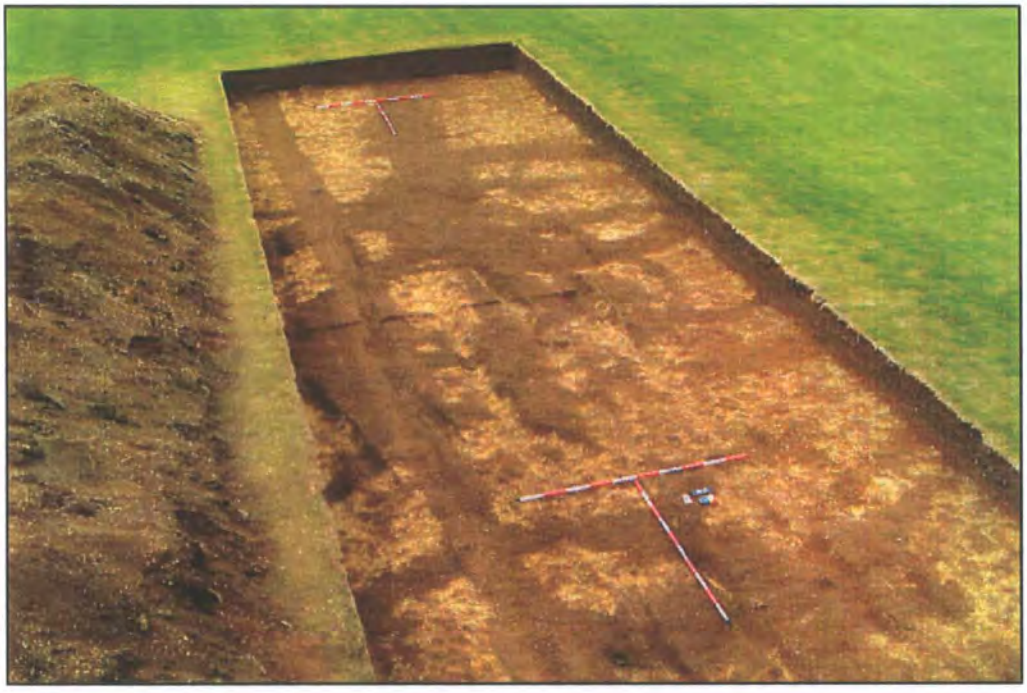

Figure 157 Pre-excavation view of barrowlets (Site 28)

Although a number of these features have already been excavated (see Figure 157), dating evidence remains somewhat scant. The current hypothesis is that they are funerary monuments, where the cremated human remains were placed in the raised area

at the centre of the barrowlet. Indications are that they came into use in the later Iron Age, when the use of the larger square barrows for inhumation was falling out of favour. As all of the barrowlets in the project area are now ploughed out, it is only in areas that have been protected by a layer of windblown sand where the possibility remains of excavating a well-preserved example of one of these features.

Dating the Anglian settlements

By carefully selecting a small number of *Grubenhäuser* from each of the Anglian settlements, it would be possible to date the range of settlement activity which ranges from the early Anglian to the end of the Middle Saxon period, a time when the modern villages of England were being established. The geophysical survey data will, for the first time, allow us to choose a representative selection from a known resource, that is each of the thirteen distinct Anglian settlements.

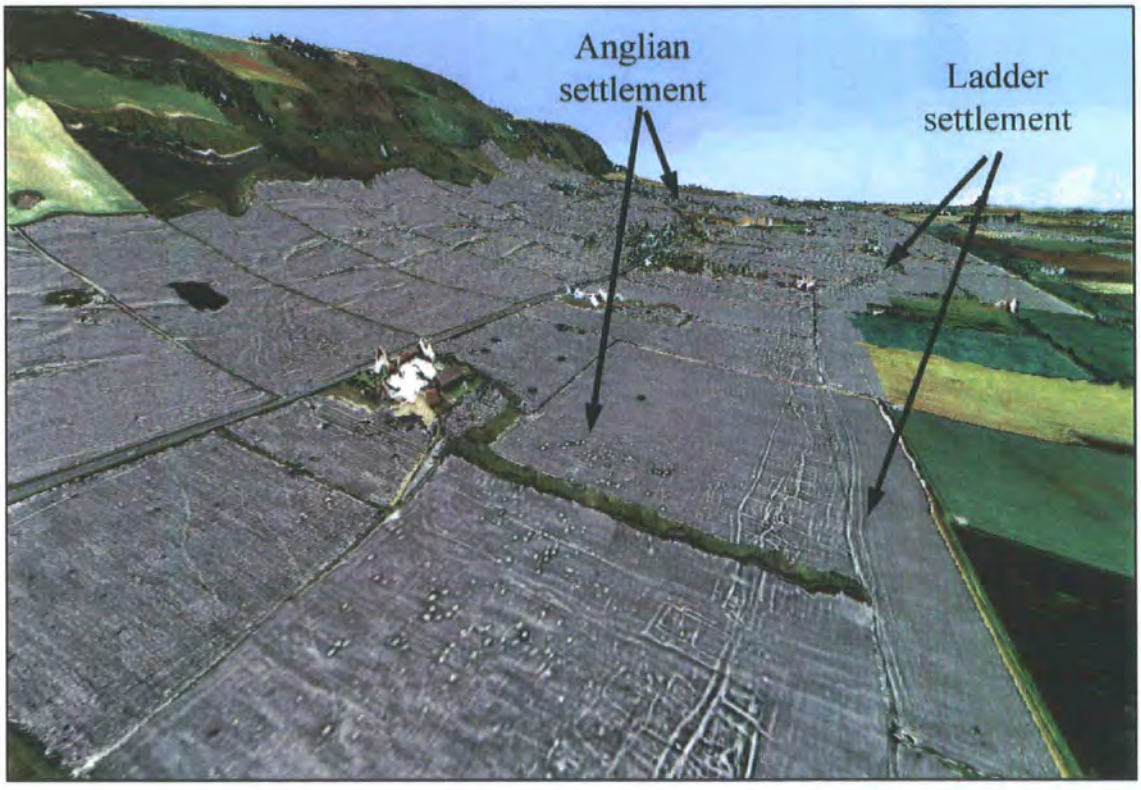

Figure 158 Geophysical survey draped onto the elevation magnified LiDAR DEM, looking west at 2 Anglian settlements

The geophysical data can now be combined with the LiDAR DEM to provide a unique topographic view of the location of the settlements. Figure 158 shows the geophysical

survey data on a Getmapping background, both subsequently draped onto the LiDAR DEM. It is only in this way that the full potential of using combined remote sensing techniques as a landscape tool can be realised, at it now becomes possible to see how the sites discovered fit into the topography of the area. We can visualise the way that the Romano-British ladder settlement (in the foreground) hugs the edge of the sandy area, as well as seeing how the Anglian settlement is here located in a similar topographic position, albeit on a slightly higher area. The location of the excavated Anglian settlement at West Heslerton is indicated by the arrow in the distance. Note that this settlement is situated in a completely different topographic setting.

The Wold entrenchments

Although not part of the case study areas, the June 1992 multi-spectral and aerial photographic data gave an excellent return of the features on the Wold top, particularly the Wold entrenchments. This is illustrated in Figure 159.

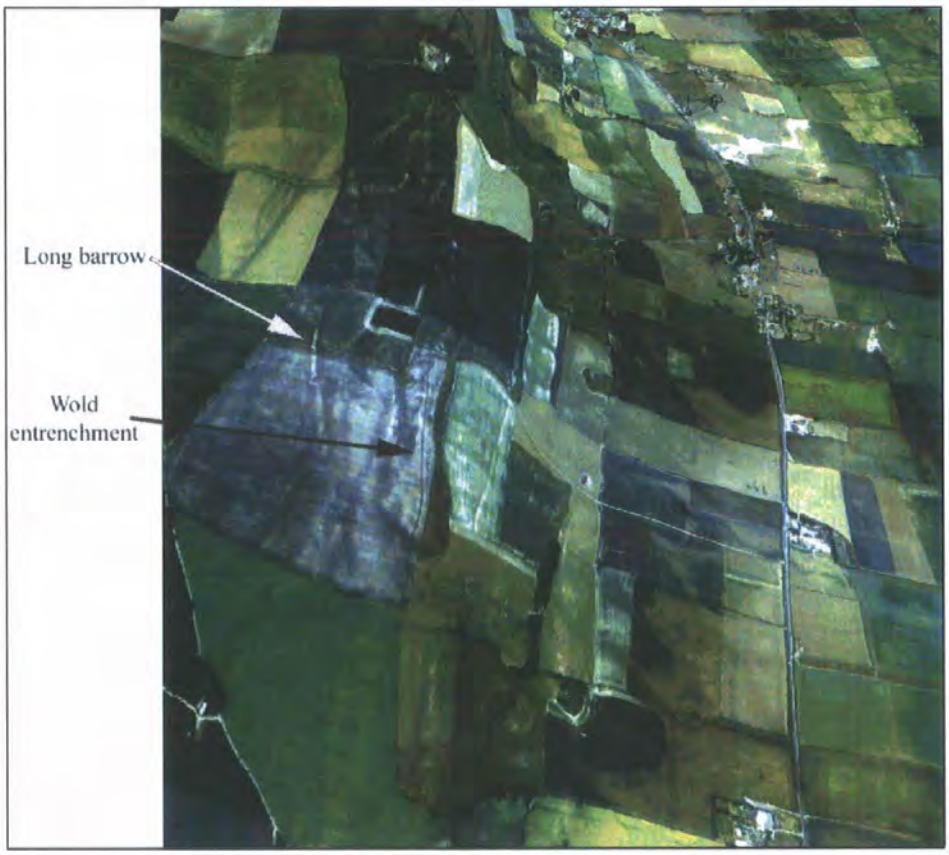

Figure 159 ATM 1268 data as an enhanced false colour image draped onto the LiDAR DEM, looking down onto the top of the Wold edge

Figure 159 uses bands 4, 3 and 2 from the Daedalus 1268 data as red, green and blue respectively. This gives a colour composite of the data, which has been enhanced to bring out some of the archaeological detail. The East Heslerton long barrow can be seen as a bright feature spanning two fields. Note that it finishes at the small circular darker area (marked as a lime kiln on early maps) and the anomaly which continues on the same alignment is in fact a fault line in the chalk. In contrast, part of the Wold entrenchments (ploughed flat at this point), can be seen as a dark green line running across the northern part of the field, before it becomes incorporated into a modern field boundary.

The potential here is to map the extent of the entrenchments, with particular reference to where these are not detected using aerial photographs. Targeted geophysical survey could then be used to demonstrate whether these gaps are real or whether the linear monuments are generally continuous.

8.3 Recommendations for further work

In order to fully assess the returns from airborne remote sensing, it would be necessary to fly over the same area at least once a week over the entire crop growing season. This would need to be carried out at least twice, once in a year when cropmark formation was good, and again in a year when cropmark formation was very poor. Although this research has indicated that both the infra-red and thermal bands contain data that is not in the visible spectrum (see Figure 95, Figure 100, Figure 114 and Figure 129 for examples) flying when cropmark formation is poor would allow the returns from the non-visible wavelengths to be assessed where aerial photography would give no returns. This project would allow much more precise timings of multispectral flights for archaeological feature detection to be established. With the development of new high

resolution multispectral scanners for use in satellites, the potential for carrying out a project on this scale is becoming increasingly likely. Further study could also investigate the possibility that certain types of cropmark are only seen vertically, as hypothesised in the CASI data comparison in Chapter 6. Although not used in this research, modern satellite images such as those produced by Ikonos and Quickbird can also provide cover of a large area at affordable prices (Quickbird coverage can currently be obtained for 24 dollars per square kilometre), and as sub1 metre resolutions are now becoming available, their use for archaeological feature detection is looking increasingly promising (Using Google Earth, go to 37"35'50.96 N 62"09'49.87 E to see an example of high resolution Quickbird data).

8.4 Environmental Assessment

Recent environmental work carried out by James Rackham as part of an English Heritage funded project undertaken by the LRC (Rackham and Powlesland, 2006) has indicated that the potential for using environmental sampling to enhance the archaeological understanding of the area still remains, although this potential is decreasing at an alarming rate. Apart from the paleochannels, where preservation of environmental remains is good, the remainder of the area is suffering from the long-term effects of modern drainage techniques.

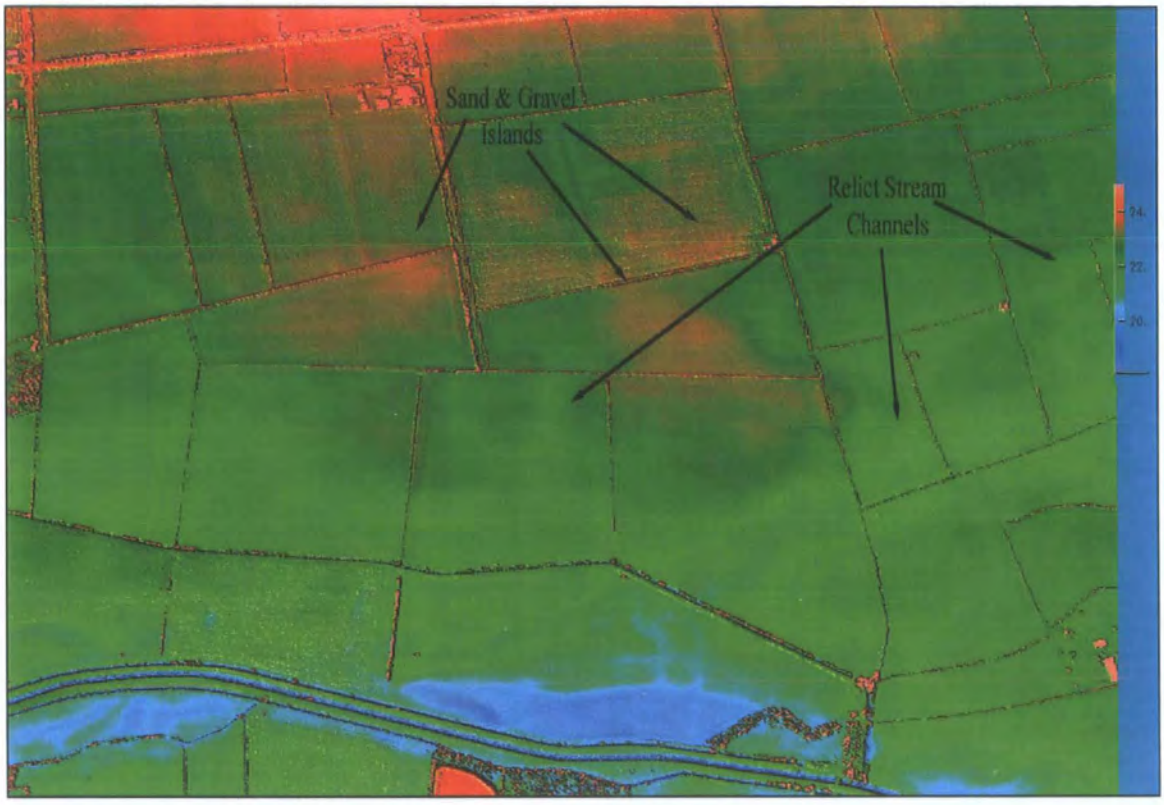

Figure 160 LiDAR image showing sand and gravel islands and relict stream channels

Remote sensing (particularly multispectral and LiDAR imagery, see Figure 160) will assist in the location of further paleochannels, enhancing the possibility of recovering undisturbed environmental remains.

8.5 Final conclusion

This type of project has the power to alter the way in which archaeologists perceive the landscape around them; that is moving away from the idea of a number of isolated sites dotted around the region towards a perception that the entire landscape at any given period was occupied and utilised. What we routinely identify as an archaeological site is in fact just one small part of the past human environment, all of which would have had a profound influence on the lifestyles of our ancestors. Remote sensing, combined with geophysical survey, should now be seen as one of the most valuable tools available to the archaeologist, both for enhancing detail of known sites and for their ability to place archaeological excavations within a landscape context. Using a combination of vectorised drawings linked to a relational database gives the researcher the opportunity to ask specific questions of the data in a way which would have been impossible only a few years ago, and the increasing availability of cheaper remote sensing data from a number of different airborne and satellite platforms will provide future researchers with an unparalleled opportunity for detailed landscape analysis.

References

Aitken, M. J. (1958) Magnetic Prospecting 1-The Water Newton Survey. *Archaeometry,* 1, pp.24-26.

Barnes, I. (2003) Aerial remote-sensing techniques used in the management of archaeological monuments on the British army's Salisbury Plain training area, Wiltshire, UK. *Archaeological Prospection*, 10, pp.83-90.

Becker H. and Fassbinder, J.W.E. (2001) Magnetic Prospecting in Archaeological Sites. *Monuments and Sites*, VI, pp.20-25.

Bewley, R.H. (2003) Aerial survey for archaeology. *The Photogrammetric Record*, 18, pp.273-292.

Bewley, R.H, Crutchley, S.P. and Shell, C.A. (2005) New light on an ancient landscape: LIDAR survey in the Stonehenge World Heritage Site. *Antiquity* 79, pp.636-647.

Brewster, T. C. M. (1952) *Two Mediaeval Habitation Sites in the Vale of Pickering.* York: Yorkshire Museum.

Brewster, T. C. M. (1957) Excavations at Newham's Pit, Staxton, 1947-8. *Yorkshire Archaeological Journal*, 39, pp.193-223.

Brewster, T.C.M. (1963) *The Excavation of Staple Howe.* The East Riding Archaeological Research Committee.

Brewster, T.C.M. (1980) *The Excavation of Garton and Wetwang Slacks.* Malton: Prehistoric Excavation Reports 2.

Brewster, T.C.M. (1981) The Devil's Hill. *Current Archaeology*, 76, pp.140-141.

Buteux, S. Gaffney, V. White, R. and van Leusen, M. (2000) Wroxeter Hinterland Project and Geophysical Survey at Wroxeter. *Archaeological Prospection*, 7(2), pp.69-80.

Caldwell, A.E. (1996) The Application of Remote Sensing in Archaeology: A Study of Crop Mark Detection in the Heslerton Parish Project Area, Vale of Pickering, North Yorkshire. Unpublished MSc thesis, University College London.

Challis, K. (2005) *Analysis of the effectiveness of Aerial Photography, LIDAR and IFSAR.* (Unpublished Birmingham Archaeological Report).

Challis, K (2006) Airborne Laser Altimetry in Alluviated Landscapes. *Archaeological Prospection* 13(2) pp.103-127.

Clark, A.J. (1996). *Seeing Beneath the Soil.* 2nd ed. B.T. Batsford Ltd: London.

Clemence, H. (1993). The Timber-Framed Structures at West Heslerton Anglo-Saxon Settlement Site: Analysis and Comparison. Unpublished undergraduate dissertation, Nottingham University.

Crawford, O.G.S. and Keiller, A. (1928) *Wessex from the Air*. Clarendon Press, Oxford.

Crutchley, S. (2006) LIDAR in the Witham Valley, Lincolnshire: An assessment of new remote sensing. *Archaeological Prospection*, 13(4), pp.251-257.

Donoghue, D.N.M. and Shennan, I. (1988a) The Application of Remote Sensing to Wetland Archaeology. *Geoarchaeology*, 3(4), pp.275-285.

Donoghue, D.N.M. and Shennan, I. (1988b) The Application of Multispectral Remote Sensing Techniques to Wetland Archaeology. *British Archaeological Reports*, 186, pp.47-59.

Donoghue, D.N.M., Powlesland, D and Pignatti, S. (2003) *Airborne thermography and spectral sensitivity analysis of the soil and soil-vegetation interface for archaeological prospection*. (Unpublished project application to the Natural Environment Research Council).

Fuller, P., Hill, I. and Leech, C. (2006) A Comparison of Archaeomagnetic Results from a Towed Magnetometer Array and Traditional Methods. *International Society for Archaeological Prospection News*, 7, pp.7-9. [online]. [Accessed 24th May 2007]. Available from World Wide Web: <http://www.bradford.ac.uk/archsci/archprospection/newsletters.php> (online member only access).

Gaffney, C. and Gater, J. (2003) *Revealing the buried past*. Tempus Publishing Ltd.

Greenwell, W. and Rolleston, G. (1877) *British Barrows*. Oxford University Press.

Gonzalez, R. and Woods, R. (1993) *Digital Image Processing*. Addison-Wesley Publishing Company.

Hampton, J. (1989) The Air Photography Unit of the Royal Commision On The Historical Monuments Of England 1965-85.. *In* Kennedy, D, (ed.) *Into the Sun: Essays in Air Photography in Archaeology*. Sheffield: J.R. Collis Publications, p.13-28.

Haralick, R.M., Dinnstein, I and Shanmugam, K. (1973) Textural features for image classification. *IEEE Transactions on Systems, Man, and Cybernetics*, SMC-3, pp.610-621.

Haughton, C.A. and Powlesland, D.J. (1999) *West Heslerton: The Anglian Cemetery*. LRC Monograph 1, North Yorkshire.

Higham, N. (1992). *Rome, Britain and the Anglo-Saxons*. London: Seaby. .

Jordan, D. (2000) Magnetic techniques applied to archaeological survey. *In*: Pasquinucci, M. and Trement, F, (eds). *Non-Destuctive Techniques Applied to Landscape Archaeology*. Oxford: Oxbow Books. p.114-124.

Jones, R. J. A. and Evans, R. (1975) Soil and crop marks in the recognition of archaeological sites by air photography. *In*: Wilson, D. R, (ed). *Aerial reconnaissance for archaeology*. London. Council for British Archaeology, Research Report No 12. p.1-11.

Kearey, P.and Brooks, M. (1991) *An introduction to Geophysical Exploration.* 2nd ed. Oxford: Blackwell Scientific Publications. p.148-218.

Kent, P. (1980) British Regional Geology Eastern England from the Tees to the Wash. Her Majesty's Stationery Office.

King, S. J. (1986) Soils in North Yorkshire VIII: *Sheet SE97N/98S (Wykeham Abbey).* Soil Survey Record Number 96. Dorking: Bartholomew Press.

Kvamme, K. (2006) Integrating Multidimensional Geophysical Data. *Archaeological Prospection*, 13(3), pp.57-72.

Lillesand, T. M. and Keifer, R.W. (1999) *Remote Sensing and Image Interpretation.* 4th ed. New York: John Wiley and Sons, Inc.

Lyall, J. and Powlesland, D. J. (1996). The application of high resolution fluxgate gradiometry as an aid to excavation planning and strategy formulation. *Internet Archaeology*, 1. [online]. [Accessed 24th May 2007]. Available from World Wide Web: <http://intarch.ac.uk/journal/issue1/lyall_toc.html>

McManus, K.B. (2003) Airborne thermography and ground geophysical investigation for detecting shallow ground disturbance under vegetation. (Unpublished PhD thesis, University of Durham)

Palmer, R. (1984) Danebury: an Iron Age Hillfort in Hampshire. An Aerial Photographic Interpretation of its Environs. RCHME Supplementary Series No.6. London.

Palmer, R. (1989) Thoughts On Some Aspects Of Air Photo-Archaeology. *In* Kennedy, D, (ed.) *Into the Sun: Essays in Air Photography in Archaeology.* Sheffield: J.R. Collis Publications, p.53-60.

Powlesland, D.J., Haughton, C.A. and Hanson, J.H. (1986) Excavations at Heslerton, North Yorkshire, 1978-82. *Archaeological Journal*, 143, pp.53-173.

Powlesland, D., Lyall, J. and Donoghue, D. (1997) Enhancing the record through remote sensing: the application and integration of multi-sensor, non-invasive remote sensing techniques for the enhancement of the Sites and Monuments Record. Heslerton Parish Project, N. Yorkshire, England. *Internet Archaeology*, 2. [online]. [Accessed 24th May 2007]. Available from World Wide Web: <http://intarch.ac.uk.ezphost.dur.ac.uk/journal/issue2/pld_toc.html> (online subscription required)

Powlesland, D. (2001) The Heslerton Parish Project: An integrated multi-sensor approach to the archaeological study of Eastern Yorkshire, England. *Remote Sensing in Archaeology.* Forte and Campagna, S. (eds). Firenze: University of Siena. p.233-255.

Powlesland, D. (2003) The Heslerton Parish Project: 20 years of archaeological research in the Vale of Pickering. *In*: Manby, T.G., Moorhouse, S. and Ottoway, P. (eds). *The Archaeology of Yorkshire: an assessment at the beginning of the 21st century.* Yorkshire Archaeological Society Occasional Paper No.3. p275-292.

Powlesland, D., Wood, I. and Morris, R. (forthcoming) Deira and York in the 7th and 8th centuries. *In*: *La ciudad medieval y su influencia territorial*, papers presented at Nájera. Encuentros Internacionales del Medievo, 2006.

Price, J.C. (1977) Thermal Inertia Mapping: A New View of the Earth. *Journal of Geophysical Research*, 82(18). pp.2582-2590.

Price, J.C. (1989) Quantitative Aspects of Remote Sensing. *In*: Asrar, G. (ed). *The Thermal Infrared Applications of Optical Remote Sensing*. New York: John Wiley & Sons. p.578-603.

Pryor, C. M. (1992) Integration of remotely sensed and ground based geophysical data for archaeological prospecting using a geographic information system; Vale of Pickering, North Yorkshire. (Unpublished MA thesis, University of Durham)

Rackham, J. and Powlesland, D.J. (2006) *Pilot Project: Environmental Assessment Project for the central Vale of Pickering*. English Heritage Project 3038. Unpublished manuscript.

Royal Commission on the Historical Monuments of England (1960) *A Matter of Time*. London: Her Majesty's Stationery Office.

Riley, D. N. (1944) The technique of air archaeology. *Archaeological Journal*, 101, pp.1-16.

Riley, D. N. (ed) (1988) *Yorkshire's Past from the Air*. Sheffield Academic Press.

Stead, I. M. (1979) *The Arras Culture*. York: Yorkshire Philosophical Society.

Scollar, I., Tabbagh, A., Hesse, A and Herzog, I. (1990) *Archaeological Prospecting and Remote Sensing*. Cambridge University Press.

Smith, L. P. (1967) *Potential Transpiration*. Technical bulletin no 16. Ministry of Agriculture, Fisheries and Food. London: Her Majesty's Stationery Office.

Shennan, I. and Donoghue, D.N.M. (1992) Remote Sensing in Archaeological Research. *Proceedings of the British Academy*, 77, pp.223-232.

Stoertz, C. (1997). Ancient landscapes of theYorkshire Wolds : aerial photographic transcription and analysis. Royal Commission on the Historical Monuments of England.

Tabbagh, J. (2003). Total Field Magnetic Prospection: Are Vertical Gradiometer Measurements Preferable to Single Sensor Survey? *Archaeological Prospection*, 10(2), pp.75-81.

Tipper, J. (2004) *The Grubenhaus in Anglo-Saxon England*. LRC Monograph 2, North Yorkshire.

Vatcher, F de M. and Vatcher H. L. (1965) Notes and News: East Heslerton Long Barrow, Yorkshire: The Eastern Half. *Antiquity,* 39(153), pp.49-52.

Vuorela, A. (1997) Satellite Image Based Land Cover and Forest Classification of

Finland. *Proceedings of the Finnish-Russian Seminar on Remote Sensing in Helsinki*, pp.42-52.

Wilson, D. R. (2000). *Air Photo Interpretation for Archaeologists*. 2nd edition. Tempus Publishing Ltd.

Winterbottom, S.J. and Dawson, T. (2005) Airborne multispectral Prospection for Buried Archaeology in Mobile Sand Dominated Systems. *Archaeological Prospection* 12(4), pp.205-219.

Warner, T.A., and Chen, X. (2001) Normalization of Landsat thermal imagery for the effects of solar heating and topography. *International journal of Remote Sensing* 22, pp.773-788.

Chapter 9 Appendices

9.1 Appendix one Geophysical survey

9.1.1 How magnetometry works

A magnetometer can detect two types of magnetism; permanent or remnant magnetism (also termed thermoremanence), and temporary magnetism. Temporary magnetisation occurs only when a magnetically susceptible material is placed in an external magnetic field. The material will then acquire a magnetic field of its own in addition to that of the outside field, but will lose this field if the external field is taken away. This occurs because of the material's magnetic susceptibility, which is the ease with which a magnetic field can pass through a material, so that the higher the material's magnetic susceptibility is, the stronger its induced magnetic field will be (Clark, 1996, p.65-66 and p.99-100). For the purposes of archaeological magnetometry the external field is provided by the Earth's magnetic core, and is thus never "off", so that magnetic techniques of archaeological prospection are not weather dependent, and can be conducted at any time.

Initially, magnetometers were used to detect the presence of kilns or furnaces, which are permanently magnetised. They acquired their thermoremanence by being fired above a temperature known as the Curie point, which varies depending on the minerals present in the material. For example, haematite will pass this point at 675 C, while for magnetite it is lower, at 565 C (Clark, 1996, p.65: Gaffney and Gater, 2003, p.37). What happens is that the iron content of the various clays present in the construction of the kiln are effectively de-magnetised at the Curie point. As the kiln subsequently cools, the iron in the material is re-magnetised with a new permanent magnetic alignment, based on the current orientation of the Earth's magnetic field.

Iron is the other major source of permanent magnetism detected in magnetometer surveys, and it produces a very strong localised signal. These peaks, or dipoles (see Figure 161), are normally displayed as small black and white peaks (in greyscale images) or very localised positive-negative signals (in trace plots) in processed survey data. Although they can pinpoint the location of buried archaeological artefacts, in practice this is a rare occurrence, and they generally tend to indicate the presence of relatively recent iron objects (i.e. horse shoes, cans, shotgun cartridges, broken ploughshares, etc).

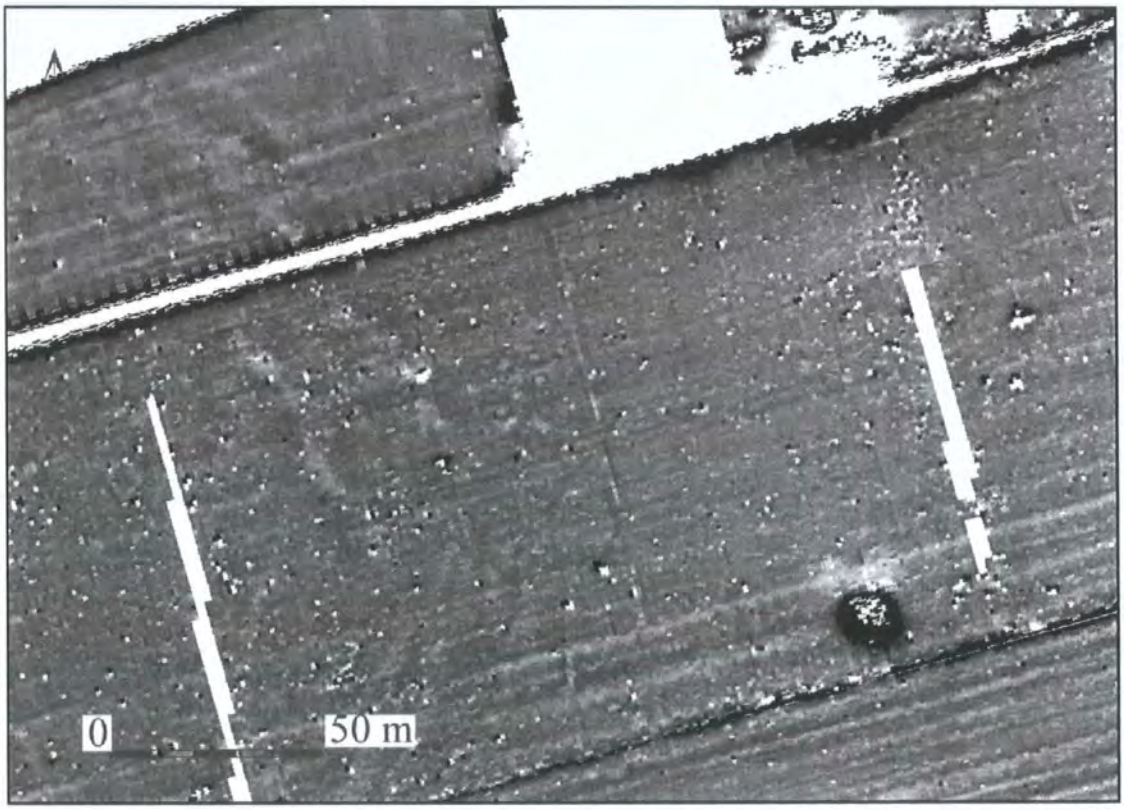

Figure 161 Note the number of dipoles present in the ploughed central field (Site 116), compared to the pasture field (Site 115) in the north-west.

However, even in the initial proton magnetometer surveys by Aitken (Aitken, 1958), it was realised that the magnetometers were also detecting much more subtle magnetic anomalies, which equated with the infill of buried ditches and pits. The detection of this "settlement" evidence has become the most prevalent use of magnetometry in archaeological geophysics today. The reason for this is that many forms human activity tend to increase the magnetic susceptibility of soils, and this enhanced material then

forms part of the fills of cut features (for example pits and ditches) present at the time of the magnetic enhancement. This human enhancement of susceptibility is primarily heat derived, through cooking, kilns, furnaces, pottery making and other activities.

Contrast in susceptibility is fundamental in the detection of these subtle archaeological features. If the contrast between the surrounding subsoil and the infilled features is not substantially different, then it is unlikely that magnetic techniques will identify these features. Also, if the overlying topsoil or ploughsoil has a substantially higher magnetic susceptibility than the contrast between the underlying infilled features and the subsoil, then the technique will only be of limited value in archaeological feature detection.

Although magnetometers are not generally used for this purpose, it is also possible to detect buried walls, which generally show up as "negative" anomalies, that is they are less magnetically susceptible than the surrounding subsoil.

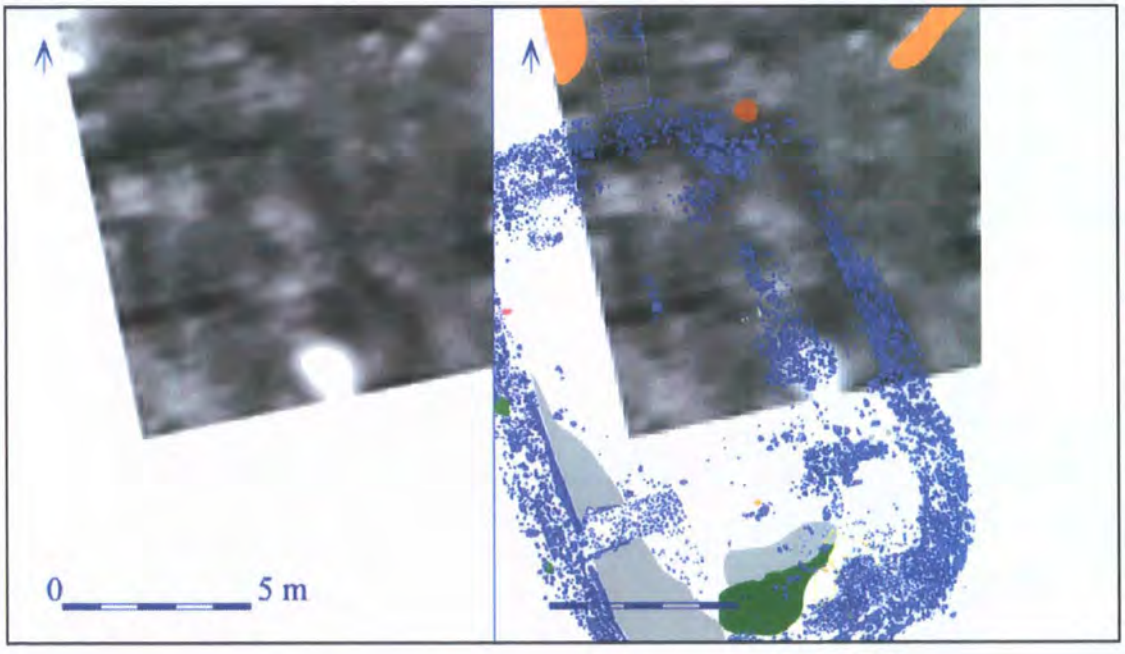

Figure 162 Wall footings detected by magnetic surveying techniques on Site 12

This can be seen in Figure 162, where the initial magnetometer survey on the left is compared with the excavated features superimposed on the right, with blue indicating

the location of a robbed out chalk wall, with only the lowest foundations remaining. While it can be seen that there is a direct correlation between the location of the wall foundation and a negative (darker) magnetic anomaly, it is also clear that a number of negative anomalies present in the magnetic survey clearly do not relate to buried wall features, and it for this reason that magnetic surveys are not generally used for the detection of buried masonry. However, large scale buildings such as Roman villas and towns (Buteux et al, 2000), as well as Medieval monasteries and abbeys (Gaffney and Gater, 2003, p.164) seem to respond well to magnetic techniques

9.1.2 Development of gradiometers

Using a single magnetic detector of any type is prone to a number of problems associated with two separate but related areas; the attitude of the detector in relation to the ground surface and the prevailing magnetic field, and the diurnal variation in the Earth's geomagnetic field. As the planet rotates, the magnetic field falls in the morning and rises at the end of the day, by 5 nT in winter, but by as much as 50 nT during summer (Clark, 1996, p.67).

In order to avoid the problems of diurnal fluctuation, differential magnetometers were devised. This involved the collection of data from two different but identical sensors at the same time; one sensor moving across the survey area, and another taking readings at a fixed location. This allowed any fluctuation in the ambient magnetic field to be adjusted for. Gradiometers are a variant on this design, with both detectors housed in a single tube. They operate by subtracting the readings of the upper, or reference sensor (measuring the Earth's magnetic field) from the lower sensor (measuring the Earth's magnetic field as well as the effect of any localised magnetic anomaly) to obtain a reading which indicates localised magnetic strength. In effect, this means that if there is no magnetic anomaly in the vicinity, then the reading obtained will be zero, although in

practice this is rare, as both soil "noise" and instrument calibration stability (or drift) will also have an effect on the readings. A factor to consider is that in a gradiometer array the sensors are usually so close together that both of them will be affected by a strong localised anomaly. However, in practice this does not detrimentally affect the ability of modern gradiometer arrays to detect both weaker and stronger anomalies.

Fluxgates are electronic magnetic detectors, and are extremely directionally sensitive, so that they are almost always used in a gradiometer array, where the two sensors are spaced at a regular intervals (usually 0.5 or 1 metre apart) in a rigid tube.

Recently, there has been much debate on whether "total field" sensors (i.e. those used in caesium magnetometers) require calibration in this way, and research carried out by Becker and Fassbinder (2001) and Tabbagh (2003) indicate that data acquired by modern stable caesium arrays can be used without the use of a differential or gradiometer setup, although more data processing may be subsequently required to remove the effects of instrument drift and diurnal variation. A total field system does not initially require that a zero reference point is found, as it measures the absolute strength of the magnetic field in nT, including that provided by the Earth. However, initial calibration and checks on the Earth's magnetic field periodic drift are required.

9.1.3 Choice of instrument

A number of factors influenced the choice of fluxgate gradiometers as the primary magnetic data collection instrument. First and foremost, they are easily carried by a single operator, and modern instruments have been designed to be very robust and portable over difficult to traverse areas. Secondly, the technology is now reasonably well understood, and processing of the data can be carried out in the field on a day to day basis. Finally, availability of this type of magnetometer is now widespread, and the

LRC owned both an FM36 and a Grad 601-2. An additional factor is the availability and cost of caesium magnetometers currently make them prohibitively expensive, although they are reducing in cost all the time. As an example, as of January 2006, a single sensor FM256 would cost around £7000, a dual sensor Grad 601-2 would cost around £9500, and each caesium sensor costs around £10000. Having said this, the fluxgate gradiometer prices over the past 10 years have seen a gradual annual increase, whereas the caesium sensors have seen a 50% reduction in price over the previous five years (that is from £20000 to £ 10000 per sensor).

The question remained that if instruments with a greater sensitivity (the fluxgates have a sensitivity of around 0.1 nT, whereas caesium instruments can be up to 10 times more sensitive, with precisions as low as 0.01 achievable) were to be used, would the results obtained be radically different?

Tests carried out with both a fluxgate gradiometer and a caesium array of four sensors (caesium array operated by English Heritage personnel) over two sites in the project area did not give an appreciably different result in terms of anomaly detection.

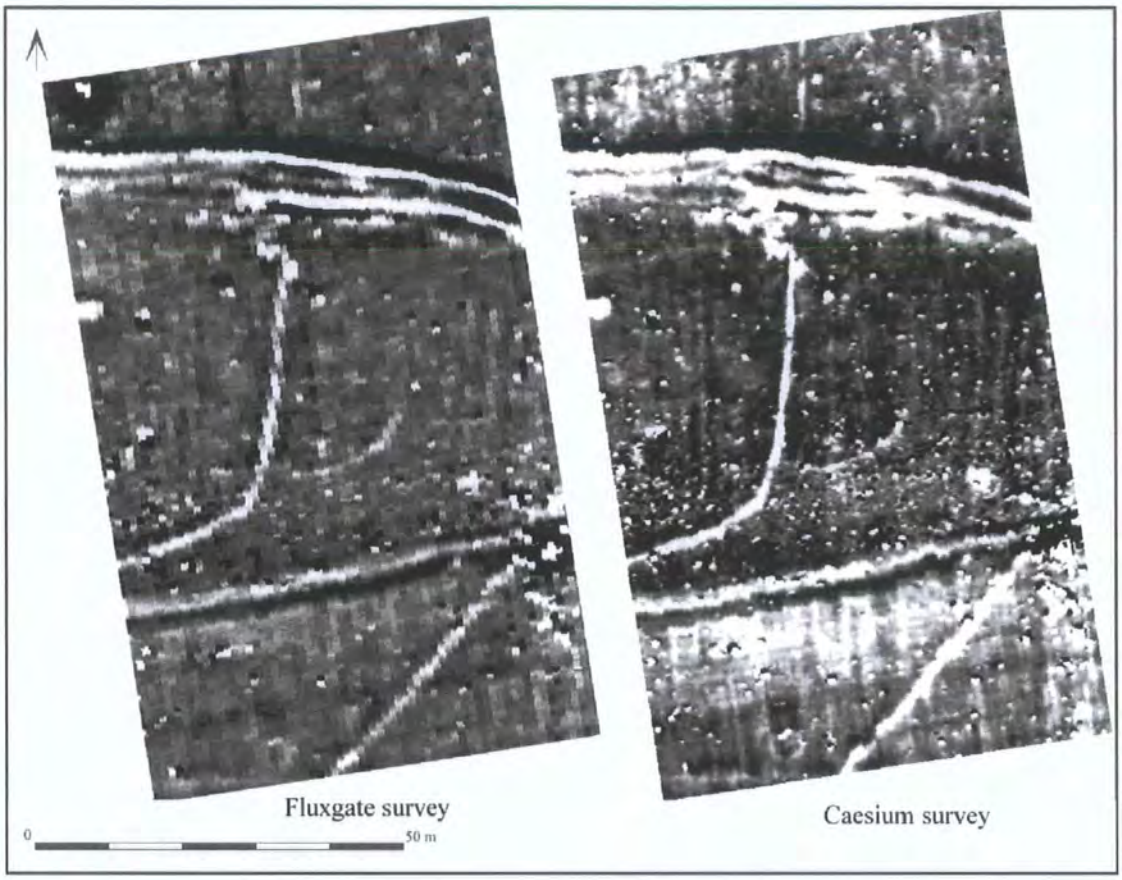

Figure 163 A comparison of a fluxgate gradiometer survey (spatial resolution 1m by 25cm) on the left and a caesium array (resolution 50cm by 12.5cm) on the right

This is illustrated in Figure 163 and Figure 164, which show the results of both types of magnetic survey techniques. While it can be seen that the higher spatial resolution of the caesium array gives a greater clarity to some of the magnetic anomalies, and that the greater sensitivity allows more depth in magnetic range to be visualised, there was no real advantage in anomaly detection to be gained by using this method, or at least not in the chosen sampled areas. The value of greater sensitivity has also been questioned by Jordan (2000, p.121). He states that the normal soil background magnetic noise is in the order of 0.1 nT, and that any weaker anomalies, while theoretically detectable using the higher sensitivity, would be lost within the higher background noise.

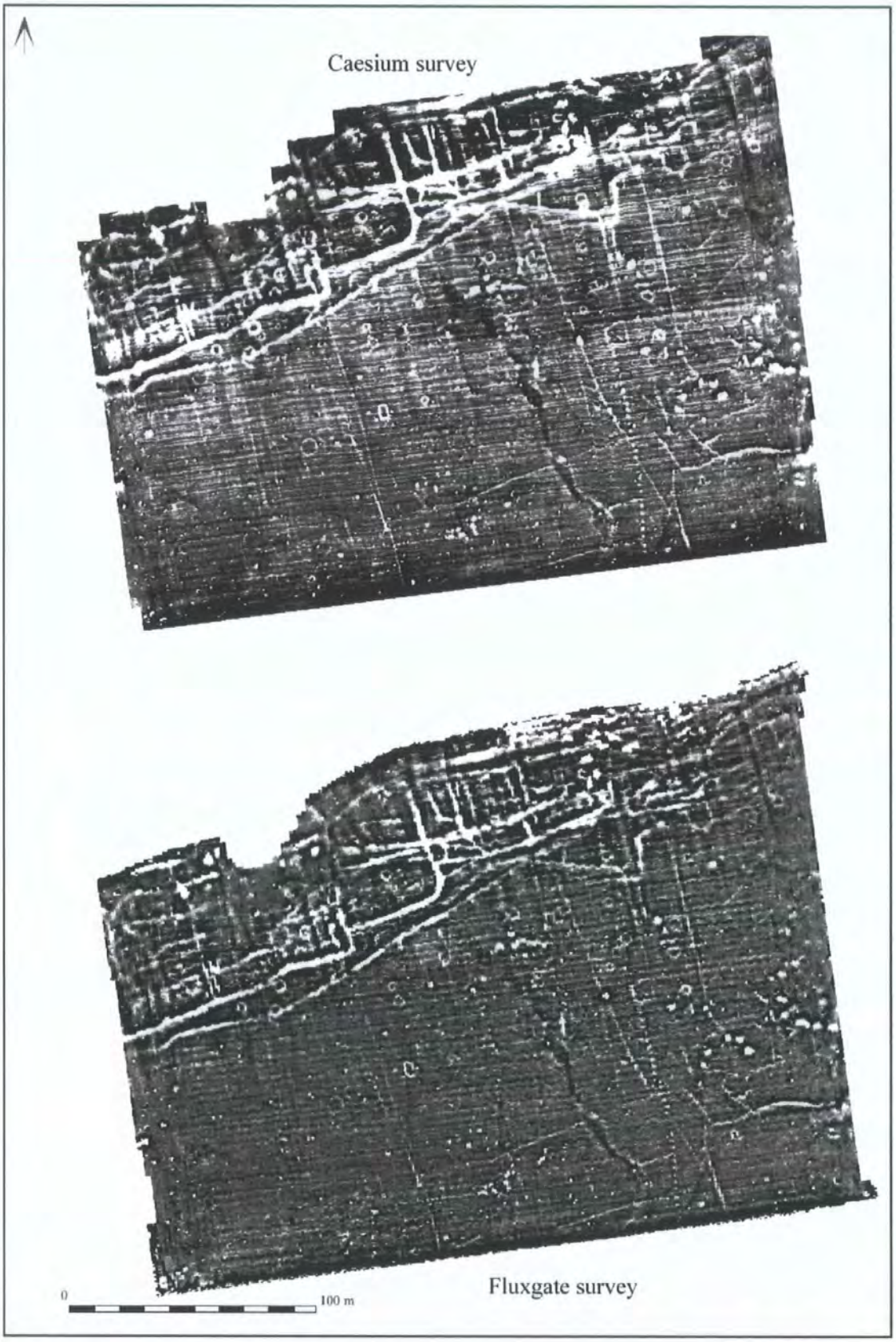

Figure 164 A comparison of fluxgate gradiometer survey (spatial resolution 1m by 25cm) below and a caesium array (resolution 50cm by 12.5cm) above

However, new developments in total field caesium arrays mean that greater areas can be covered at a higher spatial resolution, in a shorter time (Fuller et al, 2006). When this

technology has undergone further field trials and refinements, the use of caesium instruments for large scale survey could well become more widespread.

9.1.4 Zero reference point

Prior to beginning the survey, the operator should allow the sensors to establish local temperature equilibrium (taking between 20-30 minutes, depending on the array) before establishing a zero point. The zero point is a reference area which is found by walking around with the gradiometer to establish an average magnetic value, and then finding an area where a stable average reading can be obtained. The gradiometer is then set to zero over this point. This allows both negative and positive magnetic values (relative to the assigned zero) to be recorded. When necessary due to instrument drift, the gradiometer must be returned to this point to recalibrate the sensors.

9.1.5 Operator errors possible with magnetic data collection

A number of different operator errors can occur when collecting magnetic data. These problems, and how to correct them, are discussed below.

Chessboard pattern grids

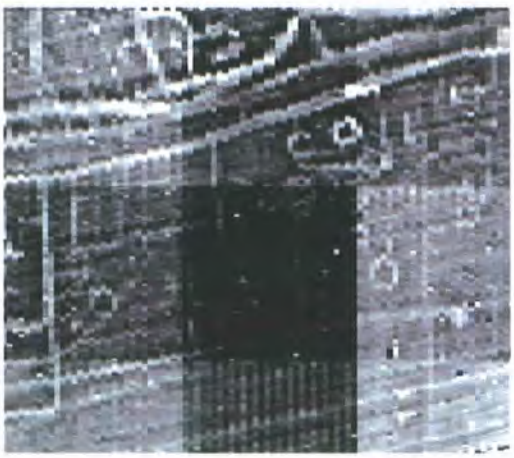

Figure 165 Chessboard pattern grids

This occurs primarily if the zero reference point chosen is not a good one (i.e. if it is near an iron object in the ground), or if the instrument is not returned, balanced and re-zeroed on the reference point at regular intervals. It can also occur if, because the area to be surveyed is large and the zero point is subsequently moved, a different underlying value is selected for the new zero point. The problem can be avoided by ensuring that the zero reference point chosen is reliable, and by regular checking of the alignment and

balance of the machine. If the zero point has to be moved, ensure that the machine is balanced and set to zero on the old point before establishing the new zero point.

Striping

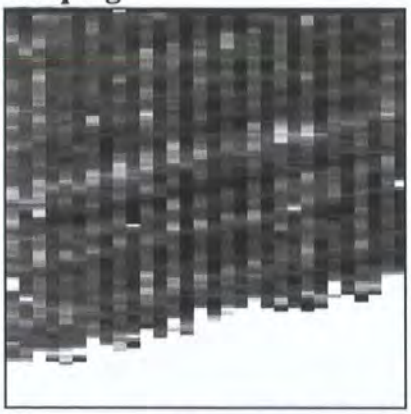

Figure 166 Traverse striping

Striping in magnetic data is mainly seen in data collected using the zigzag traverse method. It is caused by the machine being at a different alignment for alternate traverses, and the results of this can be exacerbated if the machine drift is occurring during the survey. Learning to hold the machine in the same alignment for both traverses is vital, or alternatively the parallel method of traverse will help to alleviate this problem. An extreme form of striping will occur if the operator is carrying an iron object (i.e. a set of keys in a pocket) or wearing footwear with an iron content. This form of striping is virtually impossible to deal with, as the differences in alternate traverses are so great, and the data is compromised by the magnetic effect of the iron object. It is normally necessary to re-survey the grid in these cases. Striping can occur in Bartington dual sensor array surveys when the zero reference point chosen is inappropriate, i.e. where the readings at this point for both sensors are slightly different, or if one sensor is drifting more than the other.

Banding

Figure 167 Edge banding

Banding is a problem that can be seen at the beginning or the end of each traverse (seen as a dark line across the top of Figure 167). It is commonly seen as either a lighter or darker area along the edge of the grid, and is caused by an

operator holding the instrument at a different angle when beginning or finishing each traverse. It can be solved by ensuring that walking speed is attained before beginning each traverse, and that the end of each grid is

passed over without turning the body for the next line.

Staggering

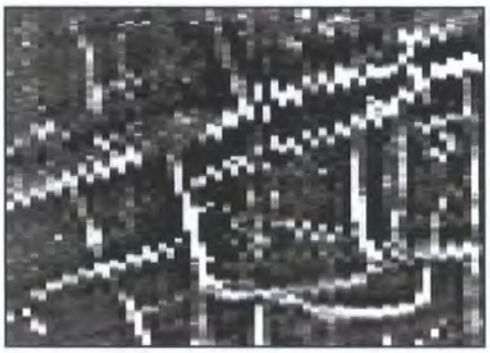

Figure 168 Zigzag or staggering errors

Staggering in the data is almost always seen only using the zigzag traverse method. It occurs when the operator does not have the machine on the markers at the same place on alternate traverses. The effect is exacerbated when surveying using a higher spatial resolution. Providing it is a consistent error, post-processing software can deal with staggering, but it would be better if the operator was made aware of this problem, and could correct it with a slightly different walking technique. The alternative is to use the parallel traverse method.

Periodic errors

Figure 169 Periodic errors

Periodic errors occur as a set of linear differences along the line of the traverse, and are caused primarily by a "loping" style of walking, where shoulders are moving up and down. It can also be caused when the operator is attempting to match his/her pace to the guide "beeps" in a striding fashion, or if the instrument is not being held firmly, but being allowed to wobble around too much. Some machines are more susceptible to this form of error then others, but the problem can generally be solved by initially slowing down the normal walking pace of the operator, so that they are forced to walk in a different way.

9.2 Resistivity

Resistivity is an active form of geophysical surveying, in that an electrical current is applied through probes which must be inserted into the ground, with the electrical resistance to the current then being measured.

The electrical resistance of the ground is almost entirely dependent upon the amount and distribution of water (or moisture) within the soil (Clarke, 1996, p.27). In fact, soil and the stones within the soil are insulators, and the current is carried by positive and negative ions in the moisture (or rather the hydrogen ions within the water) present in the pores of the soil, with conductivity increasing with porosity (Kearey and Brooks, 1991). Features underground which may equate to differences in the soil resistance can be detected with resistivity meters. In particular, stone is generally moisture resistant, and will thus generate a higher resistance signal, so that archaeologists have generally favoured the use of resistivity meters to detect the location of buried stone or masonry walls. Because of its dependence on soil moisture content, resistivity surveys will produce different results at different times, with a decrease in resistance values either during heating or after rainfall (Scollar et al, 1990, p.354)

The principles and concepts behind measuring electrical resistance are well understood (Scollar at al, 1990, p.307-335; Clark, 1996, p.27-30), but I include here a brief description of the methods generally used in archaeological prospection.

When measuring the current between just two probes, the problem arises that the contact resistance of the probes is higher than the lower resistance changes in the underlying soil in which the archaeologist is interested. This is because the probe's surface area is much smaller than the volume of ground through which we are passing

the current, and is exacerbated by the fact that the soil's conductivity is generally poor near the surface, exactly where we need to insert our probes.

This can be overcome by using a four probe system, where two probes (the mobile probes) provide the current and another two (the remote probes), provide a background reading (measuring the voltage gradient). Known as the twin electrode configuration, this system has dominated resistivity surveying for archaeological purposes, although four probe configurations such as the Wenner array or the double-dipole arrangement are now being used with increasing frequency. The separation of the probe pairs in the twin electrode configuration must conform to a strict ratio (a distance of at least 30 times the separation of the probes in the mobile pair, (i.e. a 50cm separation in the mobile probes means that the remote probes must be at least 15 metres away) so that variations in the separation of the pairs will affect readings by less than 3 per cent. This is generally assumed to be a reasonable level for archaeological surveying.

Geoscan Research RM15 resistivity meter

Figure 170 James Lyall carrying out resistance survey at Site 010 (through the nettles!)

All of the resistance surveys in the project area have been carried out using a *Geoscan Research* RM15 resistance meter, using the twin electrode configuration. The data collection was carried out using the same system as for the fluxgate gradiometer; that is in 30 metre grids using a zigzag traverse. Data was collected at 1 metre intervals in both north-south and east-west axes, thus collecting 900 readings per 30 metre grid. Generally, the resistivity meter was set up at 1mA, with a gain setting of 1, with the mobile probes spaced 50cm apart.

A further development in resistivity technique is in the application of the principles of tomography, to obtain a vertical cross-section. A linear array of electrodes provides a large number of independent readings, which in turn includes the potential for much greater depth penetration.

Figure 171 James Lyall (left) with David Stott carrying out resistance survey using the English Heritage multiplexor array on site 12, to the south of the excavated Anglian settlement at West Heslerton

Although the multiplexor has been tested at Heslerton (survey carried out by LRC personnel, data processed by EH), the results were inconclusive, possibly because the buried remains were too deep to be detected.

While no form of remote sensing can truly be said to be a repeatable experiment, this is particularly true of resistivity, because of its reliance on the moisture content within the soil to provide results. A site can be surveyed a number of times, with each successive survey giving a different response. Generally, the survey should be carried out a number of days (or weeks, depending on how well drained the site is), after rain, but before all of the soil moisture has dissipated, thus allowing a contrast to be recorded.

9.2.1 Resistivity data

When resistivity survey works, then it tends to work well, but the very way that resistance operates means that the underlying soil moisture content is vital to a successful outcome for this technique

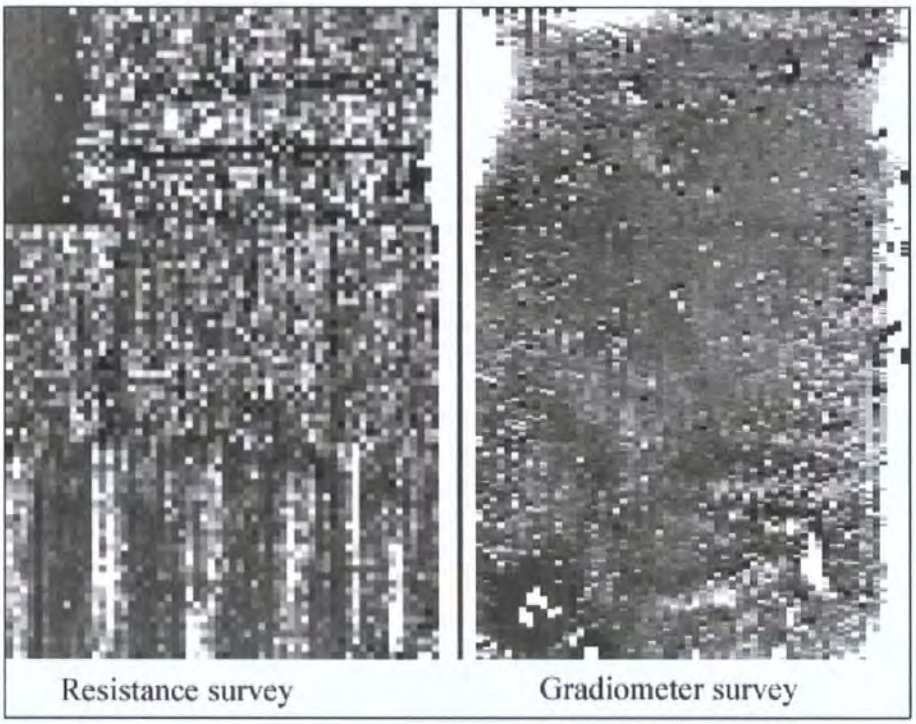

Figure 172 Comparison of resistance and gradiometer surveys

This is graphically demonstrated in Figure 172 (resistance survey on the left, area 60m by 90m) where the southernmost 2 grids were surveyed on the 14th February, 1996 when the ground was wet from rain and snow the previous day. It is clear that all we are seeing is the effect of water gathering in ploughmarks and wheel ruts down the centre of the field. In addition, the four grids in the north, surveyed previously on the 8th February, were also affected by water as the snow and frost thawed out during the duration of the survey, so that like cannot be compared to like across the four grids. The effects of this can be seen in the extreme west of the north-western grid, where standing water was encountered. The gradiometer survey on the right was carried out at the same time as the resistivity survey, and demonstrates that water (and weather conditions in general) do not effect magnetic surveying techniques. The large rectilinear anomaly in

the southern area of the magnetic survey turned out to be part of a moat surrounding a Medieval moated manor house. It is almost certain that this feature would have been detectable using resistance had the soil moisture conditions been right.

9.2.2 Operator errors possible with resistivity data collection

There are far fewer pitfalls lying in wait for the novice resistivity operator, when compared with magnetic surveying. However, some similar effects can occur.

Chessboard pattern grids

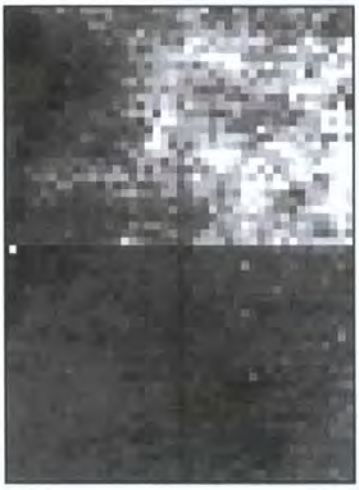

Figure 173 Chessboard pattern grids in resistivity surveys

This can occur either because the underlying ground conditions have altered between collecting the data for the grids (for instance a heavy rain shower has occurred) or when moving the remote probes after completing a grid. While post-processing software can get around the problem to some extent, best practice can help to prevent this. There is nothing we can do about rain during surveying, but the second cause of the problem can be avoided by ensuring that a reading from the mobile probes is taken before the remote probes are moved. Leaving the mobile probes in the same place, the remote probes can then be moved to their new location. Moving one of the remote probes either nearer or further away from the other, the reading previously noted on the mobile probes can be re-established with reasonable accuracy.

In addition, resistivity survey is much more sensitive to the underlying ground conditions than magnetometry. A general rule of thumb would be; if you can see standing water, snow or ice in the area you wish to survey, then come back another time. While in exceptional circumstances it is possible to obtain useful results in these conditions, you would generally be wasting your time and would have to come back again to re-survey the site anyway. This is because water near the surface allows the current to pass between the probes very easily, giving a general low resistance.

9.3 Appendix two Software used for the generation of images

A number of different software programs were used for the production of the images in the thesis, from those required for the initial data processing and manipulation, to those which created the finalised figures. Data handling and manipulations were carried out using a database, spreadsheet and a GIS/GDMS.

Access 2000
The relational database Access 2000 has been used to store all point data. In addition to all of the context and finds data from the excavations, all of the remote sensing survey data is also stored using Access.

Azgcorr version 4.5.2
Azgcorr is a program written and provided free by the NERC to end users of the data collected by NERC. It automatically geocorrects the raw ATM and CASI data, by using the navigational information taken by GPS situated at the front and back of the plane and on the wings at the time of the flight. This adjusts the image to take into account the pitch and yaw of the aircraft at the time of acquisition.

Excel 2000
The spreadsheet Microsoft Excel 2000 has been used to produce all of the tables and graphs used in the thesis.

GSYS version 5.2.674
The line between Geographic Information Systems (GIS) and Geographic Data Management Systems (GDMS), has now become so blurred as to be almost meaningless, as most modern GIS systems will deal with vector, raster and point data, derived from databases which contain 3 dimensional coordinates in real space. I have used the proprietary GIS Gsys, developed by Dominic Powlesland, for all geocorrected vector and raster data. All of the initial images for the mapped data have also been created in Gsys.

Imagine version 8.7
I have used Imagine (now owned by Leica) to georeference all of the azgcorrected ATM and CASI data. Image classification and principal component analysis was also carried out using Imagine.

Open EV
The program used for draping the remote sensing data onto the LIDAR DEM was Open EV-FW, a freeware program which allows you to "fly" over the area using the mouse. Figure 159 and Figure 158 are all screen dumps from this program.

Photoshop versions 6 and 7
Photoshop was used for final image enhancements, as well as for adding text to images.

Smart Draw version 7.31
The flowcharts (Figure 34 and Figure 65) were created using Smart Draw. A trial version of the program was downloaded from the web and this gave the user 15 free sessions. Website http://www.smartdraw.com/exp/flo/home/

Word 2000
The thesis was written and presented using the Microsoft Word 2000 word processor.

9.4 Appendix three Previous postgraduate work on the 1992 flight

Two postgraduate students have worked on various aspects of the multispectral data from the June 1992 flight. The first was Clare Pryor, who completed her MA at the University of Durham (Pryor, C.M. 1992). Clare was interested in looking at surface sedimentary deposition as well as cropmark formation. An initial comparison of the multispectral image and aerial photographic results were also compared to two small sample areas of fluxgate gradiometry. The main thrust of Clare's work was to integrate the returns from all of the remotely-sensed data into a Geographic Information System (GIS). Clare used three test areas in her research (see Figure 174).

The second student was Alison Caldwell, who gained her MSc in Remote Sensing from University College London (Caldwell, A.E. 1996). Alison was primarily interested in quantifying the returns from the different bands of the multispectral imagery in relation to the land use and underlying soils classification, with specific regard given to potential soil moisture deficit (PSMD). An initial comparison of the returns was then made with the vertical aerial photographs taken at the same time. Alison used two scales of data analysis in her research, the first of which was a large scale look at three lines of the multispectral data (lines 2a, 4c and 6), and the second looking at four test areas (see (Figure 174).

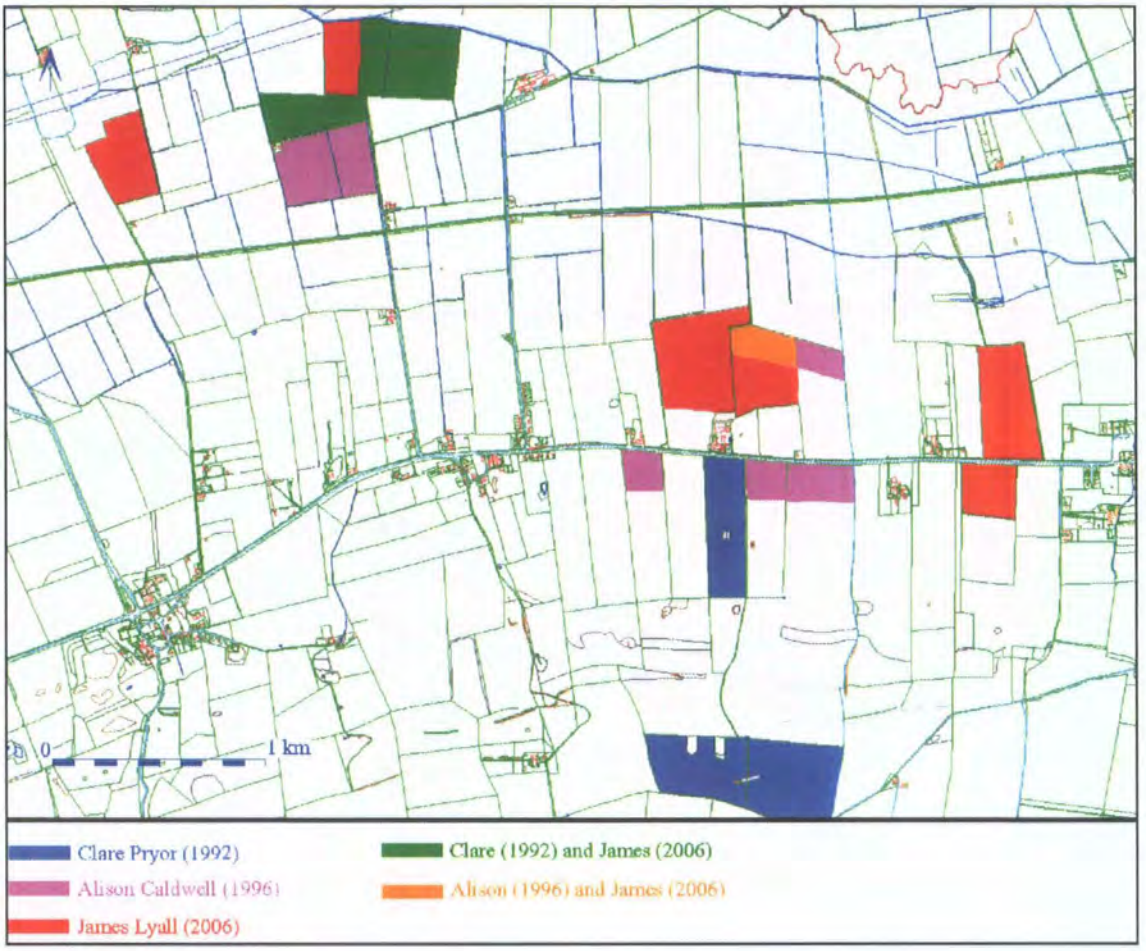

Figure 174 Showing the extent of the previous analyses in relation to the 2006 research

Because of the different research aims of the two students, neither Clare nor Alison did much in the way of georeferencing the original multispectral images, so a direct comparison of the returns from different remote sensing sources was not feasible. Alison tended to use a simple linear contrast stretch function to enhance the multispectral images. As indicated above, this does not always provide the best results for some of the more subtle features, and can also enhance some anomalies at the expense of others. She concluded that single band images were often better for anomaly detection than composites using arithmetic operations, and also that the NDVI and colour composites were not particularly helpful at finding cropmarks. She also concludes that some types of PCA might be useful, although the effects detected using PCA tended to be dominated by factors unrelated to archaeology (Caldwell, 1996, 139)

Alison did provide a number of tables totalling the numbers of anomalies from each category for her study areas, but this did not indicate whether the different returns were finding the ***same*** anomalies or not. She also totalled all of the different types of anomaly together, including archaeological, geomorphological and modern anomalies.

Both Clare and Alison worked on establishing the initial vector polygon drawings of the underlying soils, as well as creating two different land use classification drawings. I have now merged the results from the land use drawings into a single system, and have established a database (containing data on 909 different fields) which combines the results of both of their work, as well as adding in new details which were not known at the time. A unique number field had to be created, as Alison extended the area from Clare's original project zone, but duplicated some of the field numbers that Clare had used.

Landuse database updated 2005 : Table

Field Name	Data Type	Description
DRAWING	Text	Link to vector drawing
XCOORD	Text	Centroid easting
YCOORD	Text	Centroid northing
ZCOORD	Text	Height AOD
CP_Field_num	Number	Original numbers issued by Clare Pryor
Landuse_June_1992	Text	Crop at the time of the !992 multi-spectral survey
Landuse_June_2005	Text	Crop at the time of the 2005 multi-spectral survey
Unique	Number	A unique number issued for each field.
Colour	Text	Field used to overide vector drawing characteristics
Layer	Text	Field used to overide vector drawing characteristics
Shading	Text	Field used to overide vector drawing characteristics

Figure 175 Design view of the fields used in the land use database

This database will allow the land use patterns of any further flights to be easily integrated into the new system, without having to create further data structures.

9.5 Appendix four Design views of remote sensing data tables

Aerial Photographic Anomalies : Table

Field Name	Data Type	Description
Fromdraw	Text	Key_ID of individual anomaly (from digitised drawing)
Link_Key_ID	Text	Link to remote sensing correlation table
Anomaly Type	Text	Simple description of anomaly type (ie linear, circular or localised)
Sub-Type	Text	More in depth than anomaly type (ie ring ditch)
Interpretation	Text	Specific interpretation of feature (ie round barrow, round house, hay rick gully)
Cropmark Strength	Text	Strength of cropmark
Date	Date/Time	Date recorded
Master	Text	Linking anomalies that obviously belong to a single entity (ie across sites)
Master Type	Text	If the anomaly belongs to a much larger entity (ie ladder settlement or pit alignmer
Phase	Text	If appropriate, initial phasing can be inserted
Notes	Memo	Any pertinent notes relating to the anomaly
Drawn_By	Text	Drawn by (Initial transcription from AP plots)
Photo source	Text	Original transcription source photograph
Digi_By	Text	Interpreted by (interpretation by digitiser)
Site	Text	Site Number
XCOORD	Text	Easting in NGR co-ordinate system (from digitised drawing centroid)
YCOORD	Text	Northing in NGR co-ordinate system (from digitised drawing centroid)
ZCOORD	Text	Height above AOD
Cropmark Type	Text	Type of cropmark eg soil mark
Acquisition date	Date/Time	Date of photo acqisition
Group	Text	Categorisation of anomaly type

Field Properties

Figure 176 A design view of the fields in the aerial photographic anomalies database

Multi-spectral Anomalies : Table

Field Name	Data Type	Description
Fromdraw	Text	Key_ID of individual anomaly (from digitised drawing)
Link_Key_Id	Text	Link to remote sensing correlation table
Strength H/M/L	Text	Strength of anomaly
Digi_from	Text	Indicates which band the original drawing was digitised from
Band 3	Yes/No	Presence of anomaly in this band
Band 4	Yes/No	Presence of anomaly in this band
Band 5	Yes/No	Presence of anomaly in this band
Band 6	Yes/No	Presence of anomaly in this band
Band 7	Yes/No	Presence of anomaly in this band
Band 8	Yes/No	Presence of anomaly in this band
Band 10	Yes/No	Presence of anomaly in this band
Band 11	Yes/No	Presence of anomaly in this band
Band 12	Yes/No	Presence of anomaly in this band
Anomaly Type	Text	Simple description of anomaly type (ie linear, circular or localised)
Sub-Type	Text	More in depth than anomaly type (ie ring ditch)
Interpretation	Text	Specific interpretation of feature (ie round barrow, round house, hay rick gully)
Date	Date/Time	Date recorded
Master	Text	Linking anomalies that obviously belong to a single entity (ie across sites)
Master Type	Text	If the anomaly belongs to a much larger entity (ie ladder settlement or pit alignment)
Phase	Text	If appropriate, initial phasing can be inserted
Notes	Memo	Any pertinent notes relating to the anomaly
Pos_Neg	Yes/No	Positive or negative anomaly
Drawn_By	Text	Drawn by
Digi_By	Text	Interpreted by (database)
Site	Text	Site Number
XCOORD	Text	Easting in NGR co-ordinate system (from digitised drawing centroid)
YCOORD	Text	Northing in NGR co-ordinate system (from digitised drawing centroid)
ZCOORD	Text	Height above AOD
Colour	Text	Optional-potentially linked to anomaly type
Layer	Text	Optional-potentially linked to anomaly type
Shading	Text	Optional-potentially linked to anomaly type
Band 1	Yes/No	Presence of anomaly in this band
Band 2	Yes/No	Presence of anomaly in this band
Band 9	Yes/No	Presence of anomaly in this band
Source of data	Text	Indicates the original source of the data
Acquisition Date	Date/Time	Date on which the data was collected
Group	Text	Categorisation of anomaly type
Referential integrity	Text	Description of georeferencing problems

Field Properties

Figure 177 A design view of the fields in the multispectral anomalies database

Fluxgate Gradiometer Anomalies : Table

Field Name	Data Type	Description
Fromdraw	Text	Key_ID of individual anomaly (from digitised drawing)
Anomaly Type	Text	Simple description of anomaly type (ie linear, circular or localised)
Sub-Type	Text	More in depth than anomaly type (ie ring ditch)
Interpretation	Text	Specific interpretation of feature (ie round barrow, round house, hay rick gully)
Anomaly Strength 1-5	Text	Strength of anomaly
Group	Text	Categorisation of anomaly type
Date	Date/Time	Date recorded
Master	Text	Linking anomalies that obviously belong to a single entity (ie across sites)
Master Type	Text	If the anomaly belongs to a much larger entity (ie ladder settlement or pit alignment)
Phase	Text	If appropriate, initial phasing can be inserted
Strat_above	Text	If an obvious statigraphic cutting relationship is visible it can be noted here
Notes	Memo	Any pertinent notes relating to the anomaly
Strat_below	Text	If an obvious statigraphic cut by relationship is visible it can be noted here
Pos_Neg	Yes/No	Positive or negative anomaly (Negative = Y)
Drawn_By	Text	Drawn by (Initial transcription from geophysical plots)
Sheet Number	Number	Sheet number of original transcription from geophysical data
Digi_By	Text	Interpreted by (interpretation by digitiser)
Site	Text	Site Number
EXC_Key_ID	Text	Link to excavation master number
EXC_KeyID2	Text	Second link to excavation master number
XCOORD	Text	Easting in NGR co-ordinate system (from digitised drawing centroid)
YCOORD	Text	Northing in NGR co-ordinate system (from digitised drawing centroid)
ZCOORD	Text	Height above AOD
Interpretation 2	Text	Second possible interpretation
PhasePLot	Text	Phase field for plotting drawings
Project	Text	Project number
Link_Key_ID	Text	Link to Remote Sensing correlation table

Figure 178 A design view of the fields in the gradiometer anomalies database

Remote Sensing Correlation Table : Table

Field Name	Data Type	Description
MSS_1992	Text	Link to multi-spectral anomaly table
Resistance	Text	Link to resistivity anomaly table
GPR	Text	Link to ground penetrating radar table
Master1	Text	Link to Master number in context record table
Master2	Text	Link to second Master number in context record table
Number	Number	Incremental number
xcoord	Text	NGR easting
ycoord	Text	NGR northing
zcoord	Text	AOD height if applicable or known
Interpretation	Text	Feature type
Group	Text	Feature group
MSS Notes	Memo	Further notes

Figure 179 A design view of the fields in the remote sensing correlation database

9.6 Appendix five Converting image files to an ASCII file format using Imagine

Figure 180 Choosing Layer Info from the Imagine Utilities menu

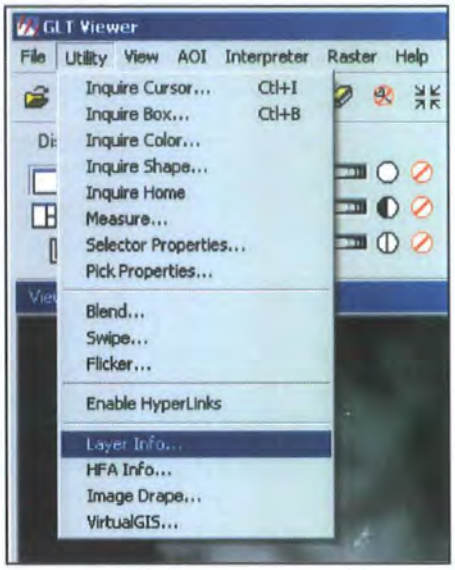

When the image is loaded in the viewer, click on the Utility menu and choose Layer Info from the submenu (see Figure 180 to the right). When the Layer Info menu has loaded, you then need to select the Pixel Data tab (highlighted in blue in Figure 181 below).

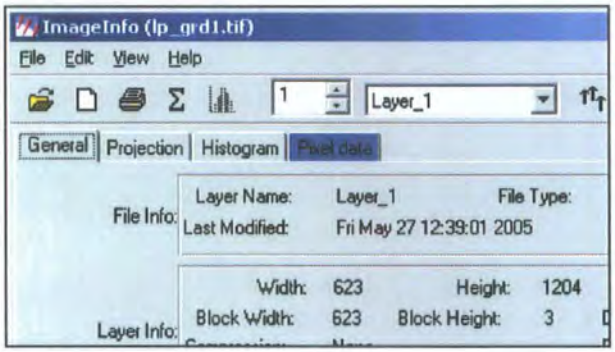

Figure 181 Selecting the Pixel Data tab from the Layer Info menu

You now have to select the Print to File from the File menu. This will bring up a dialogue which allows you to save the data in a text file format. Providing the image is in some form of map projection, the text file will consist of an easting, a northing and the data value (these are the numbers in the boxes, see Figure ?? to the left) in a tab separated file. The easiest way to deal with this file is to import it into Access and then output into the file format you want from there.

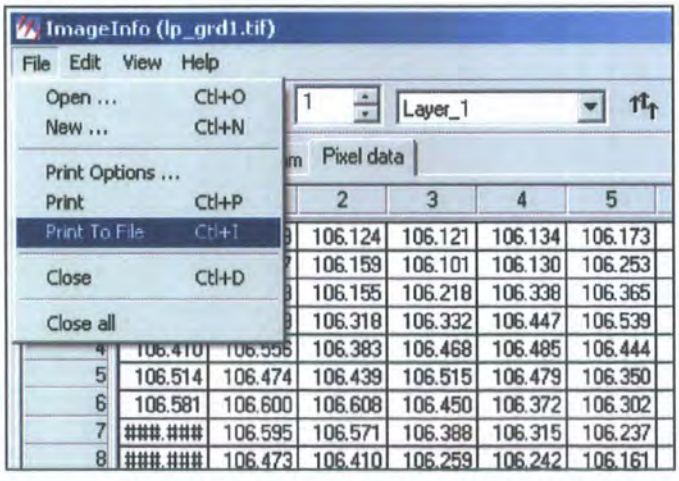

Figure 182 Choosing the Print to File dialogue from the File menu in the Pixel Data sub menu

9.7 Appendix six Hobo statistics in water from 2004

Because the Hobo which was collecting the temperatures in the body of water was stolen in 2005, it was necessary to use the figures which were obtained in 2004. These are as follows:

Air	Water	Buried	Buried
10.27	14.048	14.59	15.13

Table 27 Average temperatures in June from 02:06am to 02:46am

Air	Water	Buried	Buried
12.5	16.27	17.36	17.3

Table 28 Average temperatures from 09/06/2004 to 14/09/2004 from 02:06am to 02:46am

Air	Water	Buried	Buried
17.88	15.13	17.83	17.27

Table 29 Average temperatures in June from 09:30am to 10:45am

Air	Water	Buried	Buried
18.45	16.6	18.17	17.8

Table 30 Average temperatures from 09/06/2004 to 14/09/2004 from 09:30am to 10:45am

9.8 Appendix seven Comparison of CASI and ATM wavelengths

CASI band	Centre	Lower	Upper	ATM band	Spectral Component
1	0.407743	0.404873975	0.410612025	None	Blue
2	0.418883	0.41601037	0.42175563	1	Blue
3	0.43004	0.42716383	0.43291617	1	Blue
4	0.441214	0.438334355	0.444093645	1	Blue
5	0.452405	0.449521955	0.455288045	1	Blue
6	0.463611	0.46072461	0.46649739	2	Blue-green
7	0.474834	0.47194433	0.47772367	2	Blue-green
8	0.486072	0.483179125	0.488964875	2	Blue-green
9	0.497325	0.494428985	0.500221015	2	Blue-green
10	0.508593	0.5056939	0.5114921	2	Blue-green
11	0.519876	0.516973905	0.522778095	2	Blue-green
12	0.531173	0.52826796	0.53407804	3	Green
13	0.542484	0.53957609	0.54539191	3	Green
14	0.553809	0.55089828	0.55671972	3	Green
15	0.565147	0.562233535	0.568060465	3	Green
16	0.576498	0.57358185	0.57941415	3	Green
17	0.587862	0.58494324	0.59078076	3	Green
18	0.599238	0.59631671	0.60215929	3	Green
19	0.610627	0.60770322	0.61355078	4	Red
20	0.622026	0.61909981	0.62495219	4	Red
21	0.633438	0.63050946	0.63636654	5	Red
22	0.64486	0.641929185	0.647790815	5	Red
23	0.656293	0.653359975	0.659226025	5	Red
24	0.667737	0.66480182	0.67067218	5	Red
25	0.679191	0.676253745	0.682128255	5	Red
26	0.690655	0.687715735	0.693594265	5	Red
27	0.702128	0.699186795	0.705069205	6	Near Infra-red
28	0.71361	0.710666905	0.716553095	6	Near Infra-red
29	0.725101	0.722156085	0.728045915	6	Near Infra-red
30	0.736601	0.73365435	0.73954765	6	Near Infra-red
31	0.748109	0.745160655	0.751057345	6	Near Infra-red
32	0.759625	0.75667505	0.76257495	7	Near Infra-red
33	0.771149	0.768197495	0.774100505	7	Near Infra-red
34	0.782679	0.779726	0.785632	7	Near Infra-red
35	0.794217	0.791262595	0.797171405	7	Near Infra-red
36	0.805762	0.802806255	0.808717745	7	Near Infra-red
37	0.817312	0.81435497	0.82026903	7	Near Infra-red
38	0.828869	0.825910735	0.831827265	7	Near Infra-red
39	0.840431	0.83747159	0.84339041	7	Near Infra-red
40	0.851999	0.84903851	0.85495949	7	Near Infra-red
41	0.863572	0.8606105	0.8665335	7	Near Infra-red
42	0.87515	0.87218754	0.87811246	7	Near Infra-red
43	0.886732	0.883768655	0.889695345	7	Near Infra-red
44	0.898318	0.89535383	0.90128217	7	Near Infra-red
45	0.909907	0.90694207	0.91287193	8	Near Infra-red
46	0.921501	0.91853538	0.92446662	8	Near Infra-red
47	0.933097	0.93013077	0.93606323	8	Near Infra-red
48	0.944696	0.941729205	0.947662795	8	Near Infra-red

Table 31 CASI and ATM spectral wavelength comparison

Note that the first band of the CASI data has no ATM comparison, as it begins collecting data slightly earlier in the blue band of the EMS than the AZ-16.